

---

---

---

# 1235

TRANSPORTATION RESEARCH RECORD

---

## *In Situ Testing of Soil Properties for Transportation*

---

TRANSPORTATION RESEARCH BOARD  
NATIONAL RESEARCH COUNCIL  
WASHINGTON, D.C. 1989

**Transportation Research Record 1235**

Price: \$13.00

mode

1 highway transportation

subject areas

24 pavement design and performance

61 soil exploration and classification

62 soil foundations

63 soil and rock mechanics

64 soil science

**TRB Publications Staff**

*Director of Publications:* Nancy A. Ackerman

*Senior Editor:* Edythe T. Crump

*Associate Editors:* Naomi C. Kassabian

Ruth S. Pitt

Alison G. Tobias

*Production Editor:* Kieran P. O'Leary

*Graphics Coordinator:* Karen L. White

*Office Manager:* Phyllis D. Barber

*Production Assistant:* Betty L. Hawkins

Printed in the United States of America

**Library of Congress Cataloging-in-Publication Data**

National Research Council. Transportation Research Board.

In situ testing of soil properties for transportation.

p. cm.—(Transportation research record, ISSN 0361-1981 ; 1235)

ISBN 0-309-04962-8

1. Soils—Testing. I. National Research Council (U.S.).

Transportation Research Board. II. Series.

TE7.H5 no. 1235

[TA710.5]

380.5—dc20

[629.04'9]

90-36397

CIP

**Sponsorship of Transportation Research Record 1235**

**GROUP 2—DESIGN AND CONSTRUCTION OF TRANSPORTATION FACILITIES**

*Chairman:* Raymond A. Forsyth, California Department of Transportation

**Soil Mechanics Section**

*Chairman:* Michael G. Katona, TRW

Committee on Foundations of Bridges and Other Structures

*Chairman:* Richard S. Cheney, Federal Highway Administration, U.S. Department of Transportation

*Secretary:* Richard P. Long, University of Connecticut

*Francois J. Baguelin, Jean-Louis Briaud, Bernard E. Butler, Murty*

*S. Devata, Albert F. DiMillio, Victor Elias, Richard L. Engel,*

*Bengt H. Fellenius, George G. Goble, Richard J. Goettle III, James*

*S. Graham, Robert C. Houghton, Alan P. Kilian, Hugh S. Lacy,*

*Robert M. Leary, John F. Ledbetter, Jr., Larry Lockett, Randolph*

*W. Losch, Lyle K. Moulton, Peter J. Nicholson, Michael Wayne*

*O'Neill, Harvey E. Wahls, John L. Walkinshaw, Gdalyah Wiseman*

**Geology and Properties of Earth Materials Section**

*Chairman:* C. William Lovell, Purdue University

Committee on Soil and Rock Properties

*Chairman:* James J. Schnabel, Schnabel Engineering and Associates

*Robert C. Bachus, S. S. Bandy, Roy H. Borden, Timothy D.*

*Bowen, William H. Hightler, Robert D. Holtz, Richard H. Howe,*

*An-Bin Huang, Steven L. Kramer, C. William Lovell, Priscilla P.*

*Nelson, Sibel Pamukcu, Gerald P. Raymond, J. Allan Tice,*

*Mehmet T. Tumay, Recep Yilmaz*

G. P. Jayaprakash, Transportation Research Board staff

Sponsorship is indicated by a footnote at the end of each paper.

The organizational units, officers, and members are as of December 31, 1988.

NOTICE: The Transportation Research Board does not endorse products or manufacturers. Trade and manufacturers' names appear in this Record because they are considered essential to its object.

Transportation Research Board publications are available by ordering directly from TRB. They may also be obtained on a regular basis through organizational or individual affiliation with TRB; affiliates or library subscribers are eligible for substantial discounts. For further information, write to the Transportation Research Board, National Research Council, 2101 Constitution Avenue, N.W., Washington, D.C. 20418.

# Transportation Research Record 1235

---

## Contents

<b>Foreword</b>	<b>v</b>
<hr/>	
<b>Stiffness Profiling of Pavement Subgrades</b> <i>Glenn J. Rix and Kenneth H. Stokoe II</i>	<b>1</b>
<hr/>	
<b>In Situ Testing of Peaty Organic Soils: A Case History</b> <i>Nancy J. Nichols, Jean Benoit, and Frederic E. Prior</i>	<b>10</b>
<hr/>	
<b>Evaluation of Soil Parameters from Piezocone Tests</b> <i>Kaare Senneset, Rolf Sandven, and Nilmar Janbu</i>	<b>24</b>
<hr/>	
<b>Development of a Chart for Preliminary Assessments in Pavement Design Using Some In Situ Soil Parameters</b> <i>Sibel Pamukcu and H. Y. Fang</i>	<b>38</b>
<hr/>	
<b>Design Parameters of Cohesionless Soils from In Situ Tests</b> <i>R. Bellotti, V. N. Ghionna, M. Jamiolkowski, and P. K. Robertson</i>	<b>45</b>
<hr/>	
<b>Italian Motorway System: Experiences with In Situ Tests and Inclinometer Surveys for Urgent Remedial Works</b> <i>T. Collotta, R. Cantoni, and P. C. Moretti</i>	<b>55</b>
<hr/>	
<b>Analyses of Laterally Loaded Drilled Shafts Using In Situ Test Results</b> <i>A. B. Huang, A. J. Lutenecker, M. Z. Islam, and G. A. Miller</i>	<b>60</b>
<hr/>	
<b>Soil Stratification Using the Dual-Pore-Pressure Piezocone Test</b> <i>Ilan Juran and Mehmet T. Tuncay</i>	<b>68</b>
<hr/>	
<b>Load-Deflection Response of Piles in Sand: Performance Prediction Using the DMT</b> <i>Roy H. Borden and Robert S. Lawter, Jr.</i>	<b>79</b>
<hr/>	



# Foreword

For geotechnical purposes, in situ testing is a fast, economic, reliable, and repeatable method of obtaining data needed for classifying subsurface soils and evaluating their engineering properties. The nine papers included in this Record cover in situ tests whose uses are well established in the United States and Europe: the Cone Penetration Test (CPT), Piezocone Penetration Test (PCPT, CPTU), Dual Piezocone Penetration Test (DPCPT), Dilatometer Test (DMT), Plate Load Test (PLT), Prebored Pressuremeter Test (PMT), Self-Boring Pressuremeter Test (SBPM), Full-Displacement Pressuremeter Test (FDPM), Spectral Analysis of Surface Waves (SASW), Standard Penetration Test (SPT), and Vane Shear Test (VST, FVT).

Rix and Stokoe present results of field testing with the SASW method, which is based on the dispersive characteristics of surface waves in layered media. SASW allows detailed profiles of small-strain moduli in subgrades to be obtained before, during, and after placement of the pavement system.

Nichols et al. describe their experiences with PLT, VST, DMT, SPT, SBPM, and FDPM in areas that have peaty organic soils. These soils are extremely difficult to sample with conventional methods. Senneset et al. describe their many years of experience in using CPT and CPTU on a wide variety of soils in Norway. They demonstrate techniques for evaluating shear strength and settlement parameters in medium stiff, overconsolidated clay.

Pamukcu and Fang present a pavement design chart that includes interrelationships between soil classification and bearing values versus CPT, SPT, and SBPM results. Bellotti et al. outline cohesionless soil design parameters obtained by using CPT, SPT, and DMT. They present correlations and results from a 10-year research project involving large calibration chambers.

Collotta et al. demonstrate the importance of using inclinometer surveys as a supplement to in situ tests in the design of remedial measures for a slope stability problem along a motorway. Huang et al. discuss the use of FVT, PMT, DMT, and CPTU results to predict the lateral load displacement response of small-diameter drilled shafts in clays.

Juran and Tumay discuss field investigations indicating that PCPT has an enhanced capability to identify and classify minute loose or dense sand inclusions in clay deposits. They also cover the design, testing, de-airing, and interpretation of a new in situ probe. Borden and Lawter present the performance results of lateral load stress on two 24-in.-square prestressed concrete piles. These authors also explain a predictive method that uses DMT results for developing  $p$ - $y$  curves. The technique proves to be satisfactory for representing the observed pile response.



# Stiffness Profiling of Pavement Subgrades

GLENN J. RIX AND KENNETH H. STOKOE II

---

The Spectral-Analysis-of-Surface-Waves (SASW) method is an in situ seismic method that permits detailed profiles of small-strain moduli to be determined at both soil and pavement sites. The method, which is nondestructive, is based on the dispersive characteristic of surface (Rayleigh) waves propagating in a layered medium. One of the principal advantages of this method is that all testing is performed on the ground surface. A second advantage for evaluating the properties of pavement systems is that the method can be used to determine the stiffness of the subgrade *before*, *during*, and *after* placement of the pavement system. These advantages are illustrated using a series of tests on a silty clay subgrade performed before and after placement of a concrete slab 10 in. (0.25 m) thick. A sensitivity study of the subgrade measurements and a method of characterizing nonlinear subgrade behavior are also presented.

---

Pavement subgrades can be investigated by a variety of in situ methods. However, the in situ method or combination of methods selected depends on factors such as the purpose of the investigation, the applicability of the method, and the availability of test equipment. When the subgrade is to be characterized by in situ moduli, seismic methods are the most direct in situ methods to use.

One seismic method, the Spectral Analysis of Surface Waves (SASW) method, is especially well suited for in situ investigation of pavement subgrades. An important feature of the SASW method is that it can be used either directly on the subgrade, on the base, or on the pavement surface layer at any time during the construction and subsequent life of the pavement. The SASW method is based on the generation and measurement of stress waves (Rayleigh waves) propagating along the surface. The propagation velocities of the Rayleigh wave are directly related to small-strain elastic moduli of the material through which they propagate. If moduli at larger strains are required, then in situ measurements of small-strain moduli are combined with laboratory and/or empirical results to describe the nonlinear behavior.

The purpose of this paper is to discuss the field and analysis procedures used in the SASW method. Results from one site where tests were performed directly on the subgrade and subsequently on a concrete slab cast on the subgrade are presented. The sensitivity of the measurements and the incorporation of nonlinear subgrade behavior are also discussed.

## OVERVIEW OF SASW METHOD

The SASW method is an engineering seismic method that uses the dispersive property of surface waves to determine the shear modulus profile at soil sites and/or the Young's modulus profile at pavement sites. Several aspects of the SASW method make it particularly well suited for use by transportation engineers. The first two of these aspects are the method's nondestructiveness and nonintrusiveness. Both the source and the receivers are located on the ground surface, thereby eliminating the need for boreholes. Furthermore, because the source imparts only low-level stress waves, the testing is nondestructive. The third aspect is that the method can be used to test exposed subgrades as well as completed pavements.

The following sections briefly describe the dispersive behavior of surface waves in a layered half space and the test procedure used in SASW testing.

### Surface Wave Dispersion

To understand how surface waves can be used to determine the modulus profiles of subgrades and pavements, it is first necessary to understand surface wave dispersion in a layered profile. A dispersive wave is one in which the velocity of propagation varies with frequency (which is the same as saying that velocity varies with wavelength). Surface wave dispersion is caused by the distribution of particle motion with depth. As wavelength increases, particle motion extends to greater depths in the profile, as illustrated in Figure 1. The velocities of surface waves are representative of the material properties over depths where there is significant particle motion. For example, the particle motion of a wave that has a wavelength less than the thickness of the pavement surface layer is confined to this layer (Figure 1b). Therefore, the wave velocity is influenced only by the properties of the surface layer. The velocity of a wave with a wavelength of several feet is influenced by the properties of the surface layer, base, and subgrade because a significant portion of the particle motion is in these layers (Figure 1c). Thus, by using surface waves over a wide range of wavelengths, it is possible to assess material properties over a range of depths.

The objective in SASW testing is to make field measurements of surface wave dispersion (i.e., measurements of surface wave velocity at various wavelengths) at soil and pavement sites and then to determine the shear wave velocities of the layers in the profile. These velocities can, in turn, be used

---

G. J. Rix, Department of Civil Engineering, Georgia Institute of Technology, Atlanta, Ga. 30332. K. H. Stokoe II, Geotechnical Engineering, The University of Texas at Austin, Austin, Tex. 78712-1076.

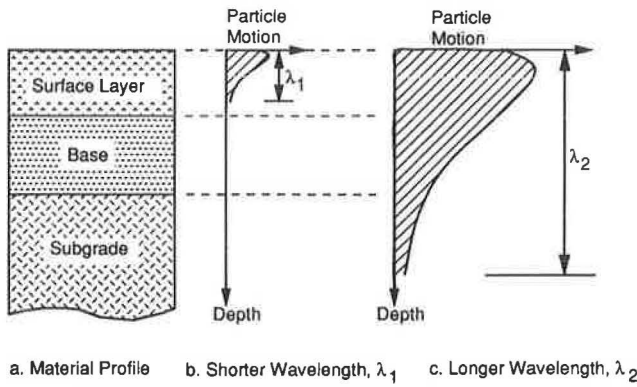


**FIGURE 1** Approximate distribution of vertical particle motion with depth for two surface waves of different wavelengths.

to calculate values of shear and Young's moduli using simple relationships from the theory of elasticity.

**SASW Test Procedure**

The procedure used to perform an SASW test can be divided into three steps: (a) field testing, (b) dispersion calculations, and (c) inversion (1). In the following sections, a brief description of each of these steps is presented.

*Equipment and Field Setup*

The configuration of source, receivers, and recording equipment used in SASW testing is shown in Figure 2. The most common types of sources used to date have been simple hammers or dropped weights that strike the ground surface and create a transient wave containing a broad range of frequencies. Recently, however, the use of electromechanical vibrators to transmit random or sinusoidal input motions to the ground has also shown promise (2).

Selection of receivers is based on the range of frequencies

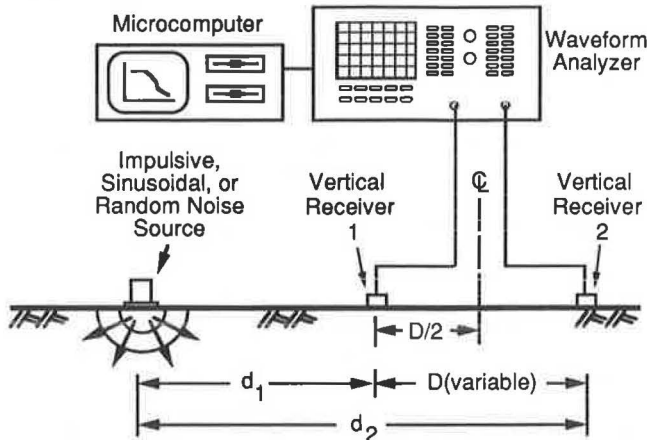


**FIGURE 2** Configuration of equipment used in field testing.

that will be used to profile the site. For subgrade profiling where the objective is to develop a profile to approximately 10 ft (3 m), the frequencies range from approximately 50 to 1000 Hz. In this range of frequencies, geophones (velocity transducers) with a natural frequency of 4.5 Hz perform well. The geophones are coupled to the soil using spikes 2 in. (5 cm) long. For profiling concrete or asphaltic pavements, much higher frequencies (up to 50 kHz) are used to generate very short wavelengths so that the pavement surface layer can be evaluated. Piezoelectric accelerometers, coupled to the pavement with mounting wax (3), are typically used in this range of frequencies.

A dual-channel fast Fourier transform (FFT) analyzer is used to record and analyze surface wave motion at the two receivers. An essential feature of this type of instrument is the ability to perform frequency domain calculations (described subsequently) in real time. Finally, a microcomputer is used to transfer data from the analyzer and to perform the dispersion calculations described in the following section.

The spacing between receivers ( $D = d_2 - d_1$  in Figure 2) varies according to the range of wavelengths used. In principle, it should be possible to use a single receiver spacing to perform an entire test. However, factors such as the attenuation of particle motion with horizontal propagation distance dictate that data from several different receiver spacings be combined for each test. For subgrade profiling, receiver spacings ranging from 1 to 16 ft (0.3 to 4.9 m) are typically used. For profiling the pavement surface layer and base materials, spacings of 0.25 to 4 ft (0.08 to 1.2 m) are employed. The distance from the source to the first receiver ( $d_1$  in Figure 2) is usually equal to the distance between receivers (1, 4).

The progression of receiver spacings at one site is illustrated in Figure 3. An imaginary centerline is established which remains fixed throughout the test. The receivers are placed equidistant from the centerline with the desired distance ( $D$ ) between them (Figure 3a). This distance is related to the minimum wavelength that must be used to profile the near-

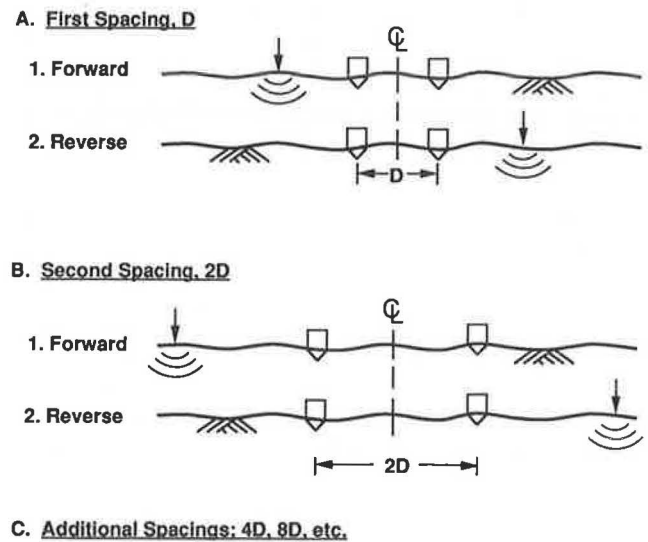


**FIGURE 3** Arrangement of source and receivers illustrating the common midpoint geometry and forward and reverse tests at each receiver spacing.



surface layers. After the measurements described in the next section are performed at this spacing, the location of the source is reversed with respect to the geophones to perform a reverse profile (Figure 3a). (The results from reverse and forward profiling are compared to check data consistency and lateral homogeneity.) The distance between the receivers is then increased (typically doubled), and the measurements are repeated at the new spacing (Fig. 3b). Testing continues in this fashion until measurements at the maximum spacing have been completed. The maximum spacing is determined by the longest wavelength required to evaluate the shear wave velocity profile to a predetermined depth. For instance, if a profile to a depth of 10 ft (3 m) is desired, a maximum wavelength from 2 to 3 times this depth should be measured.

*Dispersion Calculations*

For each source-receiver spacing, surface waves are generated by striking the soil or pavement surface with a hammer or dropped weight or by using an electromechanical vibrator to transmit random or sinusoidal input motion to the ground surface. The time histories recorded by the two receivers,  $[x(t)$  and  $y(t)]$  are transformed to the frequency domain, resulting in the linear spectra of the two signals  $[X(f)$  and  $Y(f)]$ . The cross power spectrum of the signals  $[G_{yx}(f)]$  is then calculated by multiplying  $Y(f)$  by the complex conjugate of  $X(f)$ . In addition to the cross power spectrum, the coherence function and the auto power spectrum of each signal are also calculated. It must be emphasized that all of these calculations are performed in real time by the FFT analyzer. The key data, consisting of the phase of the cross power spectrum and the coherence function, are shown in Figure 4. The coherence function represents a signal-to-noise ratio and should be nearly equal to 1 in the range of acceptable data (25 to about 150 Hz in Figure 4).

The time delay between receivers as a function of frequency, denoted as  $t(f)$ , is calculated using the phase angle of the cross power spectrum, denoted as  $\theta_{yx}(f)$ , as follows:

$$t(f) = \theta_{yx}(f)/2\pi f \tag{1}$$

where the phase angle is in radians and the frequency ( $f$ ) is in cycles/sec. The surface wave phase velocity ( $V_R$ ) is determined using

$$V_R(f) = (d_2 - d_1)/t(f) \tag{2}$$

and the corresponding wavelength of the surface wave ( $L_R$ ) is calculated from

$$L_R = V_R/f \tag{3}$$

These calculations give a dispersion curve ( $V_R$  versus  $L_R$ ) for one receiver spacing. Individual dispersion curves are then combined to form the composite dispersion curve for the site. An example of a composite dispersion curve is presented in Figure 5 for SASW testing of a silty clay subgrade.

*Inversion*

Inversion is the process of calculating the shear wave velocity (or modulus) profile using the field dispersion curve. In the inversion process, a theoretical dispersion curve is calculated for an assumed velocity profile and is then compared to the field dispersion curve. The assumed velocity profile contains a sufficiently large number of sublayers to define the variation of material properties at the site. The theoretical curve is

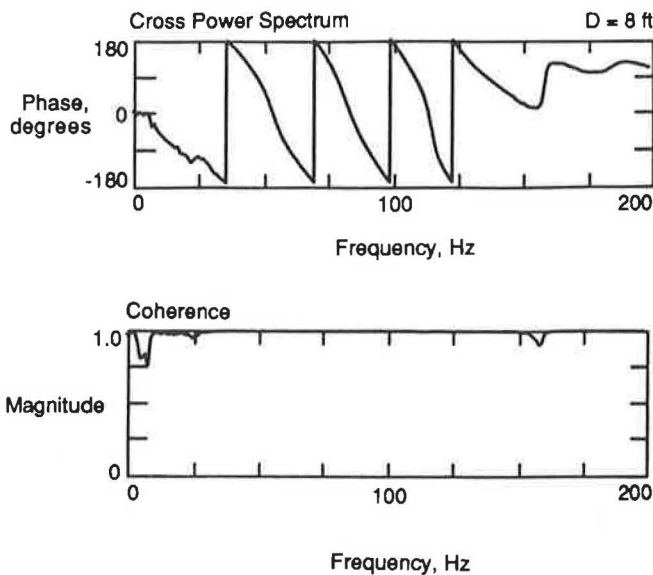


FIGURE 4 Spectral functions obtained using swept-sine input motion for a receiver spacing of 8 ft (2.4 m) on a silty clay subgrade.

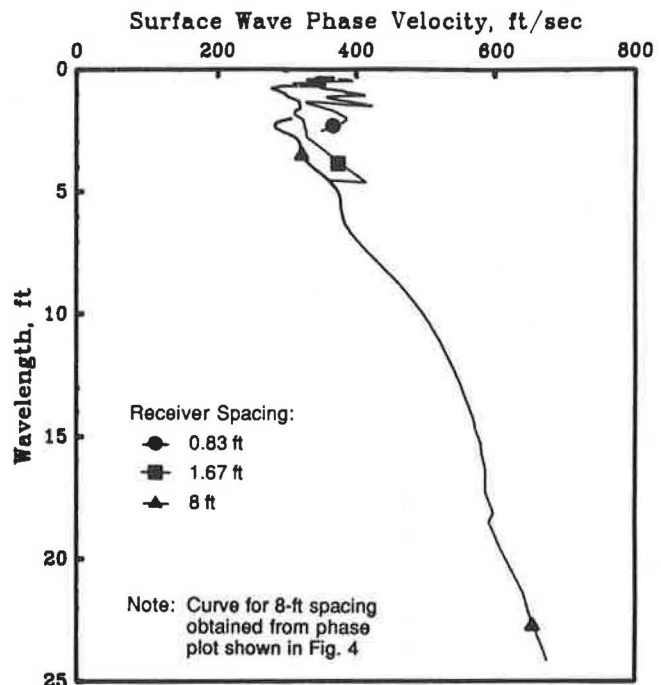


FIGURE 5 Composite dispersion curve for SASW testing of a silty clay subgrade.

calculated using a modified Haskell-Thomson matrix algorithm (1, 5, 6). The shear wave velocities and thicknesses of the sublayers in the assumed profile are adjusted by trial and error until a satisfactory match between the theoretical and field dispersion curves is obtained. Once a satisfactory match is obtained, the final profile is assumed to represent the actual site conditions. Application of inverse theory to surface wave testing has increased the accuracy of the resulting profiles and has expanded the variety of sites at which the SASW method can be used.

## SITE DESCRIPTION

A series of tests was performed to demonstrate the use of the SASW method on both subgrades and pavement sites. These tests were conducted at the Hornsby Bend test site located in Austin, Texas. A description of the soil stratigraphy and properties is presented below, along with a description of the concrete slab constructed at the site.

Soil borings show four basic strata: (a) a silty clay layer extending from the surface to 13.5 ft (4.1 m), (b) a silty clay layer interbedded with silty fine sand seams from 13.5 to 33.5 ft (4.1 to 10.2 m), (c) a loose to medium-dense, silty fine sand layer from 33.5 to 45 ft (10.2 to 13.7 m), and (d) a hard gray clay layer extending from 45 ft (13.7 m) to the maximum depth of the borings, 50 ft (15.2 m). Undrained shear strengths over the depth range of 2 to 20 ft (0.6 to 6.1 m) estimated using a pocket penetrometer are greater than 3.0 kips/ft<sup>2</sup> (144 kPa).

A concrete test slab was cast directly on the silty clay subgrade after all vegetation was removed. The slab was unreinforced and had dimensions of 8 by 12 ft (2.4 by 3.7 m) with a nominal thickness of 10 in. (25.4 cm). Class S concrete with Type I cement and a maximum aggregate size of 0.75 in. (1.91 cm) was used for the slab. The average 28-day strength determined from cylinder tests was 6,470 psi (44.5 MPa). It is believed that this slab adequately modeled a full-sized, unreinforced (or simply reinforced) pavement slab [usually 12 by 20 ft (3.7 by 6.1 m)].

## SUBGRADE PROFILING

SASW tests were performed directly on the silty clay subgrade prior to casting the slab. Three receiver spacings [0.83, 1.67, and 8 ft (0.25, 0.51, and 2.4 m)] were selected to provide data over a sufficient range of wavelengths to determine the velocity (modulus) profile to a depth of several feet. The composite dispersion curve presented in Figure 5 is the result of these measurements. The differences between the three individual dispersion curves in the wavelength range of 0.5 to 5 ft (0.15 to 1.5 m) is typical of variability often observed near the surface at soil sites. The variability at this site is most likely caused by lateral inhomogeneity and secondary structure in the silty clay.

The field dispersion curve was inverted using the procedure outlined in the section entitled "Inversion" to determine the shear wave velocity and Young's modulus profiles. The Young's modulus of each layer was derived from the shear wave velocity using the following relationship:

$$E = 2\rho V_s^2(1 + \nu) \quad (4)$$

where

- $E$  = Young's modulus,
- $\rho$  = mass density,
- $V_s$  = shear wave velocity, and
- $\nu$  = Poisson's ratio.

In the absence of direct measurements, values for mass density and Poisson's ratio are normally assumed. Reasonable values for these two parameters fall within a relatively small range and do not significantly affect the calculated value of Young's modulus ( $E$ ). In this study, however, measured values of mass density and Poisson's ratio were used.

The shear wave velocity and Young's modulus profiles for the subgrade are presented in Table 1. The values reported for the half space represent average values for the layers below 12 ft (3.7 m). The match between the composite dispersion curve shown in Figure 5 and the inverted profile given in Table 1 is shown in Figure 6. The theoretical curve agrees well with the trend of the experimental dispersion curves. However, the theoretical dispersion curve is very smooth in comparison with the experimental results and does not account for lateral variability. Until more sophisticated models of wave propagation are incorporated into inversion algorithms, it will not be possible to match the theoretical and experimental curves more exactly than is shown in Figure 6.

Finally, values of shear wave velocity determined from SASW testing are compared with those determined using an independent seismic method, the crosshole test, in Figure 7. The overall trends for the two methods are very similar, partic-

TABLE 1 VALUES OF SHEAR WAVE VELOCITY AND YOUNG'S MODULUS RESULTING FROM INVERSION OF SASW TESTS ON SILTY CLAY SUBGRADE

Layer No.	Layer Thickness (ft)	Shear		Young's Modulus (ksf)	Mass Density+ (lb-sec <sup>2</sup> /ft <sup>4</sup> )	Poisson's Ratio**
		Wave Velocity (ft/sec)	Wave			
1	1.0	376		1259	3.4	0.31
2	1.0	339		1024	3.4	0.31
3	1.0	421		1531	3.4	0.27
4	1.0	559		2699	3.4	0.27
5	1.0	952		7642	3.4	0.24
6	1.0	943		7498	3.4	0.24
7	1.0	942		7482	3.4	0.24
8	1.0	817		5492	3.4	0.21
9	1.0	817		5492	3.4	0.21
10	1.0	860		6085	3.4	0.21
11	1.0	823		5711	3.4	0.24
12	1.0	905		6906	3.4	0.24
Half Space		1018		8738	3.4	0.24

+ Determined from the average of two undisturbed samples within the upper 4 ft

\*\* Determined from compression and shear wave velocities measured by crosshole seismic testing

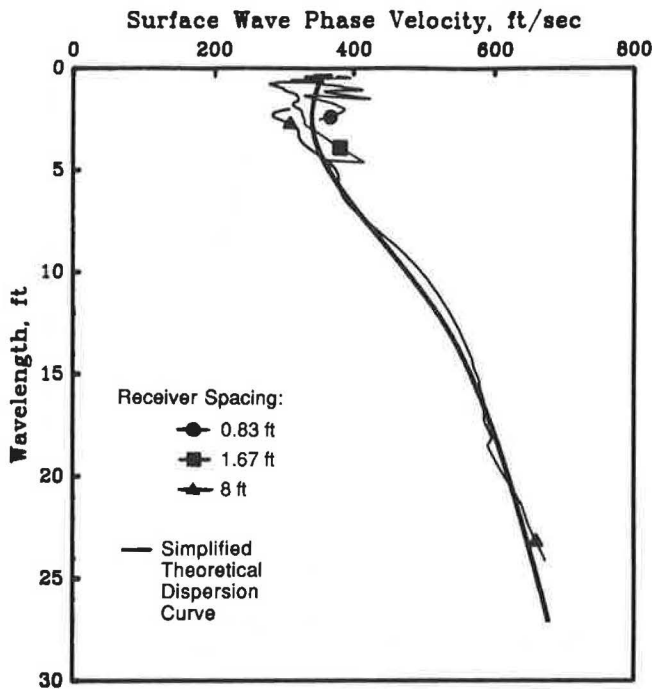


FIGURE 6 Comparison of theoretical and experimental dispersion curves for measurements of a silty clay subgrade.

ularly in light of the fact that the two tests were performed 2 years apart. Differing weather conditions (rainfall, temperature, etc.), lateral variability, and secondary soil structure are responsible for much of the difference between the results of the two test methods near the surface.

CONCRETE SLAB

Surface wave tests were also performed on the concrete slab following the same procedure used to profile the subgrade.

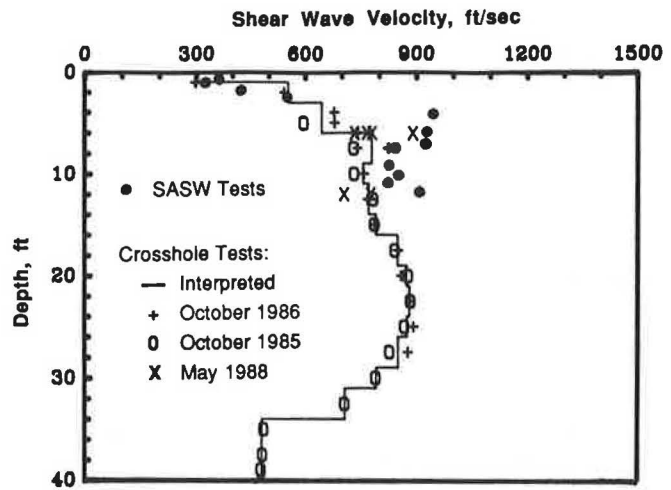


FIGURE 7 Shear wave velocity profiles from crosshole and SASW tests at the Hornsby Bend site.

In this test series, measurements were made during the time the concrete was curing so that the slab-subgrade system would appear to be many different systems, each with a different ratio of Young's modulus between the concrete and the soil. Receiver spacings of 0.83 and 1.67 ft (0.25 and 0.51 m) were used. Unfortunately, larger spacings could not be used due to the reduced size of the isolated slab.

Composite dispersion curves corresponding to two measurement times during curing of the slab are presented in Figure 8. The first curve (Figure 8a) results from measurements made approximately 5 hours after the addition of water to the cement-aggregate mixture. The curing process was actively proceeding at this time. This point is supported by the relatively low values of surface wave velocity [approximately 4,000 fps (1220 m/s)] measured at short wavelengths [less than 0.83 ft (0.25 m)] in the concrete. Fluctuations in the dispersion curves, particularly between wavelengths of 1.5 and 2 ft (0.45 to 0.6 m), are caused by reflections of waves

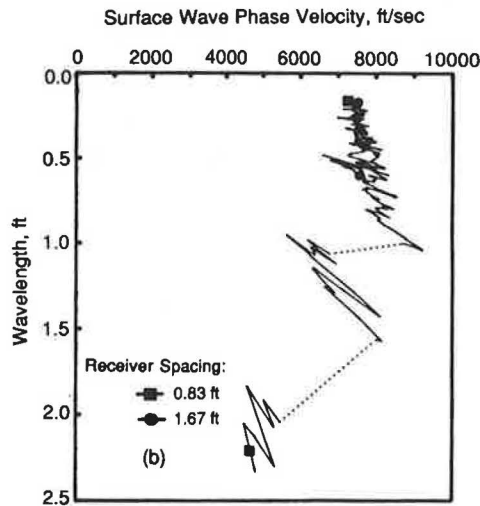
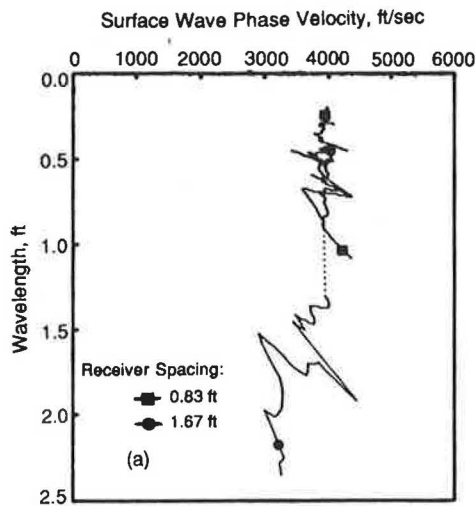


FIGURE 8 Dispersion curves for measurements on slab-subgrade system initiated (a) 5 hours and (b) 4 days after the addition of water to the cement-aggregate mixture.

from the lateral and bottom boundaries of the slab. The dotted line in Figure 8a represents a gap in the dispersion curve caused primarily by interference from reflecting waves (3).

The composite dispersion curve in Figure 8b corresponds to measurements made after 4 days, when the concrete was more fully cured. Measured surface wave velocities now range between 7,000 and 8,000 fps (2135 to 2440 m/s), which is a typical range for cured concrete. As with the earlier measurements, reflections from the lateral and bottom boundaries of the slab have caused fluctuations and gaps in the composite dispersion curve (as discussed subsequently in this section). It is important to note, however, that the dispersion curves in Figure 8 exhibit nearly constant values of phase velocity for wavelengths less than the thickness of the slab [0.83 ft (0.25 m)]. This behavior permits the modulus and the thickness of the pavement surface layer to be determined rapidly and without the need for inversion (3).

To demonstrate that surface wave measurements remain sensitive to the properties of the subgrade even in the presence of the slab, a comparison between theoretical and field dispersion curves is presented in Figure 9. This approach is followed rather than inversion of the measured dispersion curve shown in Figure 8b because the dimensions of the isolated slab did not permit measurement of sufficiently long wavelengths to use the inversion algorithm. The theoretical dispersion curve was calculated using a simplified subgrade profile, given in Table 2, supporting a concrete pavement layer of infinite lateral extent. The profile in Table 2 was simplified from the more detailed profile reported in Table 1 so that the computational effort could be reduced. The shear wave velocity assigned to the concrete was determined in the field using an independent seismic method, and the nominal thickness of the slab was used. The algorithm used to calculate the theoretical dispersion curve (4) differs from that normally used for inversion (1) in that it models more completely wave propagation in a layered profile of infinite lateral extent (at the expense of significantly more computational effort).

A comparison of the experimental and theoretical dispersion curves is shown in Figure 9. The more complete algorithm used to calculate the theoretical curve models many of the features observed in the experimental curve, especially the large excursion in the wavelength range from 0.8 to 1.4 ft (0.24 to 0.43 m). This feature is caused by body waves reflecting from the bottom of the concrete slab. The decrease in phase velocity with increasing wavelength at wavelengths longer than 1.4 ft (0.43 m) shows that surface wave measurements remain sensitive to the properties of the subgrade in the presence of the pavement surface layer. This effect would have been more clearly demonstrated if measurement of longer

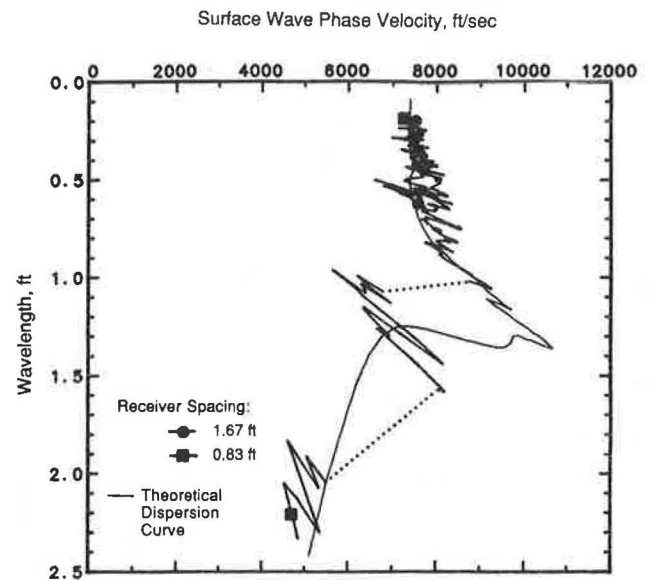


FIGURE 9 Comparison of field and theoretical dispersion curves for measurements on the slab-subgrade system.

wavelengths had not been precluded by the lateral dimensions of the slab.

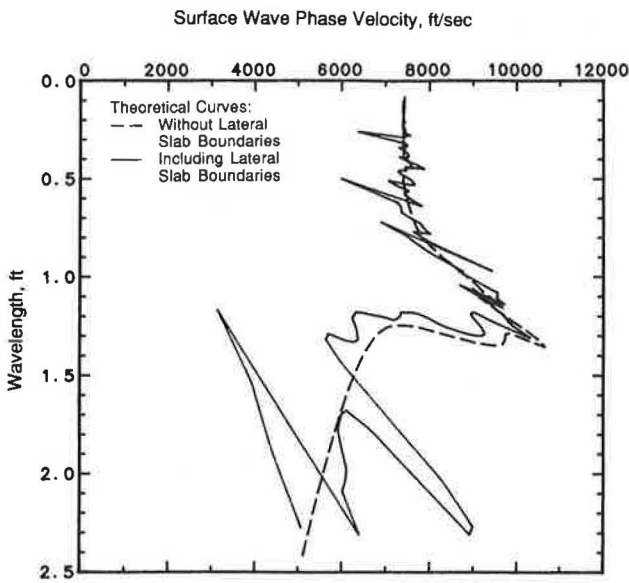
To illustrate the influence of the lateral slab boundaries on these measurements, the algorithm used to calculate the theoretical dispersion curve in Figure 9 (4) was modified to include the effects of reflected surface waves from the four edges of the slab following the procedure presented by Sheu (3). This theoretical dispersion curve is presented in Figure 10. For comparison purposes, the theoretical dispersion curve presented in Figure 9 for wave measurements of a slab-subgrade system of infinite lateral extent is also included. One can see that inclusion of the lateral boundaries results in the theoretical dispersion curve modelling essentially all of the features exhibited in the experimental curve (Figure 9). The comparison also indicates the extent to which the use of a more complete theoretical algorithm can improve surface wave testing by more accurately modelling field conditions. It is to be hoped that the computational effort needed for these algorithms can be reduced in the future so that they can be used in routine tests.

#### SENSITIVITY STUDY

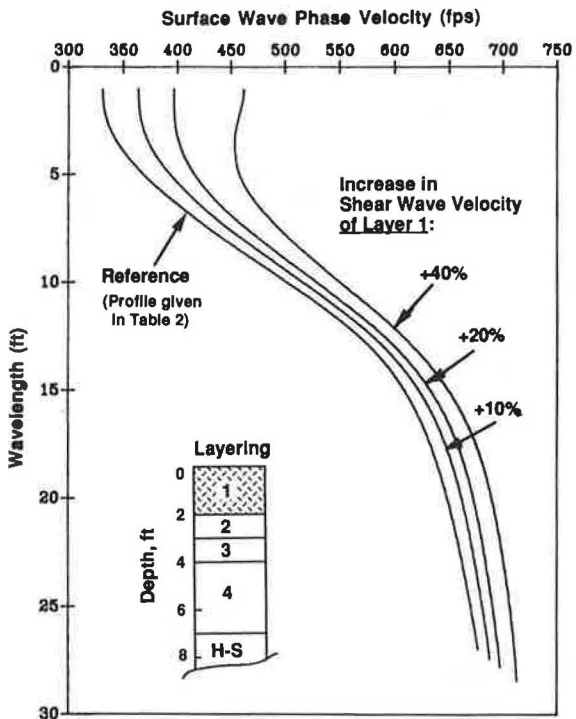
One of the questions often raised about the results obtained using the SASW method is the sensitivity of the inversion

TABLE 2 SIMPLIFIED PROFILE OF SILTY CLAY SUBGRADE USED IN ANALYTICAL STUDIES SHOWN IN FIGURES 9-13

Layer No.	Layer Thickness (ft)	Shear Wave Velocity (ft/sec)	Young's Modulus (ksf)	Mass Density (lb-sec <sup>2</sup> /ft <sup>4</sup> )	Poisson's Ratio
1	2	355	1,123	3.4	0.31
2	1	420	1,523	3.4	0.27
3	1	560	2,708	3.4	0.27
4	3	945	7,530	3.4	0.24
Half space		850	5,945	3.4	0.22



**FIGURE 10** Influence of lateral slab boundaries on the theoretical dispersion curve of the slab-subgrade system.



**FIGURE 11** Variations in the theoretical dispersion curve resulting from increasing the velocity of Layer 1 in the subgrade.

procedure. More specifically, it is desirable to estimate the resolution of the final shear wave velocity and Young's modulus profiles. A preliminary analytical study of this question was performed on the subgrade measurements using the simplified profile presented in Table 2.

Initially, the shear wave velocity of the top layer was increased by 10, 20, and 40 percent, and theoretical dispersion curves were calculated for each altered profile. (Changes of 10, 20, and 40 percent in the shear wave velocity of a layer correspond to changes of 21, 44, and 96 percent in the Young's modulus of the layer.) These "perturbed" dispersion curves are shown in Figure 11. Clearly, the shear wave velocity of the top layer exerts a large influence on the dispersion curve. Part of the reason for this large influence is that the thickness of the top layer [2 ft (0.61 m)] is a significant portion of the total depth (not including the half space) of the profile [7 ft (2.1 m)]. The large differences between the dispersion curves at short wavelengths [less than 3 ft (0.9 m)] imply that the shear wave velocity of the first layer can be resolved very accurately because shear wave velocities for the first layer which differ by as little as 10 percent shift the entire curve by an amount that results in an unsatisfactory match with the field dispersion curve. However, as illustrated in Figure 5, it is often the lateral variability at the site that controls the accuracy with which the stiffness of the top layer can be determined, rather than the resolving power of the SASW method.

The results of increasing the shear wave velocity of the second layer by 10, 20, and 40 percent are shown in Figure 12. The differences between the perturbed and unperturbed dispersion curves are less pronounced in this case. One reason is that the thickness of Layer 2 represents a smaller fraction of the total thickness of the profile than the thickness of Layer 1. The dispersion curve corresponding to an increase of 10 percent is sufficiently similar to the unperturbed curve that, in the writers' experience, a satisfactory match would likely result when considering normal site variability. An increase

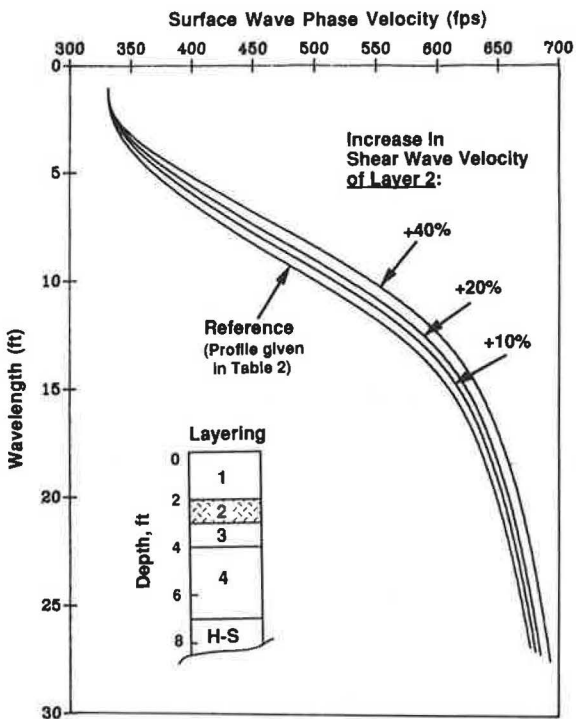


**FIGURE 12** Variations in the theoretical dispersion curve resulting from increasing the velocity of Layer 2 in the subgrade.

of 20 percent in the velocity of Layer 2 changes the dispersion curve by an amount that results in an unsatisfactory match with the field dispersion curve (Figure 5). In fact, this shift would likely result in a poor match with most field dispersion curves. Finally, a 40-percent increase in the shear wave velocity of Layer 2 produces a significant change in the dispersion curve, which further heightens the mismatch between the theoretical and field dispersion curves.

Results similar to those for variations in Layer 2 were also found for Layers 3 and 4 (7). As one would intuitively expect from an understanding of surface wave dispersion, changes in the shear wave velocity of the subgrade layers result in smaller differences between perturbed and unperturbed dispersion curves as layer depth increases and as layer thickness decreases. However, changes in shear wave velocities greater than 20 percent at this site resulted in unsatisfactory matches between theoretical and field dispersion curves.

The final comparison performed in the sensitivity study was that of "compensating" changes in wave velocities of adjacent layers. This comparison was done by increasing the shear wave velocity of Layer 2 by 20 percent and decreasing the velocity of Layer 3 by 25 percent. As shown in Figure 13, the perturbed dispersion curve differs from the unperturbed curve in two respects: (a) in the slope over wavelengths from 5 to 15 ft (1.5 to 4.6 m) and (b) in wave velocities over wavelengths from approximately 10 to 20 ft (3.1 to 6.1 m). As a result of these two differences, the perturbed dispersion curve does not satisfactorily match the field dispersion curve. In the writers' experience, potential errors caused by compensating changes can be avoided, especially for layers near the surface.

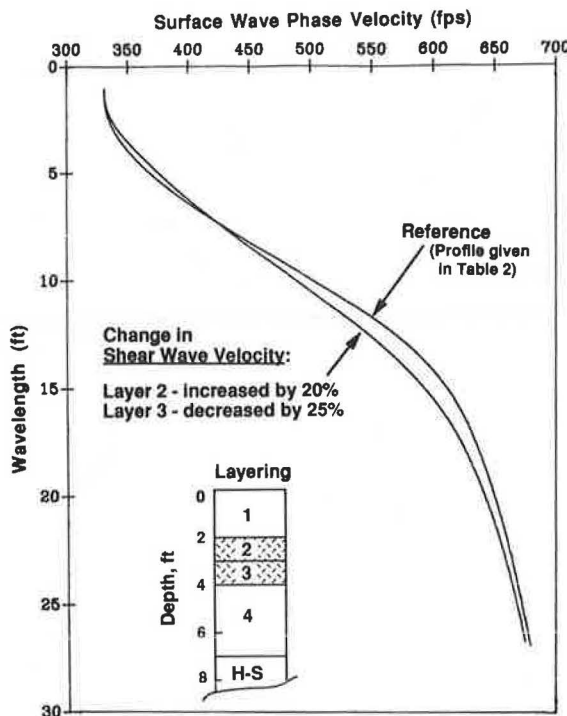


FIGURE 13 Variation in the theoretical dispersion curve resulting from "compensating" changes in subgrade layer velocities.

NONLINEAR SUBGRADE BEHAVIOR

The evaluation of subgrade moduli from the measurement of propagation velocities of stress waves, as done in seismic tests, results in the determination of small-strain elastic moduli. These moduli characterize the deformational behavior of subgrade in the range of strain where linear, elastic behavior is valid (typically at axial strains less than 0.001 percent). As illustrated in Figure 14, these moduli represent the initial slope of the stress-strain curve. The term *initial tangent modulus* is often used to refer to small-strain moduli that are commonly denoted as  $E_0$  or  $E_{max}$ . Moduli determined at higher levels of strain, where linear behavior in subgrade soils is no longer valid, are secant moduli and are denoted by  $E_1, E_2,$  etc., as shown in Figure 14.

To study the nonlinear behavior of the silty clay subgrade, undisturbed samples were taken, and torsional resonant column tests were performed. Initial tangent and secant moduli determined from one sample at four different confining pressures are shown in Figure 15. The constant value of Young's modulus at strains less than about 0.001 percent is clearly shown. To estimate nonlinear behavior in situ, the curves are first normalized with respect to the initial tangent modulus, as shown in Figure 16. The in situ modulus at any strain is then determined by multiplying the in situ modulus from the field seismic measurements by the normalized value of the

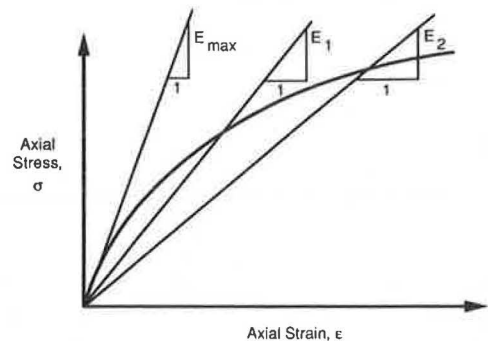


FIGURE 14 Characterization of nonlinear soil behavior by initial tangent ( $E_{max}$ ) and secant ( $E_1, E_2,$  etc.) Young's moduli.

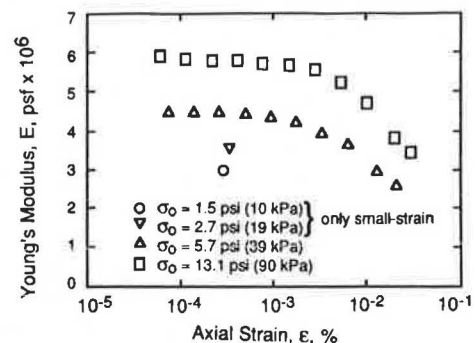
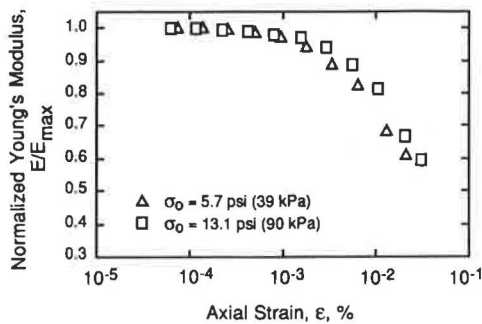


FIGURE 15 Variation in Young's modulus with strain amplitude of the silty clay subgrade.



**FIGURE 16** Variation in normalized Young's modulus with strain amplitude of the silty clay subgrade.

modulus from the laboratory test at the desired strain. This procedure can be written as:

$$E_{e,field} = E_{seismic} \cdot (E_e/E_{max})_{lab} \quad (5)$$

where

- $E_{seismic}$  = small-strain modulus determined in situ,
- $(E_e/E_{max})_{lab}$  = normalized modulus determined by cyclic laboratory test at a strain amplitude of  $\epsilon$ , and
- $E_{e,field}$  = modulus in the field at a strain amplitude of  $\epsilon$ .

For instance, if Young's modulus at a depth of 1.5 ft (0.45 m) and an axial strain of 0.01 percent is needed, the modulus from the seismic measurement (1,024 ksf in Table 1) is multiplied by 0.75. (The multiplier could be slightly reduced to about 0.70 if the confinement level was significantly lower than that used in the test.) This general approach is the same as that used in geotechnical earthquake engineering to evaluate nonlinear soil response during earthquake shaking (8).

## CONCLUSIONS

The SASW method can be used to assess the moduli of individual layers within a pavement profile at small-strain levels (< 0.001 percent) where the behavior of pavement materials is linear and elastic. An advantage of the SASW method is that it can be used to determine the modulus profile at any time during the construction and subsequent life of the pavement. Two series of tests were performed which illustrate the use of the method directly on subgrade soils and on a completed pavement. The results of these tests indicate that the SASW method remains sensitive to the subgrade properties despite the presence of the pavement surface layer.

A sensitivity study was performed on the subgrade tests to quantify the resolving power of the SASW measurements. The study revealed that the modulus of the top layer was determined within about 10 percent of the in situ value, whereas the moduli of other near-surface layers were determined within about 10 to 30 percent. One important characteristic of any site is lateral variability, which decreases the resolving power of the SASW method as variability increases. Finally, a method of characterizing nonlinear subgrade behavior by combining small-strain moduli determined in situ using seismic methods with experimental (or empirical) modulus degradation curves is presented for the silty clay subgrade.

## ACKNOWLEDGMENTS

This work was supported by the Texas State Department of Highways and Public Transportation. The authors wish to express their appreciation for this support. The authors also wish to thank D.-W. Chang and J. A. Bay for their assistance with some of the analytical studies and R. D. Andrus and D.-S. Kim for conducting the resonant column tests.

## REFERENCES

1. S. Nazarian. *In Situ Determination of Elastic Moduli of Soil Deposits and Pavement Systems by Spectral Analysis of Surface Waves Method*. Ph.D. dissertation. University of Texas at Austin, 1984, 453 pp.
2. G. J. Rix. *Experimental Study of Factors Affecting the Spectral Analysis of Surface Waves Method*. Ph.D. dissertation. University of Texas at Austin, 1988, 315 pp.
3. J.-C. Sheu. *Applications and Limitations of the Spectral Analysis of Surface Waves Method*. Ph.D. dissertation. University of Texas at Austin, 1987, 280 pp.
4. I. Sanchez-Salinerro. *Analytical Investigation of Seismic Methods Used for Engineering Applications*. Ph.D. dissertation. University of Texas at Austin, 1987, 401 pp.
5. N. A. Haskell. The Dispersion of Surface Waves in Multilayered Media. *Bulletin of the Seismological Society of America*, Vol. 43, 1953, pp. 17-34.
6. W. T. Thomson. Transmission of Elastic Waves through a Stratified Solid. *Journal of Applied Physics*, Vol. 21, 1950, pp. 89-93.
7. G. J. Rix, K. H. Stokoe II, and J. M. Roesset. *Experimental Study of Factors Affecting the SASW Method*. Research Report 1123-1. Texas State Department of Highways and Public Transportation, forthcoming.
8. F. E. Richart, Jr., D. G. Anderson, and K. H. Stokoe II. Predicting In-Situ Strain-Dependent Shear Moduli. *Proc., 6th World Conference on Earthquake Engineering*, New Delhi, India, 1977, pp. 118-121.

# In Situ Testing of Peaty Organic Soils: A Case History

NANCY J. NICHOLS, JEAN BENOIT, AND FREDERIC E. PRIOR

---

In 1985, a section of a New Hampshire roadway located over a deposit of peaty organic soil 20 ft (6 m) thick was widened and raised. On the basis of vane shear strengths, the required embankment height increase of 5 ft was implemented in three stages over a 6-month period. Two years after the initial loading, more than 6.5 ft (2 m) of vertical displacement was observed. This paper presents the results of various in situ tests conducted following these events in material located away from and below the road embankment. The tests included plate load tests, self-boring and full-displacement pressuremeter tests, standard penetration tests, field vane tests, and dilatometer tests. Assessment of the effectiveness of these tests in evaluating useful geotechnical soil parameters for embankment design over very soft peaty organic soils is discussed.

---

Construction of embankments over highly organic soil deposits is often accomplished by using design rules based on minimal characterization of soil properties with a design-as-you-go approach. Often, large and unacceptable settlements occur during and after construction. In response to these problems, organic foundations are commonly compacted with blasting or excavation and replacement methods, which alleviate the problem but at very high cost. Very soft, peaty organic soils are extremely difficult to sample undisturbed and are not well suited for conventional laboratory testing. Furthermore, peaty organic deposits are very variable within a given site, and thus extensive sampling is necessary for adequate characterization. Because of the heterogeneous and anisotropic nature of organic soils, full-scale field testing is the most accurate approach to predicting the behavior of a finished design. Such tests are generally expensive and often impractical. However, with recent advances, in situ testing methods can be used to characterize such variable deposits more economically and efficiently.

In 1985, a section of the New Boston Road in Candia, New Hampshire, was widened and raised to accommodate safer two-way traffic and to prevent flooding from the nearby North Branch River. This section of the road embankment is located over a deposit of peaty organic soil approximately 20 ft (6 m) in thickness.

After the last of three stages of fill placement, nearly 1.5 ft (0.5 m) of differential movement occurred across the centerline, separated by a longitudinal crack approximately 4.5 ft (1.4 m) deep and 100 ft (30.5 m) long. In the 2 years after the initial loading, more than 6.5 ft (2 m) of vertical displacement

was observed, twice that predicted by using a New York Department of Transportation (NYDOT) Bureau of Soil Mechanics (*I*) method based on water content. As of July 22, 1988, the settlement rate was about 2.7 in./year (6.9 cm/year) and decreasing. The design of this renovated embankment was based on vane shear strength and water content profiles.

After these events, several in situ tests were conducted to examine the properties of both the virgin material located away from the road embankment and the consolidated material below the road surface. The techniques included the use of the self-boring pressuremeter (SBPM), full-displacement pressuremeter (FDPM), standard penetration test (SPT), field vane test (VST), dilatometer (DMT), and plate load test (PLT).

This paper presents a brief overview of the composition and structure of organic soils, highlighting the differences from more conventional soil types. The New Boston Road project is summarized and used as a basis for evaluating the in situ testing investigation program. The results of the various in situ tests allow an assessment of the effectiveness of these tests in evaluating useful geotechnical soil parameters for embankment design over very soft peaty organic soils.

## COMPOSITION AND STRUCTURE OF ORGANIC SOILS

The composition of organic soil greatly depends on the extent of decomposition, which is the breakdown of organic matter by microbial processes. Decomposition leads to the disintegration of large organic particles and reduction of the organic fraction of the soil. By-products of this process include water, bacterial cells, methane gas, and nondegradable organic matter termed humus. The rate of decomposition is a function of the type of plant tissue decaying, the pH and water content of the soil, the oxygen and nutrient availability, and the type of bacteria responsible for the decomposition.

Highly organic soils are composed of both fibers and granules in varying proportions and arrangements. These geometric elements range in size from large tree trunks to clay-sized particles. An organic soil that consists predominantly of colloidal soil particles is termed amorphous-granular, whereas one that contains large particles such as roots, grasses, and leaves is termed fibrous. Electron microscope photographs of fibrous and amorphous-granular samples obtained from the site show porous diatoms coating the organic particles. The composition and structure of organic deposits are generally highly variable in plan and in cross section. Variations in types of plants, degree and rates of decomposition, water content,

---

N. J. Nichols, Haley and Aldrich, Inc., 360-8 Route 101, Bedford, N.H. 03102. J. Benoit, Department of Civil Engineering, University of New Hampshire, Kingsbury Hall, Durham, N.H. 03824-3591. F. E. Prior, State of New Hampshire Department of Transportation, Concord, N.H. 03301.



and porosity can occur over distances and depths that are much smaller than the width or thickness of a highway embankment (2).

The structure and composition of organic soils greatly affect their affinity for water and their shearing resistance. Fine-fibrous organic soils absorb and hold more water than coarse-fibrous or amorphous-granular soils. On the other hand, coarse-fibrous soils have the greatest shear strength (3). Because the structure and composition typically vary within an organic deposit, the engineering properties vary greatly as well. A brief discussion of organic soil index properties that are used as indicators of engineering behavior is presented below.

### Organic Content

The organic content is approximately equal to the percentage of weight loss measured when a dry soil specimen is submerged in a caustic solution or combusted. The fraction of mass retained is termed the ash content. Although firing methods are most commonly used, these methods may lead to overestimation of the organic content by as much as 15 percent because of the combustion of inorganic carbon (3). Various firing methods for determining the organic content were investigated by Andrejko et al. (4). Test results were found to depend significantly on sample preparation, duration of time allowed for ashing, firing temperatures, and the fraction and type of mineral matter in the specimens.

The range of organic contents associated with organic soil types depends on the system of classification. Throughout this paper, organic soils are classified according to a system introduced by Landva and Pheeney (5). "Peat" is defined as having no more than 20 percent ash content by dry weight. If a soil has more than 20 percent ash content but less than 40 percent, it is classified as a "peaty organic" soil. Moreover, "organic soil" and "soil with organic content" are defined as soils having an ash content from 40 to 95 percent, and from 95 to 99 percent, respectively.

### Water Content

Because water content increases with increasing porosity at depths below the water table, and fibrous organic soils are typically more porous than are amorphous-granular soils, water content is generally greater for peats that are more fibrous. Furthermore, because compressibility is directly related to porosity, a high water content indicates high compressibility (3). A wholly organic peat (minimal ash content) typically has a water content ranging from 750 to 1500 percent, although values greater than 2000 percent have been reported (6). The water contents of peaty organic and organic soils are generally much lower.

### Void Ratio

Void ratios typically range from 4 to 7 for amorphous-granular soils and from 7 to 15 for fibrous soils (7). However, values as low as 2 have been reported for deep amorphous deposits (8), and values as high as 28 have been reported for deep

fibrous deposits (6). Void ratios near the ground surface are generally between 2 and 5. The lower values are the results of shrinkage upon drying.

### Gas Content

Landva and La Rochelle (2) report that wholly organic peat generally contains at least 10 percent gas. Saturated organic soils containing some mineral matter (9) are likely to contain less gas. Determination of the gas content, although very difficult, is quite important because it significantly influences permeability, rate of consolidation, and pore pressure measurement.

### Specific Gravity

The specific gravity of the solids in an organic soil ranges from 1.1 to 2.5 (3). It is highest for soils having considerable mineral content. Amorphous-granular soils typically have a specific gravity of 1.9, whereas the specific gravity of fibrous soils ranges from 1.4 to 1.7. Except for wholly organic peat, specific gravity has been found to decrease linearly with increasing water content (10).

### Unit Weight

The unit weights of organic soils are usually very low due to their high porosity and low specific gravity of solids. The unit weight is highest for amorphous-granular soils and for organic soils with significant mineral content. Dry unit weights typically range from 5 to 20 pounds per cubic foot (pcf) (0.78 to 3.14 kN/m<sup>3</sup>). Saturated, wholly organic peat may have nearly the same saturated unit weight as water. Due to the low saturated unit weight of organic soils, the in situ effective stresses in organic deposits are frequently also very low.

### CASE HISTORY: NEW BOSTON ROAD, CANDIA, NEW HAMPSHIRE

A portion of the New Boston Road, located in Candia on the banks of the North Branch River near the Deerfield/Candia border (Figure 1), was renovated in 1985. The purpose of the project was to raise the road surface above seasonal flood waters and to widen it for safer two-way traffic. The plan included increases of grade and width of about 5 and 8 ft, respectively (1.5 and 2.4 m). The existing bridge was also replaced with a new structure at the proposed grade.

### Site Conditions

Before renovations, 23 test borings were drilled to depths of up to 40 ft (12 m). The stratigraphy away from the road and near the river channel (Figure 2) generally consists of about 30 ft (9 m) of highly organic soil overlying 2 to 4 ft (0.6 to 1.2 m) of sandy silt with organic content and 6 to 12 ft (1.8 to 3.6 m) of blue, poorly graded, dense sandy gravel. The bedrock surface profile is approximately U-shaped, with the

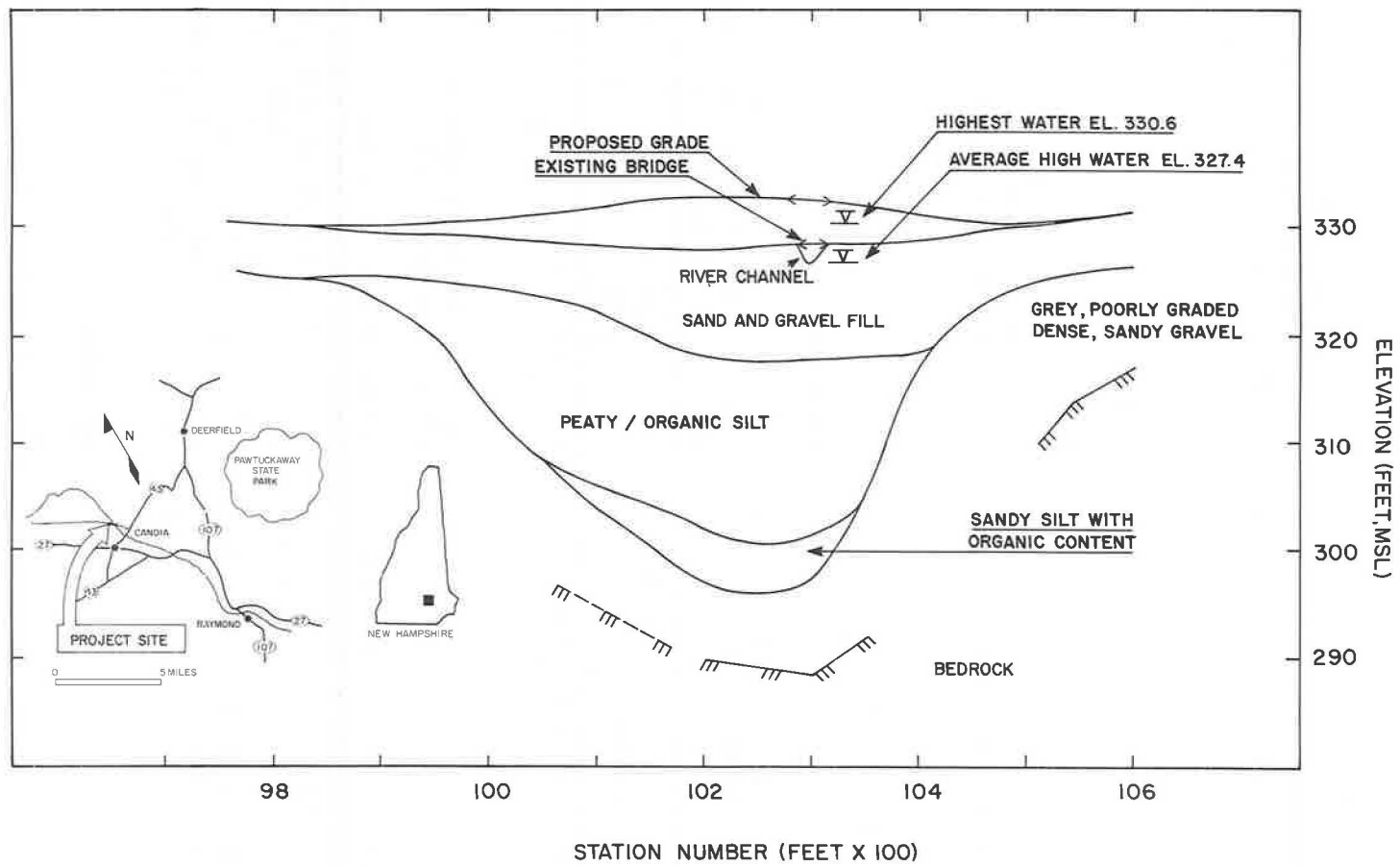


FIGURE 1 Site location and profile of the New Boston Road embankment before 1985 construction.

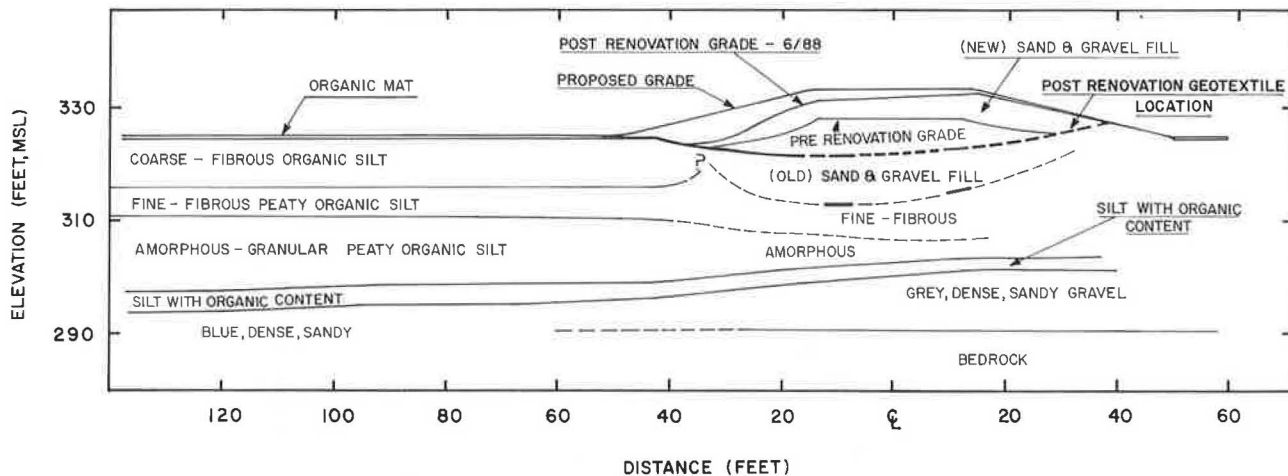


FIGURE 2 Cross-section of the New Boston Road embankment at STA 101+50 as of July 1988.

greatest depth to bedrock directly underneath the river channel (Figure 1). The highly organic deposit is deepest at about Station 102+00, where it ranges from 19 to 25 ft (5.8 to 7.6 m) in thickness and pinches out on each side of the river channel. The sand and gravel fill is deepest under the river banks, where its depth ranges from 5 to 13 ft (1.5 to 4 m). At distances greater than 175 ft (53 m) from the river channel, the depth of fill is about 5 ft (1.5 m). The water table was observed to fluctuate with stream flow, with an average elevation near the existing ground surface at the toe of the embankment.

The highly organic soil deposit is composed predominantly of fine-fibrous and amorphous-granular organic silt. The ash content was found by firing to range from 34 to 68 percent; it thus spans the borderline between peaty organic and organic silt. The fibers are both woody and nonwoody, consisting of wood fragments, twigs, rootlets, sedge, grass, and leaves. The fibrosity of the soil decreases with increasing depth. In general, coarse-fibrous organic silt is found only near the top of the organic deposit to depths of 4 and 8 ft (1.2 to 2.4 m) beneath the roadway and beneath the organic mat in the adjacent wetlands, respectively. Below this layer, the organic deposit gradually changes from fine-fibrous to amorphous. Occasional pockets of coarse-woody fibers located below the road surface are believed to be remnants of a preexisting corduroy road typical of early roadways over marshes. Pockets of sand and gravel fill are also found within the organic deposit at distances less than 50 ft (15 m) from the centerline. At depths greater than 14 ft (4.3 m), the soil is amorphous-granular with traces of fine fibers.

Before the roadway renovations, the water content of the organic soil varied with depth in a manner typical of a consolidating layer. Under the road and in the adjacent wetlands, water content increased with increasing depth to a maximum at depths of 15 to 20 ft (4.6 to 6.1 m), and then decreased from that point to the underlying blue sandy gravel (Figure 3). Water contents also increased with increasing distance from the embankment. The maximum water content measured under the roadway, 6 ft (1.8 m) left of centerline at Station 102+27, was about 500 percent. In the virgin soil

northwest of the bridge, the highest water content measurement was 850 percent. Organic contents varied similarly.

Field vane shear strength profiles were obtained before renovations at Station 102+25 near the toe and the centerline of the existing embankment (Figure 3). Measurements were obtained after insertion of a standard tapered vane through a cased borehole. The results near the toe seem to indicate an average increase of shear strength with depth, from 150 to 325 psf (7 to 16 kN/m<sup>2</sup>). Directly underneath the roadway, the results show significantly greater strengths than near the toe, as expected from consolidation processes that have taken place through time.

#### Design Settlement and Stability Analyses

Total primary settlements were estimated during the design stage by an empirical method based on water content data developed by the NYDOT. The primary settlement due to the placement of 5 ft (1.5 m) of fill was predicted to be as much as 3 ft (0.9 m). Preliminary stability analyses were performed for several embankment slopes at Station 102+25. Analyses were performed using the vane shear data according to the modified Bishop method of slices, as well as with the wedge method. Although 4:1 slopes were found safe against sliding with a safety factor of 1.25, a polypropylene woven geotextile was laid on or slightly below existing grade as a precautionary measure. Furthermore, the fill was placed in stages over a period of about 5 months.

#### Sequence of Events

In early April 1985, the existing road was graded, and the geotextile was placed loosely over the surface, with the sewn seams aligned perpendicular to the centerline of the road. To protect the geotextile, approximately 2 ft (0.6 m) of sand and gravel fill was immediately placed over the fabric. An additional 6 ft (1.8 m) of fill was placed on the embankment over the next 4 months. On September 9, 1985, a crack with a

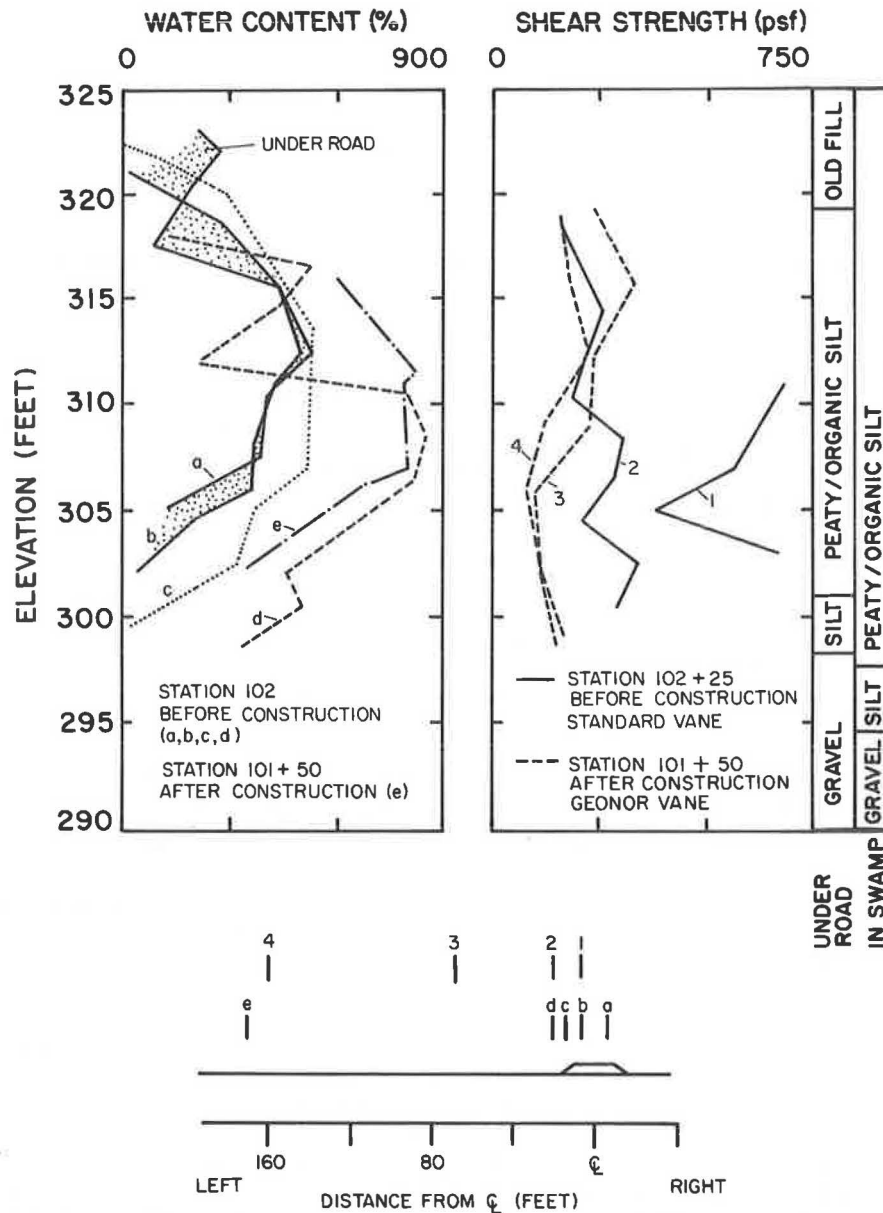


FIGURE 3 water content and vane shear strength profiles under the New Boston Road embankment before construction and in the swamp.

depth of 1 in. (2.5 cm) was first noted in the pavement across the centerline between Stations 101+50 and 102+50. On October 10, 1985, the same crack extended to a depth of 4.5 ft (1.4 m). The vertical and horizontal relative displacements across the crack were 1.34 ft (0.41 m) and 1 in. (2.5 cm), respectively. At this time, an adjacent parallel crack of much smaller dimension was observed. Moreover, a large cavity had developed under the approach slabs due to the movement of fill. In August 1986, a 1-ft (0.30-m) surcharge was added to accelerate secondary settlement. It was removed in October 1986, at which time a maintenance program of regrading and filling was initiated to maintain final conditions.

Performance of the embankment during construction was monitored by two settlement platforms and one slope inclinometer. The platforms were placed near the upper surface

of the existing road surface at offsets of 102+25, left 11, and 103+50, right 11. The latter platform was abandoned shortly after construction, because settlement at its location was minimal. The slope indicator was installed 5 months after the initiation of construction at an offset of 102+00, 37 ft left.

Vertical and horizontal displacements monitored at the west bank with the settlement platform and slope indicator, respectively, are plotted against time in Figure 4. Horizontal displacements monitored at depths of 6, 14, and 21 ft (1.8, 4.3, and 6.4 m) below the initial elevation of the settlement platform are shown. The time at zero displacement corresponds with the time of installation of the settlement platform. Total vertical displacement as of day 888 (September 3, 1987) was 6.4 ft (1.95 m), which is more than twice the amount predicted. Much of the observed vertical movement was related

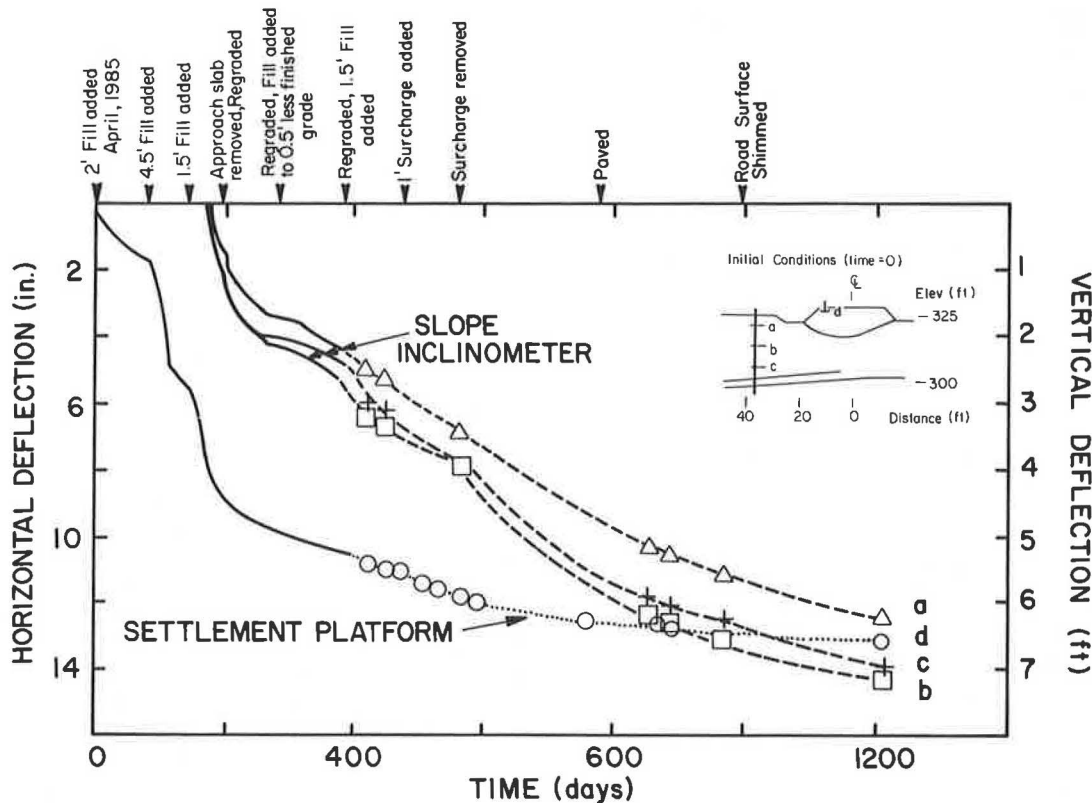


FIGURE 4 Vertical displacement as measured by the settlement platform at STA 102+25, left 11 feet, versus time; and horizontal displacements measured at depths of 6 feet, 14 feet, and 21 feet with the slope inclinometer at STA 102+00, left 37 feet, versus time.

to horizontal displacement of the embankment foundation away from the road centerline. At least 6.7 in. (17 cm) of horizontal displacement occurred within the first year after the beginning of construction. The total horizontal displacement is unknown, because the slope indicator was not installed until after most of the construction had been completed. As of July 22, 1988, about 1,210 days from installation of the settlement platform, the rates of vertical settlement and horizontal displacement at mid-depth within the organic foundation were 2.7 in./year (7.0 cm/year) and 1.2 in./year (3.1 cm/year), respectively.

#### POSTCONSTRUCTION SITE INVESTIGATION

An extensive in situ site investigation program was started 2 years after construction to ascertain the mechanisms responsible for the excessive movements and cracking of the renovated road embankment and to assess the feasibility of using in situ testing methods in organic soils. Laboratory tests were conducted to determine unit weights and water contents. Furthermore, results from a limited number of laboratory strength and compressibility tests were compared to those from in situ tests. The unit weight determined from the undisturbed tube specimens ranged from 69.4 pcf (10.9 kN/m<sup>3</sup>) under the road to 64.9 pcf (10.2 kN/m<sup>3</sup>) in the coarse-fibrous soil of the wetlands. The unit weight of the amorphous-granular soil was

about 65.5 pcf (10.3 kN/m<sup>3</sup>). Water contents before and after renovations are shown in Figures 3 and 5, respectively. After renovations, water content profiles indicate a reduction of water content at all depths. The postconstruction peak values were measured at nearly the same elevation as the preconstruction values but were 150 to 250 percent lower. This reduction indicates that the load of the new fill induced consolidation settlement.

In situ tests performed at the roadway location included standard penetration and flat plate dilatometer testing. SPT sampling was conducted continuously from the road surface through the organic deposit in two boreholes located at approximately the same station but on opposite sides of the road. Nine dilatometer tests were performed within the organic strata in a third borehole located about 30 ft (9 m) from the SPT boreholes.

In the wetland area, 2 vane shear profiles (20 tests), 4 dilatometer profiles (140 tests), 3 plate load tests, 12 full-displacement pressuremeter tests, and 3 self-boring pressuremeter tests were performed at varying distances from the embankment. The boreholes were located within a cross-section through Station 101+50 at distances left of the centerline ranging from 40 to 160 ft (12 to 49 m). Each plate load test was performed at a distance less than 30 ft (9 m) from the toe of the embankment and within 10 ft (3 m) of either a vane shear or a dilatometer testing location. The pressuremeter tests were performed outside of the influence of the

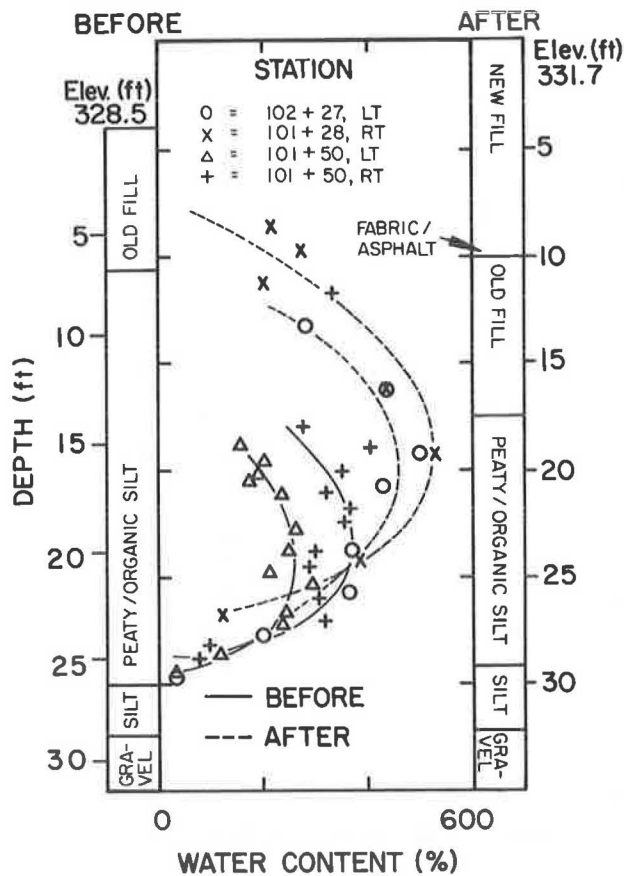


FIGURE 5 Water content profiles under the New Boston Road embankment before and after 1985 construction.

embankment at about 165 ft (50 m) left of the embankment centerline. One of the vane shear and one of the dilatometer profiles were also located in that area.

**Plate Load Testing**

Three plate load tests were performed by placing dead weights on a steel plate 1 ft (0.3 m) in diameter. In all tests, the plate was located 1 ft (0.3 m) below the organic mat. In one test, the plate was rapidly loaded and unloaded for two cycles in order to estimate the elastic properties of the upper portion of the coarse-fibrous sublayer. Deflection was found to vary linearly with the logarithm of load, with an average shear modulus of 4.1 ksf (156 kN/m<sup>2</sup>).

Two additional plate load tests were conducted to ascertain time-dependent compressibility characteristics of the coarse-fibrous soil within the pressure bulb of the plate. Applied loads were held until the deflection rate became constant with respect to the logarithm of time. As shown in Figure 6, the deflection-versus-time curves resulting from one plate load test for various load increments illustrate that, as expected, the rate of deflection decreases with time. However, this trend was occasionally interrupted by short intervals of accelerated deflection, which are believed to be related to localized bearing failure of the fibers, leading to plate tipping and consequent stress redistribution. The average constrained modulus measured by these tests was 6.1 ksf (292 kN/m<sup>2</sup>). The coefficient of secondary compression estimated from the deflection versus log of time for a consolidation stress of 0.42 tsf (40 kN/m<sup>2</sup>) is 0.038.

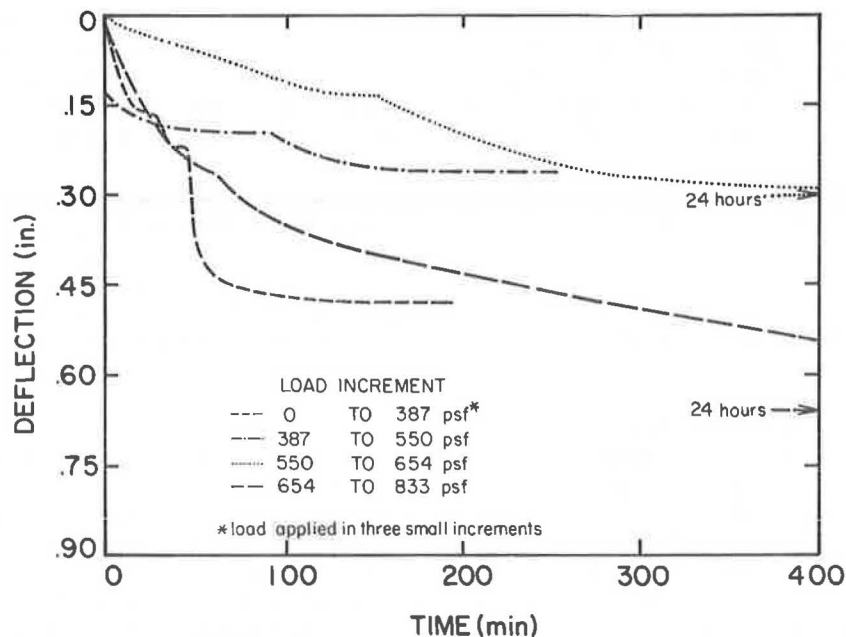


FIGURE 6 Vertical deflection of a 1-ft-diameter steel plate versus time for plate load testing of coarse-fibrous organic soil near the toe of the New Boston Road embankment.

### Standard Penetration Testing

The stratigraphy underlying the embankment at Station 101 + 50 determined from the split-spoon sampling is illustrated in Figure 2. As shown, the preexisting road surface is now located at a depth of about 10 ft (3 m). Sandy silt with organic content was encountered at a depth of 28 ft (8.5 m) in each borehole. The split-spoon samples were also used to develop the water content profiles within the embankment. Standard penetration testing in the fill above and below the geotextile yielded average penetration resistance corrected for overburden pressures ( $N$ , in blows per foot) of 34 and 23, respectively. The SPT results before construction in the organic soil below the fill ranged from 0 to 7. On average, the postconstruction values of  $N$  in the organic soil were increased by 2 blows/ft, indicating an increased density of the organic soil subsequent to construction.

### Field Vane Shear Testing

Field vane shear tests were performed after renovation with a Geonor vane apparatus at Station 101 + 35, 68 and 160 ft (21 and 49 m) left of centerline (Figure 3). The Geonor vane, which is nearly half the dimensions of the vane that was used during preconstruction investigations, was advanced according to the manufacturer's instructions for minimum soil disturbance. Rotation of the vane was commenced immediately after vane penetration and was maintained at a standard rate of 0.1 degree/sec. Due to the soft nature of the organic soil, the insertion of the Geonor vane was easily accomplished by hand.

Consistent with the vane shear profiles developed before renovations, the postconstruction profiles obtained with the Geonor vane shear apparatus (Figure 3) indicate that a sublayer with higher shear strength exists near the surface. Typically, the presence of such a sublayer is the result of overconsolidation due to water table fluctuations and other environmental and physiochemical changes. At the Candia site, the high strength values may also reflect the presence of large fibers. Landva (11) suggests that vane shear testing of fibrous soils yields estimates of shear strength that are too high due to the compression of fibers into ropelike bundles. Scatter of the vane shear data may also be due to localized fiber-induced anisotropy.

However, unlike the preconstruction vane shear strengths, the postconstruction values decrease with increasing depth and water content within the fine-fibrous sublayer. Others have found the same relation between vane shear strength, water content, and depth in fine-fibrous organic soils (3, 12). Vane shear strength reaches a minimum at a depth of about 17 ft (5.2 m), where water content is greatest and the soil is amorphous-granular. Because of the consolidating effect of lateral spreading, water content decreases and shear strength increases at locations nearer to the embankment.

### Flat Plate Dilatometer Testing

For the four dilatometer profiles conducted at the site, dilatometer indices were used to evaluate the capability of

dilatometer testing to detect changes in organic soil types. Dilatometer tests were performed at 0.75-ft (0.23-m) intervals. At three locations away from the embankment, the dilatometer blade was advanced to the base of the organic strata by hand, using two operators.

The dilatometer indices were computed assuming a hydrostatic water pressure distribution. Since marsh gases may have been present, the actual pore water pressure and effective overburden pressure probably differed from the assumed values. Consequently, the computed values of the material index ( $I_d$ ) and the horizontal stress index ( $K_d$ ) should not be quantitatively interpreted by conventional methods. On the other hand, the dilatometer modulus ( $E_d$ ) is computed independent of pore water and overburden pressures, and thus the measured values of  $E_d$  should be representative of the in situ soil characteristics.

Values of the DMT indices at Station 101 + 50 and 160 ft (49 m) from the centerline are shown in Figure 7. These profiles show several of the same trends found at other DMT testing locations. For instance, at all locations away from the embankment,  $E_d$  and  $I_d$  tend to decrease with increasing depth within the upper coarse-fibrous sublayer and remain fairly constant with depth in the amorphous-granular sublayer. The near-surface reductions of  $E_d$  and  $I_d$  correspond to a reduction of fibrosity and soil stiffness. Moreover,  $K_d$  noticeably decreases with depth within the upper half of the amorphous-granular sublayer and increases with depth in the lower half. This trend parallels that of the water content profiles and mirrors that of the vane shear strength profiles. Because of significant scatter, the changes of  $K_d$  with depth in the coarse-fibrous sublayer are unclear. There does not appear to be any clear trend for all the DMT indices in the fine-fibrous sublayer. The DMT index value averages and ranges for each of the sublayers are listed in Table 1.

Although the  $I_d$  and  $K_d$  values found from testing beneath the road are similar to those found at other locations in the amorphous-granular soil, the  $E_d$  values from the road sounding are much higher than elsewhere (Figure 8). The consistency of  $I_d$  reflects the fairly homogeneous composition of the Candia organic soil, whereas the variation of  $E_d$  manifests the greater consolidation and resulting increases in stiffness of the embankment foundation.

According to the chart developed by Marchetti (13) for the determination of soil type and unit weight based on  $E_d$  and  $I_d$ , the high values of  $E_d$  inaccurately place the stiff organic foundation soil in the silty clay category. Moreover, the  $E_d$  values for the virgin amorphous-granular and fine-fibrous soil are less than the  $E_d$  values earmarked in the chart for muck and peat. In all cases, the chart overestimates the unit weight of the Candia highly organic soil by a factor of about 1.5.

Dilatometer determinations of constrained modulus and undrained shear strength are based on  $K_d$  and  $E_d$ . Because much uncertainty is associated with the calculated value of  $K_d$  due to the unknown hydraulic conditions in the organic soils and uncertain drainage conditions during DMT testing, the reliability of the dilatometer undrained shear strength and constrained modulus values are questionable. The constrained modulus ( $M$ ) was calculated at every DMT test depth. Because  $M$  is proportional to  $E_d$ , it varies with depth and distance from the embankment according to the same trends as  $E_d$ . Away from the embankment and under the road surface, the

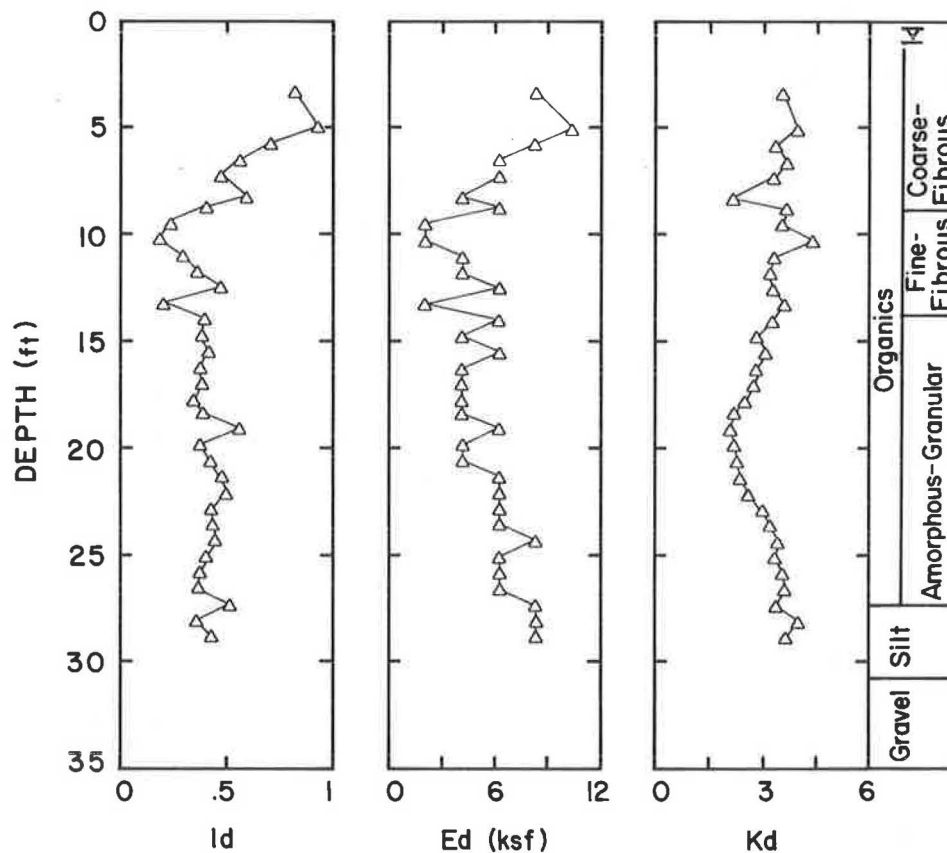


FIGURE 7 Profiles of Id, Ed, and Kd at STA 101+50, 160 feet left.

TABLE 1 DILATOMETER INDICES

Index	Road Foundation: Fine-Fibrous Amorphous		Wetlands					
	Range	Avg.	Coarse-Fibrous		Fine-Fibrous		Amorphous-Granular	
			Range	Avg.	Range	Avg.	Range	Avg.
Id	0.4-0.7	0.50	0.3-5.2	1.09	0.1-0.7	0.43	0.1-1.4	0.46
Ed (ksf)	37-117	68.0	4-113	17.1	2-15	8.6	2-15	7.2
Kd	0.7-2.0	1.4	1.4-17.3	5.6	1.2-11.9	4.9	0.2-7.5	3.4

constrained modulus of the highly organic soil ranged from 2.5 to 64.3 ksf (120 to 3080 kN/m<sup>2</sup>) and 31.7 to 100.3 ksf (1520 to 4800 kN/m<sup>2</sup>), respectively.

In general, dilatometer testing measured an increase of shear strength with depth in the coarse-fibrous sublayer and a decrease with depth from the top to the middle of the amorphous-granular sublayer. As shown in Figure 9, dilatometer shear strength values in the uppermost fibrous soil far from the embankment were generally half of those near the toe. Under the embankment, the shear strength values were much higher, thus reflecting the expected increase in strength due to consolidation of the embankment foundation.

#### Pressuremeter Testing

The pressuremeter used at the Candia site is of the British self-boring type designed by the University of New Hampshire

to have three levels of strain measurement arms along the length of the probe, which independently track the thin flexible rubber membrane expansion. After insertion of the probe into the ground with minimum disturbance, the pressure used to expand the membrane and its deflection are recorded continuously. For each strain arm, values of the in situ horizontal stress, shear modulus, and shear strength can be determined from the test results. On each side of the probe are located two pore pressure cells, which can also measure pore water pressures during probe expansion. Self-boring was accomplished using drilling guidelines appropriate for soft clays to achieve minimum disturbance during probe insertion (14). Full-displacement pressuremeter tests were also conducted using the self-boring probe fitted with a 60-degree cone tip. It was pushed into the ground at a rate of advance ranging from 24 to 30 in./min (61 to 76 cm/min).

Even for the pressuremeter tests in which the rate of advance of the probe was most rapid, negligible excess pore pressures



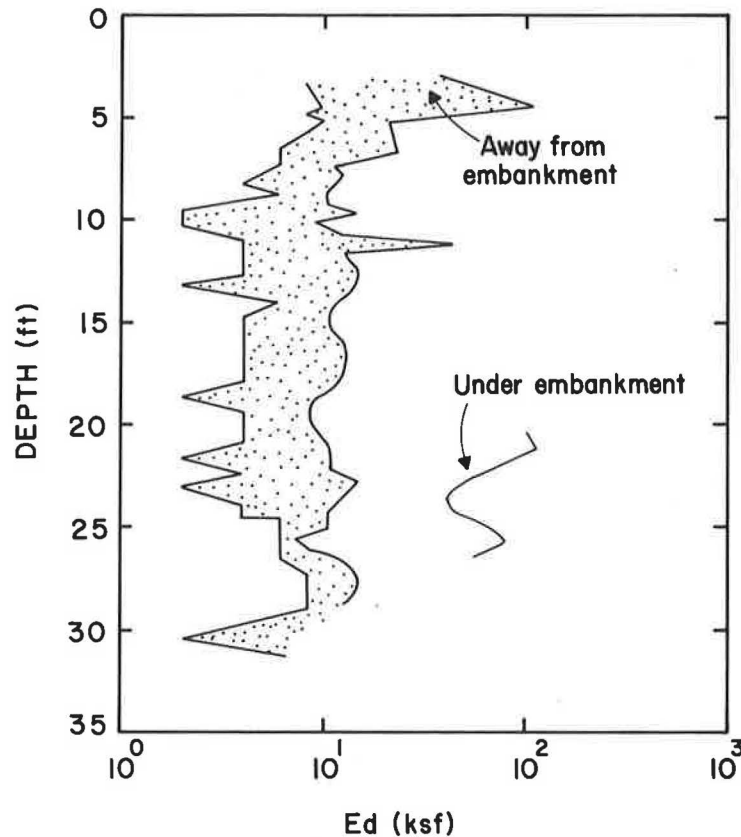


**FIGURE 8** Profiles of  $E_d$  under the New Boston Road embankment and in the adjacent marsh.

were measured after penetration. Moreover, during all tests the difference between pore pressure cell readings at different depths was less than the estimated difference in the hydrostatic pressure at those elevations. Pore pressure response and pore pressure measurement may have been affected by the presence of gases in the organic soil, by seepage forces, or by incomplete saturation of the pore pressure cells.

Typical total-pressure-versus-strain curves for the expansion of a single strain arm during SBPM and FDPM testing at the Candia site are depicted in Figure 10. As shown, the shapes of the expansion curve are significantly different. However, elastic properties obtained from the unload-reload cycles are similar and in agreement with findings by others (15).

Total horizontal stress in the ground was measured from the total pressure at which expansion begins to occur for each of the strain arms. In general, SBPM measurements of total horizontal stress were similar to those from FDPM measurements. This is contrary to findings by other investigators (16), which have shown FDPM testing to yield greater lateral stress than SBPM testing.

As shown in Figure 11, the total horizontal stress estimates in the wetlands range from slightly less than hydrostatic to slightly greater than total overburden pressure. Since total horizontal stress cannot be less than hydrostatic in a fully saturated medium with a single piezometric surface, one or more unusual factors must be influencing the existing stress state or measurement technique. The same factor(s) may also

be related to the unusually low effective stresses measured by the pore pressure cells.

Also shown in Figure 11 are the values of limit pressure from both SBPM and FDPM testing. The limit pressure was defined as the pressure corresponding to 100-percent volume change. The shaded area bounds the lower and upper values of limit pressure. This area seems to indicate that the lowest resistance is at the transition between the fine-fibrous and amorphous zone. Below that transition, the limit pressures increase with depth in a manner similar to that observed in the total horizontal stress measurements. For both SBPM and FDPM tests conducted in the coarse-fibrous zone, the results show significant scatter, probably due to the high heterogeneity from the presence of roots and twigs.

As shown in Figure 12, the shear modulus values estimated by pressuremeter testing generally decrease with depth to the top of the amorphous zone. This trend is evident from both the SBPM and FDPM test results, although at each depth the average SBPM shear modulus values appear to be slightly less than the average FDPM values. Below the transition, the values seem to increase with depth. The shear modulus values found with different strain arms at the same depth differ by as much as 75 percent.

The shear strength values estimated from the SBPM data using the Gibson and Anderson method (17) ranged from 54 to 86 psf (2.6 to 4.1 kN/m<sup>2</sup>). This method assumes undrained conditions and elastoplastic behavior. The values obtained

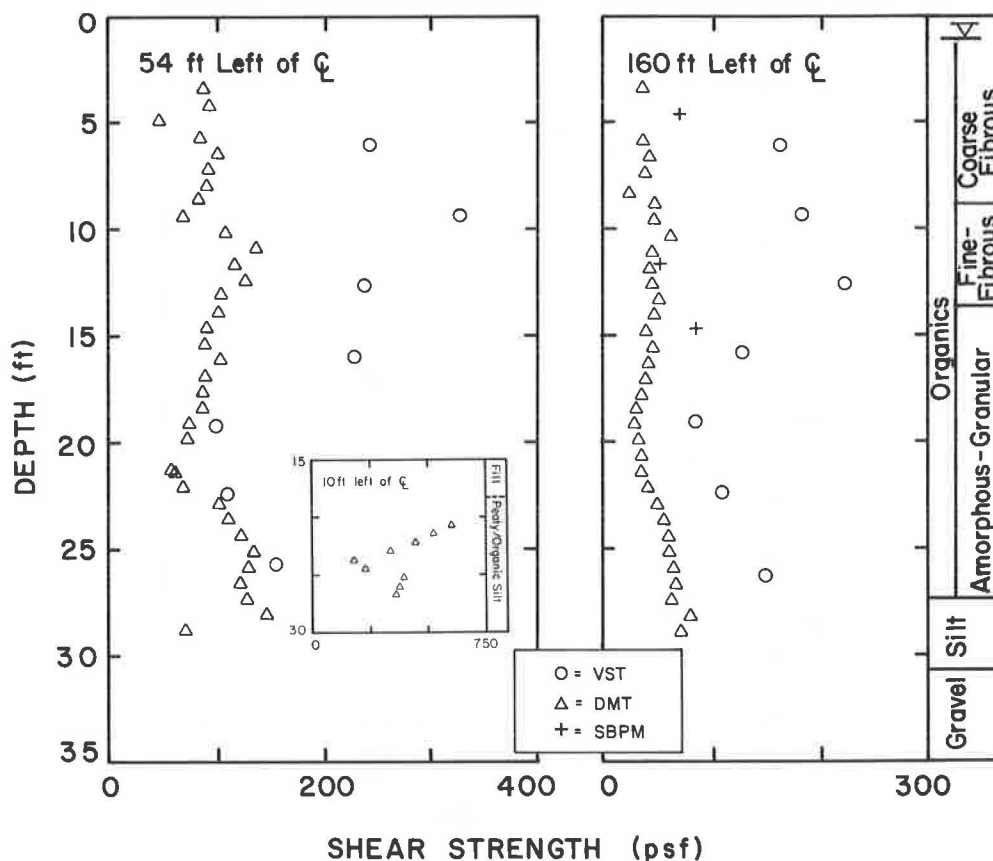


FIGURE 9 Shear strength profiles obtained by vane shear, dilatometer, and self-boring pressuremeter testing.

are shown in Figure 9. The undrained shear strength may also be estimated using an empirical method introduced by Ménard (18) based on the difference between the limit pressure and the horizontal stress. The difference, divided by a factor that generally varies between 4.5 and 7.5, can be used to evaluate the shear strength. As experience grows for a certain soil type and region, this empirical method increases in accuracy. From Figure 11, it is evident that two nearly constant zones of differences exist within the fibrous and the amorphous layers.

#### SUMMARY OF COMPRESSIBILITY AND SHEAR STRENGTH CHARACTERISTICS

The DMT estimates of the constrained modulus were found to depend greatly on location, increasing from an average of 6.6 ksf (320 kN/m<sup>2</sup>) in the virgin soil to 58 ksf (2780 kN/m<sup>2</sup>) at the embankment. Although this trend is consistent with expectations due to the consolidating effect of the embankment, the values of the constrained modulus obtained in and near the embankment appear to be too high considering the large magnitude of observed settlement. The amount of settlement predicted to occur in response to embankment renovation, according to Schmertmann's procedure (19) and the DMT estimates of  $M$  obtained near the toe, is 0.28 ft (0.09 m), which is only 4 percent of the 6.5 ft (2 m) measured at

the settlement platform. The average constrained modulus measured by plate load testing in the coarse-fibrous soil was 6.1 ksf (290 kN/m<sup>2</sup>). This value is similar to the 6.6 ksf (320 kN/m<sup>2</sup>) estimated by the DMT in the virgin fine-fibrous and amorphous-granular organic soil.

In general, secondary compression of an organic foundation is as significant as initial (elastic and primary) compression (6, 9, 20). The observed behavior of the New Boston Road embankment and the plate load and pressuremeter test estimates of soil compressibility indicate that the Candia organic foundation responded to loading in the usual fashion. Recall that the settlement of the embankment was most rapid immediately after the placement of fill, although long-term settlement of appreciable magnitude continues to occur. Estimates of initial and secondary settlement from the field and laboratory test results range from 1.1 to 2 ft (0.3 to 0.6 m) and from 1.5 to 2 ft (0.5 to 0.6 m), respectively.

According to the results of the VST, DMT, and SBPM testing, the shear strength increases with depth within the fibrous soil, decreases with depth from the top to the middle of the amorphous-granular sublayer, and thereafter increases with depth. However, as shown in Figure 9, the vane shear strength values are greater than either DMT or SBPM shear strength values by a factor of about 2.

The reliability of the dilatometer and pressuremeter compressibility and shear strength estimates is uncertain. DMT and SBPM testing methods are based on the assumption of

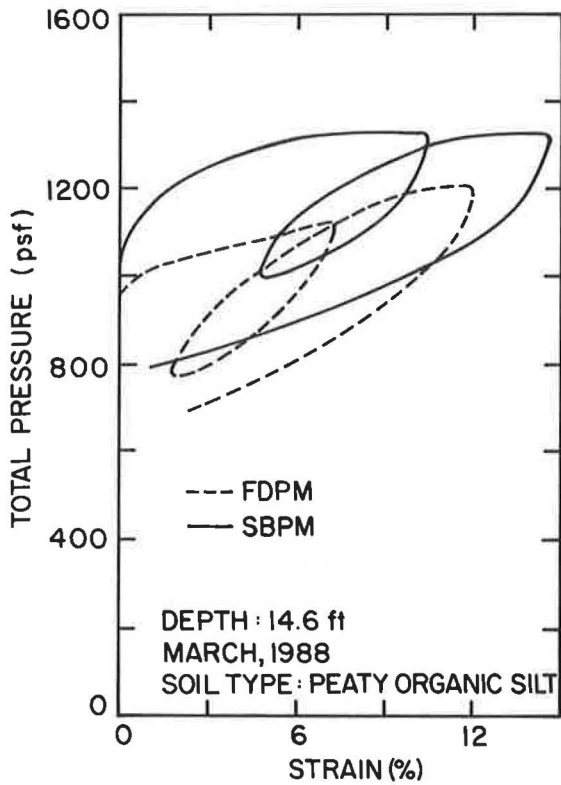


FIGURE 10 Typical total-pressure-versus-strain curves for self-boring and full-displacement pressuremeter testing in the Candia virgin peaty organic silt.

undrained conditions; yet drained conditions may prevail due to the unusually high permeability of the organic soil. The DMT and SBPM testing methods also fail to account for the unusually large magnitude of strain that accompanies compression and failure of the organic soil as indicated by laboratory consolidation and strength testing. In addition, considerable uncertainty is associated with  $K_d$  and  $I_d$ , and thus with DMT correlations. Consequently, estimates of shear strength and constrained modulus are uncertain because of the difficulty of pore water pressure estimation in the presence of marsh gas.

CONCLUSION

In accord with field and laboratory test estimates of the shear moduli, constrained moduli, and coefficients of secondary compression, the maximum prediction of combined initial and secondary settlement of the New Boston Road embankment 3 years after renovation is 4 ft (1.2 m). This is similar to the 3 ft (0.9 m) predicted with the NYDOT empirical method based on water content. Yet it is about 2.5 ft (0.8 m) less than the cumulative settlement monitored by the settlement platform at this time. The discrepancy could be explained by lateral spreading as manifested by decreasing water content, increasing shear strength, and increasing stiffness at distances closer to the embankment. Vertical settlement occurs as a result of compression in both the horizontal and vertical directions. The predictions made from the laboratory and in situ soil test results assume compression in one direction only.

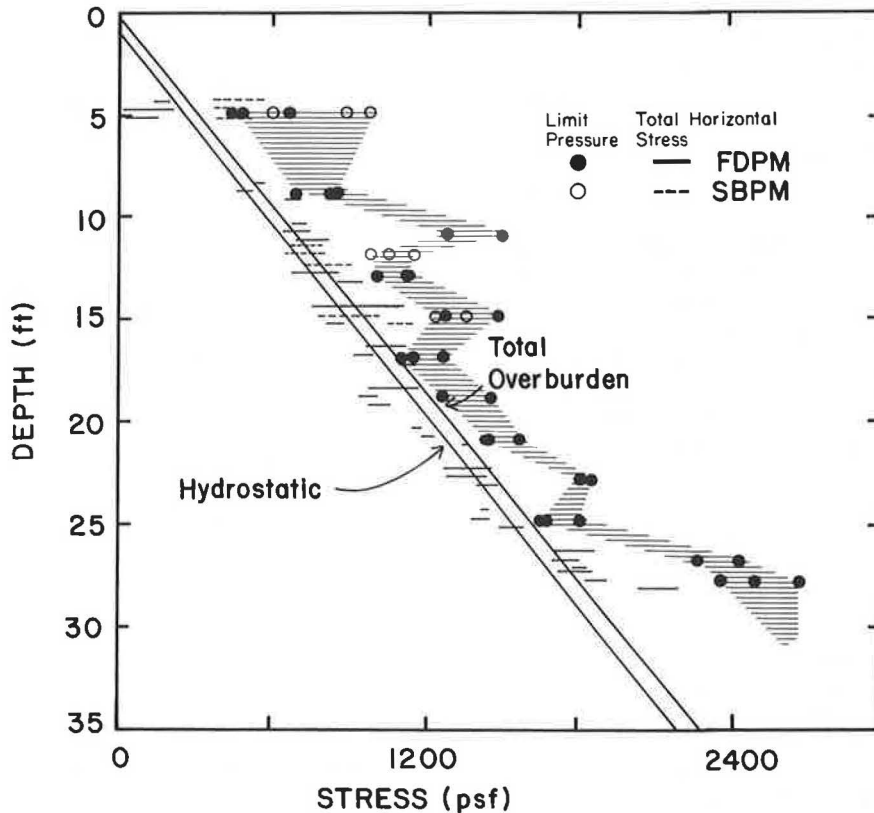


FIGURE 11 Total horizontal stress and limit pressure profiles measured by self-boring and full-displacement pressuremeter testing in the Candia virgin peaty organic silt.

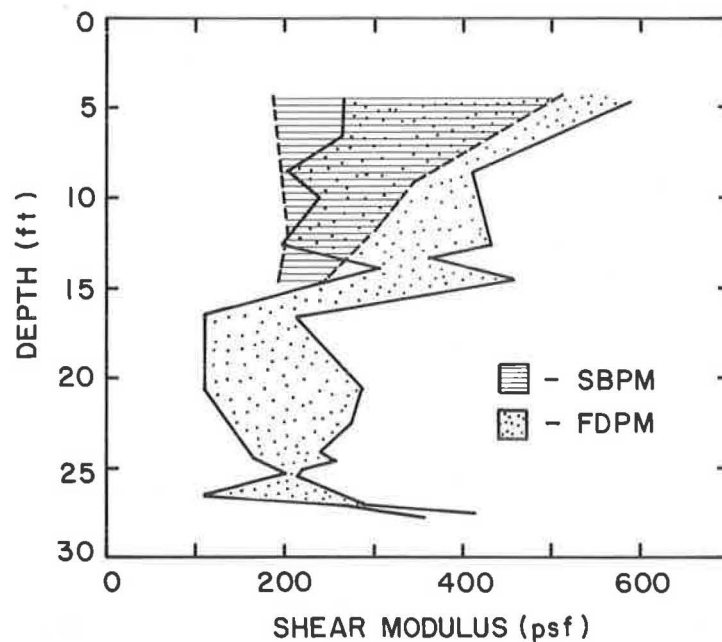


FIGURE 12 Shear modulus profiles measured by self-boring and full-displacement pressuremeter testing in the Candia virgin peaty organic silt.

Localized embankment slope failure may also account for some of the discrepancy. However, it is impossible to separate the horizontal displacements due to slow lateral shear from those due to rapid horizontal compression by analyzing the measurements of a single slope inclinometer. Moreover, the longitudinal cracks that developed over several months after construction and which revealed minimal horizontal displacement were not typical of circular shear failure.

Dilatometer testing was found to yield useful information in an efficient and economical manner. DMT profiling was fast, simple, and, where the soil was particularly soft, did not require the use of a drill rig. Despite problems of  $K_d$  and  $I_d$  interpretation due to the presence of marsh gas, variations of  $E_d$  yielded valuable information regarding changes of organic soil type from fibrous to amorphous-granular and changes of soil stiffness with distance from the embankment. With further DMT experience in organic soils, Marchetti's chart for the determination of soil type and unit weight could probably be modified to include different types of organic soils. Moreover, the accuracy of DMT test results could be improved by modifying the blade for greater expansion and by installing a more sensitive membrane.

As indicated by the shape of the SBPM expansion curves, advancement of the pressuremeter into the Candia organic soil with the self-boring technique probably induced some soil disturbance. However, comparison of the SBPM curves with the FDPM expansion curves suggests that the self-boring technique still induced less disturbance than the full-displacement technique. Thus there is hope that further adaptation of the SBPM apparatus and technique to the fibrous and gaseous nature of organic soils will minimize this effect. Moreover, pore pressure cell performance in partially saturated, gaseous organic soils should be improved. It is possible that methods of analysis based on limit pressure are better suited for use in highly compressible soils. As with the DMT, the pressure-

meter needs to be expanded to larger strains to truly model the observed behavior of organic soils.

#### ACKNOWLEDGMENTS

The writers would like to express their appreciation of Michael J. Atwood, Craig R. Findlay, Adam N. Jones, and Louis A. Nejame for their help during postconstruction in situ and laboratory soil testing.

#### REFERENCES

1. New York Department of Transportation, Soil Mechanics Bureau. *Design Manual*. New York Department of Transportation, New York, March 1978.
2. A. O. Landva and P. La Rochelle. Compressibility and Shear Characteristics of Radforth Peats. In *Testing of Peats and Organic Soils* (P. M. Jarrett, ed.), ASTM STP 820, ASTM, Philadelphia, Pa., 1983, pp. 141–156.
3. I. C. MacFarlane. Engineering Characteristics of Peat. In *Muskeg Engineering Handbook* (I. C. MacFarlane, ed.), University of Toronto Press, Toronto, Canada, 1969, chapter 4.
4. J. J. Andrejko, F. Fiene, and A. D. Cohen. Comparison of Ashing Techniques for Determination of the Inorganic Content of Peats. In *Testing of Peats and Organic Soils* (P. M. Jarrett, ed.), ASTM STP 820, ASTM, Philadelphia, Pa., 1983, pp. 5–20.
5. A. O. Landva and P. E. Pheaney. Peat Fabric and Structure. *Canadian Geotechnical Journal*, Vol. 17, 1980, pp. 416–435.
6. L. Casagrande. Construction of Embankments across Peaty Soils. *Journal of the Boston Society of Civil Engineers*, Vol. 53, No. 3, pp. 272–317.
7. K. Karesniemi. Dependence of Humification Degree on Certain Properties of Peat. *Proc., 4th International Peat Congress*, Vol. 2, 1972, pp. 273–282.
8. S. F. Hillis and C. O. Brawner. The Compressibility of Peat and Reference to Major Highway Construction in British Columbia.

- Proc., 7th Muskeg Research Conference*, Ottawa, Canada, Technical Memorandum 71. NRC Associate Committee on Soil and Snow Mechanics, National Research Council, Ottawa, Canada, 1961, pp. 204–227.
9. W. G. Weber. Performance of Embankments Constructed over Peat. *Journal of the Soil Mechanics and Foundations Division, ASCE*, Vol. 95, No. SM1, 1969, pp. 53–77.
  10. N. D. Lea and C. O. Brawner. Highway Design and Construction over Peat Deposits in Lower British Columbia. In *Highway Research Record 7*. HRB, National Research Council, Washington, D.C., 1963, pp. 1–33.
  11. A. O. Landva. Vane Testing in Peat. *Canadian Geotechnical Journal*, Vol. 17, No. 1, 1980.
  12. T. J. Kaderabek, D. Barreiro, and M. A. Call. In Situ Tests on a Florida Peat. In *Use of In Situ Tests and Geotechnical Engineering* (S. P. Clemence, ed.), ASCE Geotechnical Special Publication 6. ASCE, New York, 1986, pp. 649–666.
  13. S. Marchetti. In-Situ Tests by Flat Dilatometer. *Journal of Geotechnical Engineering*, Vol. 106, No. GT3, 1980, pp. 299–321.
  14. J. Benoit and G. W. Clough. Self-Boring Pressuremeter Tests in Soft Clay. *Journal of Geotechnical Engineering*, Vol. 112, No. 1, 1986, pp. 60–78.
  15. N. J. Withers, L. H. J. Schaap, and C. P. Dalton. The Development of the Full Displacement Pressuremeter. In *The Pressuremeter and Its Marine Applications* (J. L. Briaud and M. E. Audibert, eds.), ASTM STP 950. ASTM, Philadelphia, Pa., 1986, pp. 38–56.
  16. A. Marsland and D. Windle. Developments in Offshore Site Investigation. *Oceanology International, Brighton*, Vol. 1, 1982.
  17. R. E. Gibson and W. F. Anderson. In-Situ Measurement of Soil Properties with Pressuremeter. *Civil Engineering and Public Works Review*, Vol. 56, 1961, pp. 615–618.
  18. L. Ménard. Mesurement in-situ des propriétés physiques des sols. *Annales des Ponts et Chaussées, Paris*, Vol. 127, No. 3, 1957, pp. 357–377.
  19. J. H. Schmertmann. Dilatometer to Compute Foundation Settlement. In *Use of In Situ Tests in Geotechnical Engineering* (S. P. Clemence, ed.), ASCE Geotechnical Special Publication No. 6, (ASCE, New York, 1986, pp. 303–321.
  20. L. Samson and P. LaRochelle. Design and Performance of an Expressway Constructed over Peat by Preloading. *Canadian Geotechnical Journal*, Vol. 9, 1972, pp. 447–466.

---

*Publication of this paper sponsored by Committee on Soil and Rock Properties.*

# Evaluation of Soil Parameters from Piezocone Tests

KAARE SENNESET, ROLF SANDVEN, AND NILMAR JANBU

The interpretation and evaluation of soil parameters determined by cone penetration tests (CPTs) have been a part of our research program for the last 15 to 20 years. A theoretical framework has been established, and CPT results have been compared and calibrated to laboratory data for a wide variety of soils. The pore pressure measurements that enable us to find effective shear strength parameters, as well as settlement parameters (such as the coefficient of consolidation) have been especially useful. In general, piezocone penetration test data have proved to be very useful and valuable additions to sampling and laboratory investigations. In some soils, we believe that the in situ method provides us with better data because sampling and laboratory handling may give us disturbed samples and erroneous results. In this paper, our interpretation and evaluation of piezocone data are demonstrated for a medium-stiff, overconsolidated clay.

Cone penetration tests (CPTs) with measurement of cone resistance ( $q_c$ ) and sleeve friction ( $f_s$ ) during penetration have been used in Norway since the early 1950s. In the early 1970s, the first attempts were made to measure the pore pressures developed around conically shaped piezometers ( $I$ ). These tests clearly showed that large pore pressures could be developed during penetration of fine-grained clays and silts.

The introduction of the piezocone (2,3) in the mid-1970s provided new possibilities for the interpretation of soil parameters and the identification of soil type. In particular, the simultaneous measurement of cone resistance ( $q_c$ ) and pore pressure ( $u_T$ ) in a piezocone penetration test (CPTU) permits the interpretation of test results in terms of effective stresses.

At the Norwegian Institute of Technology (NTH), research on the interpretation of piezocone test results has concentrated on the development of rational interpretation methods based on well-known theoretical principles. The methods have been applied to test records from various soil types, and systematic correlations have been made between laboratory reference parameters and interpreted values from CPTU data.

In this paper, the interpretation methods are demonstrated for Glava clay from the Trondheim region. This is a medium-stiff, overconsolidated clay of medium to low sensitivity. The following parameters have been interpreted and evaluated:

## Soil strength parameters:

- Undrained shear strength ( $s_u$ ), and
- Effective shear strength parameters [attraction ( $a$ ) and friction ( $\tan \phi'$ )];

## Deformation parameters:

- Compression moduli ( $M_i$  and  $M_n$ ),
- Stress history, preconsolidation pressure ( $\sigma'_c$ ), and
- Coefficient of consolidation ( $c_v$ ).

A classification chart that may aid in the classification of soil type on the basis of CPTU recordings is also presented.

## CPTU MEASUREMENTS AND CORRECTIONS

In a piezocone penetration test, the following recordings are usually made:

- Cone resistance ( $q_c$ ),
- Total pore pressure ( $u_T$ ) at reference location (Figure 1), and
- Sleeve friction ( $f_s$ ).

The terminology and symbols used in a CPTU are summarized in Figure 2. When the cone is subjected to water pressure on all sides, a shift in zero values will usually be recorded both for friction and cone resistance readings (4). The reason for this effect can be seen in Figure 1: the water pressures act on the end areas of the conical part and the friction sleeve, respectively, due to the jointed design of the cone. For most types of cones in practical use, these end areas are not equal in size, and an unbalanced force will occur during penetration. Therefore the recorded cone resistance  $q_c$  will be smaller than the true value, and the sleeve friction will be larger. To account for these effects, certain corrections should be applied to the original recordings (4,5). Equation 1 shows the correction to be applied to cone resistance:

$$q_T = q_c + (1 - a) \cdot u_T \quad (1)$$

where

- $q_T$  = corrected total cone resistance,
- $a$  = net area ratio ( $A_n/A_q < 1$ ) (Figure 1), and
- $u_T$  = total pore pressure at reference level (Figure 1).

Equation 2 shows the correction to be applied to sleeve friction:

$$f_T = f_s - (1 - k_s b) \cdot c \cdot u_T \quad (2)$$

where

- $f_T$  = corrected sleeve friction,

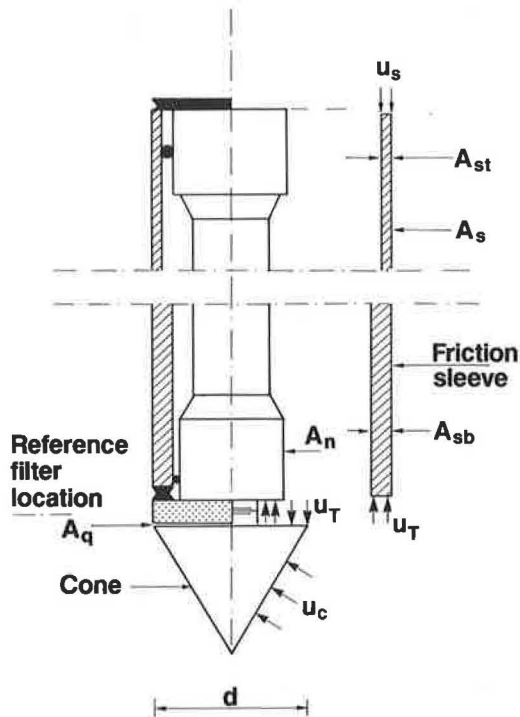


FIGURE 1 Correction of measured cone resistance for pore pressure effects.

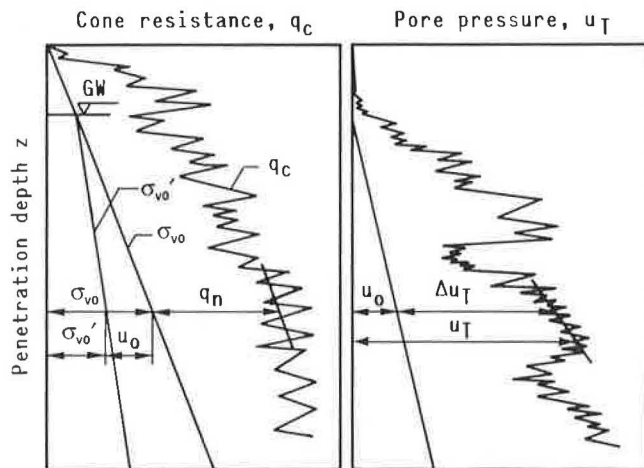


FIGURE 2 CPTU measurements and notations.

$b$  = sleeve end area ratio ( $A_{st}/A_{sb} < 1$ ) (Figure 1),  
 $c$  = sleeve area ratio ( $A_{sb}/A_s < 1$ ) (Figure 1),  
 $u_T$  = total pore pressure at reference filter location, and  
 $k_s = u_s/u_T \approx 0.6$  to  $0.8$  in soft clays.

These corrections may be important in soft clays and silts, where large pore pressures are generated during penetration. In coarse soils, the corrections are practically negligible because almost drained conditions prevail in the surrounding soil. To interpret the cone penetration process in terms of effective stresses, the pore pressures must be measured somewhere on or in the vicinity of the conical part. Two different locations have frequently been used for the pore pressure element:

- On the conical part, either at the tip or at mid-height of the cone,
- On the cylindrical part, immediately behind the cone neck. (This location has been recommended in a proposal to the International Society for Soil Mechanics and Foundation Engineering (6). It is referred to in this paper as the reference filter location.)

No specific filter location provides optimal pore pressure measurements for all practical applications. Unfortunately, the relative magnitude of the penetration pore pressure depends on where on the cone it is measured. Generally, the largest pore pressure is generated in the compression zone beneath the cone, whereas significantly lower pore pressure may be developed along the cylindrical part. Several researchers (7,8) have indicated that pore pressure behind the cone may be empirically related to pore pressure measured at the conical part.

The following expression may be used to adjust the pore pressure measured on the cone to make it correspond to the reference value (9):

$$u_T = u_0 + k(u_c - u_0) \quad (3)$$

where

- $u_0$  = hydrostatic or initial in situ pore pressure,
- $u_c$  = measured total pore pressure, and
- $k$  = adjustment factor.

The adjustment factor  $k$  is primarily a function of soil type, soil properties, and the exact filter location on the cone. Experience from penetration tests in various soil types using cones with different filter locations is summarized in Table 1.

In some heavily overconsolidated clays and in very dense sands, negative pore pressures may exist at the reference level although positive pore pressures are measured on the cone. In such materials, negative values of  $k$  should be selected.

#### SITE AND LABORATORY INVESTIGATIONS— GLAVA CLAY

Interpretation of CPTU records from the medium-stiff, overconsolidated marine Glava clay has been selected for this paper. The clay is homogeneous, but some silt lenses are present in the upper parts of the profile. The clay is dry crusted down to about 1.5 m. Results from index tests and special tests in the laboratory are presented in Figure 3. The ground-

TABLE 1 EMPIRICAL VALUES OF  $k$  FOR ADJUSTMENT OF PORE PRESSURES

Soil Type	Filter Location	
	Cone Face, Mid-Height	Cone Tip
Normally consolidated clay	0.6–0.8	0.7–0.9
Slightly overconsolidated, sensitive clays	0.5–0.7	0.6–0.8
Heavily overconsolidated clays	0–0.3	0.1–0.3
Loose, compressible silts	0.5–0.6	0.5–0.7
Dilatant, dense silts	0–0.2	0.1–0.3
Loose, silty sands	0.2–0.4	0.5–0.6

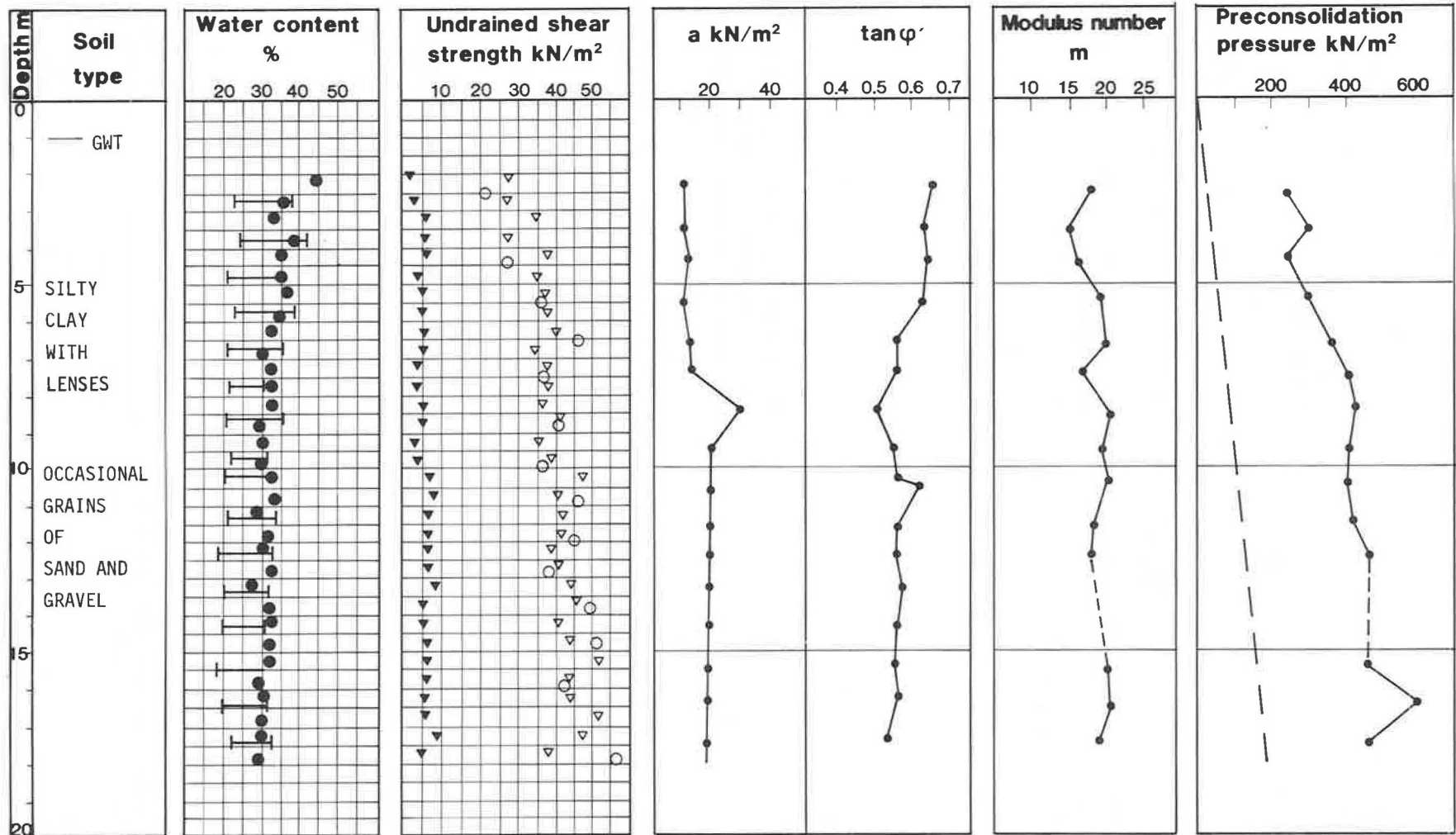


FIGURE 3 Soil profile for Glava clay.



water table is located at a depth of 1.0 m, and the initial pore pressure distribution ( $u_0$ ) is hydrostatic.

The laboratory testing program was performed on undisturbed clay samples obtained with the Geonor Ø 54 mm piston sampler. It included conventional index tests, CIU triaxial compression tests, and continuous-loading oedometer tests. The aim of this test program was to establish reference strength and deformation parameters for comparison with in situ parameters interpreted from the CPTU records.

The site investigations included three cone penetration tests with pore pressure measurements. A 10-cm<sup>2</sup>/60-degree piezocone with the filter at the reference location immediately behind the cone was used for all tests. Typical records of corrected cone resistance  $q_T$  and reference pore pressure  $u_T$  are shown in Figure 4.

The most important aspect of piezocone testing is the saturation of the pore pressure transducer system. Insufficient saturation may cause a delayed response to rapid changes in the pore pressure. The following procedure produced good results in Glava clay:

1. Saturation of filters before field work by (a) applying vacuum on submerged filters and (b) flushing with de-aired water; and
2. Preparation for field use by (a) applying high vacuum on the dismantled cone at the site for approximately 1 hour, (b) performing final cone assembly with the cone and filter submerged in de-aired water, and (c) sealing the filter with a rubber membrane before lowering the penetrometer down to the water level in a predrilled hole.

**SOIL STRENGTH**

The cone penetration process involves many aspects of soil behavior that may complicate the development of a realistic analytical interpretation model. For example,

- Stresses and pore pressures around the cone vary in both vertical and radial directions;
- Singularities, high stress gradients, and high pore pressure gradients are present because of the cone geometry;

- The geometrical shape and extent of plastified zones at failure are unknown; and
- The penetration takes place continuously, and large strains are imposed on the surrounding soil.

Considering these aspects, one may easily realize that a closed-form analytical solution to the cone penetration problem may be difficult to conceive. Analytical models from CPTU data for penetration of soil hence include simplifying assumptions and approximations that should be considered when evaluating interpreted parameters.

**Undrained Shear Strength**

The undrained shear strength ( $s_u$ ) may be estimated from the cone data by using a theoretical relationship of the following form (10):

$$s_u = \frac{q_T - \sigma}{N_c} \tag{4}$$

where

- $q_T$  = total corrected cone resistance,
- $N_c$  = bearing capacity factor, and
- $\sigma$  = in situ stress [either vertical overburden pressure ( $\sigma_{v0}$ ), horizontal pressure ( $\sigma_{h0} = K_0\sigma_{v0}$ ), or octahedral pressure ( $\sigma_{oct} = 1/3(\sigma_{v0} + 2\sigma_{h0})$ )].

Various theoretical approaches have been introduced to determine the bearing capacity factor  $N_c$ ; these include bearing capacity theory (11,12), cavity expansion methods (13,14) and numerical approaches using linear or nonlinear soil models (15,16). However, a generally accepted theoretical model for determination of  $s_u$  has not yet been developed. Hence the interpretation of  $s_u$  is usually estimated from empirical relationships (17) such as

$$s_u = \frac{q_T - \sigma_{v0}}{N_{kT}} \tag{5}$$

where  $N_{kT}$  denotes a cone factor, including shape and depth factors.

The cone factor  $N_{kT}$  is usually determined from a reference value for  $s_u$ , either from a field vane test or a laboratory triaxial compression test. Values for  $N_{kT}$  seem to range from 10 to 15 for normally consolidated clays, and from about 15 to 19 for overconsolidated clays. Empirical values of  $N_{kT}$  are usually higher than the values of  $N_c$  obtained by theoretical models.

The large scatter in values of  $N_{kT}$  often limits the ability to produce a successful interpretation of  $s_u$  from CPTU data. Local correlations at the site are hence usually recommended, which, in fact, is not a very consistent procedure. Many reasons for the reported scatter may be relevant to mention; for example,

- The undrained shear strength is not a unique measure of the soil strength;
- The obtained value depends on the type of test performed;

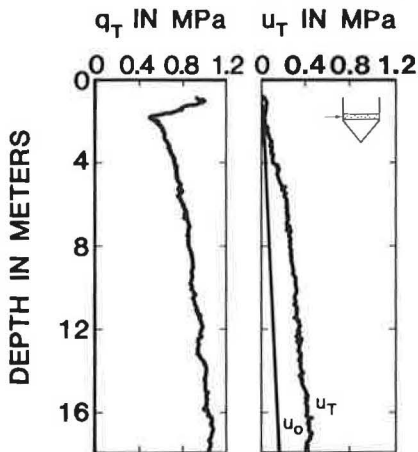


FIGURE 4 CPTU records for Glava clay.

- The obtained value of  $s_u$  is strain rate dependent; and
- The reference  $s_u$  for many empirical methods has been different.

The latter point may be discussed in further detail. It is well known that the maximum shear stress obtained in a clay sample subjected to triaxial compression depends on the consolidation stress level. Usually the samples are consolidated to the present in situ stress level, where the at-rest coefficient  $K'_0$  is anticipated or approximated from empirical relationships. Overconsolidated soils were previously consolidated at higher stresses than those acting on the deposit today. These stress conditions may also be simulated in the consolidation phase for a triaxial test sample.

In Figure 5, a principal graph for the peak shear stress as a function of the consolidation stress  $\sigma'_{3c}$  is shown for Glava clay. The band reveals quite interesting tendencies:

- A large scatter is seen in the maximum shear stress ( $\tau_{max}$ ) for samples consolidated to the present in situ overburden pressure.
- Samples consolidated to or past the overconsolidation pressure indicate that there exists an upper limit of the maximum obtainable shear stress in the clay. This limit will correspond to the undrained shear strength  $s_u$ .

For Glava clay, values of  $N_{kT}$  based on  $\tau_{max}$  values from  $\sigma'_{vo}$ -consolidated test samples range from about 12 to 18. If the average peak shear stress from  $\sigma'_c$ -consolidated samples is utilized, the corresponding range becomes about 7 to 10. These empirically based values are in better agreement with reported theoretical values of the bearing capacity factor  $N_c$ .

Further research will be carried out in other types of clay to evaluate whether this approach has general applicability. If so, it may help narrowing the scatter in  $N_{kT}$  values and may perhaps explain the often-reported discrepancies between theoretical and empirical values.

**Effective Shear Strength**

The effective shear strength parameters, friction ( $\tan \phi'$ ) and attraction ( $a$ ), over a stress range  $\Delta\sigma'$  are defined by the Mohr-

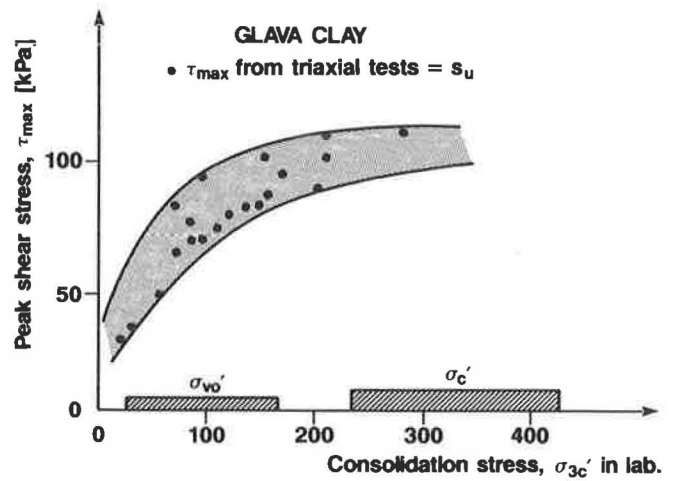


**FIGURE 5** Principal graph of peak shear stress ( $\tau_{max}$ ) versus consolidation stress  $\sigma'_{3c}$  for Glava clay.

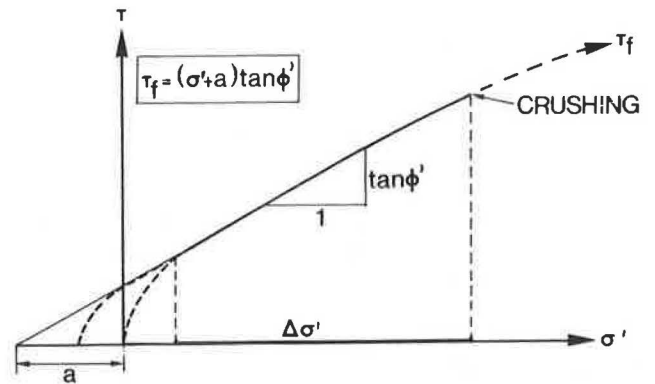


**FIGURE 6** Definition of strength parameters in the Mohr-Coulomb criterion.

Coulomb failure criterion in Figure 6. Over a given range of working stresses, the strength envelope may best be approximated by the expression

$$\tau_f = (\sigma' + a)\tan \phi' \tag{6}$$

where  $\tau_f$  denotes shear strength, and  $\sigma'$  denotes effective normal

**TABLE 2** TYPICAL VALUES OF ATTRACTION ( $a$ ) AND FRICTION ( $\tan \phi'$ ) (18)

	Shear Strength Parameters				
	$a$ (kPa)	$\tan \phi'$	$\phi'$	$N_m$	$B_q$
Clay					
Soft	5–10	0.35–0.45	19–24	1–3	0.8–1.0
Medium	10–20	0.40–0.55	19–29	3–5	0.6–0.8
Stiff	20–50	0.50–0.60	27–31	5–8	0.3–0.6
Silt					
Soft	0–5	0.50–0.60	27–31		
Medium	5–15	0.55–0.65	29–33	5–30	0–0.4
Stiff	15–30	0.60–0.70	31–35		
Sand					
Loose	0	0.55–0.65	29–33		
Medium	10–20	0.60–0.75	31–37	30–100	<0.1
Dense	20–50	0.70–0.90	35–42		
Hard, stiff soil, OC, cemented	>50	0.8–1.0	38–45	100	<0

stress on the failure plane. The term attraction ( $a$ ) is interpreted from the design stress range as the negative intercept of the normal stress axis ( $\sigma'$ ). The classical term cohesion ( $c$ ) is related to the attraction by the expression:

$$c = a \cdot \tan \phi' \quad (7)$$

Typical ranges of the shear strength parameters for some common soil types are given (18) in Table 2. The table may be useful for evaluating the parameter values interpreted from CPTU data.

It is important to note that a large silt content may increase the parameter values for clays but may reduce the parameter values in sands for otherwise similar conditions. Moreover, the presence of active clay minerals such as smectite and montmorillonite will decrease friction below the values given in Table 2.

*Theoretical Framework*

The framework for effective stress interpretation has been the conventional bearing capacity approach based on the theory of plasticity. In the case of cone penetration in well-draining soils, which allow no excess pore pressure buildup in the soil, the formula for plane strain bearing capacity may be written (19) as

$$q_T + a = N_q(\sigma'_{v0} + a) \quad (8)$$

where

- $\sigma'_{v0}$  = effective overburden pressure (at reference location),
- $N_q$  = theoretical bearing capacity factor, and
- $a$  = attraction.

In fine-grained soils, excess pore pressures will be generated around the cone and will decrease the ultimate bearing capacity. This is accounted for in the expression below (19):

$$q_n = (N_q - 1)(\sigma'_{v0} + a) - N_u \Delta u_T \quad (9)$$

where

- $q_n = q_T - \sigma_{v0}$  = net cone resistance,
- $\Delta u_T$  = excess pore pressure at reference location, and
- $N_u$  = theoretical bearing capacity factor.

When the excess pore pressure is measured in the test, one can insert (19)

$$\Delta u_T = B_q q_n \quad (10)$$

[where  $B_q$  denotes pore pressure ratio ( $\Delta u_T/q_n$ )] into Equation 9 and obtain

$$q_n = N_m(\sigma'_{v0} + a) \quad (11)$$

where  $N_m = (N_q - 1)/(1 + N_u B_q)$ .

For the drained case,  $B_q = 0$ , and Equation 11 becomes similar to Equation 8.

The expression for the bearing capacity factor  $N_q$  may be written in the following way (18):

$$N_q = N_f \exp[(\pi - 2\beta)\tan \phi'] \quad (12)$$

where  $N_f$  equals  $\tan^2(45 + \frac{1}{2}\phi')$ , and  $\beta$  is the angle of plastification.

Figure 7 shows values of  $N_q$  as a function of  $\phi'$  and  $\beta$ , including an "empirical graph" for  $\beta$  based on various in situ strength tests in sands and silts. The band is extrapolated to cover clays. A definition of the angle of plastification ( $\beta$ ) in the idealized geometrical failure pattern is also included in Figure 7.

A theoretical solution of the bearing capacity factor  $N_u$  as a function of soil friction ( $\tan \phi'$ ) and base roughness ( $r$ ) has recently been developed at NTH (20). In the typical range of friction values in clays and silts where the term  $N_u \Delta u_T$  is significant, i.e., when  $\tan \phi'$  is in the range 0.3 to 0.7, the theoretical solution may be reasonably well approximated (19) by

$$N_u \sim 6 \tan \phi' (1 + \tan \phi') \quad (13)$$

The plane strain bearing capacity solution is hence primarily a function of the soil friction ( $\tan \phi'$ ) and the angle of plastification ( $\beta$ ).

*Soil classification*

An impression of soil type may be gained from recorded values in a CPTU. If one uses the dimensionless parameters  $N_m = q_n/(\sigma'_{v0} + a)$  and  $B_q = \Delta u_T/q_n$ , the possible type of soil may be identified by using Table 2 (18).

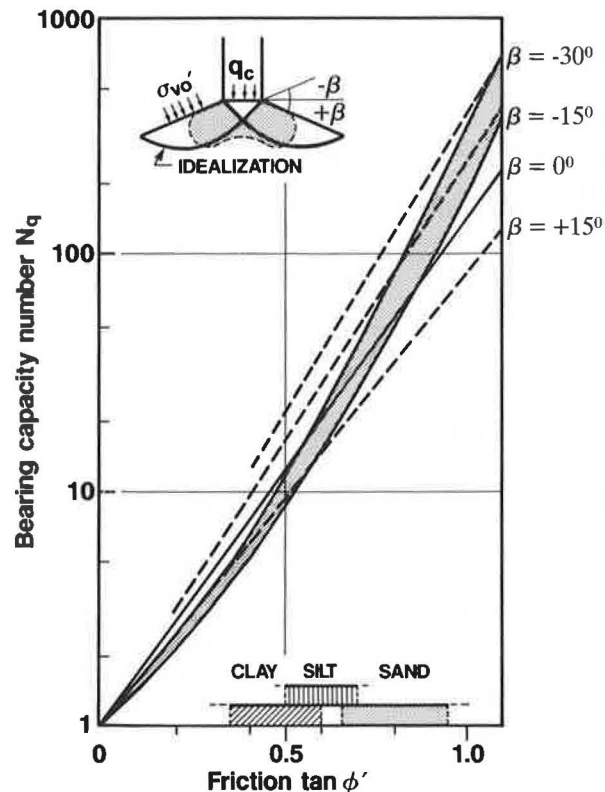


FIGURE 7 The bearing capacity factor  $N_q$ .

The modified classification chart shown in Figure 8, which is based on values of  $q_T$  and  $B_q$ , may be used for the same purpose (18). One should note that the values of  $B_q$  should be developed from the reference pore pressures measured immediately behind the cone, and that the corrected cone resistance  $q_T$  should be utilized in the classifications. The chart in Figure 8 may also be used when negative pore pressures are recorded at the reference location. The information on soil type and penetration conditions obtained from the classification may be valuable for the interpretation of strength parameters described later in this section.

*Interpretation Method—Friction*

The interpretation procedure is based on the following CPTU data:

- Corrected cone resistance ( $q_T$ ), and
- Excess pore pressure at reference location ( $\Delta u_T$ ).

Moreover, the following initial stress conditions in the penetrated soil must be known:

- Total overburden pressure ( $\sigma_{v0}$ ),
- Initial pore pressure distribution ( $u_0$ ), and
- Effective overburden pressure ( $\sigma'_{v0} = \sigma_{v0} - u_0$ ).

The following dimensionless parameters can then be found directly from the CPTU recordings: (a) the cone resistance number ( $N_m$ ):

$$N_m = \frac{q_T - \sigma_{v0}}{\sigma'_{v0} + a} = \frac{q_n}{\sigma'_{v0} + a} = \frac{N_q - 1}{1 + N_u B_q} \quad (14)$$

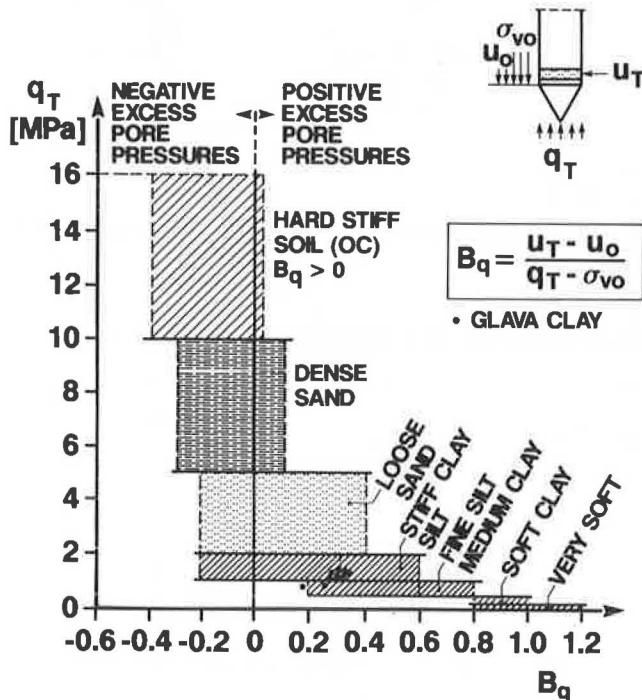


FIGURE 8 Chart for classification of soil type on the basis of CPTU recordings.

and (b) the pore pressure ratio ( $B_q$ ):

$$B_q = \frac{u_T - u_0}{\sigma'_{v0} + a} = \frac{\Delta u_T}{q_n} \quad (15)$$

The choice was made to derive values of  $B_q$  from the pore pressures measured on the reference filter location. The attraction values in Equation 14 may be evaluated theoretically or chosen on the basis of information on soil type and soil conditions.

The friction ( $\tan \phi'$ ) is then found from an interpretation chart, as shown in Figure 9. Because the interpreted value depends on the angle of plastification, several charts have to be developed in order to cover a range of possible values of  $\beta$ . In the example shown in Figure 9a,  $\tan \phi' = 0.66$  is determined from  $N_m = 12$  and  $B_q = 0.2$ . The interpretation procedure is, however, well suited for computer-assisted interpretation and presentation of results, and a computer program has been developed for the purpose (21).

*Angle of Plastification*

The angle of plastification ( $\beta$ ) expresses an idealized geometry of the generated failure zones around the advancing cone. This idealization requires that cone penetration be simulated as a quasistatic process. The value of  $\beta$  is hence difficult to assess, both experimentally and theoretically. However, it is reasonable to believe that  $\beta$  depends on soil properties such as compressibility and stress history, plasticity, and sensitivity. The easiest way to estimate typical values of  $\beta$  in various soils is to perform correlations between laboratory-determined  $\tan \phi'$  and interpreted values from CPTU. Results from such studies in various soil types performed at NTH over the recent years are summarized in Table 3. Information on soil type and soil conditions may be gained from the previously shown classification chart and table.

*Attraction*

Attraction ( $a$ ) may be estimated directly from the CPTU records, both for drained and undrained penetration (1,18). The suggested methods are applicable when relatively homogeneous soil deposits or layers are penetrated. In cases where such estimates cannot be obtained, it is suggested that typical values from triaxial tests on similar soils be used (9) (Table 2).

In CPTU interpretations, one may often obtain larger values than are usually found by triaxial testing. This may be due to sample disturbance of suction in the pores. However,

TABLE 3 TENTATIVE VALUES OF THE ANGLE OF PLASTIFICATION  $\beta$  IN VARIOUS SOIL TYPES (9)

Soil Type	Tentative Values of $\beta$ (degrees)
Dense sands, overconsolidated silts, high plastic clays, low-compressible overconsolidated clays	-20 to -10
Medium sands and silts, sensitive clays, high-compressible clays	-5 to +5
Loose silts, clayey silts	+10 to +20

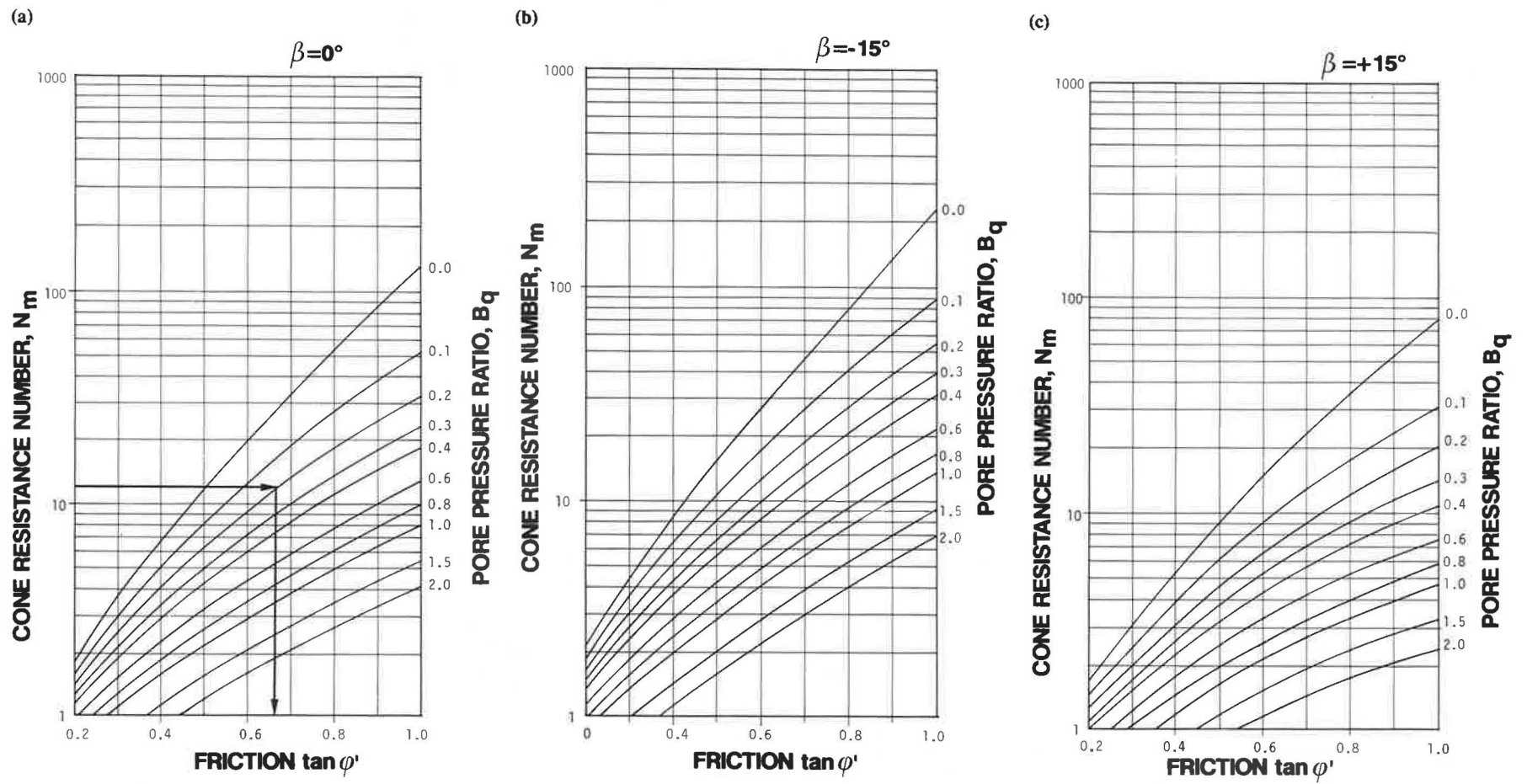


FIGURE 9 (a) Interpretation diagram for  $\beta = 0$  degrees; (b) interpretation diagram for  $\beta = -15$  degrees; (c) interpretation diagram for  $\beta = +15$  degrees.

uncertainties in the determination of attraction have only small effects on interpreted friction at greater penetration depths ( $z > 10$  m).

*Results for Glava Clay*

In Figure 10, values of  $\tan \phi'$  interpreted from CPTU are compared to reference values obtained from triaxial compression tests. In the upper 10 m of the profile,  $\beta = -15$  degrees provided the best correspondance to the reference values, whereas  $\beta \sim 0$  degrees was appropriate below this depth. Attraction values determined from triaxial tests were used in the interpretation. Similar values of  $\beta$  have been found for other overconsolidated clays as well (9).

Further research will be carried out in order to gain more confidence in the selection of  $\beta$  values in various soils.

**SOIL DEFORMATION PARAMETERS**

The penetration of a cone imposes large strains in the surrounding soil, and the distribution of stresses and pore pressures are complex and difficult to predict. This is in contradiction to real design problems, where relatively small strains are developed and a reasonable prediction of the effective stresses may be obtained. Hence, predictions of deformation moduli from CPTU data are usually based on empirical or semiempirical relationships.

The introduction of the piezocone made it possible to include pore pressure dissipation tests in situ. Much attention has been devoted to interpreting the results of such tests in order to estimate flow and consolidation characteristics of the soil.

In this section, simple methods of approximating soil deformation and consolidation parameters from CPTU data are presented and demonstrated for Glava clay. It should be stressed

that the methods are aiming only at a rough estimate of the parameter values. Laboratory tests should be carried out in order to establish design values of the deformation parameters for clays.

**Compression Moduli**

The compressibility of the soil may conveniently be expressed by the tangent modulus ( $M$ ) (22), where

$$M = d\sigma'/d\epsilon \tag{16}$$

The tangent modulus varies with the effective stress  $\sigma'$  in different ways for various soil types. It has been found that all types of variations may be described by the following general expression (22):

$$M = m \cdot \sigma_a \cdot \left(\frac{\sigma'}{\sigma_a}\right)^{1-a} \tag{17}$$

where

- $m$  = modulus number,
- $\sigma_a$  = reference stress (= 100 kN/m<sup>2</sup>), and
- $a$  = stress exponent ( $-1 \leq a \leq 1$ ).

A definition of the tangent modulus from the stress-strain behavior of the soil is shown in Figure 11. The same figure also shows the principal behavior of the tangent modulus for an overconsolidated clay. For the preconsolidated stress range, a constant modulus is indicated ( $a = 1$ ), whereas the modulus increases linearly ( $a = 0$ ) for stresses above the preconsolidation pressure  $\sigma'_c$ . The tangent modulus may be determined from a laboratory oedometer test.

In the CPTU interpretations, the vertical deformation moduli may be expressed as a function of the net cone resistance  $q_n$ . For clays, a linear interpretation model is suggested for the estimation of values of  $M$  for the preconsolidated stress range (Figure 11). The expression reads (19)

$$M_i = m_i \cdot q_n \tag{18}$$

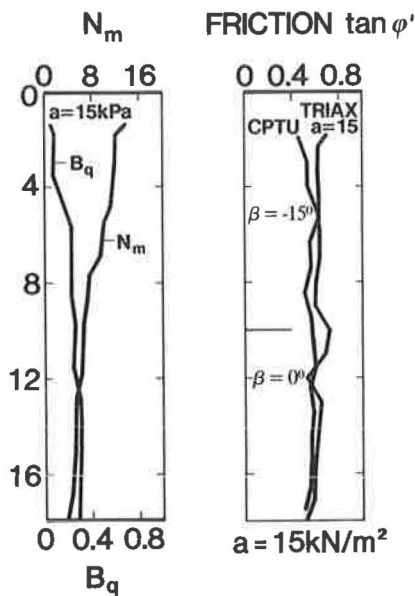


**FIGURE 10** Comparison between in situ and laboratory values of  $\tan \phi'$  for Glava clay.

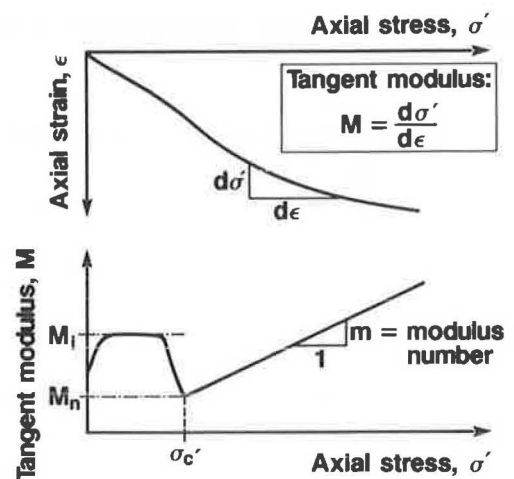


**FIGURE 11** Definition of deformation moduli from CPTU.

The in situ modulus number  $m_i$  ranges from 5 to 15 in most clays (19). In the normally consolidated stress range, one may combine

$$M = m(\sigma'_{v0} + a) \quad (19)$$

and

$$q_n = N_m(\sigma'_{v0} + a) \quad (20)$$

and get

$$M_n = m_n \cdot q_n \quad (21)$$

where

- $m_n$  = in situ modulus number ( $m/N_m$ ),
- $m$  = oedometer modulus number, and
- $N_m$  = cone resistance number.

Common values of  $m_n$  in clays may range from 4 to 8 (9). As shown in Figure 11,  $M_n$  corresponds to the oedometer modulus occurring at the preconsolidation pressure  $\sigma'_c$ .

In Figure 12, interpreted values of  $M_i$  are shown for Glava clay. Corresponding values of the oedometer modulus show good agreement with an average interpretation of  $10 \cdot q_n$ , and generally plot within the suggested range of  $\pm 5 \cdot q_n$ .

The modulus  $M_n$  at  $\sigma'_c$  is shown in Figure 13. Interpreted values compare well with the upper limit of  $8 \cdot q_n$ . The exam-

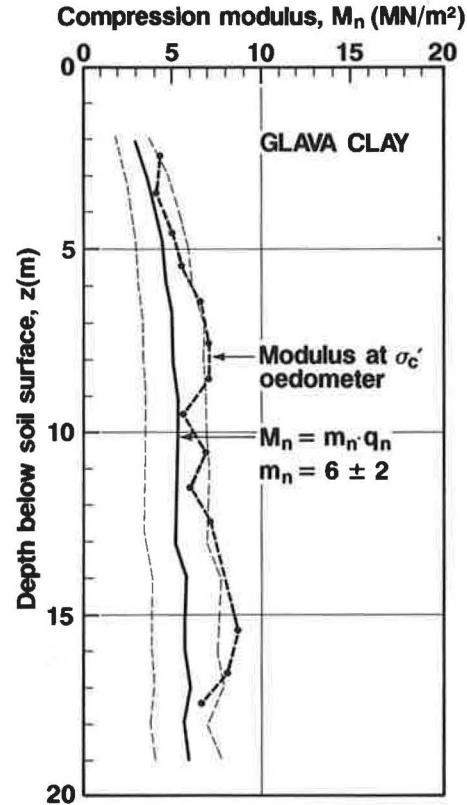


FIGURE 13 Compression modulus  $M_n$  for Glava clay.

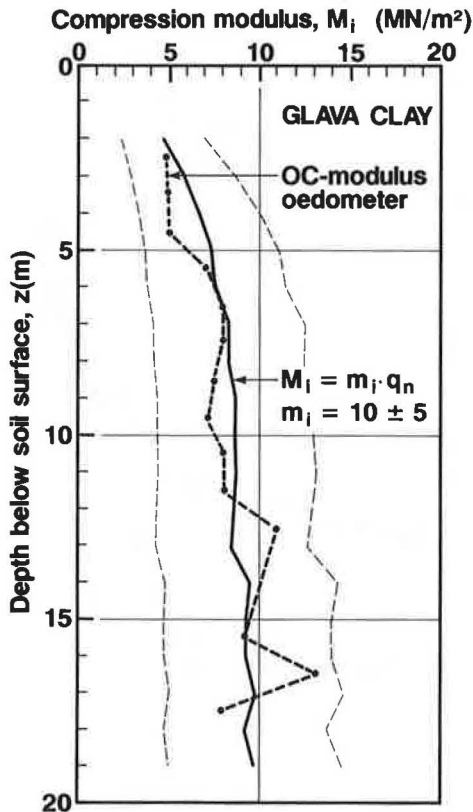


FIGURE 12 Compression modulus  $M_i$  for Glava clay.

ples indicate that, for clays, compression moduli may be fairly well predicted from simple, semiempirical relationships.

#### Stress History and Preconsolidation Pressure

Several methods have recently been presented for evaluation of the stress history of a soil on the basis of in situ tests (4). Such methods may give supplementary information besides the determination of the preconsolidation pressure from oedometer tests. A reliable interpretation of preconsolidation stress level is particularly important in soil types where it is difficult to obtain undisturbed, high-quality samples.

#### Cone Resistance in Preconsolidated Clays

It has previously been shown that the bearing capacity expression on total stress basis may be written as

$$q_T - \gamma z = N_c \cdot s_u \quad (22)$$

where

- $N_c$  = bearing capacity factor,
- $\gamma$  = unit weight of soil, and
- $z$  = depth below soil surface.

For normally consolidated clays, the undrained shear strength may be expressed as:

$$s_u = \alpha_u \cdot (\gamma - \gamma_w) \cdot z = \alpha_u \cdot \gamma' \cdot z \quad (23)$$

By combining Equations 22 and 23, one obtains:

$$q_T = (N_c \cdot \alpha_u \cdot \gamma' / \gamma + 1) \cdot \gamma \cdot z = K_c \cdot \gamma \cdot z \quad (24)$$

where  $K_c$  is the cone resistance factor.

Typical values of  $\alpha_u$  range from 0.2 to 0.25, whereas  $N_c$  theoretically may vary between 6 and 10 in most bearing capacity approaches. The ratio  $\gamma' / \gamma$  lies approximately in the range from 0.5 to 0.6. The average value of  $K_c$  is hence close to 2.

Consequently, the theoretical cone resistance for a marine, homogeneous, normally consolidated clay may be written:

$$q_T \cong 2\bar{\gamma} \cdot z \quad (25)$$

where  $\bar{\gamma}$  is the average total unit weight of soil.

The stress history of a clay deposit may hence be evaluated by plotting a straight line  $2\bar{\gamma} \cdot z$  on the  $q_T - z$  record. If the  $q_T$  recordings plot is close to the theoretical line, the clay is most likely normally consolidated. If  $q_T$  is significantly larger than  $2\bar{\gamma} \cdot z$ , the clay may be in an overconsolidated state. Figure 14 shows this evaluation principle applied to CPTU records from overconsolidated Glava clay.

*Approximation of Preconsolidation Pressure*

When pore pressures are measured in a piezocone test, the in situ preconsolidation pressure  $\sigma'_c$  may be approximated from the expression published by Sandven et al. (9):

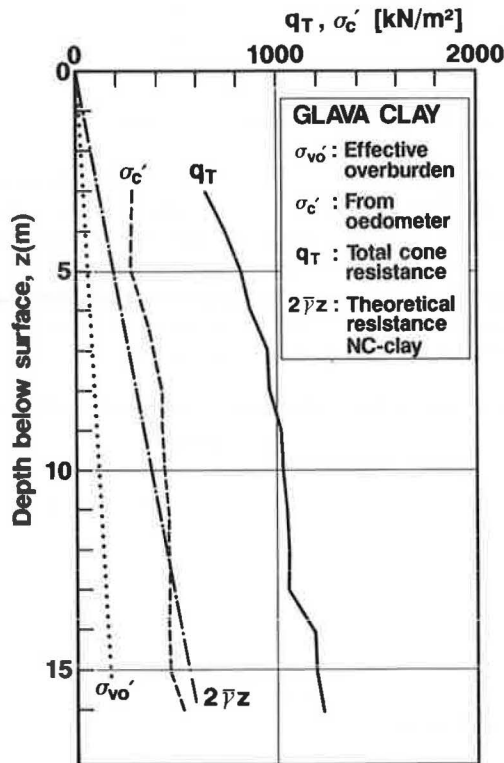


FIGURE 14 Cone resistance  $q_T$  versus preconsolidation pressure  $\sigma'_c$  for Glava clay.

$$\sigma'_c + a = \frac{q'_T + a}{N_{qc}} \quad (26)$$

where  $q'_T = q_T - u_T$  is the effective cone resistance, and  $N_{qc}$  is a bearing capacity coefficient defined by

$$N_{qc} = \frac{N_q + N_u B_q}{1 + N_u B_q} \quad (27)$$

The theoretical principles for this solution are similar to those applied for the interpretation of effective soil friction outlined in the section entitled "Soil Strength." In this approach, it is assumed that the effective cone resistance ( $q'_T$ ) depends on the preconsolidation stress ( $\sigma'_c$ ), the excess pore pressure around the cone ( $\Delta u_T$ ), and the effective shear strength parameters  $a$  and  $\tan \phi'$ . These factors are expressed in the bearing capacity coefficient  $N_{qc}$ , shown in Figure 15. The hatched area in the diagram reflects the variation in the product  $N_u B_q$  when the Prandtl solution for  $N_q$  ( $\beta = 0$  degrees) is used. The basis for the diagram is presently the subject of further research; hence the diagram may be modified when more data become available. Interpreted preconsolidation pressures from CPTU data for Glava clay are compared to corresponding values determined from oedometer tests in Figure 16. Some discrepancies are seen between the two values, especially below a depth of 10 m. However, continued research and further correlations in other clay types may improve the agreement between in situ and laboratory parameters.

**Coefficient of Consolidation**

When performing cone penetration tests in slow-draining soils, excess pore pressures will be generated in the surrounding soil. If the continuous cone penetration is stopped, this excess

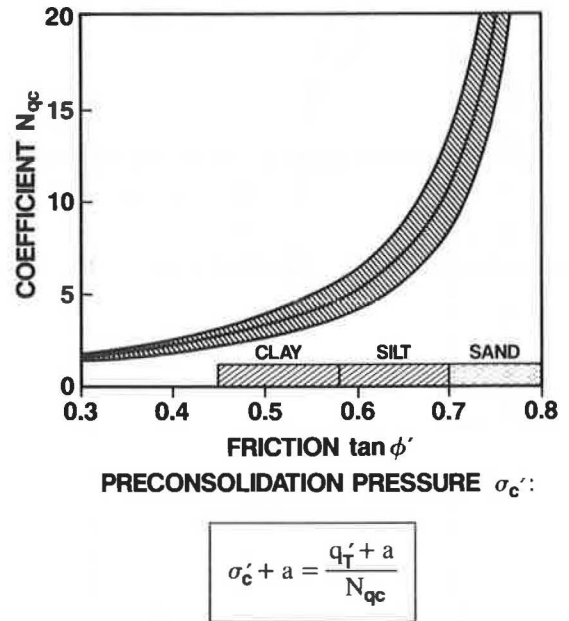


FIGURE 15 Bearing capacity coefficient  $N_{qc}$  for interpretation of preconsolidation pressure  $\sigma'_c$ .



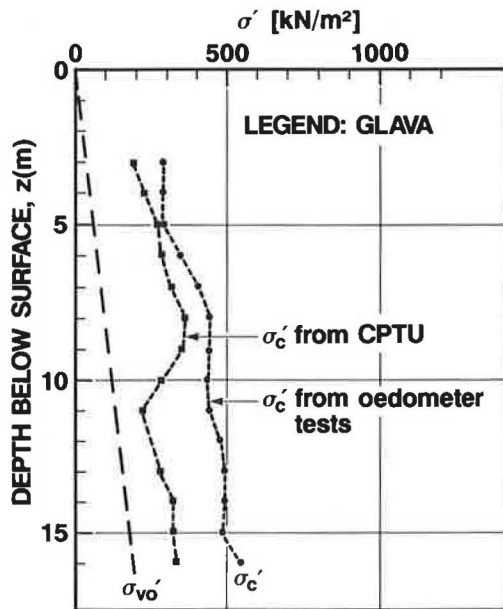


FIGURE 16 In situ and laboratory values of the preconsolidation pressure  $\sigma'_c$  for Glava clay.

pore pressure will start to dissipate, and the decay of pore pressure with time can be monitored.

*Theoretical Considerations*

Cone indentation in soils may be modelled by the expansion of a cylindrical or spherical cavity in an elastic, perfectly plastic medium (13,14). The cavity expansion is characterized by the development of a spherical or cylindrical plastic zone ( $\tau_f = s_u$ ) near the cone. Outside this zone, the soil is in a state of elastic equilibrium ( $\tau_f < s_u$ ). The extension of the plastified zone depends on the rigidity index of the soil ( $I_r = G/s_u$ , where  $G$  is the shear modulus of the soil). Several models based on cavity expansion theory have been developed in

order to interpret the coefficient of consolidation ( $c$ ) from dissipation test results (23). This parameter may be defined as follows:

$$c = \frac{M \cdot k}{\gamma_w} \tag{28}$$

where

- $M$  = deformation modulus,
- $k$  = soil permeability, and
- $\gamma_w$  = unit weight of water.

Vertical ( $c_v$ ) and radial ( $c_r$ ) values of the coefficient of consolidation are usually somewhat different in natural soil deposits. At NTH, two different approaches are used to interpret dissipation test data (19). Both approaches are based on cylindrical cavity expansion theory, and should hence yield values for the radial coefficient of consolidation. Using the time-factor approach,

$$c_r = r_0^2 \cdot \frac{T}{t} \tag{29}$$

where

- $r_0$  = probe diameter,
- $T$  = time factor, and
- $t$  = time to reach given level of dissipation.

Using the rate-factor approach,

$$c_r = r_0^2 \cdot \lambda_c \cdot \left| \frac{\Delta \dot{u}_T}{\Delta u_T} \right| \tag{30}$$

where

- $\lambda_c$  = rate factor,
- $\Delta \dot{u}_T$  = rate of pore pressure dissipation at given dissipation level, and
- $\Delta u_T$  = initial excess pore pressure at  $t = 0$ .

A principal graph of test recordings and terminology is given in Figure 17, and values for the rate factor  $\lambda_c$  and time factor

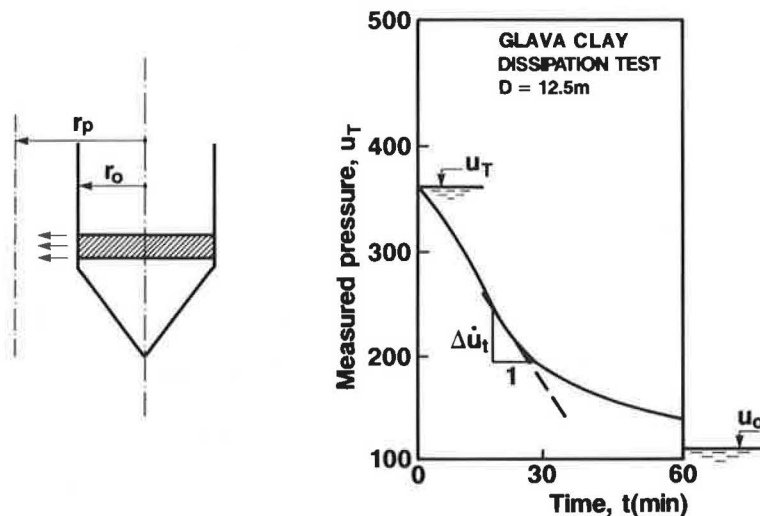


FIGURE 17 Principal graph and terminology for interpretation of CPTU dissipation tests.

$T$  are shown in Figures 18 and 19, respectively. Both factors depend on soil properties (rigidity index  $I_r$ ) and degree of dissipation ( $U_T$ ), where  $U_T$  (in percent) may be written as

$$U_T = \frac{\Delta u_t}{\Delta u_T} = \left| \frac{u_t - u_0}{u_T - u_0} \right| \cdot 100 \quad (31)$$

where

- $u_t$  = pore pressure at given time  $t$ ,
- $u_T$  = initial pore pressure at  $t = 0$ , and
- $u_0$  = initial in situ pore pressure before penetration.

The coefficient of consolidation may vary with the effective stress level. It is, however, usually evaluated at a 50-percent degree of dissipation.

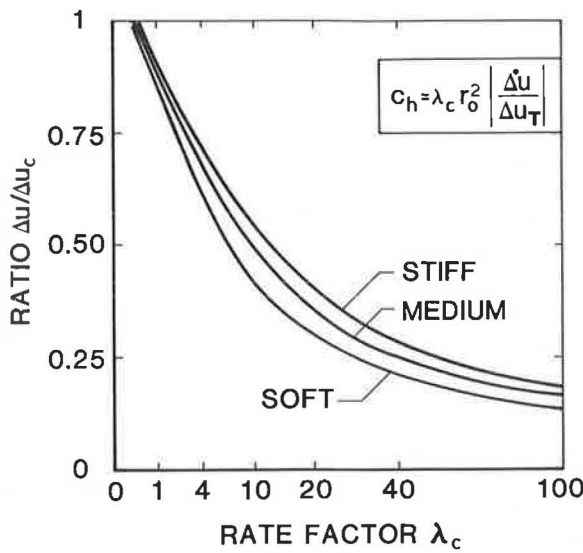


FIGURE 18 Diagram for interpretation of rate factor  $\lambda_c$ .

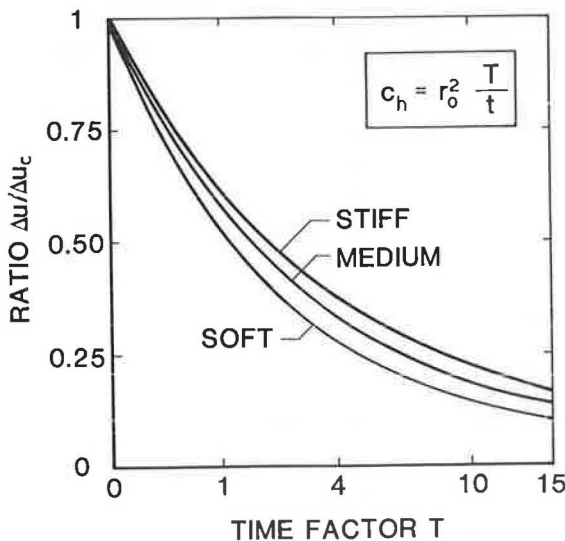


FIGURE 19 Diagram for interpretation of time factor  $T$ .

Several factors may complicate a successful interpretation of dissipation test data. For example (24),

- The dissipation curves are very sensitive to the initial distribution of the excess pore pressure in the plastic zone;
- Consolidation may take place in both vertical and horizontal directions;
- Soil behavior near the cone is complex, due to remolding during penetration, soil anisotropy effects, and soil macrostructure and stratification; and
- A rigid and sufficiently saturated pore pressure measuring system is necessary to give high-quality, reliable test results.

However, it seems that one-dimensional models based on cavity expansion theory may provide reasonably reliable predictions of the coefficient of consolidation. Interpreted values may correspond to values in the preconsolidated stress range in a laboratory test sample, at least for dissipation levels below 50 percent. This is because parts of the consolidation process will take place with the soil in an overconsolidated state. If a value of the coefficient of consolidation in the normally consolidated (NC) stress range is wanted, one may hence wait past the 50-percent level of dissipation.

Results

Dissipation tests were carried out at five different levels in Glava clay. A piezocone with the filter located at the cylindrical part was used for the test, and hence it was assumed that the dissipation mainly takes place in the radial direction. Continuous consolidation tests were performed on undisturbed samples from the same level in the profile. These tests were performed on both vertically and horizontally oriented samples to evaluate the consolidation properties in both directions. In situ and laboratory values of the coefficient of consolidation are compared in Figure 20. In general, values predicted by the interpretation models are of the same order of magnitude as those determined on horizontal samples in the oedometer tests.

In the interpretations, the coefficient of consolidation has been evaluated at 50-percent pore pressure dissipation, and for medium-stiff soil conditions ( $I_r = 45$ ). The laboratory values have been selected as the average from the preconsolidated stress range. In this clay, the radial coefficient of consolidation was slightly greater than the vertical.

CONCLUSIONS

Piezocone tests are a very promising method of obtaining realistic values of strength and deformation parameters in many soil types. The piezocone is also an excellent tool for the determination of soil stratification and the identification of soil type. Its potential for obtaining estimates of engineering soil parameters, along with its excellent determination of soil layering, has established the piezocone test as one of the outstanding and most promising methods of in situ investigation.

The test is today the dominant in situ method for offshore

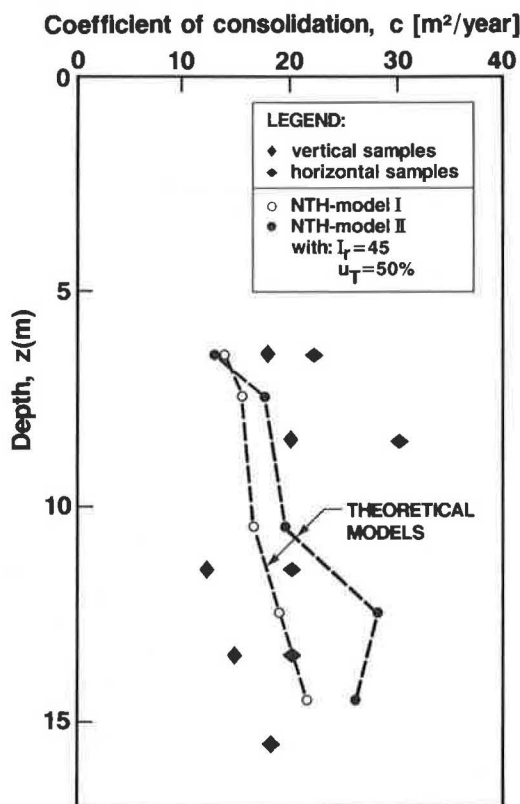


FIGURE 20 Comparison of in situ and laboratory values for the coefficient of consolidation ( $c$ ).

site investigations on the Norwegian Continental Shelf. It is particularly useful in deposits where it may be difficult to obtain undisturbed soil samples for onshore laboratory investigations. Research carried out in many countries and institutions further illustrates the potential of the test. It is reasonable to believe that new and improved interpretation models will emerge from this research and thus further improve the quality of the interpreted parameters.

## REFERENCES

1. N. Janbu and K. Senneset. Effective Stress Interpretation of In Situ Static Cone Penetration Tests. *Proc., 1st European Symposium on Penetration Testing, ESOPT I*, Stockholm, Sweden, Vol. 2.2, 1974, pp. 181–195.
2. B. A. Torstensson. Pore Pressure Sounding Instrument. *Proc., Conference on In Situ Measurement of Soil Properties*, Raleigh, N.C., Vol. 1, 1975, pp. 48–54.
3. A. E. Z. Wissa, R. T. Martin, and I. E. Garlenger. The Piezometer Probe. *Proc., Conference on In Situ Measurement of Soil Properties*, Raleigh, N.C., Vol. 1, 1975, pp. 536–545.
4. R. Campanella, P. K. Robertson, and D. Gillespie. Cone Penetration Testing in Deltaic Soils. *Canadian Geotechnical Journal*, Vol. 20, No. 1, 1983, pp. 23–35.
5. J. M. Konrad. Piezo-Friction-Cone Penetrometer Testing in Soft Clays. *Canadian Geotechnical Journal*, Vol. 24, 1987, pp. 645–652.
6. Technical Committee on Penetration Testing, International Society for Soil Mechanics and Foundation Engineering. International Reference Test Procedure. Proposal to International Society for Soil Mechanics and Foundation Engineering, Orlando, Florida, 1988.
7. T. Lunne, H. P. Christoffersen, and T. I. Tjelta. Engineering Use of Piezocone Data in North Sea Clays. *Proc., 11th International Conference on Soil Mechanics and Foundation Engineering*, San Francisco, Calif., 1985.
8. R. Campanella and P. K. Robertson. Current Status of the Piezocone Test. *Proc., 1st International Symposium on Penetration Testing, ISOPT-1*, Orlando, Fla., Vol. 1, 1988, pp. 93–116.
9. R. Sandven, K. Senneset, and N. Janbu. Interpretation of Piezocone Tests in Cohesive Soils. *Proc., 1st International Symposium on Penetration Testing, ISOPT-1*, Orlando, Fla., Vol. 2, 1988, pp. 939–955.
10. J. M. Konrad and K. T. Law. Undrained Shear Strength from Piezocone Tests. *Canadian Geotechnical Journal*, Vol. 14, 1987, pp. 392–405.
11. G. G. Meyerhof. The Ultimate Bearing Capacity of Wedge-Shaped Foundations. *Proc., 4th International Conference on Soil Mechanics and Foundation Engineering*, London, England, 1957, pp. 105–109.
12. K. Terzaghi. *Theoretical Soil Mechanics*. John Wiley & Sons, New York, 1943.
13. R. Hill. *The Mathematical Theory of Plasticity*. Oxford University Press, Oxford, England, 1950.
14. A. S. Vesic. Expansion of Cavities in Infinite Soil Mass. *Journal of the Soil Mechanics and Foundation Engineering Division, ASCE*, Vol. 98, No. SM3, 1972, pp. 265–290.
15. M. M. Baligh. Strain Path Method. *Journal of Geotechnical Engineering*, Vol. 111, No. 9, 1985, pp. 1108–1136.
16. G. Housley and C. I. Teh. Analysis of the Piezocone in Clay. *Proc., 1st International Symposium on Penetration Testing, ESOPT-1*, Orlando, Fla., Vol. 2, 1988, pp. 777–783.
17. T. Lunne and A. Kleven. Role of CPT in North Sea Foundation Engineering. In *Cone Penetration Testing and Experience* (G. M. Norris et al., eds.), ASCE, New York, 1981, pp. 49–75.
18. K. Senneset and N. Janbu. Shear Strength Parameters Obtained from Static Cone Penetration Tests. In *Strength Testing of Marine Sediments*, ASTM STP 883, Philadelphia, Pa., 1985, pp. 41–54.
19. K. Senneset, N. Janbu, and G. Svanø. Strength and Deformation Parameters from Cone Penetration Tests. *Proc., 2nd European Symposium on Penetration Testing, ESOPT II*, Amsterdam, The Netherlands, Vol. 2, 1982, pp. 863–870.
20. S. Kirkebø. *Re-evaluation of the Bearing Capacity Factors  $N_q$ ,  $N_\gamma$ , and  $N_u$* . Diploma thesis. Geotechnical Division, Norwegian Institute of Technology, 1986.
21. K. Eggereide. Program Documentation for DATCPT (in Norwegian). O. Kummeneje A/S, Report No. 0.5024.3, 1985.
22. N. Janbu. Soil Compressibility as Determined by Oedometer and Triaxial Tests. *Proc., 3rd European Conference on Soil Mechanics and Foundation Engineering*, Wiesbaden, Germany, Vol. 1, 1963, pp. 19–25.
23. B. A. Torstensson. The Pore Pressure Probe. *Proc., NGF, Geoteknikdagen, Oslo*, 1977, pp. 34.1–34.15.
24. J. N. Levadoux and M. M. Baligh. Consolidation after Undrained Piezocone Penetration: I, Prediction. *Journal of Geotechnical Engineering*, Vol. 112, No. 7, 1986, pp. 707–726.

# Development of a Chart for Preliminary Assessments in Pavement Design Using Some In Situ Soil Parameters

SIBEL PAMUKCU AND H. Y. FANG

Much information has been generated from in situ soil tests conducted over the last two decades. Because of variations in mechanical and procedural details and the intended use of these tests, the information can be too specific, fragmented, or sometimes difficult to interpret. There is a need to gather and present this information on a common basis. The work presented in this paper introduces a practical approach that aims to address part of this need and to incorporate some in situ parameters in preliminary estimations for pavement design. The results of the study are preliminary. Nevertheless, the impact is twofold: the study is an initial effort to gather and present various in situ test information on a common basis and introduces direct utility of some in situ test parameters in broad estimation of bearing parameters in pavement design. The results of a great number of tests have been used to establish correlations between some in situ tests, and also to establish correlations between in situ parameters and soil properties. The well-known correlations are those between cone penetration (CPT) and standard penetration (SPT) tests, and between the soil type and the cone penetration, dilatometer (DMT), and pressuremeter (PMT) parameters. Four such correlations were incorporated into an existing design chart that included approximate interrelationships between soil classification, modulus of subgrade reaction, and California bearing ratio (CBR). The new correlations (SPT, CPT, PMT) were based on soil classification.

A chart showing approximate interrelationships between soil classification and bearing values has been satisfactorily utilized for rapid estimation of design parameters for foundations of pavements ( $I$ ). After an estimate of soil classification has been made, the chart can be very useful in arriving at approximate values for bearing and modulus of subgrade reaction in pavement design. The advent of in situ testing methods, and the rapid and often systematic manner with which soil data are obtained using these methods, have resulted in the accumulation of new information. The incorporation of this information into the currently used chart is timely.

Variations in the mechanics and procedures of the in situ tests, as well as problems encountered in data interpretation, can make it difficult to correlate parameters obtained through these tests. The existing correlations are often based on soil index properties and soil classification (2–5). The various in situ test parameters are used to predict the shear strength, stiffness, bearing capacity, or settlement of foundation soils.

Some of these parameters, or mathematical combinations of different measurements in a particular test, are also used as indices or coefficients with which to classify soils and predict overconsolidation ratio, consistency, or relative density. In this paper, such indices or parameters (6–10) were studied to establish the graphical correlations between them on the basis of soil classification.

The updated chart is basically intended as a quick reference with which to make reliable first approximations of the California bearing ratio (CBR) and modulus of subgrade reaction ( $k$ ) based on the measured in situ properties. The chart can be used to classify the soil or to estimate in situ properties once soil classification has been performed in the laboratory. Another important feature of the new chart is that it presents a comparison of soil classification predictions by three in situ tests.

## BACKGROUND

### Some In Situ Tests

Results of three tests are utilized in this study: the cone penetration test (CPT), the standard penetration test (SPT), and the self-boring pressuremeter test (SBPMT or PAF).

### Standard Penetration Testing

SPT (ASTM D1587) is one of the oldest sounding methods. It was developed in 1927. The blow count per foot ( $N$ ) is correlated with the relative density, the unit weight, and the angle of internal friction of soils.  $N$  is also used to estimate the allowable bearing capacity ( $q_a$ ) and elastic modulus ( $E_s$ ) of shallow foundations. Some correlations of SPT result in large scatter, and therefore the use of SPT alone is not generally recommended for design purposes. A well-known correlation of SPT and CPT is  $q_c/N$  versus mean grain size ( $D_{50}$ ) (6), shown in Figure 1. A more recent study presents the relationship between normalized CPT parameters and the SPT blow count ( $N$ ), as shown in Figure 2 (3). The basic advantages of using SPT are that the procedure has been widely used for a long time, resulting in a significant buildup of experience, and it is relatively simple and economical.

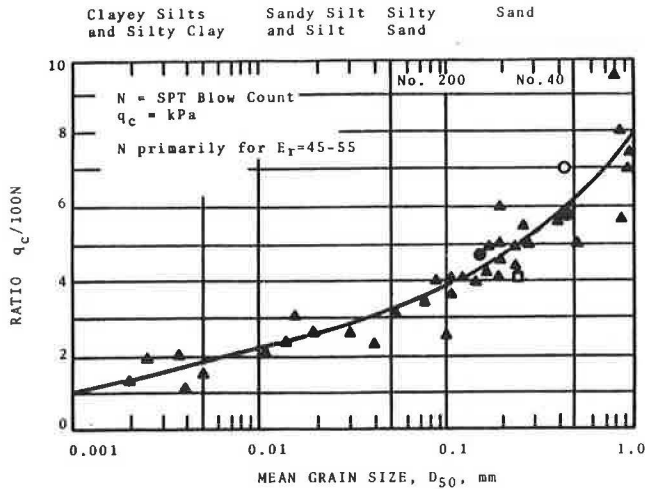


FIGURE 1 Relationship between grain size ( $D_{50}$ ) and  $q_c/100N$  ratio (6). ( $E_r$  = standard energy ratio;  $q_c$  = cone tip bearing.)

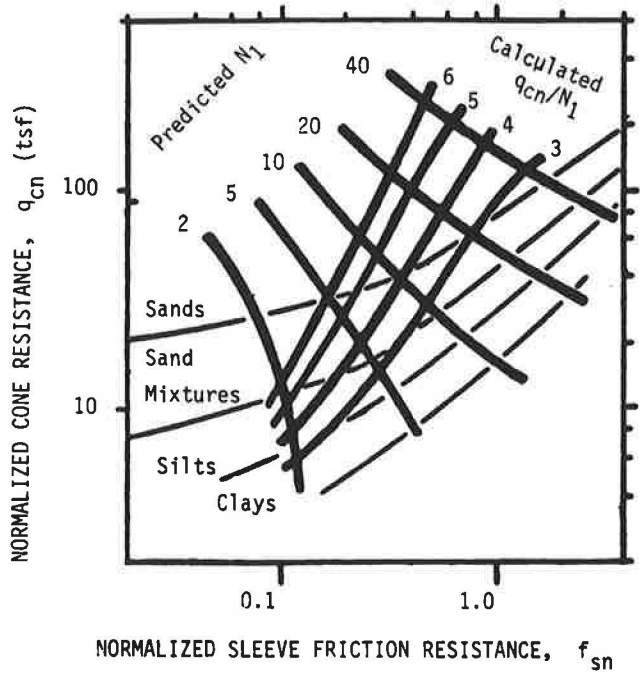


FIGURE 2 Normalized SPT blow count per foot versus normalized CPT parameters (3).

Cone Penetration Testing

Cone penetration testing (ASTM D3441) has become a versatile and reliable tool for continuous subsurface investigation. There are various types of cone penetrometers available (e.g., mechanical, electric, and seismic cones, and piezocones), and use has widened significantly over the years. The accumulation of information has resulted in the development of soil classification charts, as shown in Figures 2 and 3 (7). CPT data has much less scatter than SPT data, and its interpretation is more reliable; it is therefore recommended for foundation design purposes. The parameters obtained from CPT tests—tip bearing ( $q_c$ ), sleeve friction ( $f_s$ ), excess pore pressure ( $\Delta u$ ) with piezocone, and various mathematical com-

binations of these parameters—have been correlated with undrained shear strength ( $s_u$ ), ultimate bearing of shallow and deep foundations, the internal friction angle for sands, the elastic modulus ( $E_s$ ), the overconsolidation ratio (OCR), and soil classification (2,4,5,11-18).

Pressuremeter Testing

The borehole pressuremeter test has been widely used in France since it was first developed by Ménard in 1956 (19-22). Discussions of pressuremeter tests have been published by a number of investigators (21,23,24). The self-boring pressuremeter was developed to overcome some of the problems associated with the borehole PMT (i.e., borehole preparation and soil expansion) in the mid 1970s in France and England (19,25). Both of these pressuremeter tests have gained considerable usage, both in research and in practice, in the United States in recent years (26-29). The parameters obtained from PMT are used to predict bearing capacity and settlement of shallow foundations, and bearing capacity and axial and lateral displacement of piles. Some of the soil parameters obtained through PMT are undrained shear strength ( $s_u$ ), coefficient of lateral earth pressure at rest ( $K_0$ ) and tangent ( $E$ ) and secant ( $E_s$ ) soil moduli. The soil identification coefficient ( $\beta$ ), given in Equation 9, and net pressure applied at 20-percent strain ( $p_{20}$ ), are used to classify soils, as shown in Figure 4.

Bearing Values in Design of Pavements and Their Foundations

The existing design chart that provides approximate interrelationships of soil classification and bearing values includes ASTM soil classification (USC ASTM D2487); AASHTO soil classification (AASHTO M145); FAA soil classification, resistance value ( $R$ ) (ASTM D2844, AASHTO T190); modulus of subgrade reaction ( $k$ ) (Portland Cement Association); bearing value (ASTM D1195, D1196, or AASHTO T221, T222); and California bearing ratio (CBR) (ASTM D1883, AASHTO T193). This chart (1) has been used by practitioners to arrive at approximate numbers for the bearing values once a soil classification has been obtained through laboratory analysis. The chart is a rapid and reliable means of obtaining preliminary estimates of the required values of bearing.

The new chart presented here incorporates two soil classification systems (ASTM and AASHTO), the modulus of subgrade reaction, and the CBR. This is both for reasons of simplicity, and because of the existence of correlations between these parameters and the in situ parameters. These correlations were used in preparation and also in verification of the chart. The modulus of subgrade reaction ( $k$ ) is used in concrete pavement design. The thickness of the pavement can be determined through a design chart based on  $k$  and single axle load. The modulus of subgrade reaction is defined as the pressure per unit deformation of the subgrade. In the field, the determination of  $k$  for concrete pavement design is generally done for a deformation of 0.05 in., using a 30-in.-diameter plate. CBR is a punching shear test developed by the California Division of Highways. It is used by the U.S. Army

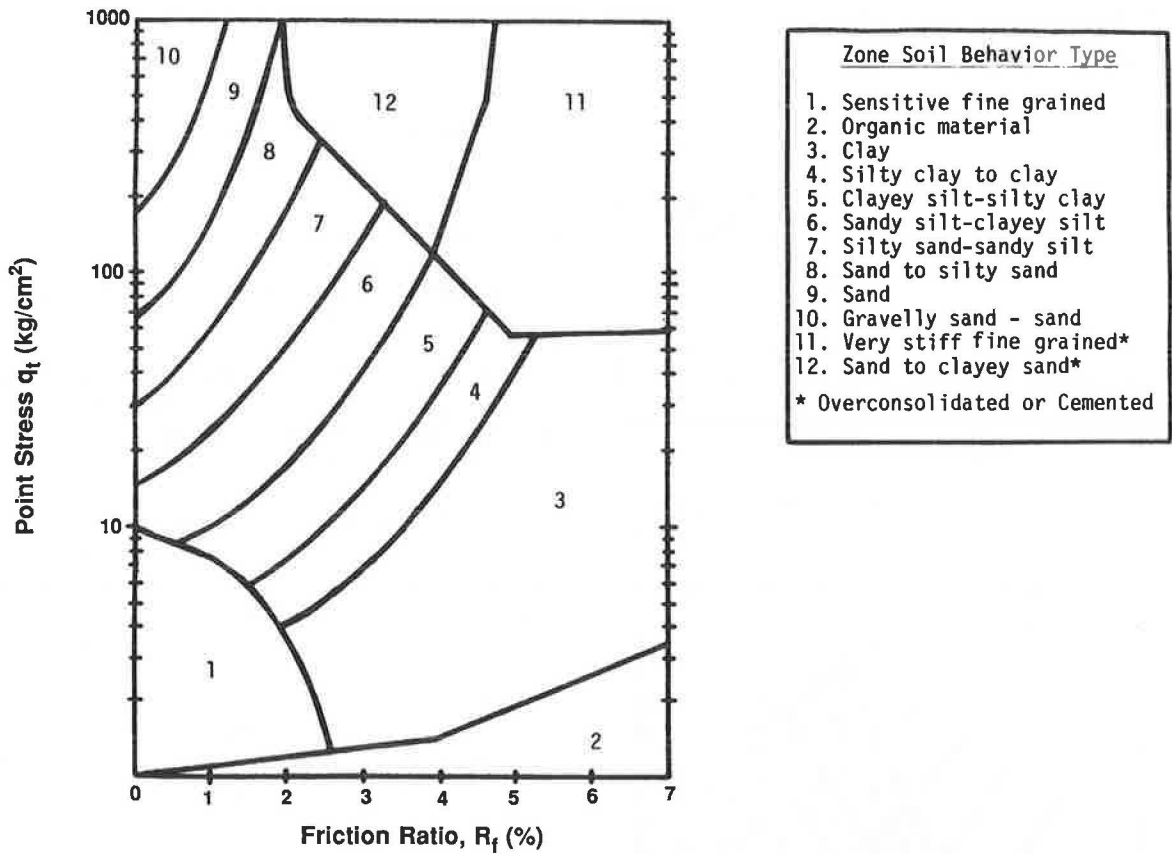


FIGURE 3 Soil classification system from CPT data (7).

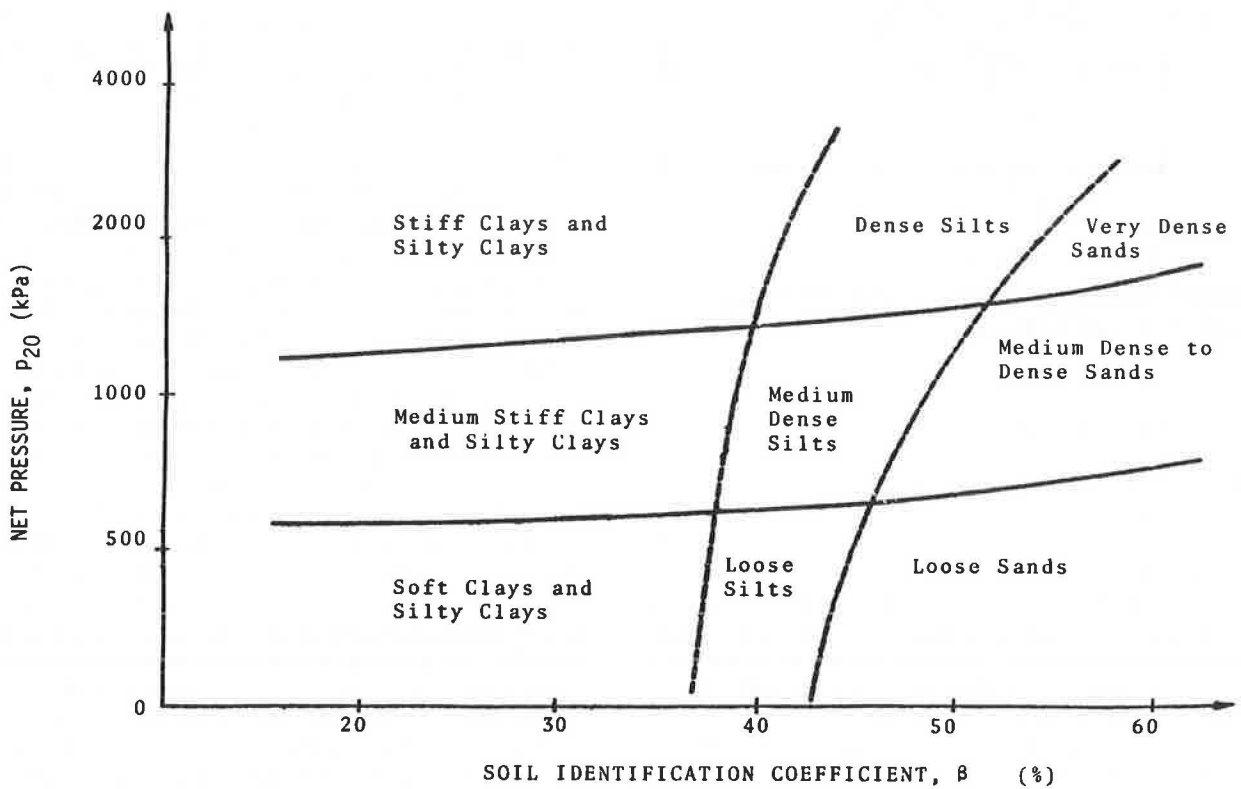


FIGURE 4 Soil classification based on self-boring pressuremeter data (9).

Corps of Engineers and by a number of highway departments to evaluate the bearing value of subgrade soils.

### DEVELOPMENT OF THE NEW CHART

A number of existing correlations were used in the development of the new chart. These correlations are presented with their references in Table 1. The intent was neither to disprove nor to verify these correlations but rather to use them as tools to develop the chart. The reader and possible users of the chart should be fully aware that these correlations and assumptions may or may not prove to be valid for certain soil types as new information and data bases develop. In such cases, modification of the chart would be warranted. Furthermore, it should be noted that it is important to verify the predictions and estimations made from this chart through field testing to ensure reliability and consistency. The work presented here does not include such verification.

Figure 5 shows the new chart. The CPT-SPT correlation was done using the  $q_c/100N$ -versus- $D_{50}$  relationship shown in Figure 1. The following equations were employed to arrive at approximate allowable bearing capacity values using the  $k$  and CBR values from the new chart (refer to Table 1 for references):

$$X_1 = q_c/q_a \quad (1)$$

$$q_c = 280 \times \text{CBR} \quad (2)$$

$$k = 40 \times \text{SF} \times q_a \quad (3)$$

$$k = 40 \times 280 \times \text{SF} \times \text{CBR}/X_1 \text{ (kPa/m)} \quad (4)$$

Using a safety factor (SF) of 3, which is an appropriate value for shallow foundations, the  $X_1$  values were evaluated. The chart description of soil type with respect to these values was found as follows:

$$q_c/10 < q_a < q_c/12 \quad \text{sand} \quad (5)$$

TABLE 1 CORRELATIONS USED IN DEVELOPMENT OF THE NEW CHART FOR PAVEMENT DESIGN

Correlation	Reference
$q_c/100 N$ vs. $D_{50}$ (Figure 1)	Robertson et al., 1983 (6)
$q_{cn}$ vs. $f_{sn}$ and $N$ (Figure 2)	Olsen and Farr, 1986 (3)
$q_t$ vs. $R_f$ (Figure 3)	Robertson et al., 1986 (7)
$p_{20}$ vs. $\beta$ (Figure 4)	Becue et al., 1986 (9)
$G_{p0}/G_{p2}$ and $G_{p2}/G_{p5}$ (Table 2) ratios vs. soil type	Jesequel and Le Mehaute, 1979 (20)
$q_c = 280 \times \text{CBR}$ (kPa)	Scala, 1954 (30); Sanglerat, 1972 (12)
$k = 40 \times \text{SF} \times q_a$ (kN/m <sup>2</sup> · m)	Bowles, 1988 (31)
$q_a = q_c/X_1$	Sanglerat, 1972 (12)

NOTE:  $q_c$  = cone tip bearing;  $N$  = SPT blow count/ft;  $D_{50}$  = mean grain size;  $q_{cn}$  = normalized cone tip bearing;  $f_{sn}$  = normalized sleeve friction;  $q_t$  = corrected tip bearing w.r.t. area ratio and pore pressure;  $R_f$  =  $f_s/q_t$  = friction ratio (%);  $p_{20}$  = SBPMT pressure at 20% strain (net pressure);  $\beta$  = SBPMT soil identification coefficient (%);  $G_{p0}$ ,  $G_{p2}$ ,  $G_{p5}$  = SBPMT shear moduli at 0% (initial), 2%, 5% strain; CBR = California bearing ratio;  $k$  = modulus of subgrade reaction;  $q_a$  = allowable bearing capacity; SF = safety factor; and  $X_1$  = factor that depends on soil and foundation type.

$$q_c/6 < q_a < q_c/10 \quad \text{clayey silt, silt, sandy silt} \quad (6)$$

$$q_c/4 < q_a < q_c/6 \quad \text{clay} \quad (7)$$

These values agree with the estimates given for shallow foundations with SF = 3 in cohesive and cohesionless soils, as summarized by Sanglerat (12). Using Equations 1 and 3 and the  $q_c/100N_{55}$  ratio from the new chart, approximate  $N$  values were estimated for different  $k$  values corresponding to different soil types. The resulting equations were:

$$X_2 = q_c/100N \quad (8)$$

$$N = (k \times X_1)/(40 \times 3 \times 100 \times X_2) \quad (9)$$

The calculated  $N$  values varied from 14 for well-graded sands to 2 for high-plasticity clays. These values were recognized to be somewhat on the low side. Backcalculating  $q_c$  using these  $N$  values resulted in good agreement with the  $q_c$  values that are shown in Figure 3 to correspond to various types of soils.

Figure 6 shows the variation of  $q_c/N$  with  $R_f/N$  calculated from Figure 2, and superimposed on it is the trend of the same data estimated from the chart. The chart values were found from the approximate relation between  $q_c/100N_{55}$  and  $q_c/100R_f$ . As observed from Figure 6, the values obtained from the chart that correspond to  $q_c/N$  values of 3, 4, 5, and 6 (where  $q_c$  is in tsf) fall well within the limits seen for soil classification ranges that correspond to the chart classification.

Finally, Figure 4 was utilized to correlate SBPMT parameters. The soil identification coefficient ( $\beta$ ) was directly related to the ASTM soil classification with respect to clays, silts, and sands. The following expression and the ratios presented in Table 2 (20) were utilized to arrive at the  $G_{p0}/p_{20}$  correlation shown in the new chart.

$$\beta = (p_{20} - p_5)/p_{20} \quad (9)$$

$$G_{p5} = p_5/0.05 \quad (10)$$

When using Table 2, average values of clay and sand ratios were calculated for silts.

### CONCLUSIONS

The new chart presented here incorporates parameters from three different in situ tests. The original chart has been used in pavement design to provide preliminary estimation of a range of bearing values corresponding to a given soil classification. The new additions to the chart increase its versatility. The chart presents a comparison of soil classification predictions using parameters from three different in situ tests. It can be used to make preliminary estimates of the bearing values of subgrade soil, and of the classification of subgrade soil with given in situ parameters. It can also be used to derive approximate correlations between different in situ parameters, to verify test results, or to identify areas where a more extensive and detailed data base is needed. The chart is based on various existing correlations and assumptions. In the future, new findings and enlarged data bases may warrant updating

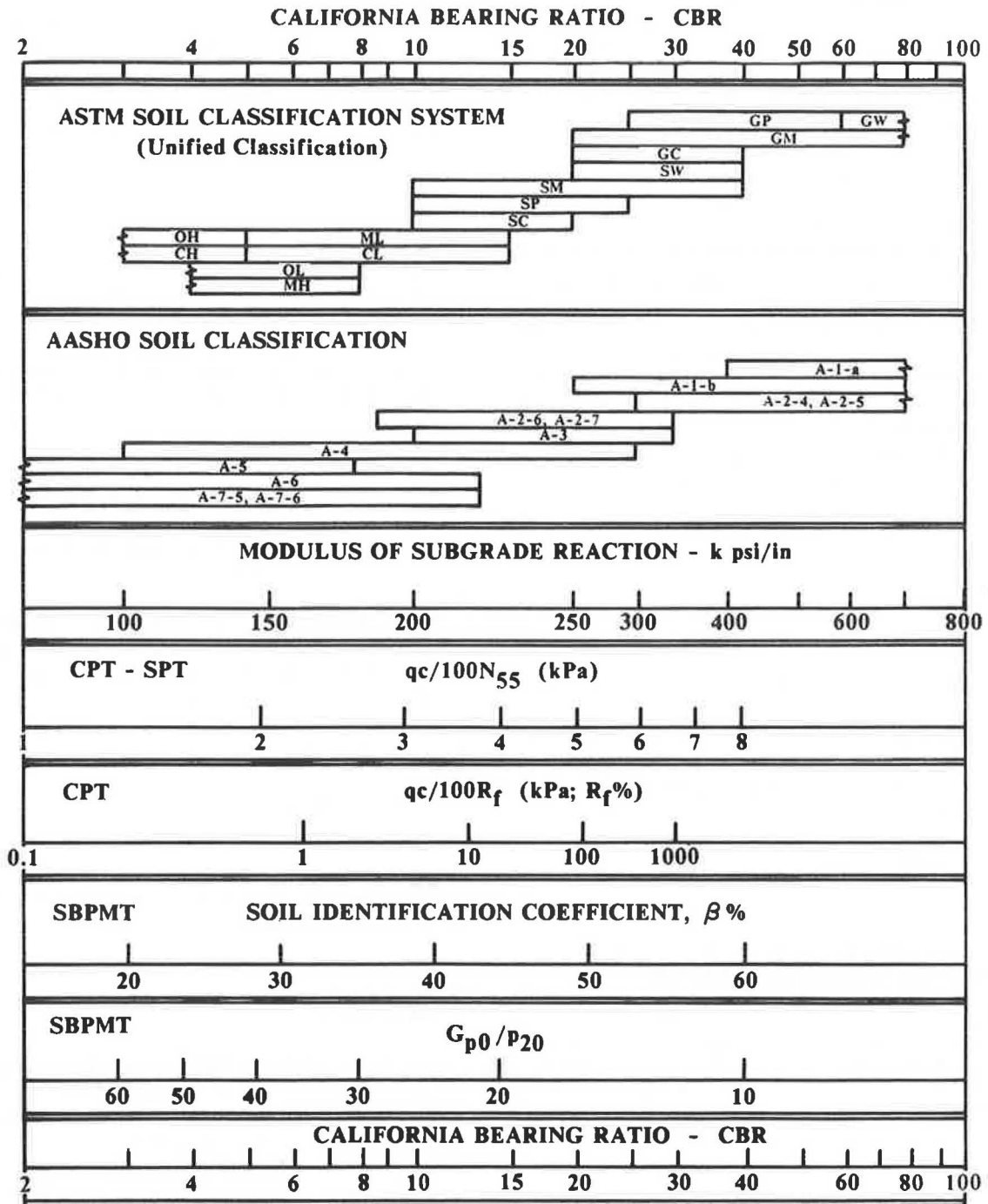


FIGURE 5 New chart for approximate interrelationships between soil classification, bearing values, and some in situ parameters ( $q_c$ , cone tip bearing;  $N_{55}$ , SPT blow count/ft at a standard energy ratio of 55;  $R_f$ , friction ratio (%);  $G_{p0}$ , shear modulus at 0% strain;  $p_{20}$ , pressure at 20% strain; CBR, California Bearing Ratio).



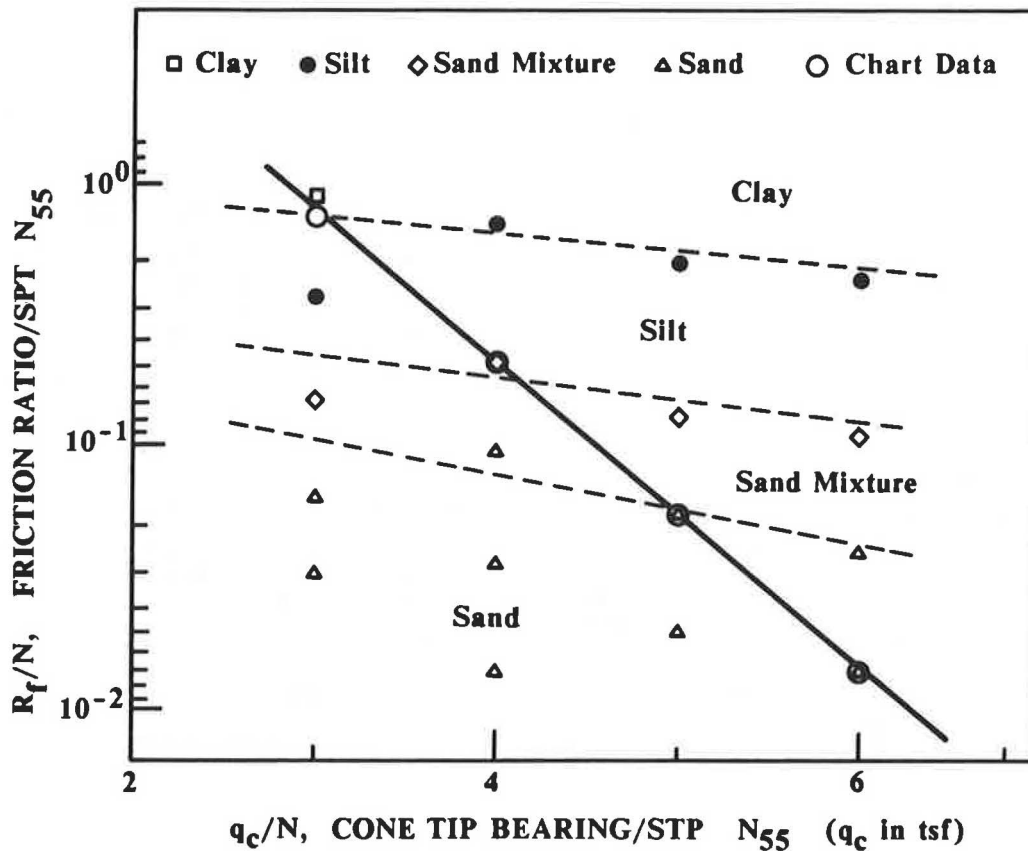


FIGURE 6 Comparison of the variation of  $R_f/N$  versus  $q_c/N$  from Olsen and Farr correlation (3) and the new chart with respect to soil classification.

TABLE 2 CORRELATIONS BETWEEN SBPMT AND PMT MODULI (20)

	$G_{p0}/G_{p2}$	$G_{p2}/G_{p5}$	$G_{p2}/G_M$	$G_{p5}/G_M$	$G_{p0}/G_M$
Clays	2.09	1.72	5.42	3.03	11.3
Sands	1.19	1.29	3.47	2.53	4.1

or modification of this chart. It should also be noted that field verification of the chart's predictions may be essential for reliable use of the chart.

REFERENCES

- Portland Cement Association. *PCA Soil Primer*. Portland Cement Association, Skokie, Ill. 1973.
- G. Aas, S. Lacasse, T. Lunne, and K. Hoeg. Use of In Situ Tests for Foundation Design on Clay. In *Use of In Situ Tests in Geotechnical Engineering* (S. P. Clemence, ed.), ASCE Geotechnical Special Publication No. 6, ASCE, New York, 1986, pp. 1-30.
- R. S. Olsen and J. V. Farr. Site Characterization Using the Cone Penetrometer Test. In *Use of In Situ Tests in Geotechnical Engineering* (S. P. Clemence, ed.), ASCE Geotechnical Special Publication, No. 6, ASCE, New York, 1986, pp. 854-868.
- P. K. Robertson and R. G. Campanella. Interpretation of Cone Penetration Tests: Part I, Sand. *Canadian Geotechnical Journal*, Vol. 20, 1983, pp. 718-733.
- P. K. Robertson and R. G. Campanella. Interpretation of Cone Penetration Tests: Part II, Clay. *Canadian Geotechnical Journal*, Vol. 20, 1983, pp. 734-745.
- P. K. Robertson, R. G. Campanella, and A. Wightman. SPT-

- CPT Correlations. *Journal of Geotechnical Engineering*, Vol. 109, No. 11, 1983, pp. 1449-1459.
- P. K. Robertson, R. G. Campanella, D. Gillespie, and J. Greig. Use of Piezometer Cone Data. In *Use of In Situ Tests in Geotechnical Engineering* (S. P. Clemence, ed.), ASCE Geotechnical Special Publication No. 6, ASCE, New York, 1986, pp. 1263-1280.
- S. Lacasse and T. Lunne. Dilatometer Tests in Sand. In *Use of In Situ Tests in Geotechnical Engineering* (S. P. Clemence, ed.), ASCE Geotechnical Special Publication No. 6, ASCE, New York, 1986, pp. 686-699.
- J. P. Becue, B. Francoise, and P. Le Tirant. Proposed Method for Application of Pressuremeter Test Results to Designing of Offshore Foundations. In *The Pressuremeter and Its Marine Applications* (L. J. Briaud, ed.), ASTM STP 950, ASTM, Philadelphia, Pa., 1986, pp. 357-375.
- F. J. Baquelin, M. G. Bustamante, and R. A. Frank. The Pressuremeter for Foundations: French Experience. In *Use of In Situ Tests in Geotechnical Engineering* (S. P. Clemence, ed.), ASCE Geotechnical Special Publication No. 6, ASCE, New York, 1986, pp. 31-46.
- M. T. Tumay and M. Fakhroo. Pile Capacity in Soft Clays Using Electric QCPT Data. *Proc., Session on Cone Penetration Testing and Experience*, ASCE, St. Louis, Mo., 1981, pp. 434-454.
- G. Sanglerat. *The Penetrometer and Soil Exploration*. Elsevier Publishing Co., New York, 1972.
- H. T. Durgunoglu and J. K. Mitchell. Static Penetration Resistance of Soils: Part I, Analysis. In *In-Situ Measurement of Soil Properties*, ASCE Geotechnical Special Publication, ASCE, New York, Vol. 1, 1975, pp. 151-171.
- M. Jamiolkowski, R. Lancellotta, L. Tordella, and M. Battaglio. Undrained Strength from CPT. *Proc., 2nd European Symposium on Penetration Testing, ESOPT II*, Amsterdam, The Netherlands, Vol. 2, 1982, pp. 599-606.

15. B. J. Douglas and R. S. Olsen. Soil Classification Using Electric Cone Penetrometer. *Proc., Session on Cone Penetration Testing and Experience*, ASCE, St. Louis, Mo., 1981, pp. 209–227.
16. M. M. Baligh, V. Vivatrat, and C. C. Ladd. Cone Penetration in Soil Profiling. *Journal of the Geotechnical Engineering Division*, ASCE, Vol. 106, No. GT4, 1980, pp. 447–461.
17. P. W. Mayne. CPT Indexing of In Situ OCR in Clays. In *Use of In Situ Tests in Geotechnical Engineering* (S. P. Clemence, ed.), ASCE Geotechnical Special Publication No. 6, 1986, pp. 780–793.
18. J. H. Schmertmann. *Guidelines for Cone Penetration Test, Performance and Design*. Report 5 No. FHWA-TS-78-209. FHWA, U.S. Department of Transportation, 1978.
19. F. Baquelin et al. Self-Boring Placement Method of Soil Characteristics Measurement. *Proc., Conference on Subsurface Exploration for Underground Excavation and Heavy Construction*, ASCE, 1974, pp. 312–322.
20. J. F. Jezequel and A. Le Mahute. *The Self-Boring Pressuremeter Model 76 (PAF 76) User's Manual*. (J. Canou, translator; M. T. Tumay, ed.). Geotechnical Engineering Report No. GE-84/05. Louisiana State University, Department of Civil Engineering, November 1984 (original publication, 1979), 104 pp.
21. E. Winter. Suggested Practice for Pressuremeter Testing in Soils. *Geotechnical Testing Journal*, Vol. 5, No. 3, 1982, pp. 85–88.
22. J. L. Briaud and M. Gambin. Suggested Practice for Drilling Boreholes for Pressuremeter Testing. *Geotechnical Testing Journal*, Vol. 7, No. 1, 1984, pp. 36–40.
23. H. Y. Fang. Discussion of Pressuremeter Correlation Study. In *Highway Research Record 284*, HRB, National Research Council, Washington, D.C., 1969, pp. 61–62.
24. J. H. Schmertmann. *Measurement of In Situ Shear Strength*. State-of-the-Art Paper to Session III, *Proc., Conference on In Situ Measurement of Soil Properties*, Raleigh, N.C., Vol. 2, 1975, pp. 57–139.
25. C. P. Wroth. In Situ Measurement of Initial Stresses and Deformation Characteristics. *Proc., Conference on In Situ Measurement of Soil Properties*, Raleigh, N.C., Vol. 2, ASCE, New York, 1986, pp. 181–230.
26. J. L. Briaud. Pressuremeter and Foundation Design. In *Use of In Situ Tests in Geotechnical Engineering* (S. P. Clemence, ed.), ASCE Geotechnical Special Publication No. 6, ASCE, New York, 1986, pp. 74–115.
27. J. Canou and M. T. Tumay. Field Evaluation of French Self-Boring Pressuremeter PAF 76 in Soft Deltaic Louisiana Clay. In *The Pressuremeter and Its Marine Applications* (L. J. Briaud and M. E. Audibert, eds.), ASTM STP 950, ASTM, Philadelphia, Pa., 1986, pp. 97–118.
28. G. W. Clough and G. M. Denby. Self-Boring Pressuremeter Study on San Francisco Bay-Mud. *Journal of the Geotechnical Engineering Division*, ASCE, Vol. 106, No. GT1, January 1980, pp. 45–63.
29. J. Benoit and G. W. Clough. Self-Boring Pressuremeter Tests in Soft Clay. *Journal of Geotechnical Engineering*, Vol. 112, No. 1, 1986, pp. 60–78.
30. A. J. Scala. The Use of Cone Penetration in Determining the Bearing Capacity of Soils: Simple Methods of Flexible Pavement Design Using Cone Penetrometers. *Proc., Australia-New Zealand Conference on Soil Mechanics and Foundation Engineering*, 2nd, Canterbury University, 1954, pp. 73–84.
31. J. E. Bowles. *Foundation Analysis and Design*, 4th ed., McGraw-Hill Book Company, New York, 1988.

---

*Publication of this paper sponsored by Committee on Soil and Rock Properties.*

# Design Parameters of Cohesionless Soils from In Situ Tests

R. BELLOTTI, V. N. GHIONNA, M. JAMIOLKOWSKI, AND P. K. ROBERTSON

A critical review of interpretation methods for estimating the design parameters of cohesionless soils from in situ test methods is presented. The latest correlations and results from more than 10 years of research using large calibration chambers are presented and discussed. Correlations are also evaluated and discussed using field data from several well-documented sites. Emphasis is placed on the estimation of in situ state parameters ( $D_R$ ), soil stiffness ( $G$ ,  $E'$ ), and soil strength ( $\phi'$ ) using in situ test methods such as the cone penetration test (CPT), the standard penetration test (SPT), and the flat dilatometer test (DMT). Guidelines are provided regarding the limitations of existing interpretation methods.

One of the major advantages of in situ testing is that it can be used to test soil deposits in which undisturbed sampling is very difficult and often unreliable. Hence the use of in situ testing, especially penetration testing, in cohesionless soils has always played an important role in geotechnical engineering.

In this paper the authors attempt to summarize the experience that they have gained from more than 10 years of research using in situ test techniques in cohesionless soils. This research has included controlled laboratory studies using large calibration chambers (CCs), as well as field experience in many natural deposits.

Because of space limitations, discussion will be limited to the evaluation of relative density, deformation moduli, and friction angle from various penetration tests (i.e., SPT, CPT, and DMT).

The methods for interpreting in situ tests used to obtain geotechnical parameters can be divided into three main categories (1):

- The soil elements follow very similar effective stress paths. Therefore, with appropriate assumptions on drainage conditions and stress-strain relationships, the solution of a more or less complex boundary value problem can lead to the determination of stress-strain and strength characteristics. This category of interpretation method is used for tests including pressuremeter tests, especially the self-boring pressuremeter test (SBPT), and seismic tests.

- The soil elements follow different effective stress paths depending on the geometry of the problem and the magnitude of the applied load. In this case, a rational interpretation of the test is very difficult. Even with appropriate assumptions concerning the drainage conditions and soil model, the solu-

tion of a complex boundary value problem leads to something like "average" soil characteristics. Comparisons between these average values and the behavior of a typical soil element tested in the laboratory, or the use of these values in the specific design calculation, are far from straightforward. Typical examples of tests subject to this category of interpretation method are the plate load test (PLT) and the cone penetration test (CPT) when interpreted for evaluating soil strength.

- The soil elements follow different effective stress paths, and the in situ test results are empirically correlated to selected soil properties. Typical examples are the widely used correlations between penetration resistance measured in the standard penetration test (SPT) and CPT and deformation moduli ( $E$ ). Because these correlations are purely empirical in nature, they are subject to many limitations, which are not always fully recognized by potential users. In addition, it is important to recognize that these empirical correlations are formulated for either fully drained or fully undrained conditions.

Interpretations of all penetration tests fall into the last two groups.

The major sources of uncertainty in the interpretation of many in situ tests are related to the following:

- Complex boundary value problem;
- Complex, and often unknown, drainage conditions;
- Complex variation in stress and strain levels; and
- Complex influence of stress path-dependent soil behavior, i.e., anisotropy, and plasticity.

Because of these uncertainties, interpretation of most penetration tests is based on empirical correlations to selected soil properties. Because of the purely empirical nature of these correlations, it is important to be aware of their many limitations. Often the correlations are only partly able to account for soil nonlinearity and plasticity, as well as other complexities in natural soils, such as mineralogy, in situ stress state, stress-strain history, cementation, sensitivity, anisotropy, and structure (fabric).

To fully define soil behavior, it is necessary to identify the following main characteristics:

- Initial state, which includes stress-strain history;
- Strength;
- Deformation; and
- Flow and consolidation.

For most soils, this requires a minimum of about 9 or 10 independent parameters. Unfortunately, most existing pen-

R. Bellotti, ENEL-CRIS, Via Ornato, 90/14, Milano, Italy. V. N. Ghionna and M. Jamiolkowski, Technical University of Turin, Department of Structural Engineering, Corso Duca degli Abruzzi, 24 I-10129 Turin, Italy. P. K. Robertson, Civil Engineering Department, University of Alberta, Edmonton, Alberta, Canada, T6G 2G7.

etration tests only provide 2 or 3 independent measurements for interpretation. Therefore, it is presently impossible to fully identify all the parameters that control soil behavior. However, there is clearly potential in the newer combined in situ tests that provide additional *independent* measurements, such as the seismic cone penetration test (2,3) and the cone pres-suremeter test (4,5).

**DISCUSSION OF EXISTING CORRELATIONS**

The term *initial state* incorporates the following:

- Macro- and microstructure;
- Initial total vertical and horizontal geostatic stresses ( $\sigma_{v,0}$  and  $\sigma_{h,0}$ , respectively);
- Initial pore pressure ( $u_0$ ), which is not necessarily hydro-static;
- Initial void ratio ( $e_0$ ) and/or relative density ( $D_R$ ); and
- Vertical yield stresses ( $\sigma'_{vy} = \sigma'_p$ ) or overconsolidation ratio (OCR).

Unfortunately, most of the initial state factors are difficult to individually identify and quantify using in situ testing, espe-cially penetration tests, because the penetration resistance is generally influenced to different degrees by almost all of the factors.

The dominant influence of initial horizontal stress ( $\sigma'_{h0}$ ) on penetration resistance has long been well recognized on the basis of the results of large calibration chamber tests (6-11).

Figure 1 presents a summary of CPT penetration resistance ( $q_c$ ) data for very dense Ticino sand obtained from calibration chamber tests. The CPT  $q_c$  data has been correlated with the effective horizontal stress acting on the boundary of the CC during penetration ( $\sigma'_{h75}$ ). Because the  $q_c$  data was obtained at a penetration depth of 75 cm in the 1.5-m-deep CC, the horizontal stress has been designated  $\sigma'_{h75}$ . Details of the method adopted for measuring  $\sigma'_{h75}$  have been described by Belotti et al. (8). Figure 1, which refers to very dense samples, shows that the influence of CC size and boundary effects is essen-tially removed if correlations are based on the effective hori-zontal stress acting on the boundary at the time of penetra-tion. The data in Figure 1 also indicate the dominant influence of the in situ horizontal stress on penetration resistance.

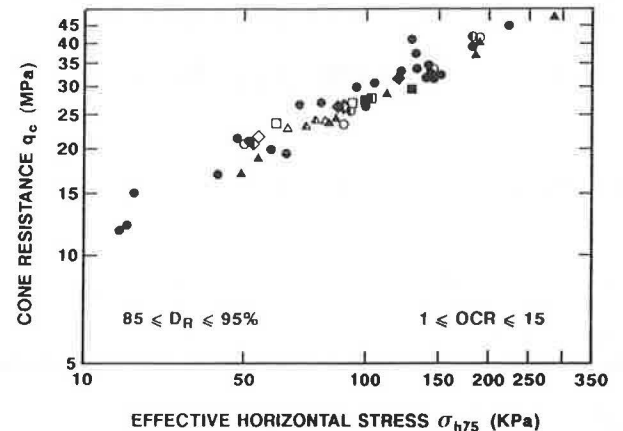
The importance of  $\sigma'_{h0}$  for the penetration resistance mea-sured by any penetration test (e.g., SPT or CPT) has impor-tant implications for the interpretation of parameters such as relative density ( $D_R$ ) and friction angle ( $\phi'$ ).

On the basis of extensive CC studies (7, 12), the following relationship has been derived for Ticino sand (TS) to evaluate  $D_R$  (see also Figure 2):

$$D_R = \frac{1}{2.38} \ln \left( \frac{q_c}{248(\sigma'_{h0})^{0.55}} \right) \tag{1}$$

where  $q_c$  and  $\sigma'_{h0}$  are in kPa (1 ton/ft<sup>2</sup> = 107 kPa = 0.107 MPa). As noted, this correlation was based on CC data, where  $d_c$  denotes cone diameter, and 20 mm  $\leq d_c \leq$  35.7 mm;  $D_R$  denotes relative density, and 16 percent  $\leq D_R \leq$  98 percent; OCR denotes overconsolidation ratio, and 1  $\leq$  OCR  $\leq$  15.

$$q_c = 28 f p_a \left( \frac{\sigma'_{h75}}{p_a} \right)^{0.55} \quad p_a = 1 \text{ bar}, \quad R^2 = 0.94$$



SYM	●	○	□	■	◇	△	▽	◇	◇	
d (mm)	35.7	25.4	20.0	35.7	25.4	20.0	35.7	25.4	20.0	
Boundary conditions	B1 $\sigma'_v = \text{CONST.}$ $\sigma'_h = \text{CONST.}$			B2 $\epsilon_v = 0$ $\epsilon_h = 0$			B3 $\sigma'_v = \text{CONST.}$ $\epsilon_h = 0$		B4 $\sigma'_h = \text{CONST.}$ $\epsilon_v = 0$	

FIGURE 1 Cone resistance versus effective horizontal stress as measured in 59 calibration chamber tests in very dense Ticino sand.

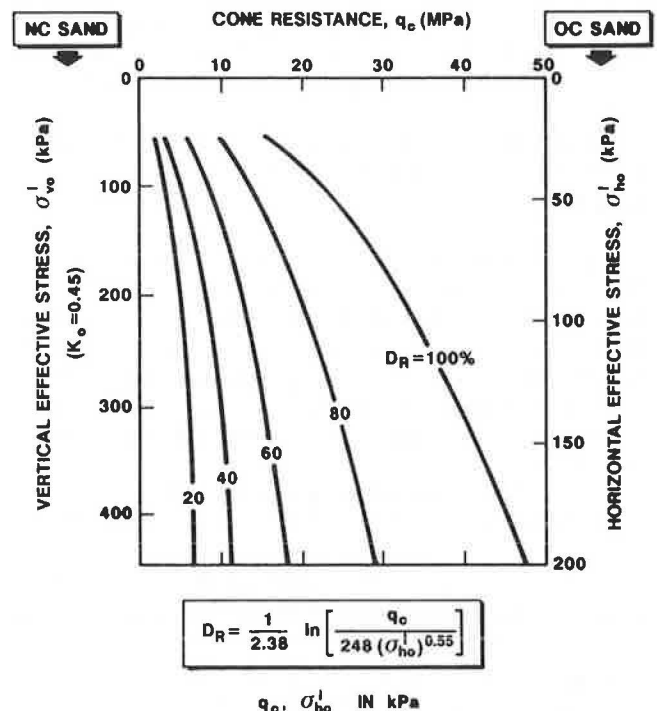


FIGURE 2 Relative density correlation for uncemented, unaged silica sand (Ticino sand) [after Baldi et al. (12)].

Bellotti et al. also derived this correlation from CC data, using all the available boundary conditions (8).

Robertson and Campanella (13) have stressed the importance of the effect of sand compressibility on penetration resistance. Figure 3 illustrates the variation in the  $D_R$  correlations from CC studies around the world due to changes in sand compressibility for predominantly silica sands (14). Highly compressible sands, such as sands with a high carbonate content (greater than 80 percent), may fall outside the range shown in Figure 3.

Figure 2 can be used as a guide for evaluation of in situ relative density ( $D_R$ ) for clean, predominantly silica sand. Figure 3 can be used to evaluate the uncertainties involved in the determination of  $D_R$  from  $q_c$  for sands that may be more or less compressible than Ticino sand. The compressibility of sands tends to increase with decreasing uniformity of grading, increasing angularity of grains, increasing fines content, and increasing mica or carbonate content. Ticino sand is a uniform, clean, predominantly silica sand ( $D_{50} = 0.53$  mm) with subangular to subrounded grains. For normally consolidated (NC) sands, the vertical effective stress ( $\sigma'_{v0}$ ) can be applied to Figure 2, assuming  $K_0 = 0.45$ . If overconsolidated (OC) sands are encountered, the horizontal effective stress ( $\sigma'_{h0}$ ) should be applied in Figure 2. However, the application to OC sands is difficult because of the inherent difficulties in evaluating an appropriate value of  $K_0$ .

Recently, Skempton (15) has demonstrated the importance of aging in the interpretation of the SPT in cohesionless soils. Because the CC correlations were developed on pluvially

deposited unaged and uncemented sands, it is likely that the  $D_R$ -versus- $q_c$  correlations (Figure 2) will lead to overestimation of  $D_R$  when applied to natural sand deposits. However, the same correlations will underestimate  $D_R$  if they are applied to more crushable and compressible sands or to sands containing more than 5 to 10 percent fines.

In conclusion, the evaluation of  $D_R$  from penetration resistance suffers from some uncertainties because all the correlations were established on freshly deposited, uncemented sands, and because the correlations are referenced to  $\sigma'_{v0}$ , so that their application is correct only in NC, unaged sand deposits.

## DEFORMATION CHARACTERISTICS

There has always been great practical interest in estimating deformation characteristics (moduli) from penetration resistance in cohesionless soils (16–18), because undisturbed sampling is almost impossible or is not cost-effective. However, as mentioned earlier, the interpretation of penetration tests suffers from many limitations that make the assessment of deformation characteristics very difficult. The matter is further complicated by the tenuous links to the relevant drainage conditions, stress paths, and stress or strain level of the specific design project.

The deformation characteristics of a given soil depend on

- The stress and strain history of the deposit, intended in the broadest sense of the term (10);
- The current level of mean effective stress;
- The induced level of shear strain;
- The effective stress path followed, reflecting both soil anisotropy and plasticity; and
- A time factor whereby factors such as viscous hardening (aging) and creep (in shear) influence the stress-strain response.

Therefore, the correct, safe use of correlations between penetration resistance and soil moduli is influenced, at least qualitatively, by the engineer's skill in taking all of the above factors into account.

In the last decade, significant improvements in our theoretical understanding of the stress-strain behavior of sands, combined with a large number of experimental observations, have resulted in a more rational understanding of the reliability and limitations of such empirical correlations.

These findings can be summarized as follows:

1. The influence of overconsolidation on a cohesionless soil can be considered twofold: strain hardening due to accumulated plastic strains, and an increase in  $K_0$  (i.e.,  $K_0^{OC} > K_0^{NC}$ ). The latter is conventionally linked with mechanical overconsolidation and possibly aging, whereas plastic hardening generally appears as a consequence of all types of preconsolidation mechanisms, i.e., aging, cementation, desiccation, low-strain cyclic stress history, and so forth.

2. Small- and large-scale laboratory (CC) tests have shown that penetration resistance is strongly influenced by the current level of  $\sigma'_{h0}$  and is almost totally insensitive to the effects of plastic strain hardening (19). This indicates that the large strains caused by penetration mostly destroy the effects of

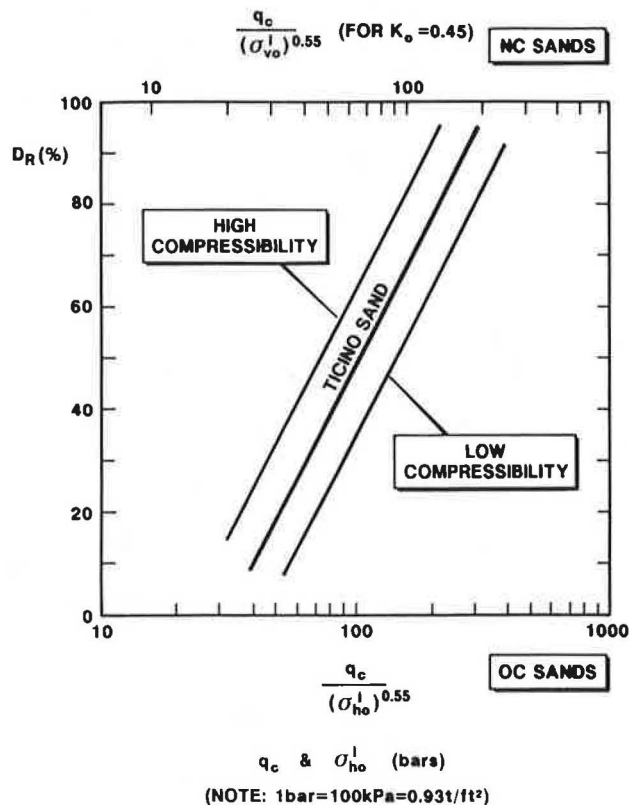


FIGURE 3 Influence of compressibility on evaluation of relative density from CPT.

plastic hardening, which is often the predominant factor caused by overconsolidation.

3. Results of CC tests show that all kinds of penetration resistances are more sensitive to  $\sigma'_{h0}$  than to  $\sigma'_{v0}$ .

Figures 4 and 5 show correlations between the CC results of CPTs and flat dilatometer tests (DMTs), and the deformation characteristics ( $E'_s$ ) of the predominantly silica Ticino sand (TS) (9,12).

The following comments should be of help in the examination of these figures:

- Cone resistance is denoted by  $q_c$ , and  $E_D$  is the dilatometer modulus measured at mid-height in pluvially deposited CC specimens.
- $E'_s$  corresponds to the secant drained Young's modulus inferred from  $CK_0D$  triaxial compression tests performed on pluvially deposited TS in a Bishop-Wesley triaxial cell. The  $E'_s$  values refer to a given effective mean consolidation stress ( $\sigma'_{m0}$ ) and to a level of axial strain ( $\bar{\epsilon}_a$ ) of 0.1 percent in OC sand and 0.1 and 0.25 percent in NC sand. On the basis of a numerical study of shallow foundations in TS performed using finite element methods, Battaglio and Jamiolkowski (20) concluded that these values of  $\bar{\epsilon}_a$  correspond to the upper limit and operational range of the average strain levels of practical interest for OC and NC sand.

A review of Figures 4 and 5 reveals some common features, which can be summarized as follows:

- Even for the same sand, the ratio of the reference modulus ( $E'_s$ ), to the penetration test result ( $q_c, E_D$ ) is substantially

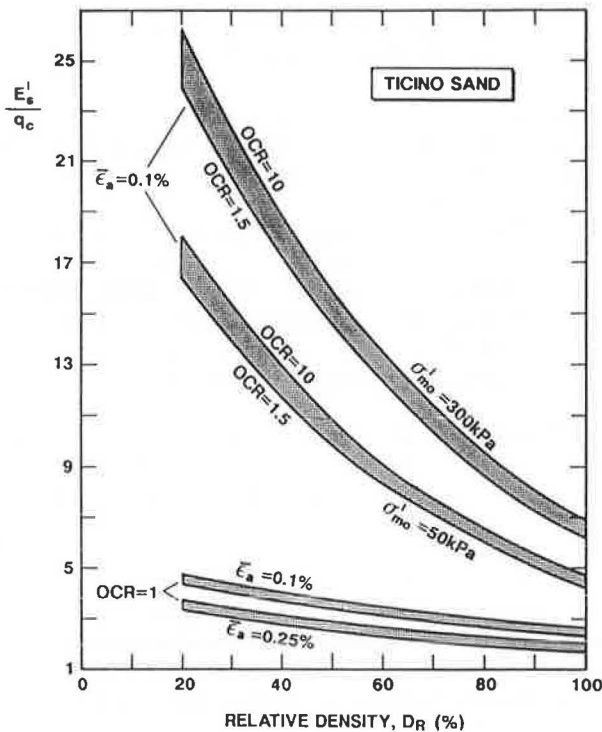


FIGURE 4 Drained Young's modulus of Ticino sand versus cone resistance.

FOR NC TICINO SAND		
(37 TESTS):	$\frac{E'_s}{E_D} = 1.05 \pm 0.25$	
TICINO	1	●
	1.5 to 8.5	○
FOR OC TICINO SAND		
(22 TESTS):	$\frac{E'_s}{E_D} = 3.66 \pm 0.80$	
HOKKSUND	1	■
	3.0 to 8.3	□

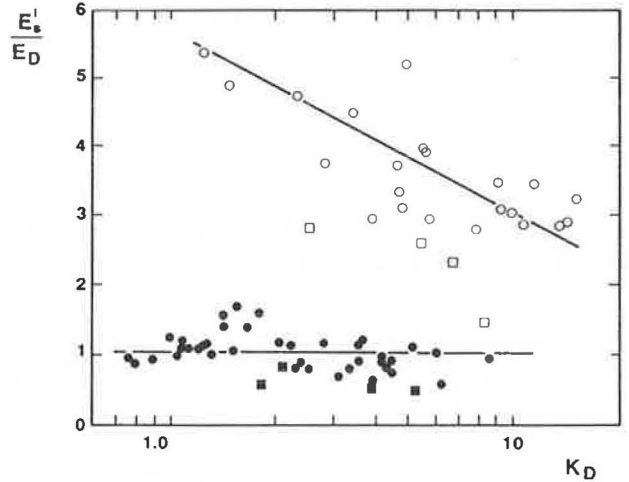


FIGURE 5 Drained Young's modulus versus dilatometer modulus from CC tests.  $E'_s$  = drained Young's modulus from TX- $CK_0D$  tests at  $\epsilon_a = 0.1\%$ .

higher for mechanically OC specimens than for NC specimens. This trend, which is observed in all silica sands and for all kinds of penetration tests validated in CCs around the world, reflects very high sensitivity of the reference moduli and low sensitivity of the penetration test results to the strain and stress history of the sand.

- The ratio under discussion decreases as the relative density ( $D_R$ ) of sand increases. This reflects the different effects of a change in  $D_R$  on the reference modulus and the penetration resistance.

In view of the above statements it appears obvious that, for a given sand, no unique correlation exists between penetration resistance and the nonlinear deformation moduli. The nonlinear moduli are defined here as the moduli at a strain level greater than the elastic threshold strain  $\gamma_t^e$  (21). Below  $\gamma_t^e \approx 10^{-5}$ , the shear modulus is practically constant and equal to the maximum shear modulus ( $G_0$ ).

The above statements result from CC studies performed on freshly deposited silica sands. Further research is necessary to evaluate to what extent these findings are applicable to natural sands and to sands that are not silica. The writers believe, however, that at least qualitatively similar overall trends should be expected in natural aged sands.

For natural aged sand deposits (age  $\geq 1,000$  years), the writers believe that the correlations between penetration resistance and moduli, for example  $E'_s$  and  $q_c$ , may lie somewhere between the NC and OC sand correlations developed for unaged sands in the CC studies, as shown in Figure 6.

The correct application of empirical correlations between

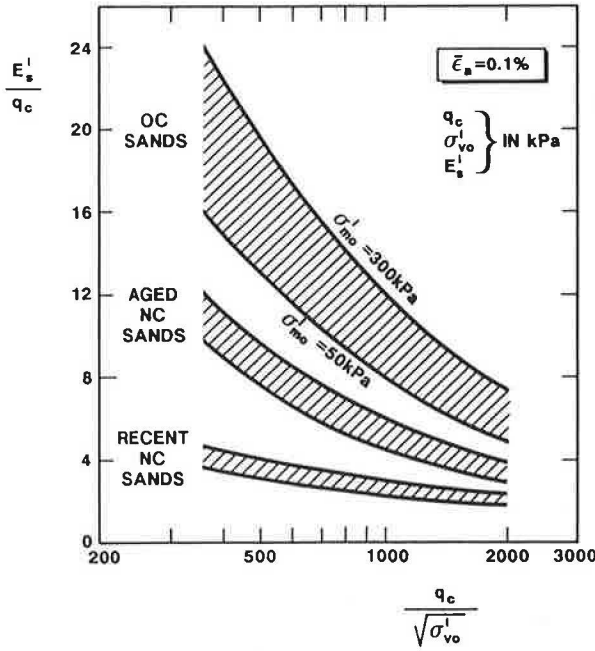


**FIGURE 6** Evaluation of drained Young's modulus from CPT for silica sands.

penetration resistance and moduli must take into account the strong influence of stress and strain history. Most existing methods that estimate the settlement of shallow foundations on sands from SPT, CPT, and DMT results make a clear distinction between NC and OC sands. However, in practice, the OCR of sands is usually unknown, which is a major limitation of these correlations. Further developments are required to quantify the improvement due to stress history and to evaluate this stress history on the basis of results of penetration tests or other in situ tests.

The foregoing statements and comments lead to a rather negative attitude as far as the reliability of existing correlations between penetration resistance and nonlinear deformation moduli is concerned. However, correlations with the maximum shear modulus ( $G_0$ ) measured at shear strain levels less than  $10^{-5}$  are a notable exception (13, 22–27).

A large amount of experimental data show that  $G_0$  in cohesionless soils is influenced very little by the stress and strain history. For a given sand,  $G_0$  is primarily a function of three variables (28):

$$G_0 = f(D_R, \sigma'_a, \sigma'_b) \quad (2)$$

where

- $\sigma'_a$  = effective stress acting in the direction of seismic wave propagation, and
- $\sigma'_b$  = effective stress acting in the direction of soil particle displacement.

These same basic variables ( $D_R$  and  $\sigma'$ ) influence penetration resistance. This suggests that correlations between  $G_0$  and penetration resistance (e.g.,  $q_c$  or  $N_{SPT}$ ) might be more reliable than those relating penetration resistance to larger strain moduli. To support this point, an example of the Ohta

and Goto correlation (23) between  $N_{SPT}$ , corrected to an energy ratio of 60 percent, and shear wave velocity ( $V_s$ ), is shown in Figure 7, where it is compared with measured  $V_s$  from cross-hole (CH) tests. Figure 7 shows that the Ohta and Goto (23) correlation provides a good estimate of  $V_s$  for clean Holocene sands. However, with increasing age and gravel content, the correlation underestimates the shear wave velocity.

Examples of CPT and DMT correlations for the evaluation of  $G_0$  are shown in Figures 8 and 9. These correlations are based on extensive CC studies. Figures 8 and 9 also include data from crosshole and seismic cone penetration tests performed at the Po River sand site, near Viadana, Italy. Although the CC data was obtained on recently deposited, unaged sand, the results in Figures 8 and 9 for Viadana Po River sand, which has an age of up to about 20,000 years at 30 m depth, show remarkably good agreement.

The application of correlations such as those shown in Figures 7 through 9 depends heavily on the development of a link between the evaluated moduli and the geotechnical design problem. The type of link will depend on the "average" strain level expected in the design problem. Geotechnical engineers have traditionally considered small strain moduli ( $G_0$ ) to be applicable only to dynamic problems, such as machine foundations or low-magnitude earthquakes. However, recent studies (20,29) have shown that with an appropriate correction for strain level, the  $G_0$  moduli can also be useful for most well-designed static foundation problems in sand. These studies have shown that for most well-designed foundations in sand, the "average" strain in the soil is generally less than 0.1 percent.

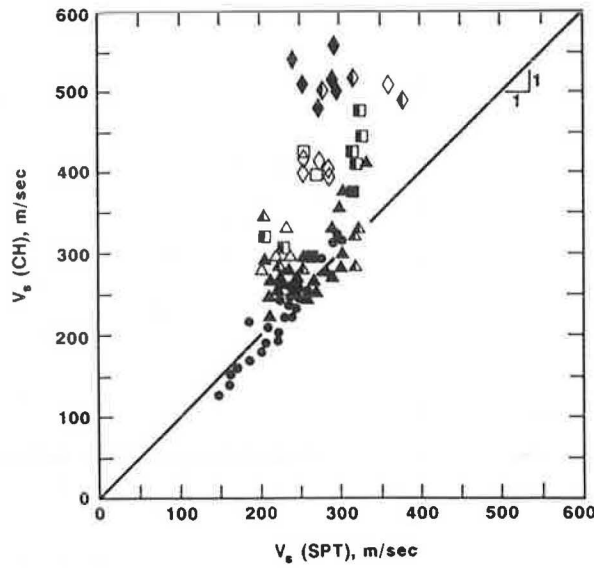
### SHEAR STRENGTH

Interpretation of in situ test results to assess shear strength has always been done with reference to either fully undrained or fully drained conditions (saturated cohesive deposits or cohesionless deposits, respectively). In coarse-grained soils where penetration takes place under drained conditions, the test results are used to evaluate the drained shear strength expressed as the friction angle ( $\phi'$ ). In fine-grained saturated soils where penetration takes place under essentially undrained conditions, the test results are used to evaluate shear strength in terms of total stresses expressed as the undrained shear strength ( $s_u$ ). The results of penetration testing involving intermediate (partially drained) conditions cannot be rationally interpreted at present.

The most important aspect of the shear strength behavior of granular soils is their nonlinear failure envelope (30,31). Because of the nonlinearity of the strength envelope, the angle  $\phi'$  of a given sand is not uniquely defined but depends on the magnitude of the effective normal stress on the failure plane at failure ( $\sigma'_{ff}$ ). Therefore, any value of  $\phi'$  inferred from in situ test results corresponds to a secant angle of friction whose magnitude is related to some value of  $\sigma'_{ff}$ .

For many in situ tests,  $\sigma'_{ff}$  is usually taken as the average value acting on the failure plane around the in situ device. Unfortunately, the evaluation of  $\sigma'_{ff}$  around most in situ test devices is difficult, especially for penetration tests.

Existing methods for estimating  $\phi'$  from penetration test results are based on the following:



LOCATION	AGE	FINES CONTENT %	GRAVEL CONTENT %	D <sub>60</sub> mm	N. OF TEST	V <sub>s</sub> (SPT) / V <sub>s</sub> (CH) ±1SD	[Er] %	SYMBOL	
VIADANA PO RIVER SAND	HOLOCENE	0 TO 28	0	0.1 TO 0.4	29	1.01±0.11	7.2	●	
SALUGGIA DORA RIVER SAND AND GRAVEL	HOLOCENE	8 TO 22	0 TO 10	0.5	10	0.74±0.09	26.5	■	
			10 TO 50	0.3 TO 0.6				□	
			>50	7 TO 11				△	
GIOIA TAURO SAND AND GRAVEL	HOLOCENE ? PLEISTOCENE	1 TO 20	0 TO 10	0.1 TO 0.5	33	0.89±0.12	14.0	▲	
			10 TO 50	0.3 TO 1.0				△	
			>50	3 TO 6				△	
TRINO VERCELLESE PO RIVER SAND AND GRAVEL	PLEISTOCENE	8 TO 25	0 TO 10	0.2 TO 0.5	16	0.61±0.09	36.5	◆	
			10 TO 12	10 TO 50				0.2 TO 0.6	◇
			6 TO 10	>50				4.2 TO 10.8	◇

FIGURE 7 Shear wave velocity from N<sub>SPT</sub> [using formula by Ohta and Goto (23)].

- Empirical correlations, where the nonlinearity of the strength envelope may or may not be included.
- Bearing capacity theories based on rigid plastic soil models. These theories are unable to account for the influence of soil compressibility or crushability.
- Cavity expansion theories, which can account for nonlinearity of strength envelope and soil compressibility. However, they require a knowledge of additional soil parameters such as K<sub>0</sub>, G, and volumetric strain (ε<sub>v</sub>); their use in practice is therefore difficult.

The cavity expansion theories (32,33), have been shown to model the measured response of cone penetration extremely well (12,34). However, the cavity expansion analysis is somewhat complex and requires considerable input data regarding soil compressibility and shear strength.

Bearing capacity theories, such as those presented by Durgunoglu and Mitchell (35), will give conservatively low estimates of φ' for compressible sands (i.e., carbonate sands).

A recent approach that deserves further comment is the empirical method developed by Bolton (36). The shear strength of cohesionless soils is related to the rate of dilation at failure, which in turn depends on the relative density, the level of mean effective stress, and the soil compressibility. These factors are reflected in Rowe's stress-dilatancy theory (37), which

recently was given a simple but conceptually sound formulation by Bolton (36,38). Bolton (36) showed that the peak secant friction angle (φ'<sub>s</sub>) from triaxial tests of many sands can be estimated from the empirical expression

$$\phi'_s = \phi'_{cv} + 3I_R \tag{3}$$

where φ'<sub>cv</sub> is the friction angle at constant volume, and I<sub>R</sub> is a relative dilatancy index given by

$$I_R = D_R(Q - \ln p'_f) - 1 \tag{4}$$

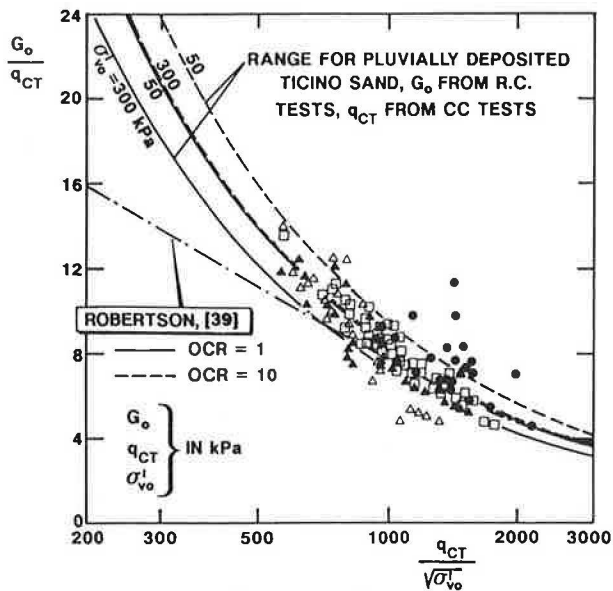
D<sub>R</sub> being the relative density, p'<sub>f</sub> the mean effective stress at failure, and Q a constant depending on the compressibility and mineralogy of the sand. Bolton (36) suggested a general value of Q = 10 for most silica sands.

The generalized variation of φ'<sub>s</sub> - φ'<sub>cv</sub> for silica sand proposed by Bolton (36) is shown in Figure 10. Figure 11 presents results of triaxial tests on Hokksund sand to evaluate Bolton's generalized formulation. Although Hokksund sand is a predominantly silica sand, Bolton's formulation underpredicts φ'<sub>s</sub> by about 2 to 3 degrees.

Bolton's formulation represents a useful tool for evaluating φ'<sub>s</sub> from cone penetration resistance (q<sub>c</sub>). A method that uses Bolton's formulation to derive φ'<sub>s</sub> was proposed by Jamiol-

INCREASING AGE





	SITE	SOIL	G <sub>0</sub> SOURCE	BOREHOLE
△	VIADANA	MEDIUM SAND	CROSS-HOLE	4017
▲	VIADANA	MEDIUM SAND	SEISMIC CONE	4017
□	S. PROSPERO	MEDIUM SAND	SEISMIC CONE	16 17
●	GIOIA TAURO	SAND WITH GRAVEL	CROSS-HOLE	209 219

DEPTH BELOW G.L. CONSIDERED: 5.5 TO 43.5 m

FIGURE 8 Correlation of  $q_{CT}$  versus  $G_0$  in uncemented, predominantly quartz sands. Depth below ground level considered: 5.5–43.5 m.

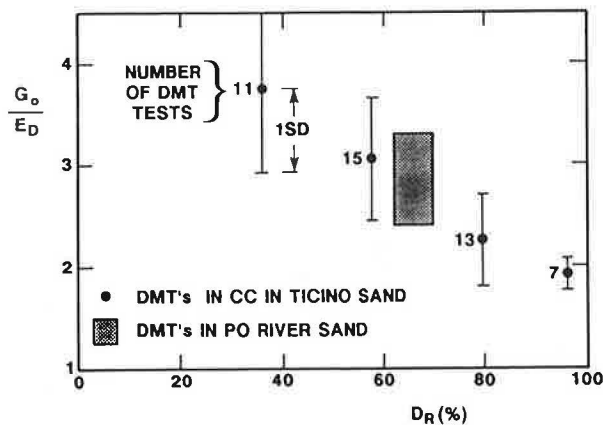


FIGURE 9  $G_0$  versus  $E_d$  for Ticino sand ( $G_0$  from RCTs) and Po River sands ( $G_0$  from cross-hole test).

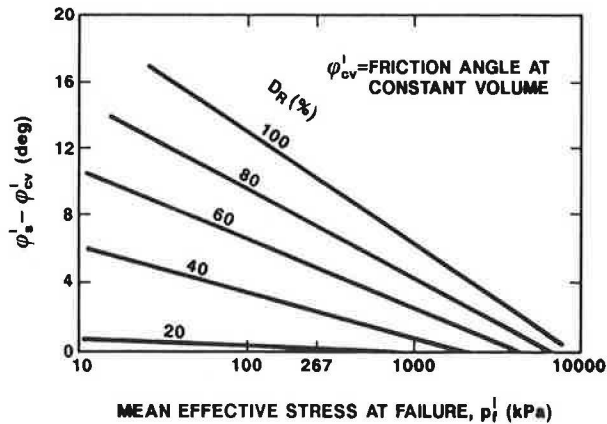


FIGURE 10 Generalized variation of triaxial peak  $\phi'_s$  with mean effective stress [after Bolton (36)].

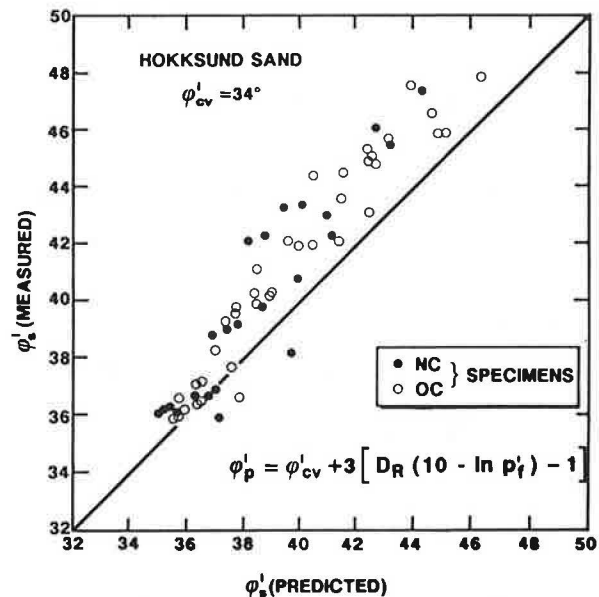


FIGURE 11 Validation of Bolton's dilatancy theory (38).

kowski et al. (1). Figure 12 shows the proposed correlation for silica sand relating CPT  $q_c$  to peak secant friction angle  $\phi'_0$  defined at a stress level of  $\sigma'_{ff} = 267$  kPa.

The peak secant friction angle in Figure 12 has been defined at a specific stress level ( $\sigma'_{ff} = 267$  kPa) because of the non-linearity of the failure envelope. This stress level results from the application of the nonlinear strength envelope proposed by Baligh (33) where;

$$\tan \phi'_s = \tan \phi'_0 + \tan \alpha \left( \frac{1}{2.3} - \log_{10} \frac{\sigma'_{ff}}{p_a} \right) \quad (5)$$

where

- $\phi'_s$  = peak secant friction angle at  $\sigma'_{ff}$
- $\sigma'_{ff}$  = effective normal stress on the failure plane at failure,
- $p_a$  = reference stress, assumed equal to 98.1 kPa,
- $\phi'_0$  = secant angle of friction at  $\sigma'_{ff} = 267$  kPa, and

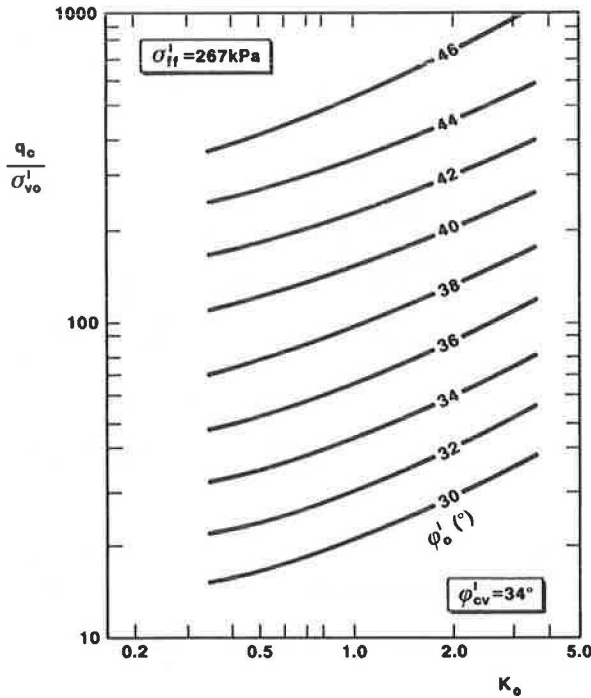


**FIGURE 12** Friction angle  $\phi'_o$  of silica sand using Bolton's stress-dilatancy theory (36) [adapted from Jamiolkowski et al. (1)].

$\alpha$  = angle that describes the curvature of the failure envelope.

Full details on the derivation of the correlation shown in Figure 12 are given by Jamiolkowski et al. (1).

Baldi et al. (12) have shown that  $\alpha$  increases with increasing  $D_R$ . As a first approximation, the value of  $\alpha$  can be evaluated for silica sands using the following expression:

$$\alpha = \left( \frac{D_R - 0.2}{0.8} \right) \cdot 10 \quad \text{for } \alpha \geq 0 \text{ degrees} \quad (6)$$

The  $\phi'_s$  mobilized at stress levels higher than  $\sigma'_{ff} = 267$  kPa can be evaluated using Baligh's (33) expression (Equation 5) and an estimate of  $\alpha$  calculated from Equation 6. The variation of  $\phi'_s$  with stress level can also be estimated using Figure 10 and the following relationship to relate  $\sigma'_{ff}$  to  $p'_f$ , which is derived from Mohr's circle at failure:

$$p'_f \approx \sigma'_{ff} \left( \frac{3 - \sin \phi'_s}{3 \cos^2 \phi'_s} \right) \quad (7)$$

However, the correct evaluation and application of  $\phi'_s$  also require an evaluation of the appropriate average stress at failure applicable to the relevant design problem (30).

To evaluate the effectiveness of the correlation shown in Figure 12, a comparison was made between measured  $\phi'_s$  in triaxial tests and those obtained from CPT  $q_c$ . Results of the comparison for Hokksund sand, which is a uniform, medium ( $D_{50} = 0.4$  mm) silica sand, is shown in Figure 13.

Figure 13 shows good agreement between measured  $\phi'_s$  and predicted  $\phi'_s$  using Figure 12. However, Bolton's formulation again tends to underpredict  $\phi'_s$  by about 2 degrees for Hokksund sand (see Figure 11). To incorporate variations in sand compressibilities, there is a need to define the empirical constant  $Q$  in relation to sand compressibility and mineralogy. Fortunately, the prediction of  $\phi'_s$  from penetration resistance is not sensitive to moderate variations in sand compressibility, especially for predominantly silica sands.

A review of Figure 12 also shows that the prediction of  $\phi'_s$  is not sensitive to  $K_o$ . Therefore, if  $K_o$  is unknown it is reasonable to assume a value of  $K_o \approx 0.5$  for most NC sands and  $0.5 \leq K_o < 1.0$  for most OC sands in order to evaluate  $\phi'_s$ .

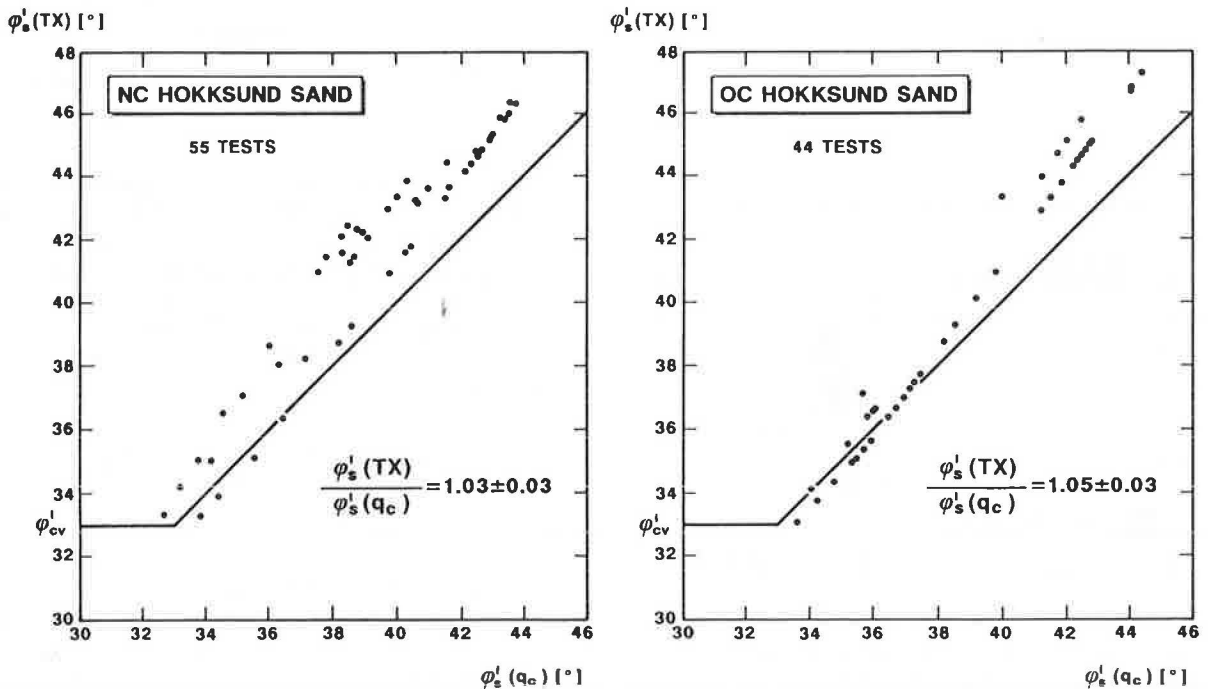


**FIGURE 13** Evaluation of  $\phi'_s$  from CPT ( $q_c$ ) for Hokksund sand using Bolton's stress-dilatancy theory (36).

To improve the interpretation of  $\phi'_s$  from penetration test results, further improvements are required to take into account

- Soil compressibility,
- In situ stress state ( $K_0$ ); and
- Nonlinearity of the strength envelope ( $\sigma'_{ff}$ ).

However, when  $\phi'_s$  is to be evaluated from penetration tests in predominantly silica sands, reasonable predictions can be obtained using correlations such as that shown in Figure 12.

## SUMMARY

A brief review of interpretation methods for estimating design parameters of cohesionless soils on the basis of in situ tests has been presented. This discussion has concentrated on the interpretation of relative density ( $D_R$ ), deformation moduli ( $E'_s$ ,  $G_0$ ), and friction angle ( $\phi'$ ) from cone penetration tests (CPT) and the flat dilatometer test (DMT), and  $G_0$  from the standard penetration test (SPT).

Experience gained from over 10 years of testing using large calibration chambers has shown that the existing empirical correlations are often unable to fully account for complexities in natural soils resulting from stress-strain nonlinearity, mineralogy, in situ stress state, stress-strain history, and aging. Research has also shown the following main points:

- Penetration resistance ( $q_c$ ,  $N_{SPT}$ ) is dominated by the in situ horizontal stress ( $\sigma'_{h0}$ );
- Correlations for the evaluation of  $D_R$  are strongly influenced by soil compressibility;
- No unique correlations exist between penetration test results ( $q_c$ ,  $E_D$ ) and nonlinear deformation moduli ( $E'_s$ ,  $M_t$ ) because the correlations are strongly influenced by the stress history (OCR) of the deposit;
- Good correlations exist between penetration resistance ( $q_c$ ,  $N_{SPT}$ ) and the small strain shear modulus ( $G_0$ ), at least for most clean, unaged, silica sands; and
- Correlations between penetration resistance ( $q_c$ ) and peak secant friction angle ( $\phi'_s$ ) are not very sensitive to in situ ( $K_0$ ).

Further improvements are required to account for soil compressibility and in situ stress state in the interpretation of penetration tests in cohesionless soils. Further developments are also required to improve the link between interpreted geotechnical parameters and specific design problems.

## ACKNOWLEDGMENTS

The writers would like to acknowledge the support provided by the Hydraulic and Structural Research Center of the Italian National Electricity Board (ENEL-CRIS) of Milan, the Experimental Institute for Models and Structures (ISMES) of Bergamo, the Technical University of Turin, and the University of British Columbia.

## REFERENCES

1. M. Jamiolkowski, V. N. Ghionna, R. Lancellotta, and E. Pasqualini. New Correlations of Penetration Tests for Design Prac-

- Proc., *Penetration Testing 1988, ISOPT-1*, Orlando, Fla., 1988.
2. R. G. Campanella and P. K. Robertson. A Seismic Cone Penetrometer to Measure Engineering Properties of Soil. *Proc., 54th Annual International Meeting and Exposition of the Society of Exploration Geophysicists*, Atlanta, Georgia, 1984.
3. P. K. Robertson, R. G. Campanella, D. Gillespie, and A. Rice. Seismic CPT to Measure In Situ Shear Wave Velocity. *Journal of Geotechnical Engineering*, Vol. 112, No. 8, 1986, pp. 791-803.
4. N. J. Withers, L. H. J. Schaap, K. J. Kolk, and J. C. P. Dalton. The Development of the Full Displacement Pressuremeter. In *The Pressuremeter and Its Marine Applications* (L. J. Briaud and M. E. Audibert, eds.), ASTM STP 950, ASTM, Philadelphia, Pa., 1986.
5. R. G. Campanella and P. K. Robertson. Research and Development of the UBC Cone Pressuremeter. *Proc., 3rd Canadian Conference on Marine Geotechnical Engineering*, Newfoundland, Canada, 1986.
6. J. Holden. *Research on the Performance of Soil Penetrometers*. Churchill Fellowship 1970, Country Road Board of Victoria, 1971.
7. J. H. Schmertmann. An Updated Correlation between Relative Density,  $D_R$ , and Fugro-Type Electric Cone Bearing,  $q_c$ . Unpublished report. U.S. Army Waterways Experiment Station, Vicksburg, Miss., 1976.
8. R. Bellotti, G. Bizzi, and V. Ghionna. Design, Construction and Use of a Calibration Chamber. *Proc., 2nd European Symposium on Penetration Testing, ESOPT II*, Amsterdam, The Netherlands, 1982.
9. G. Baldi, R. Bellotti, V. Crippa, C. Fretti, V. N. Ghionna, M. Jamiolkowski, D. Ostricati, E. Pasqualini, and S. Pedroni. Laboratory Validation of In Situ Tests. *Proc., 11th International Conference on Soil Mechanics and Foundation Engineering*, San Francisco, Calif. AGI Jubilee Volume, 1985.
10. M. Jamiolkowski, C. C. Ladd, J. T. Germaine, and R. Lancellotta. New Developments in Field and Laboratory Testing of Soils. Theme Lecture, *Proc., 11th International Conference on Soil Mechanics and Foundation Engineering*, San Francisco, Calif., 1985.
11. G. Houlsby and R. Hitchmann. *Calibration Chamber Tests of a Cone Penetrometer in Sand*. Oxford University Report OUEL 1699/87, Soil Mechanics Report No. SMO74/87. Oxford University, Oxford, England, 1987.
12. G. Baldi, R. Bellotti, N. Ghionna, M. Jamiolkowski, and R. Lancellotta. Interpretation of CPT's and CPTU's: Part II, Drained Penetration on Sands. *Proc., 4th International Geotechnical Seminar on Field Instrumentation and In Situ Measurements*, Nanyang Technical Institute, Singapore, 1986.
13. P. K. Robertson and R. G. Campanella. Interpretation of Cone Penetration Tests. *Canadian Geotechnical Journal*, Vol. 20, 1983.
14. R. Lancellotta. Analisi di affidabilità in ingegneria geotecnica. *Atti Istituto Scienza Costruzioni*, No. 625, Politecnico di Torino, 1983.
15. A. W. Skempton. Standard Penetration Test Procedures and the Effects in Sands of Overburden Pressure, Relative Density, Particle Size, Aging, and Overconsolidation. *Géotechnique*, Vol. 36, No. 3, pp. 425-447.
16. K. Terzaghi and R. B. Peck. *Soil Mechanics in Engineering Practice*. John Wiley & Sons, New York, 1948.
17. E. De Beer. Settlements Records of Bridges Founded on Sand. *Proc., 2nd International Conference on Soil Mechanics and Foundation Engineering*, Rotterdam, The Netherlands, 1948.
18. G. G. Meyerhoff. Discussion of Session 1. *Proc., 4th International Conference on Soil Mechanics and Foundation Engineering*, London, England, 1957.
19. J. R. Lambrechts and G. A. Leonards. Effects of Stress History on Deformation of Sand. *Journal of the Geotechnical Engineering Division, ASCE*, Vol. 104, No. GT11, 1978.
20. M. Battaglio and M. Jamiolkowski. Analisi delle deformazioni. *XIII Ciclo Conferenze di Geotecnica di Torino, Italy*, 1987.
21. R. Dobry, D. J. Powell, F. Y. Yokel, and R. S. Ladd. Liquefaction Potential of Saturated Sand—The Stiffness Method. *Proc., 7th World Conference on Earthquake Engineering*, Istanbul, Turkey, 1980.
22. Y. Ohta and N. Goto. Estimation of S-Wave Velocity in Terms of Characteristic Indices of Soil (in Japanese). *Bitsuri-Tanko*, Vol. 29, No. 4, 1976, pp. 34-41.

23. Y. Ohta and N. Goto. Empirical Shear Wave Velocity Equations in Terms of Characteristic Soil Indexes. *Earthquake Engineering and Structural Dynamics*, Vol. 6, 1978.
24. D. W. Sykora and K. H. Stokoe. *Correlations of In-Situ Measurements in Sands of Shear Waves Velocity, Soil Characteristics and Site Conditions*. Geotechnical Engineering REP GR 83-33. University of Texas at Austin, 1983.
25. R. Bellotti, N. Ghionna, M. Jamiolkowski, R. Lancellotta, and G. Manfredini. Deformation Characteristics of Cohesionless Soils from In Situ Tests. *Proc., In Situ '86*, ASCE Specialty Conference, Virginia Tech, Blacksburg, Va., 1986.
26. G. J. Rix. *Correlation of Elastic Moduli and Cone Penetration Resistance*. M.S. thesis. University of Texas at Austin, 1984.
27. D. Lo Presti. *Behaviour of Ticino Sand during Resonant Column Test*. Ph.D. thesis. Technological University of Turin, Turin, Italy, 1987.
28. S. H. H. Lee and K. H. Stokoe. *Investigation of Low-Amplitude Shear Wave Velocity in Anisotropic Material*. Geotechnical Engineering Report GR86-6. Civil Engineering Department, University of Texas at Austin, 1986.
29. R. J. Jardine, D. M. Potts, A. B. Fourie, and J. B. Burland. Studies of the Influence of Non-Linear Stress-Strain Characteristics in Soil Structure Interaction. *Géotechnique*, Vol. 36, No. 3, 1986.
30. E. E. De Beer. Influence of the Mean Normal Stress on the Shear Strength of Sand. *Proc., 6th International Conference on Soil Mechanics and Foundation Engineering*, Montreal, Quebec, Canada, 1965.
31. A. S. Vésic and G. W. Clough. Behaviour of Granular Materials under High Stresses. *Journal of the Soil Mechanics and Foundations Division, ASCE*, Vol. 94, No. SM3, 1968.
32. A. S. Vésic. Expansion of Cavities in Infinite Soil Mass. *Journal of the Soil Mechanics and Foundations Division, ASCE*, Vol. 98, No. SM3, 1972.
33. M. M. Baligh. Cavity Expansion in Sand with Curved Envelopes. *Journal of the Geotechnical Engineering Division, ASCE*, Vol. 102, No. GT11, 1976.
34. J. K. Mitchell and J. Keaveany. Determining Sand Strength by Cone Penetrometer, *Proc., In-Situ '86*, ASCE Specialty Conference, Virginia Tech, Blacksburg, Virginia, 1986.
35. H. T. Durgunoglu and J. K. Mitchell. Static Penetration Resistance of Soils: Part I, Analysis. *Proc., Conference on In Situ Measurement of Soil Properties*, Raleigh, N.C., Vol. 1, ASCE, New York, 1975.
36. M. D. Bolton. The Strength and Dilatancy of Sands. *Géotechnique* Vol. 36, No. 1, 1986.
37. P. W. Rowe. The Stress-Dilatancy Relation for Static Equilibrium of an Assembly of Particles in Contact. *Proceedings of the Royal Society*, 1962.
38. M. D. Bolton. *The Strength and Dilatancy of Sands*. CUED/D-Soils/TR 152. University of Cambridge, Cambridge, England, 1984.

---

Publication of this paper sponsored by Committee on Soil and Rock Properties.

# Italian Motorway System: Experiences with In Situ Tests and Inclinometer Surveys for Urgent Remedial Works

T. COLLOTTA, R. CANTONI, AND P. C. MORETTI

**This paper deals with the philosophy adopted by the company Autostrade SpA for the maintenance of a motorway network about 2700 km long. A case study of a slope failure is presented to illustrate the application of this philosophy. In particular, a possible misjudgment in the design of remedial works performed only on the basis of quick in situ tests is reported. Because of the importance of inclinometer surveys in dealing with slope failures, some useful observations about processing criteria for inclinometer data are presented. The procedures adopted to avoid or, when possible, to overcome instrumentation errors are also discussed.**

Since the opening of the first multilane motorways in the 1960s, routine landslide monitoring has consisted almost entirely of on-site inspections by maintenance personnel. In cases that appeared particularly severe, geotechnical investigations that involved the installation of monitoring devices were performed as well.

The design of the remedial measures can be divided into the following typical stages:

1. Retrieval of all the available information, such as the original design, technical reports, investigation data, and accounts of the construction works (measurement logbooks).
2. Drafting of a preliminary study that includes the following items: (a) geological and geomorphological analysis (e.g., photointerpretation, in situ survey) leading to a comprehensive definition of the slide area; (b) stratigraphic and geotechnical characterization of the soils involved in the slide; (c) indication of the first measures to be undertaken; and (d) a program of in situ and laboratory tests and/or a monitoring system.
3. Execution of the in situ and laboratory tests and reading of the monitoring instruments.
4. Final design of the remedial measures.

Unless comprehensive data are already available, the average time required to go from Stage 1 through Stage 4, after a slide has been reported, is of the order of 8 to 12 months, which can be broken down as follows:

- One to two months to acquire the necessary data and draw up the preliminary study;
- Two to three months to perform the soil investigation;

- Three to five months to carry out the laboratory tests and to obtain significant data from the monitoring system;
- Two months for the final design of the remedial measures.

The progression of the mass movement usually "respects" the time required for investigations and design. In some cases, however, slides may undergo sharp acceleration and seriously interfere with normal traffic, thus calling for emergency actions. In such cases, "on-the-spot" decisions regarding measures to be adopted may result in extremely difficult and unreliable designs unless specific data are readily available. According to the authors' experience, these specific data must consist of:

- The results of quick in situ tests, such as cone penetration tests (CPTs), standard penetration tests (SPTs), dilatometer tests (DMTs), and stratigraphic boreholes.
- A technical and historical data bank relevant to the region that includes the area under consideration (*I*). The data bank should contain the characteristics of a significant number of registered landslides, including: (a) the type of failure, e.g., according to the classification presented by Varnes (2); (b) the volume of soil involved; and (c) indications that allow designers to know whether the slip surfaces usually develop along particular stratigraphic interfaces recurring in the region.
- Geotechnical parameters of the soil involved and/or correlations that are specific for the region considered. For example, using the results of laboratory tests conducted on more than 150 samples relevant to 20 sites along the "Autostrade SpA" network, a correlation linking residual friction angle, gradation, and index properties of cohesive soils was found (Figure 1). The correlation is very useful as a guide in the urgent design of remedial works when the data from an extensive laboratory program is not readily available.

Without an adequate data bank, the analysis, based only on quick in situ tests, may be unreliable. The following example shows, for a specific landslide, a possible misjudgment in the selection of an "urgent" design based on the analysis of the few data available instead of the complete data listed in Stages 1 through 4.

The landslide under consideration is situated along the Naples-Bari motorway (A16) in the southern Apennines region. The landslide area, 400 m long and about 70 m wide, was defined by means of geomorphological analysis (photo-

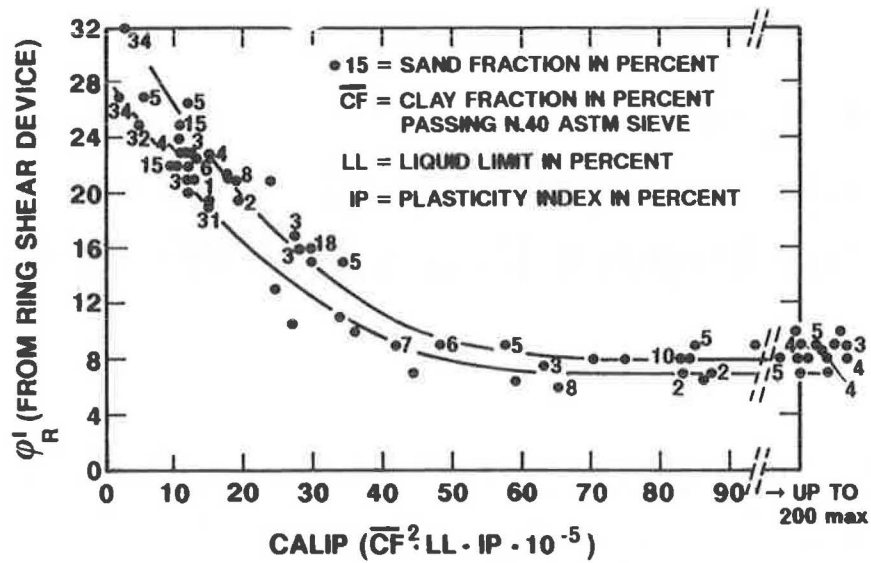


FIGURE 1 Correlation between residual friction angle, gradation, and index properties of cohesive soils.

interpretation and in situ survey) and is shown in Figure 2. A geotechnical investigation was performed in this area to a maximum depth of 35 m from ground level. The investigation consisted of

- Five geotechnical boreholes, four of which were instrumented with inclinometric tubes. In each borehole, several

SPT tests were conducted and undisturbed samples were obtained.

- Four boreholes instrumented with Casagrande piezometers (two cells in each borehole).
- Ten continuous dynamic penetrometer tests.

The location of this investigation is shown in Figure 2. The

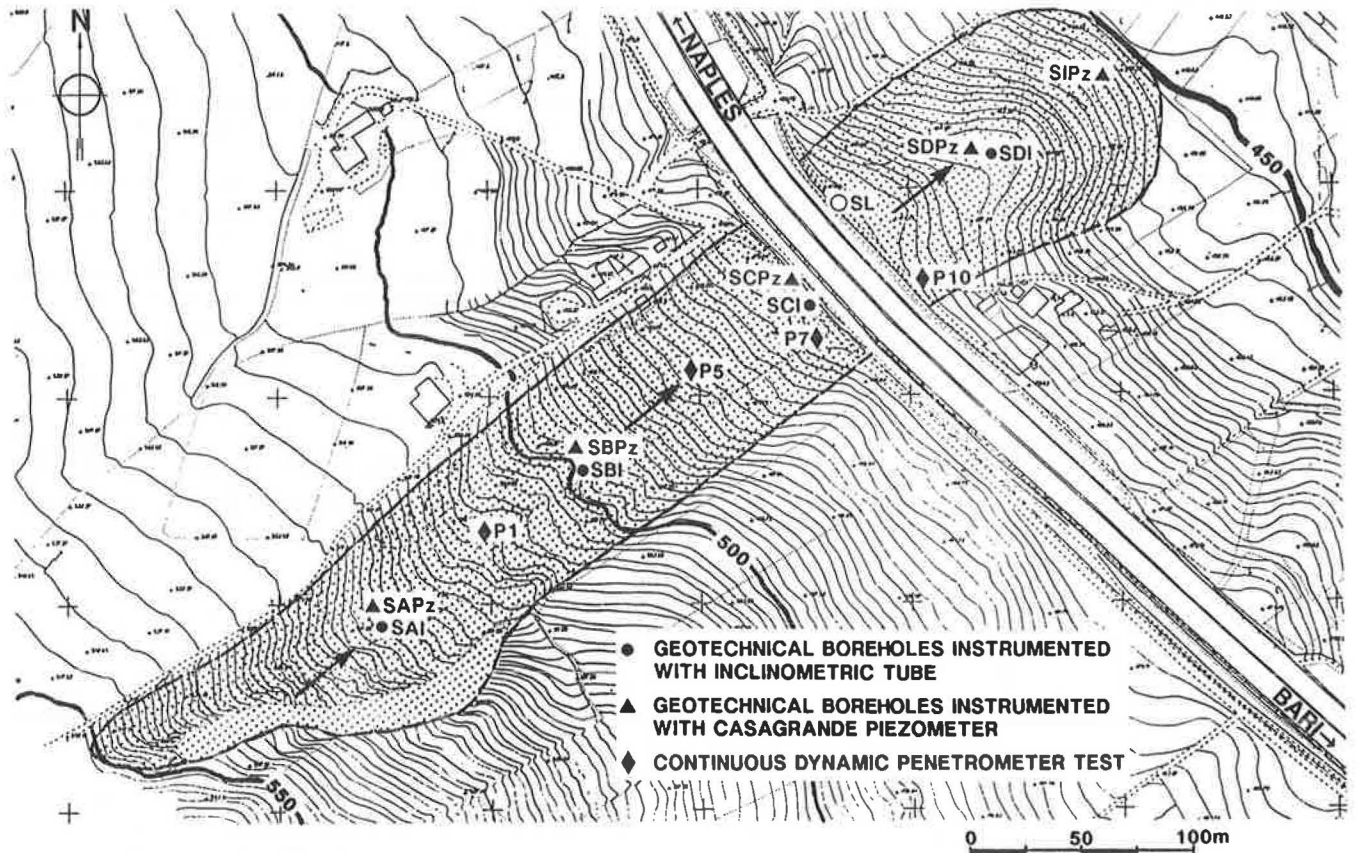


FIGURE 2 Plan of slide area.

soil in this area consists of an upper formation of brown soft clayey silt, 8.0 to 10.0 m thick, and a base formation of grey-blue marly clay. Gradation, index properties, and strength parameters of the two formations are shown in Table 1.

On the basis of the preliminary data (geomorphological analysis, boreholes, and penetrometer test profiles), we concluded that the area involved is indeed that defined in Figure 2, the slip surface developed along the interface between the clayey silt, and the marly clay formations. This conclusion appears to be justified by the following considerations:

- Penetrometric profiles and SPT values show a marked increase in resistance just below the interface (Figure 3);
- $N_{SPT}$  values in the marly clay formation are always very high, ranging between 50 blows/ft to refusal (more than 50 blows/15 cm);
- The flow type of the landslide suggests the development of shallow slide surfaces; and
- Residual friction angles inferred from back analyses show

a good agreement with the values obtained from the correlation in Figure 1.

Preliminary data therefore seemed sufficient for an "urgent" design. Fortunately, because the soil investigation was carried out as a part of a general monitoring program of the motorway network and the rate of movement was low, it was possible to wait for the results of the inclinometer readings before undertaking the remedial works.

The examination of inclinometer results (Figure 3) clearly showed a slide surface much deeper (19.0 m) than the one inferred from the preliminary data (10.0 m).

On the basis of the above example, we can make the following statements: If we do not have a sufficient data bank available, the design of urgent remedial works must be carried out with extreme caution. In this case the design should involve only works of temporary nature. The design of the final works should always be supported by the acquisition of the complete instrumentation data, particularly inclinometer data.

TABLE 1 SOIL PARAMETERS

	Upper Formation	Base Formation
Unified Soil Classification System symbol	CL-CH	CL-CH
Clay fraction (%)	35-40	38-43
Liquid limit (%)	45-50	48-53
Plasticity index (%)	27-29	28-30
Water content (%)	22-25	12-15
Unit weight of soil (kN/m <sup>3</sup> )	20-21	22-23
Apparent cohesion intercept (kPa)	150	>800
Effective angle of internal friction (degrees)	25-27	- <sup>a</sup>
Effective cohesion intercept (kPa)	0.0	- <sup>a</sup>
Residual angle of internal friction (degrees)	17-19	16-17
Residual cohesion intercept (kPa)	0.0	0.0

<sup>a</sup>Unavailable data

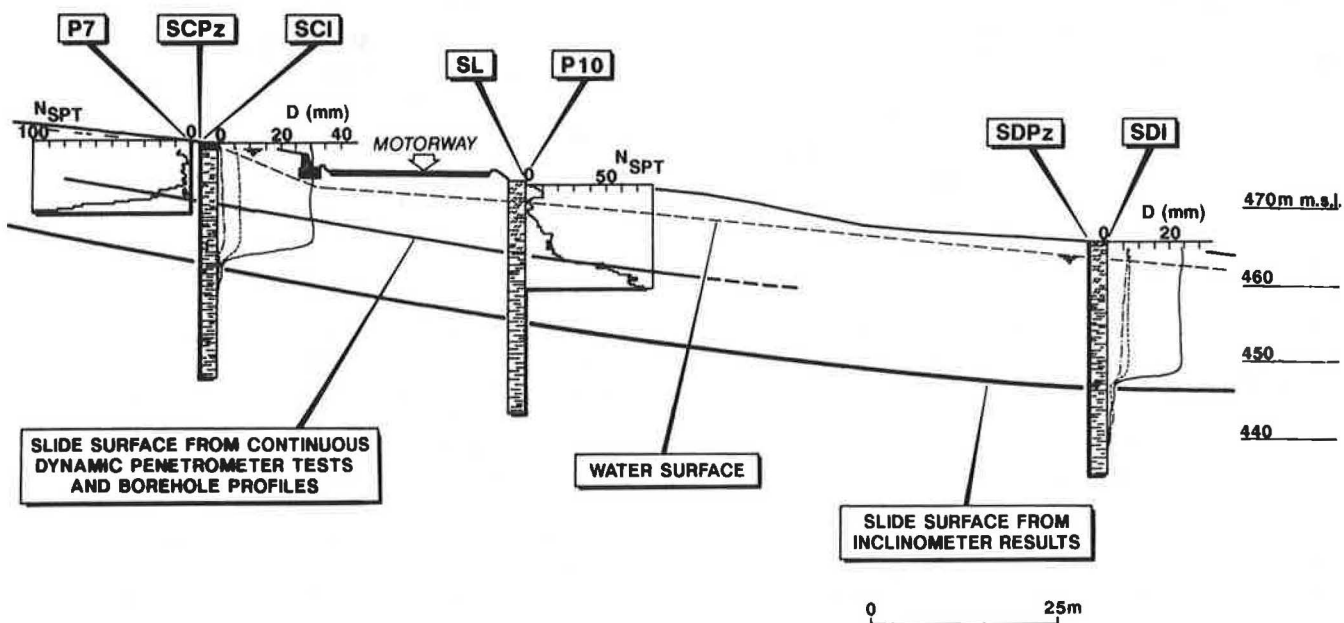


FIGURE 3 Typical section.  $D$  = horizontal displacement; dot-dashed line = December 14, 1987; dashed line = January 26, 1988; solid line = March 16, 1988.

It is the authors' experience that the time required for the acquisition of significant inclinometer data can be substantially reduced by operating with rigorous specifications concerning the technical characteristics of the instrumentation, tube installation, and the acquisition and processing of records.

Before showing the possible effects of instrumentation errors on the quality of the readings, it appears necessary to provide some definitions that will aid in understanding the material that follows.

- A reading is a set of measurements along the inclinometer tube;
- Measurement processing in terms of *integrated absolute displacements* gives the actual planimetric and altimetric position of each measurement point with respect to the vertical passing through the center of the tube toe;
- Measurement processing in terms of *integrated differential displacements* gives the tube deformation with respect to the initial tube profile corresponding to the "zero reading"; and
- Measurement processing in terms of *local differential displacements* gives the displacement at each measurement elevation, without integration. The displacements are with respect to the "zero reading."

The effects of possible instrumentation errors on the quality of the processed readings are shown in Figures 4 and 5, with reference to the landslide under consideration. From this information we can draw some useful conclusions:

- When data is processed in terms of integrated differential displacements (Figure 4), instrumentation errors can totally invalidate the final results or, at best, allow the determination of the slip surface depth only when large displacements are involved (15/03/1988 readings on Figure 4b and c).
- When data is processed in terms of local differential displacements (Figure 5), the instrumentation errors can be almost entirely overcome, thus allowing, in this particular case, the determination of the slip surface depth from the second reading, with a time savings of about 2 months.

Given the fact that in most cases the local differential method allows even rather significant instrumentation errors to be overcome, the best way to measure meaningful data quickly is by

- Reducing vertical deviation of the inclinometer tubes during the installation stage (< 1.5 percent);
- Using a biaxial inclinometer torpedo; and
- Performing periodic calibration of the equipment to determine the variations in the rotational shift of the sensor (small electrical or mechanical alignment shift of the sensor azimuth relative to the torpedo wheels) and in the sensitivity of the sensor and readout unit.

For situations in which the results of calibration tests are not available, the authors have adopted a procedure, consisting of the following steps, for an approximate evaluation of the variation in the sensitivity of the equipment and in the rotational shift of the sensor:

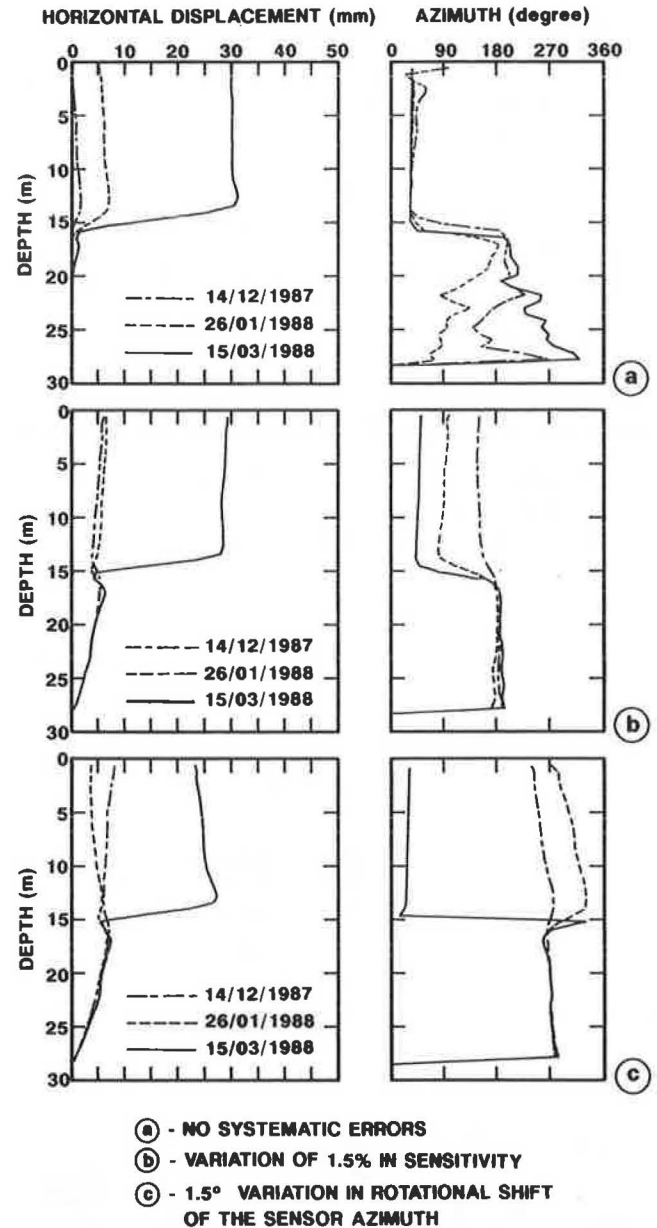


FIGURE 4 Measurement processing in terms of integrated differential displacements.

- Locating a short segment of the inclinometric tube that is certainly below the slip surface. This can be done in two ways: (a) by examining the stratigraphic-geotechnical data; (b) by performing a preliminary local differential elaboration of the readings. The latter procedure will, in general, produce a diagram similar to that shown in Figure 6. In this diagram, the lined area represents the sum of the systematic errors (variation in sensitivity and/or rotational shift), while the dotted area represents the shear zone deformations; below this zone, the soil is certainly stable.

- Processing data in terms of integrated absolute displacement (including "zero reading").

- Fixing a reference elevation ( $z$ ) within the tube length below the slip surface. Given the fact that below the slip surface the absolute position of the point can not change with



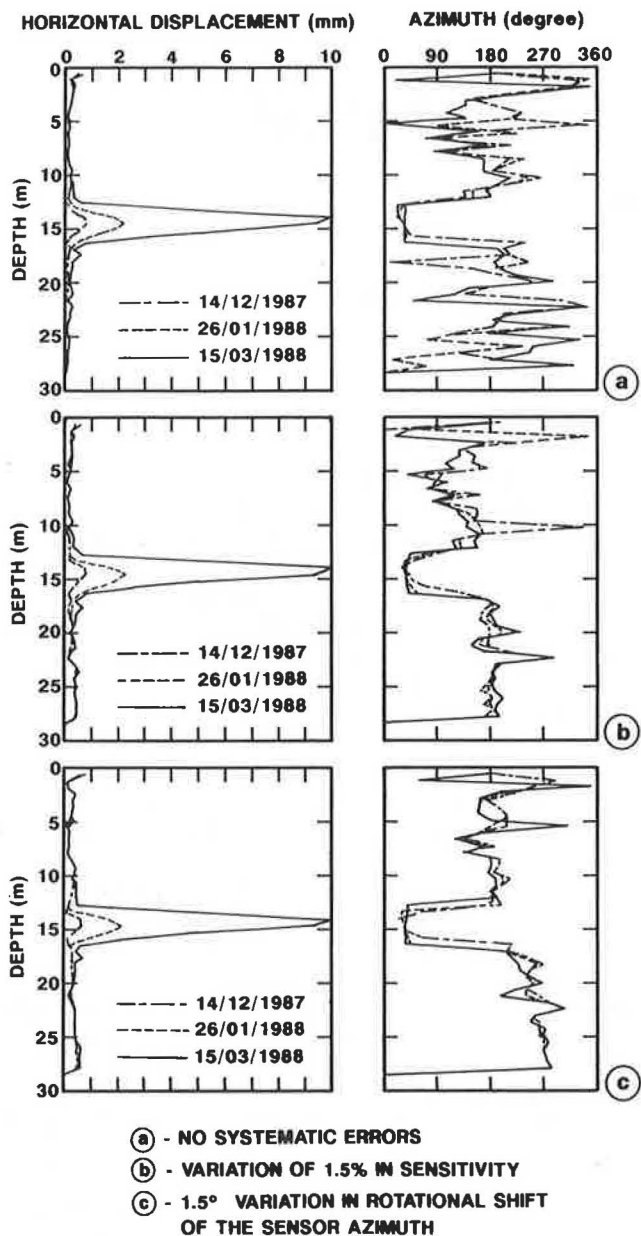


FIGURE 5 Measurement processing in terms of local differential displacements.

time, we can say that at the reference elevation, the ratio between the absolute displacement corresponding to the  $n$ th reading and the one corresponding to the zero reading gives the sensitivity variation of the torpedo and readout unit. Moreover, the difference between the azimuth values represents the rotational shift of the sensor.

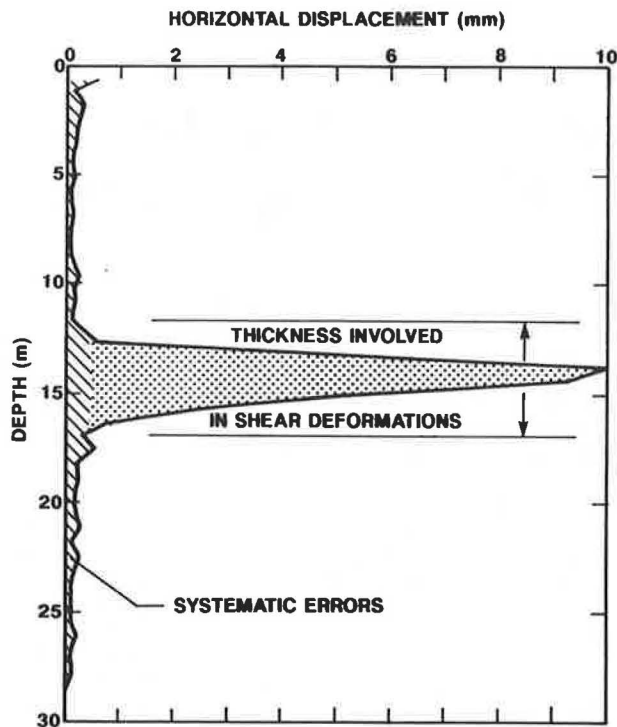


FIGURE 6 Determination of the soil thickness involved in the movement.

### CONCLUSIONS

For a specific landslide, we have reported a misjudgment in the design of remedial works performed only on the basis of quick in situ tests. We recommend that the design of the final works should always be supported by the acquisition of complete instrumentation data, particularly inclinometer data. Moreover, we have proposed criteria to facilitate quick measurement of meaningful data. These criteria involve tube installation, reading equipment calibration, and measurement processing.

### REFERENCES

1. T. Collotta, P. C. Moretti, and C. Viola. A Slope Instability Data-Bank: Present Usefulness, Future Developments. *Proc. 5th International Symposium on Landslides*, Lausanne, Switzerland, Vol. 2, 1988, pp. 1143-1146.
2. D. J. Varnes. Slope Movement Types and Processes. In *Special Report 176: Landslides: Analyses and Control* (R. L. Schuster and R. J. Krizek, eds.), TRB, National Research Council, Washington, D.C., 1978, pp. 11-33.

Publication of this paper sponsored by Committee on Soil and Rock Properties.

# Analyses of Laterally Loaded Drilled Shafts Using In Situ Test Results

A. B. HUANG, A. J. LUTENEGGER, M. Z. ISLAM, AND G. A. MILLER

To predict the lateral load-displacement response of small-diameter drilled shafts in desiccated clays, a series of in situ tests was performed at a field test site in Massena, New York. These tests included piezocone, flat dilatometer, field vane, and prebored pressuremeter. Four cast-in-place concrete shafts with diameters of 152 and 305 mm and lengths of 1.5 to 3.0 m were installed at the site. Predictions of the lateral load-deformation relationships were made prior to the pile load tests using a finite difference program and results from in situ tests. Comparisons were made between the predicted and the measured response of each drilled shaft. This paper describes the use of in situ tests in the analyses of relatively small and short, laterally loaded drilled shafts in desiccated clays and presents a discussion of the efficacy of the approach.

Many methods are available for analyzing single laterally loaded piles. They vary from relatively simple closed-form solutions (1,2) to sophisticated three-dimensional finite element techniques (3). A common approach is to treat the pile-soil system as a linear elastic beam resting on a series of Winkler springs that have nonlinear force-displacement relationships (4). The problem of a laterally loaded pile can then be described by a differential equation:

$$EI \frac{d^4 y}{dx^4} + P_x \frac{d^2 y}{dx^2} - p = 0 \quad (1)$$

and

$$p = E_s(x,y)y \quad (2)$$

where

- $P_x$  = axial load,
- $y$  = lateral deflection of pile,
- $x$  = length along the pile,
- $p$  = soil reaction,
- $EI$  = flexural stiffness of the pile, and
- $E_s$  = soil reaction modulus.

This well-known approach involves some serious drawbacks. The most noticeable one is that  $E_s$  is not a soil parameter but also depends intrinsically on the geometry and flexural rigidity of the piles as well as the boundary conditions (5). However, the method remains popular because of its simplicity and its capability to handle nonlinear  $p$ - $y$  relationships.

Case histories and methods of using laboratory and/or in situ test results to estimate the necessary soil  $p$ - $y$  relationships have been reported by many authors [e.g., Briaud et al. (6); Gazioglu and O'Neill (7); and Robertson et al. (8)]. Commonly used in situ test methods include pressuremeter (PMT), field vane (FVT), and plate load tests. The use of flat dilatometer test (DMT) results in analyzing laterally loaded piles is relatively new. Regardless of methods used in the reported cases, they all have the drawback of being highly empirical. Also, only limited information is available as to the relative performance of each method. In fact, there appears to be a general lack of available data on small-diameter shafts founded within a desiccated clay crust.

The project reported herein concentrates on the behavior of small-diameter drilled shafts founded in a stiff clay crust and subjected to lateral loads. Foundations of this type are often used for structures such as guiderail poles, light poles, and transmission towers, where the foundation load in the axial direction is low compared to potential loads in the lateral direction. The relatively low cost and widespread location of these structures often do not justify elaborate subsurface explorations and analyses for each structural unit in the design of the foundations. In situ tests offer potentially cost-effective ways of providing the parameters necessary for valid analyses of such foundations.

In addition to laboratory tests, piezocone (CPTU), field vane, flat dilatometer, and pressuremeter tests were performed at the test site. Four concrete drilled shafts were installed. Table 1 shows the dimensions of these shafts. Results from FVT, PMT, and DMT were used to establish the necessary  $p$ - $y$  relationships and predict the lateral response of the piles using a finite difference program. All predictions were made before the lateral load tests. The paper describes the details of these analyses and presents a discussion of the efficacy of the methods utilized.

## SOIL CONDITIONS AT THE TEST SITE

The test site is located on Barnhart Island about 1 km north of the Snell Lock along the Saint Lawrence Seaway Canal, north of the village of Massena, New York. Field and laboratory investigations conducted at the test site indicate that the soils generally consist of Champlain Sea marine sediments, which occur throughout the Saint Lawrence Lowlands. The upper 2 to 3 m consists of highly overconsolidated and often fissured clays, as indicated by the results of CPTU (Figure 1) and FVT (Figure 2). Beneath this desiccated crust, the marine

A. B. Huang, M. Z. Islam, and G. A. Miller, Department of Civil and Environmental Engineering, Clarkson University, Potsdam, N.Y. 13676. A. J. Lutenecker, Department of Civil Engineering, University of Massachusetts, Amherst, Mass. 01003.

TABLE 1 DIMENSIONS OF THE DRILLED SHAFTS

Case	Diameter (cm)	Length (cm)
I	15.2	152
II	15.2	304
III	30.5	152
IV	30.5	304

clays are softer, slightly overconsolidated, and often sensitive. A summary of the soil conditions and a piezocone profile at the site are presented in Figure 1.

The upper 1 m of soil at the site is highly variable and contains abundant small sand lenses. Below this, the materials are more uniform and are generally classified as CH-CL according to the Unified Soil Classification System. Figure 2 presents the results of field vane tests along with other shear

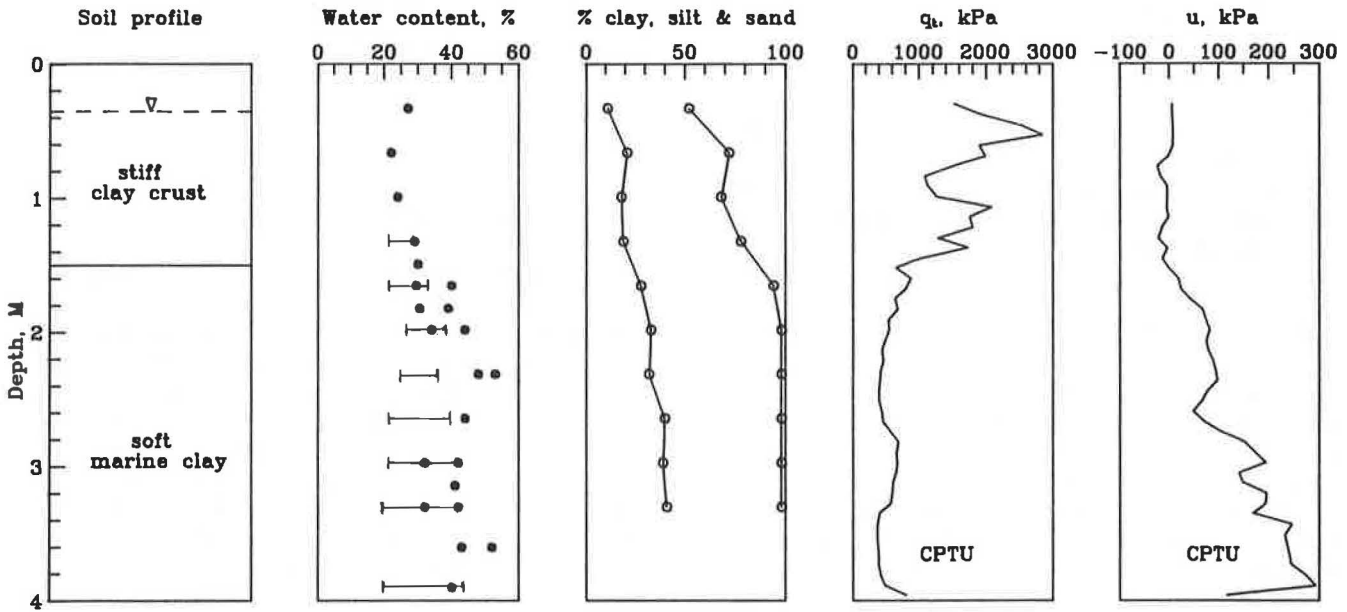


FIGURE 1 Soil profile at the test site.

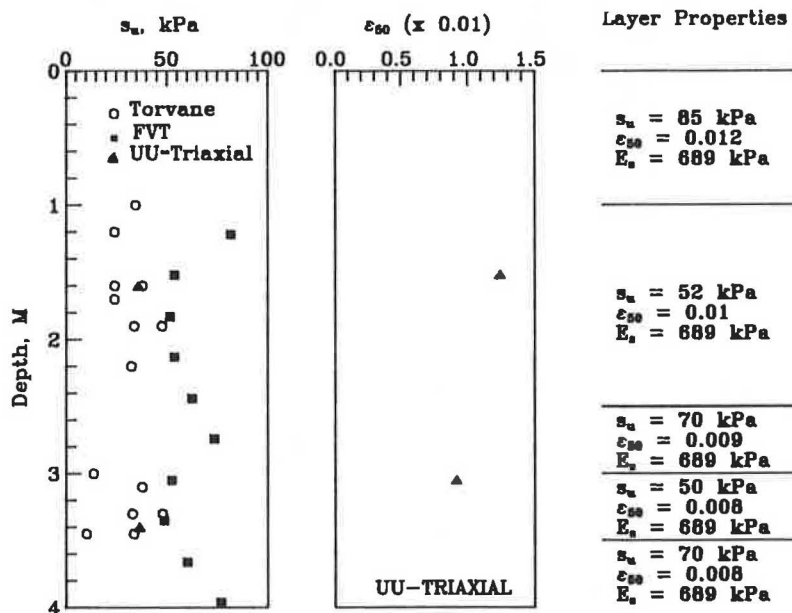


FIGURE 2 Soil layering using the FVT data.

strength measurements. These results are typical of marine deposits in the area.

## PREDICTING LATERAL LOAD RESPONSE

### The Numerical Technique

A finite difference program was written to solve Equation 1. The technique follows that of Reese and Allen (4). The pile is divided into segments such that the flexural stiffness ( $EI$ ) and a nonlinear  $p$ - $y$  relationship or the so-called  $p$ - $y$  curve can be defined for each segment. The program is capable of handling general loading conditions at the shaft top that include axial load ( $P_x$ ), bending moment, and lateral load. Zero moment and axial load were applied at the shaft top in all computations included herein, as they were the conditions applied in the field load tests. The following sections describe the details of constructing  $p$ - $y$  curves using results from each of the three in situ test methods and predictions of the lateral load response for the drilled shafts.

### Field Vane Tests (FVTs)

Reese and Allen (4) recommended that for submerged clays, the  $p$ - $y$  curves be established based on a profile of undrained shear strength ( $s_u$ ) and  $\epsilon_{50}$ , the axial strain at 50 percent of the peak principal stress difference in a triaxial compression test. For soft clay soils that are normally or lightly overconsolidated, Matlock (9) recommended the FVT as the preferable method to determine the in situ undrained shear strength. Although this is not exactly the case for the clay crust, undrained shear strengths from FVT were used in establishing the  $p$ - $y$  curves. This is primarily due to the lack of good-quality samples for laboratory testing, as is usually the case for clay crusts.

The  $p$ - $y$  relationships were established according to the "integrated clay method" proposed by Gazioglu and O'Neill (7). This semiempirical method considers the effects of soil ductility, nonlinear dependence on pile diameter, and relative stiffness of soil and pile. It is applicable to both soft and stiff clays, as the name implies. A critical pile length ( $L_c$ ) is computed first as

$$L_c = 3(EI/E_s D^{0.5})^{0.286} \quad (3)$$

where

- $D$  = diameter of the pile,
- $EI$  = flexural stiffness of the pile, and
- $E_s$  = average soil modulus.

The lateral load-deflection relationships are unaffected by penetration beyond  $L_c$  according to Gazioglu and O'Neill (7). The critical depth ( $x_{cr}$ ) is related to  $L_c$  by the following equation:

$$x_{cr} = L_c/4 \quad (4)$$

A reference deflection ( $y_c$ ) is defined as follows:

$$y_c = 0.8\epsilon_{50} D^{0.5} (EI/E_s)^{0.125} \quad (5)$$

The ultimate soil resistance ( $p_u$ ) is determined by

$$p_u = 0.75N_p s_u D \quad (6)$$

and

$$N_p = 3 + 6(x/x_{cr}) \leq 9 \quad (7)$$

where  $x$  is the depth below ground surface. The lateral reaction ( $p$ ) at depth  $x$  is then computed as

$$p = 0.5(y/y_c)^{0.387} p_u \quad (8)$$

Figure 2 shows the layering of the soil profile and parameters used in establishing the  $p$ - $y$  curves and Figure 3 shows the typical shape of a  $p$ - $y$  curve established on the basis of this method.

### Pressuremeter Tests (PMTs)

Because of its lateral expansion, the pressuremeter provides a close simulation of a laterally loaded drilled shaft. At least seven methods (6) have been proposed to derive the  $p$ - $y$  relationships and select the critical depths. Some of these methods are also applicable to self-boring pressuremeter tests. Full-displacement pressuremeter tests have been used to evaluate laterally loaded driven piles (8). Because only drilled shafts are involved herein, the  $p$ - $y$  curves were established on the basis of a series of prebored, three-cell Ménard pressuremeter tests following the procedures recommended by Baguelin et al. (10). PMTs were conducted in hand-augered holes of 76-mm nominal diameter. Because of the size of the pressuremeter probe, it was necessary to perform tests at alternate depths in two adjacent boreholes.

This method considers the effects of pile dimensions and derives the subgrade reaction modulus ( $k$ ) using the pressuremeter modulus ( $E_M$ ), the pressuremeter creep pressure ( $p_f$ ), and the limit pressure ( $p_l$ ), as shown in Figure 4 and the following equation:

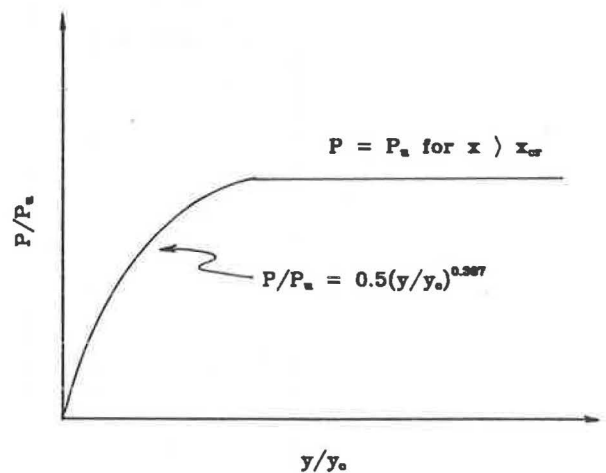


FIGURE 3 The  $p$ - $y$  curve using the "integrated clay method."

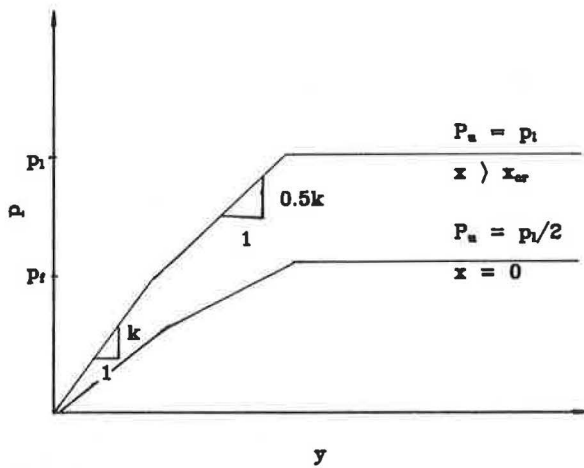


FIGURE 4 The  $p$ - $y$  curve using the PMT method.

$$\frac{1}{k} = \frac{1}{9E_M} \left[ 2D_o \left( \lambda_d \frac{D}{D_o} \right)^\alpha + \alpha \lambda_c D \right] \quad (9)$$

where

- $E_M$  = pressuremeter modulus,
- $\lambda_d, \lambda_c$  = shape factors that depend on the length-to-diameter ratio of the pile,
- $\alpha$  = rheological factor that depends on soil type and stress history (for overconsolidated clays,  $\alpha = 1$ ), and
- $D_o = 60$  cm as a reference diameter.

Values of  $\lambda_d$  and  $\lambda_c$  have been proposed by Baguelin et al. (10) for foundations with different geometries. A critical depth ( $x_{cr}$ ) equivalent to twice the pile diameter was used, as suggested by Baguelin et al. (10). Values of  $k$  and  $p_1$  above the

critical depth (Figure 4) are adjusted according to a reduction factor ( $\lambda_z$ ), calculated as follows:

$$\lambda_z = (1 + x/x_{cr})/2 \quad (10)$$

On the basis of the results of PMTs, the soil was divided into three layers for analysis, as shown in Figure 5. The  $p$ - $y$  relationships were then determined for each layer.

**Flat Dilatometer Tests (DMTs)**

The use of the DMT in analyzing laterally loaded piles is relatively new, and only a few cases have been reported (5,11,12). The potential advantages of using the DMT for this situation include:

- During the DMT membrane expansion, the soil is stressed in the lateral direction.
- Because of the small size of the instrument, the DMT is capable of providing soil modulus values at much closer intervals than are normally obtained with a pressuremeter; therefore, more detailed analyses that account for soil layering can be made. Typically, DMT tests are conducted at 0.3-m intervals, as was the case herein.
- The results of the DMT are more reproducible than those of the PMT, since the DMT does not involve different methods of inserting the probe (e.g., use of auger, self-boring pressuremeter, or Shelby tube) and is therefore much less operator-dependent.

Although the value of the DMT modulus ( $E_D$ ) is obtained after full displacement of the soil resulting from inserting the blade, Lutenegeger (11) has indicated that  $E_D$  is slightly higher than but close to the pre-bored PMT modulus ( $E_M$ ), at least for the marine clays tested in the Massena area. Also, the

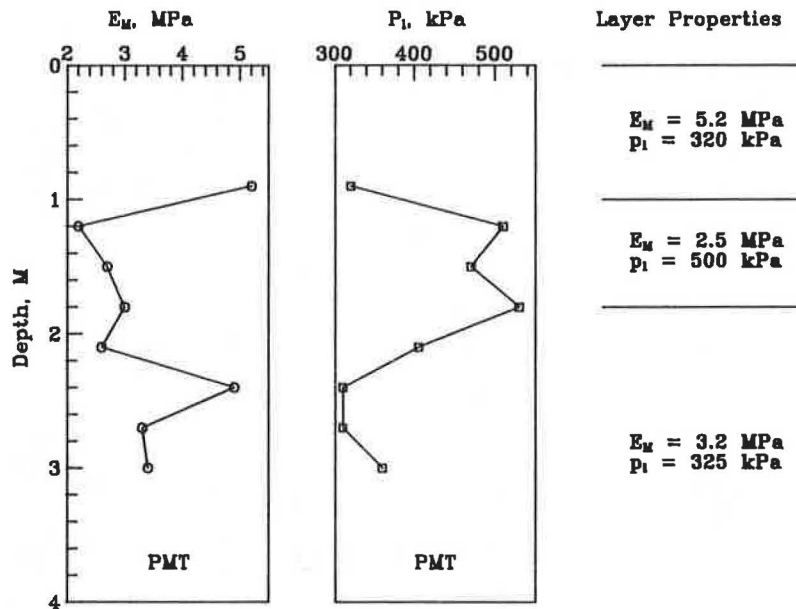


FIGURE 5 Soil layering using the PMT data.

PMT limit pressure ( $p_l$ ) is approximately equivalent to the average of the DMT lift-off pressure  $P_0$  and the 1-mm expansion pressure ( $P_1$ ), i.e.,  $0.5(P_0 + P_1)$ . Because of these similarities and for the sake of simplicity, it was decided to adopt the PMT method as described above in using the DMT data for the analyses. Therefore, modifying Equation 9 results in

$$\frac{1}{k} = \frac{1}{9E_D} \left[ 2D_o \left( \lambda_d \frac{D}{D_o} \right)^\alpha + \alpha \lambda_c D \right] \quad (11)$$

and the PMT limit pressure ( $p_l$ ) is replaced with  $0.5(P_0 + P_1)$ . Figure 6 shows the results of the DMT tests and layering of the soil and parameters used in establishing the  $p$ - $y$  curves. As mentioned previously, the DMT provides data with a much higher resolution, and this is reflected in the more detailed layering of the soil profile indicated.

The use of subgrade reaction modulus as proposed by Gabr and Borden (12) is another possible method of using the DMT for the analyses. However, it requires knowing in situ horizontal stress and therefore may be very subjective, especially in clay crust.

### RESULTS AND COMPARISON

#### Field Load Tests

Four small-diameter drilled shafts (see Table 1 for dimensions) were installed at the site and allowed to cure for 30 days before load tests were conducted. Holes were drilled with a truck-mounted drill rig using continuous-flight augers and were filled with concrete immediately after drilling. Four No. 4 rebars were placed concentrically throughout the full length in each shaft. Concrete cylinders were taken during casting, and compression tests on these cylinders were con-

ducted on the same day as the load test. The compressive strength of the concrete cylinders had an average value of 22 800 kPa. The lateral load tests were performed in close conformance with ASTM Standard D3966. Lateral loads were applied at the ground surface ( $x = 0$ ), and two shafts were tested simultaneously by placing the hydraulic cylinder and load cell between them. Each load increment was maintained for 10 minutes. Free rotation was allowed at the shaft head at the ground surface.

#### Predictions

Qualitatively, all methods predicted similar patterns in deflection and soil reaction, as well as bending moment. As an example, Figure 7 shows the predicted deflection profiles of the shafts in all four cases (Table 1) according to the numerical analyses using results from the DMT, as the lateral load on the pile head varied from 2 to 20 kN. Except in Case II, the deflection of shafts was close to a rigid body rotation. Figure 8 shows the distribution of soil lateral reaction (force per unit length of shaft) according to results from the DMT, as the lateral load reached 10 kN. For the longer shafts (Cases II and IV), the soil lateral reaction from below the clay crust was rather insignificant. Figure 9 shows the predicted responses of the shaft for Case IV under a lateral load of 10 kN based on the three in situ test methods. It is clear that the added length of shafts in Cases II and IV did not cause any significant increase of lateral resistance due to the much softer soil conditions at the lower level.

Quantitatively, however, predictions from different methods are significantly different. For example, the displacement at the ground surface predicted by the PMT was 100 percent larger than that predicted by DMT. A discussion on the possible reasons for these discrepancies will be presented later.

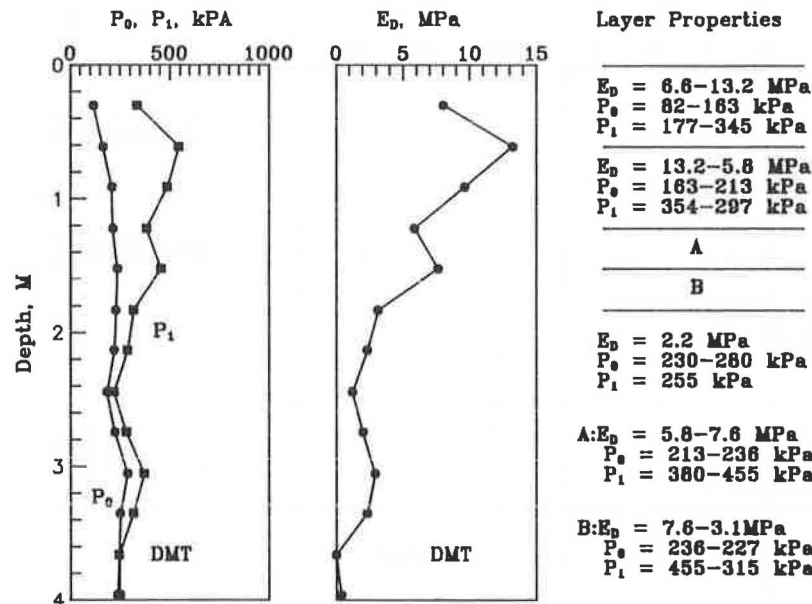


FIGURE 6 Soil layering using the DMT data.

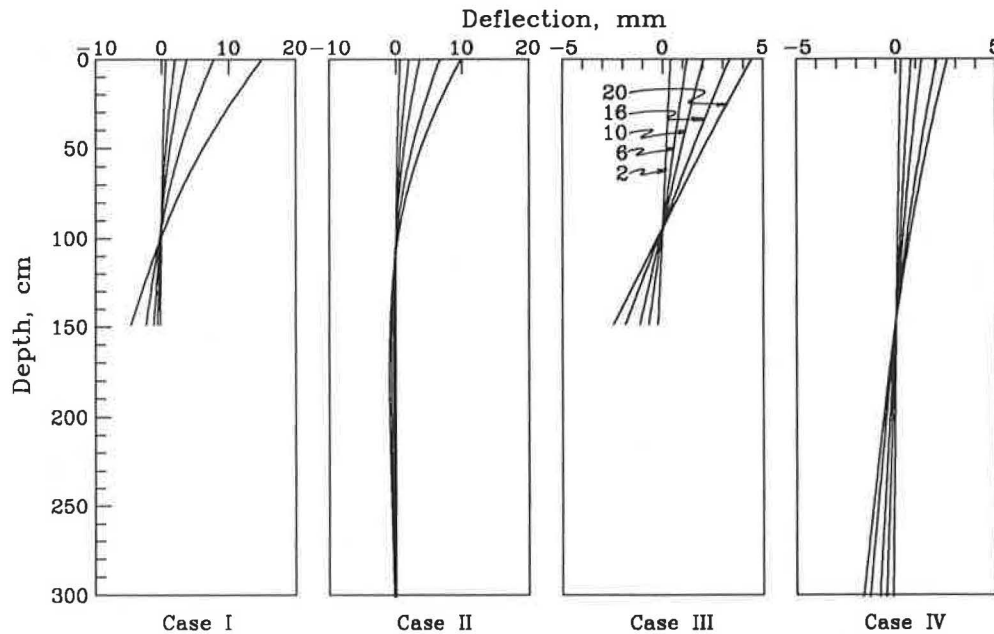


FIGURE 7 The predicted shaft deflection profiles.

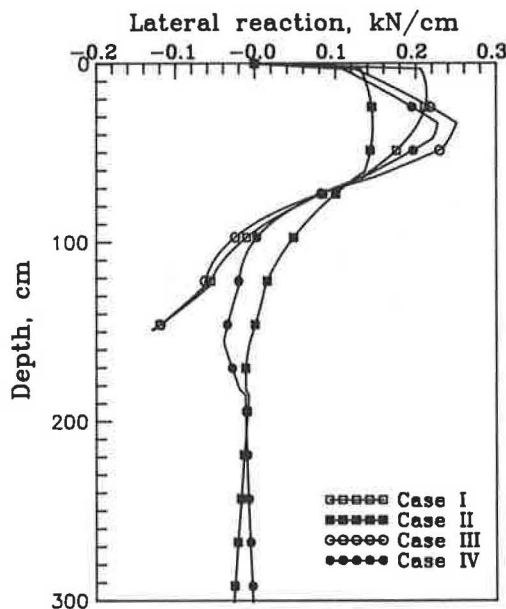


FIGURE 8 The predicted soil lateral reaction.

Comparison

Figures 10 and 11 show the predicted and measured displacement versus lateral load for all four cases. In all the field loading tests, the longer shafts (Cases II and IV) had more displacements than the shorter ones (Cases I and III). This contradicts all the predictions. One possible explanation is that there was more soil disturbance during drilling for longer shafts. The softening caused by disturbance might have offset the limited additional resistance from the extra length below

a depth of 150 cm where the soil stiffness was much lower, as previously described.

The analytical solutions employed do have some built-in scale effects, e.g., critical depths, ignoring the influence of pile characteristics on the *p-y* curves, etc. The results did show that as the shaft diameter doubled in Cases III and IV, much closer predictions were obtained, as shown in Figure 11.

CONCLUSIONS

The determination of the engineering properties (i.e., strength and modulus) of desiccated clay crust is a difficult and challenging task. The use of in situ tests is attractive, as it is essentially impossible to obtain good-quality samples for laboratory testing (13). Studies by Bauer and Tanaka (14) indicate that in addition to the variable and fissured nature of desiccated clays, the interpreted undrained shear strength and modulus are very sensitive to different in situ test methods. They further suggest that a larger number of in situ tests is required to characterize the soil properties and to obtain statistically meaningful average values.

In establishing the *p-y* curves, there are significant differences in selecting the critical depths and subgrade reaction moduli among the available methods that involve in situ tests. These discrepancies are accentuated by the variable nature of the clay crust at the test site. No data in this study suggest that any one in situ test method is consistently better than the others in predicting the performance of this class of laterally loaded drilled shafts. It appears that the procedures for analyzing laterally loaded drilled shafts are limited in their usefulness in their present form for the unique combination of small shaft diameters and shaft location in a clay crust with somewhat variable properties. Further studies are warranted specifically for drilled shafts installed in clay crust. The improved

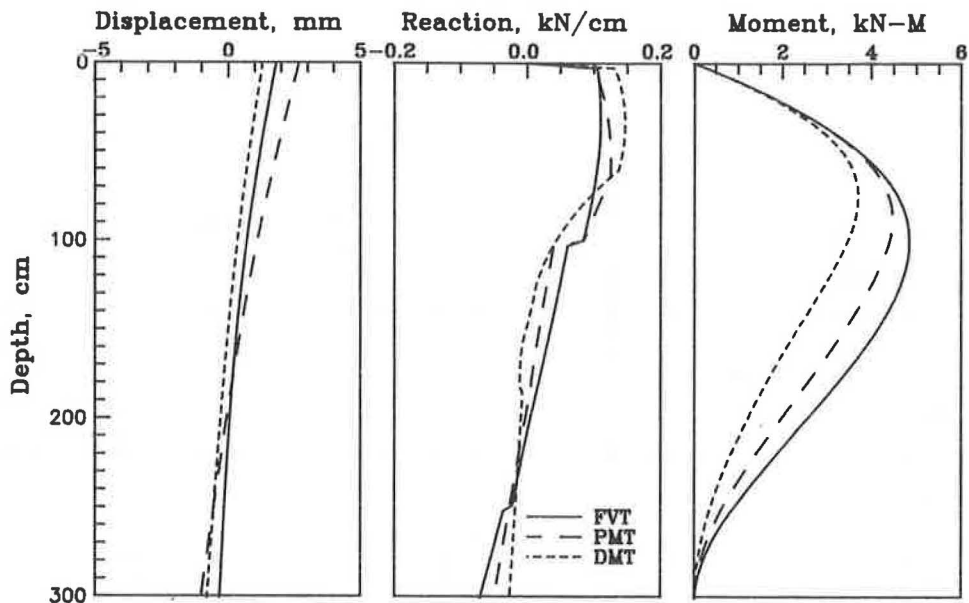


FIGURE 9 Predicted responses from different methods.

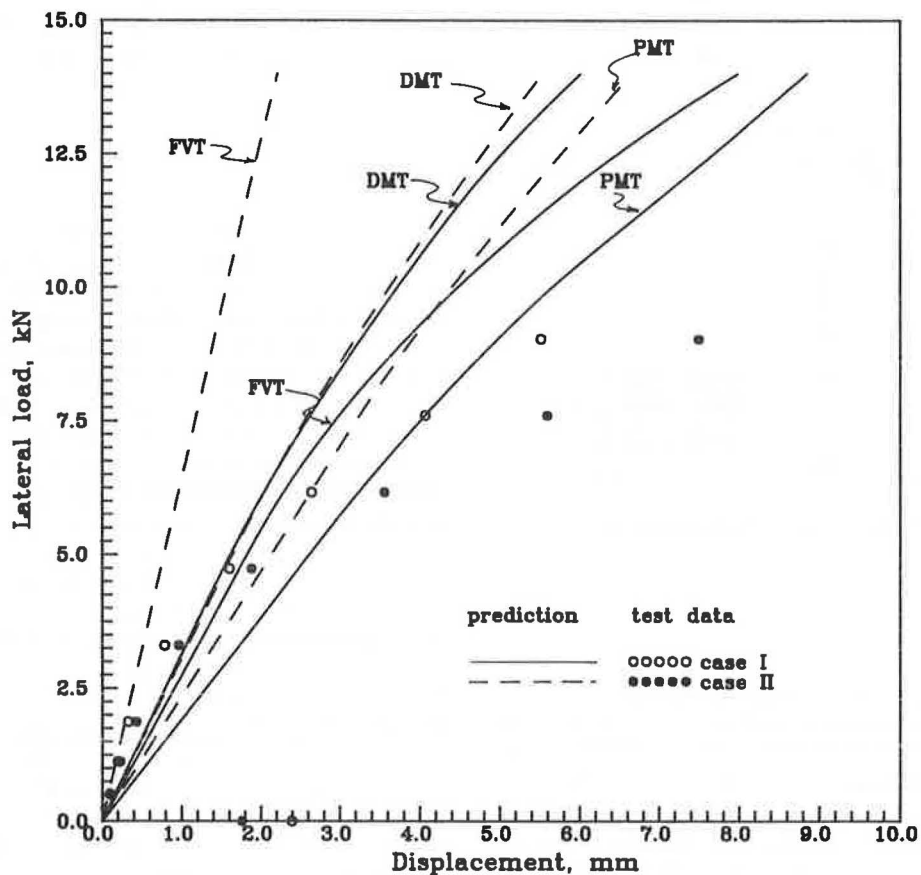


FIGURE 10 Predicted and measured displacement for Cases I and II.



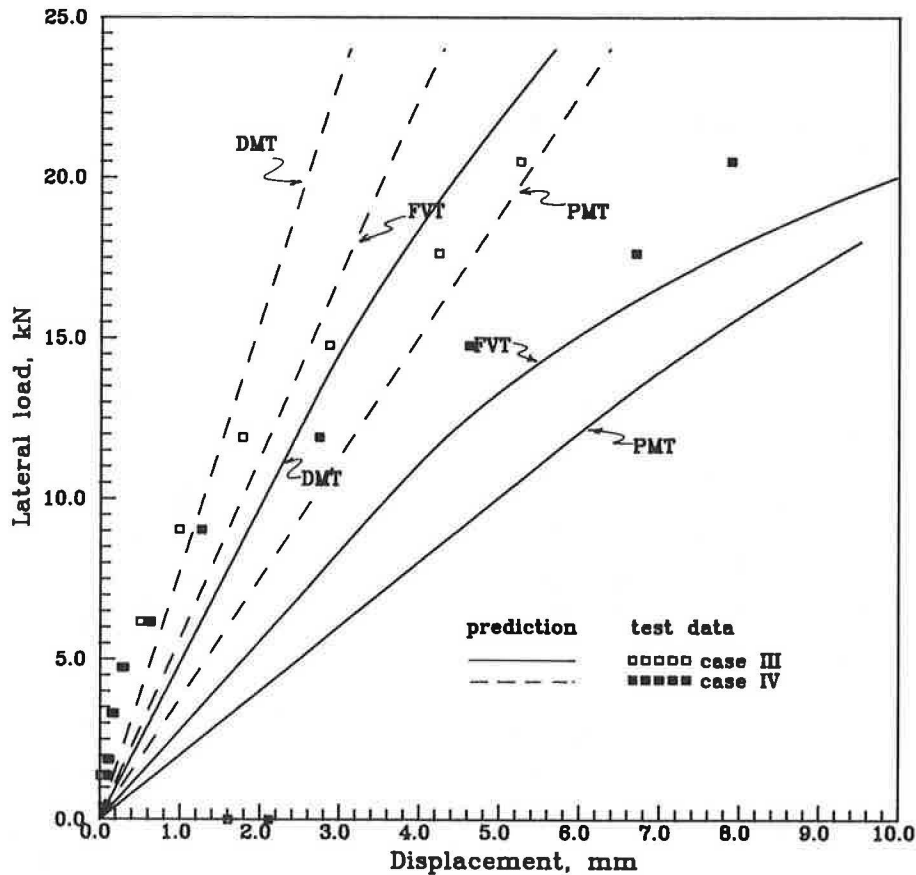


FIGURE 11 Predicted and measured displacement for Cases III and IV.

procedure should consider the scale effects of the small-diameter shafts and the existence of fissures.

## REFERENCES

1. B. B. Broms. Lateral Resistance of Piles in Cohesive Soils. *Journal of the Soil Mechanics and Foundation Engineering Division, ASCE*, Vol. 90, No. SM2, 1964, pp. 27–63.
2. B. B. Broms. Lateral Resistance of Piles in Cohesionless Soils. *Journal of the Soil Mechanics and Foundation Engineering Division, ASCE*, Vol. 90, No. SM3, 1964, pp. 123–156.
3. C. S. Desai and G. C. Appel. 3-D Analysis of Laterally Loaded Structures. *Proc., 2nd International Conference on Numerical Methods in Geomechanics*, Blacksburg, Va., 1976, pp. 405–418.
4. L. C. Reese and J. D. Allen. *Drilled Shaft Design and Construction Guidelines Manual*, Vol. 2, *Structural Analysis and Design for Lateral Loading*. U.S. Department of Transportation Offices of Research and Development Implementation Division HDV-22, Washington, D.C., 1977, 227 pp.
5. M. Jamiolkowski and A. Garassino. Soil Modulus for Laterally Loaded Piles. *Proc., Special Session No. 10, 9th International Conference on Soil Mechanics and Foundation Engineering*, Tokyo, Japan, 1977, pp. 43–57.
6. J. L. Briaud, T. Smith, and B. Meyer. Laterally Loaded Piles and the Pressuremeter: Comparison of Existing Methods. In *Laterally Loaded Deep Foundations: Analysis and Performance* (J. A. Langer et al., eds.), ASTM STP 835, ASTM, Philadelphia, Pa., 1984, pp. 97–111.
7. S. M. Gazizoglu and M. W. O'Neill. Evaluation of  $p$ - $y$  Relationships in Cohesive Soils. *Proc., Analysis and Design of Pile Foundations, ASCE National Convention*, San Francisco, Calif., 1984, pp. 192–213.
8. P. K. Robertson, J. M. O. Hughes, R. G. Campanella, and A. Sy. Design of Laterally Loaded Displacement Piles Using a Driven Pressuremeter. In *Laterally Loaded Deep Foundations: Analysis and Performance* (J. A. Langer et al., eds.), ASTM STP 835, ASTM, Philadelphia, Pa., 1984, pp. 229–238.
9. H. Matlock. Correlations for Design of Laterally Loaded Piles in Soft Clay. Paper No. OTC 1204, *Proc., 2nd Annual Offshore Technology Conference*, Houston, Tex., 1970, pp. 578–588.
10. F. Baguelin, J. F. Jézéquel, and D. H. Shields. *The Pressuremeter and Foundation Engineering*. Trans Tech Publications, Gower Publishing Co., Brookfield, Vt., 1978, 617 pp.
11. A. J. Lutenegeger. Current Status of the Marchetti Dilatometer Test. *Proc., Penetration Testing 1988, ISOPT-1*, Orlando, Fla., 1988, pp. 137–156.
12. M. A. Gabr and R. H. Borden. Analysis of Load Deflection Response of Laterally Loaded Piers Using DMT. *Proc., Penetration Testing 1988, ISOPT-1*, Orlando, Fla., 1988, pp. 513–520.
13. M. Jamiolkowski, C. C. Ladd, J. T. Germaine, and A. Lancelotta. New Developments in Field and Laboratory Testing of Soils. Theme Lecture, *Proc., 11th International Conference on Soil Mechanics and Foundation Engineering*, San Francisco, Calif., 1985, Vol. 1, pp. 57–154.
14. G. E. Bauer and A. Tanaka. Penetration Testing of a Desiccated Clay Crust. *Proc., Penetration Testing 1988, ISOPT 1*, Orlando, Fla., 1988, pp. 477–488.

Publication of this paper sponsored by Committee on Soil and Rock Properties.

# Soil Stratification Using the Dual-Pore-Pressure Piezocone Test

ILAN JURAN AND MEHMET T. TUMAY

**Among in situ testing techniques presently used in soil stratification and identification, the electric quasistatic cone penetration test (QCPT) is recognized as a reliable, simple, fast, and economical test. Installation of pressure transducers inside cone penetrometers to measure pore pressures generated during a sounding has added a new dimension to QCPT—the piezocone penetration test (PCPT). In this paper, some of the major design, testing, de-airing, and interpretive problems with regard to a new piezocone penetrometer with dual pore pressure measurement (DPCPT) are addressed. Results of field investigations indicate that DPCPT provides an enhanced capability of identifying and classifying minute loose or dense sand inclusions in low-permeability clay deposits.**

The construction of highway embankments and reclamation projects in deltaic zones often requires continuous soil profiling to establish the stratification of heterogeneous soil deposits. It is of particular significance to identify in these freshly deposited soils the presence of loose sandy layers that could potentially liquefy. The piezocone penetration test (PCPT) offers the unique capability of continuous, detailed, and simultaneous monitoring of the excess pore water pressures generated during penetration, along with the conventional measurements of tip resistance and/or sleeve friction. Therefore, during the last 15 years, PCPT has been extensively used in geotechnical investigations to establish soil stratification.

Significant research has been conducted by several investigators (1–17) to evaluate the effect of the main design, testing, and performance parameters (specifically: the cone shape, diameter and apex angle, and configuration; as well as the location of the piezometric element, and the penetration rate) on the pore water pressures measured during penetration.

Most of these studies have been conducted in fine-grained low-permeability soils. They have demonstrated that the location of the piezometric element has a major effect on the magnitude of pore water pressures measured ( $u_t$ ). The fundamental differences in the strain paths at the cone tip and along the penetrometer shaft result in a significantly different pore water pressure response. At the cone tip, the soil is subjected to both maximum compression and interface shear. The generated pore water pressures ( $u_t$ ) are primarily dominated by the increase of normal stress which can be related to the point resistance. Along the penetrometer shaft, and in particular immediately behind the cone friction sleeve, the soil is subjected mainly to shearing, and the measured pore water pressures depend primarily on the tendency of the sat-

urated soil to dilate or contract during shearing. The pore water pressures measured at the cone tip and the shaft *immediately* behind the cone tip were found to be highly dependent upon the stress history, sensitivity, and stiffness-to-strength ratio of the soil. Therefore, several charts dealing with soil classification and stress history [i.e., overconsolidation ratio (OCR)] have been developed using the point resistance and the excess pore water pressures measured *immediately* behind the tip (18–20) and at the cone tip (6,16), respectively.

Interpretation of excess pore water pressures ( $\Delta u = u_t - u_0$ , where  $u_0$  is hydrostatic water pressure) measured in sandy soils, and their use in soil classification, are more complex because the magnitude of these pore water pressures is highly dependent upon the ratio of the penetration rate to hydraulic conductivity of the soil. However, an attempt has been made to incorporate pore pressures measured in silty fine sands at the standard penetration rate of 2 cm/sec in the classification charts. Moreover, as the pore water pressures measured along the penetrometer shaft immediately behind the tip were found to be highly sensitive to the dilatant/contractive behavior of these soils (20,21), the piezocone appeared to provide a unique testing capability for identifying potentially liquefiable loose sand seams in freshly deposited stratified soils.

To enhance this capability, the concept of a “dual piezocone” was proposed by Tumay and Juran (22); it would allow simultaneous measurement of the pore water pressures at the tip, and along the penetrometer shaft behind the friction sleeve, together with tip resistance and sleeve friction. The LSU/Fugro Dual Pore Pressure Piezocone depicted in Figure 1 was later designed and fabricated (23–25). This paper first presents the design considerations pertaining to the development of the dual-pore-pressure piezocone penetration test (DPCPT) and discusses the results of soundings conducted in Louisiana in normally consolidated clay deposits, and in France in relatively heterogeneous soils of Flandria clay, with inclusions of loose and dense sand layers.

## DUAL-PORE-PRESSURE PIEZOCONES PENETROMETER—DESIGN AND DE-AIRING CONSIDERATIONS

Previous experimental and theoretical studies (1,5,6,16,17,26–31) have shown the individual merits of piezocones with pore pressure measurement capabilities on the shaft immediately behind the cone tip or the midsection of the cone tip. It has been proposed that piezometric measurement on the cone tip is best suited for investigations regarding soil classification,

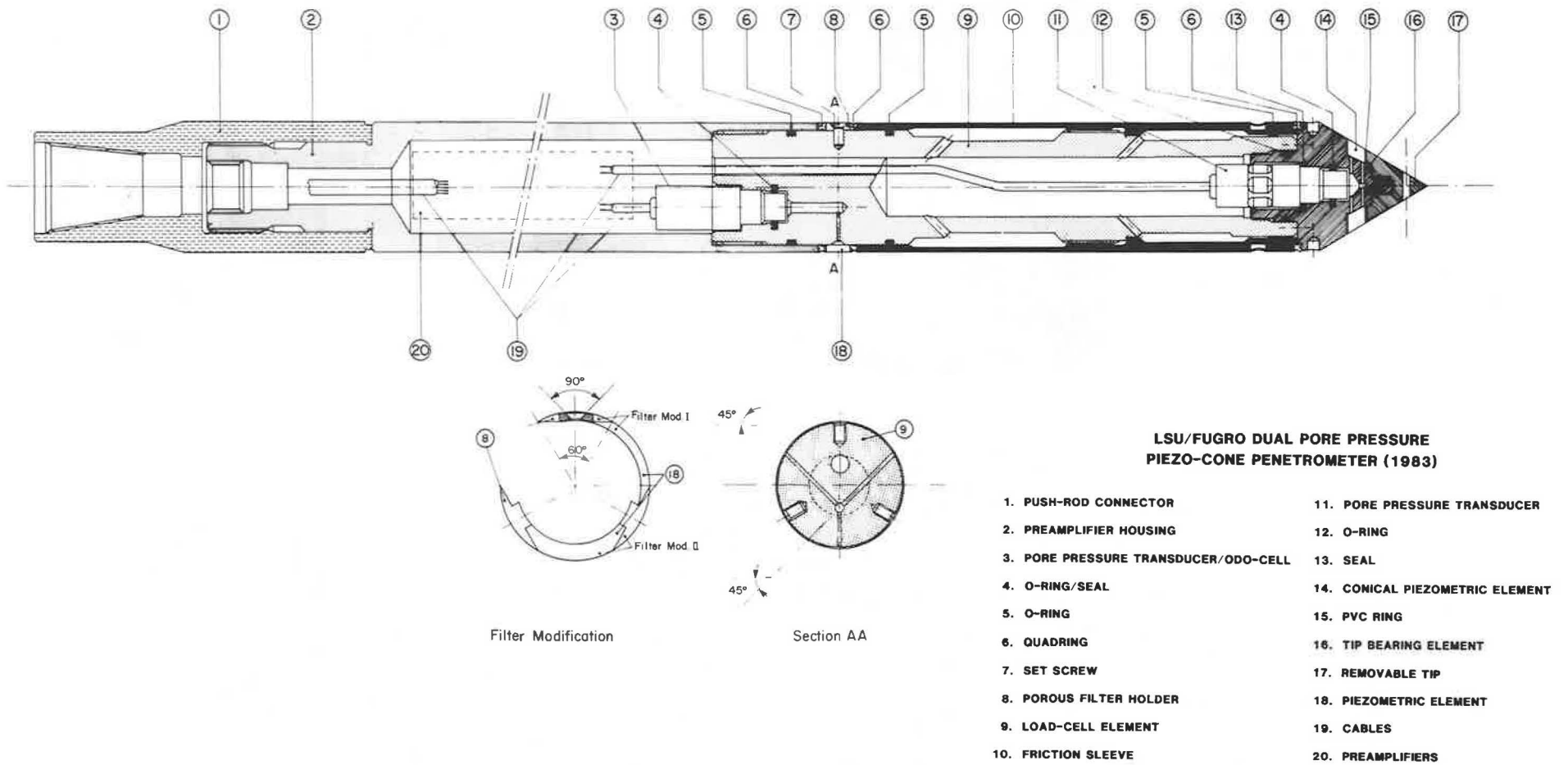
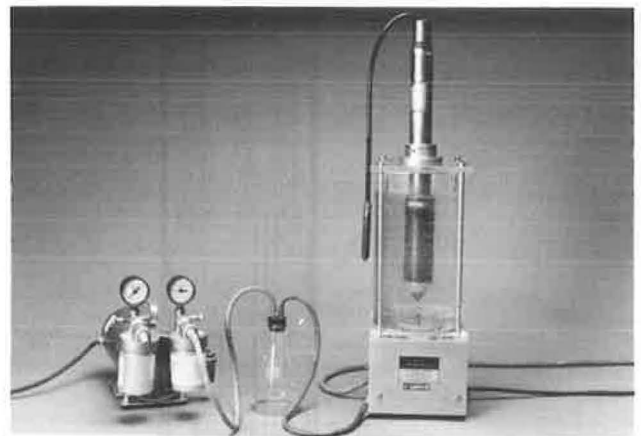
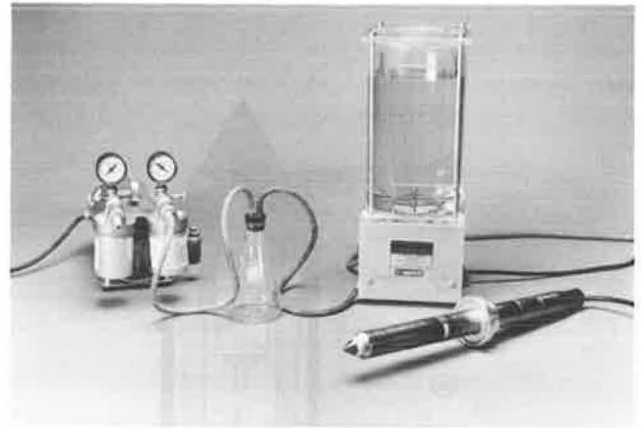


FIGURE 1 Cross-sectional view of DPCPT (23-25).

whereas the pore pressures measured along the shaft tend to reflect the stress history of the sediments penetrated. Theoretical studies by Al-Awkati (26), Tumay and Yilmaz (32), Acar and Tumay (16), and Kioussis et al. (17) have further hypothesized the likelihood of the presence of a significant unloading zone (i.e., tendency toward separation of the soil and shaft interface) immediately behind the cone tip, extending approximately twice to three times the radius of the shaft. The concept of the dual-pore-pressure piezocone penetration test (DPCPT) has thus evolved from the necessity of making reliable measurements of pore pressures generated during a CPT for proper soil stratification/classification and stress history (OCR) identification. The respective locations of the piezometric elements were initially envisaged to be on the face of the cone tip and at the mid-section of the friction sleeve about 3 cone diameters behind the cone. Observations on the wear of the cone tip and friction sleeve with respect to penetrometer use (5) have demonstrated these locations to be subjected to maximum soil-penetrometer interaction. Due to practical reasons, however, the piezometric element on the shaft was finally emplaced behind the friction sleeve 17 cm behind the tip of a 15-cm<sup>2</sup> cone. Figure 1 shows the cross-sectional view of the LSU/Fugro DPCPT. The dual pore pressure measurement configuration of this probe takes into account the basic parameters of design, namely: (a) identical pore pressure transducers, (b) identical material properties (i.e., compressibility, pore size, hydraulic conductivity, etc.) of piezometric element, (c) equal pore pressure chamber volumes, (d) compressibility and viscosity of pore pressure chamber fluid, (e) equal thickness of piezometric elements, and (f) equal lateral surface area of piezometric elements in contact with soil to ensure compatible and comparable pore measurements at two locations during a sounding. The piezometric elements used in LSU/Fugro DPCPT were ceramic (aerolith 10) with a hydraulic conductivity of  $10^{-2}$  cm/sec and a nominal filtration grade of 15 microns. Calibration tests conducted in the lab to check compliance proved it unnecessary to use viscous fluids (i.e., glycerin, silicone oil, etc.) instead of water in the pore pressure chamber (25).

One of the most important aspects of the PCPT is the complete saturation of the pressure-sensing cavities (i.e., the piezometric element and the pore pressure chamber). Complete saturation is essential because compressible gas bubbles inside the measuring system would lead to an increase in the response time, affecting the accuracy and repeatability of results. The traditional de-airing technique used for piezometric elements is boiling and/or the application of  $10^{-2}$  to  $10^{-3}$  mm Hg vacuum. Vacuum saturation of the piezometric element and pressure-sensing cavities using special portable attachments on the cone tip in the field have been successfully used in the past (31). However, with the addition of a second piezometric element, the sheer size of the probe, which needed to be bodily housed in a portable vacuum chamber, became problematic. The saturation of the measuring system has to be done before each test and, in principle, may be influenced by the operator. Thus, a new technique that could easily and repeatedly be carried out in the field was needed.

Figure 2 depicts the Nold DeAerator system, modified to achieve saturation of the DPCPT by mechanically generating the phenomena of nucleation and cavitation, by which gases are removed from their dissolved state at much higher rates



**FIGURE 2** General view of the Nold DeAerator modified for DPCPT de-airing (34).

than are possible with conventional heat-boiling and vacuum methods (33). The unit consists of a sealed tank, an electric motor, a magnetic clutch, an impeller, and a water-powered aspirator. A vacuum, applied through a hollow support tube, draws water into the tank via an intake valve; the motor is energized, rotating the impeller.

Cavitation forms at ultra-high vacuum around the impeller vanes, violently agitating and breaking liquid into a fine, mist-like spray (nucleation). Centrifugal force hurls the released gases (air, hydrogen sulfide, sulfur dioxide, methane, radon, etc.) outward; they then bubble up to the partially evacuated space above the liquid surface and are withdrawn through the vacuum tube (34).

#### **PENETRATION TESTS WITH THE DUAL-PORE-PRESSURE PIEZOCONE PENETROMETER**

Field verification and calibration tests of the DPCPT were conducted in Louisiana (24,33,35) and in France (36,37). A series of 19 tests were completed at sites in Dunkerque, France, and Grand Isle and Norco, Louisiana, with four different

types of cone penetrometers: (a) the 10-cm<sup>2</sup> Fugro electrical cone measuring the point resistance ( $q_c$ ) and sleeve friction ( $f_s$ ) (QCPT); (b) the 10-cm<sup>2</sup> Fugro piezocone measuring pore water pressure ( $u_t$ ) at the middle of the cone tip, as well as point resistance ( $q_c$ ) (PCPT); (c) the 15-cm<sup>2</sup> piezocone measuring  $q_c$ ,  $f_s$ , and  $u_t$  at the middle of the tip (PCPT); and (d) the 15-cm<sup>2</sup> dual-pore-pressure piezocone measuring  $q_c$ ,  $f_s$ , and  $u_t$  at the middle of the tip and behind the friction sleeve on the penetrometer shaft (DPCPT). The main objective of these penetration tests was to evaluate the effect of the cone diameter, the penetration rate, and the location of the piezometric elements on the measured soil response parameters.

Figure 3 shows the soil profile established by self-boring pressuremeter tests (PMTs) and piezocone penetration tests (PCPTs) in the Dunkerque site. The site consists of an upper sandy layer, 16 m deep, underlain by a Flandria clay layer. The soil profile obtained by DPCPT sounding at the Grand Islé, Louisiana, site is depicted in Figure 4. A 16-m-deep loose and dense sand layer with inclusions of silt and clay, underlain by Belize Delta clay with sand/silt lenses, closely parallels the characteristics of the Dunkerque site. In both soil profiles, the upper part of the clay layer includes loose and dense sand layers that are of specific interest in evaluating the stratification capability of the DPCPT and specifically the sensitivity of dual pore water pressure measurement in loose and dense sand/silt inclusions.

**Effect of Cone Diameter**

Figure 5 shows typical CPT and PCPT soil profiles at Dunkerque obtained with the 10-cm<sup>2</sup> and 15-cm<sup>2</sup> cones. The cone diameter is found to have practically no effect on the point resistance and excess pore water pressures measured at the tip, provided that the cone diameter ( $d$ ) and the shaft diameter ( $D$ ) are the same (i.e.,  $d/D = 1$ ). However, cone diameter does affect the measured sleeve friction: the 10-cm<sup>2</sup> cone systematically yields values about 20 percent higher than those obtained with the 15-cm<sup>2</sup> cone.

**Effect of Penetration Rate**

Figure 6 shows the PCPT profiles at Dunkerque of  $q_c$  and the excess pore pressure  $\Delta u$  obtained with the 15-cm<sup>2</sup> cone at penetration rates of 0.2 cm/s and 10 cm/s. The penetration rate is also found to have no appreciable effect on the  $q_c$  values recorded in the sand and clay layers. However, it has a significant effect on the pore water pressures measured in the sand. At the penetration rate of 0.2 cm/s, the measured pore water pressures approach the hydrostatic  $u_0$ , whereas the penetration at the rate of 10 cm/s generates pore water pressures that reach 4 times  $u_0$ .

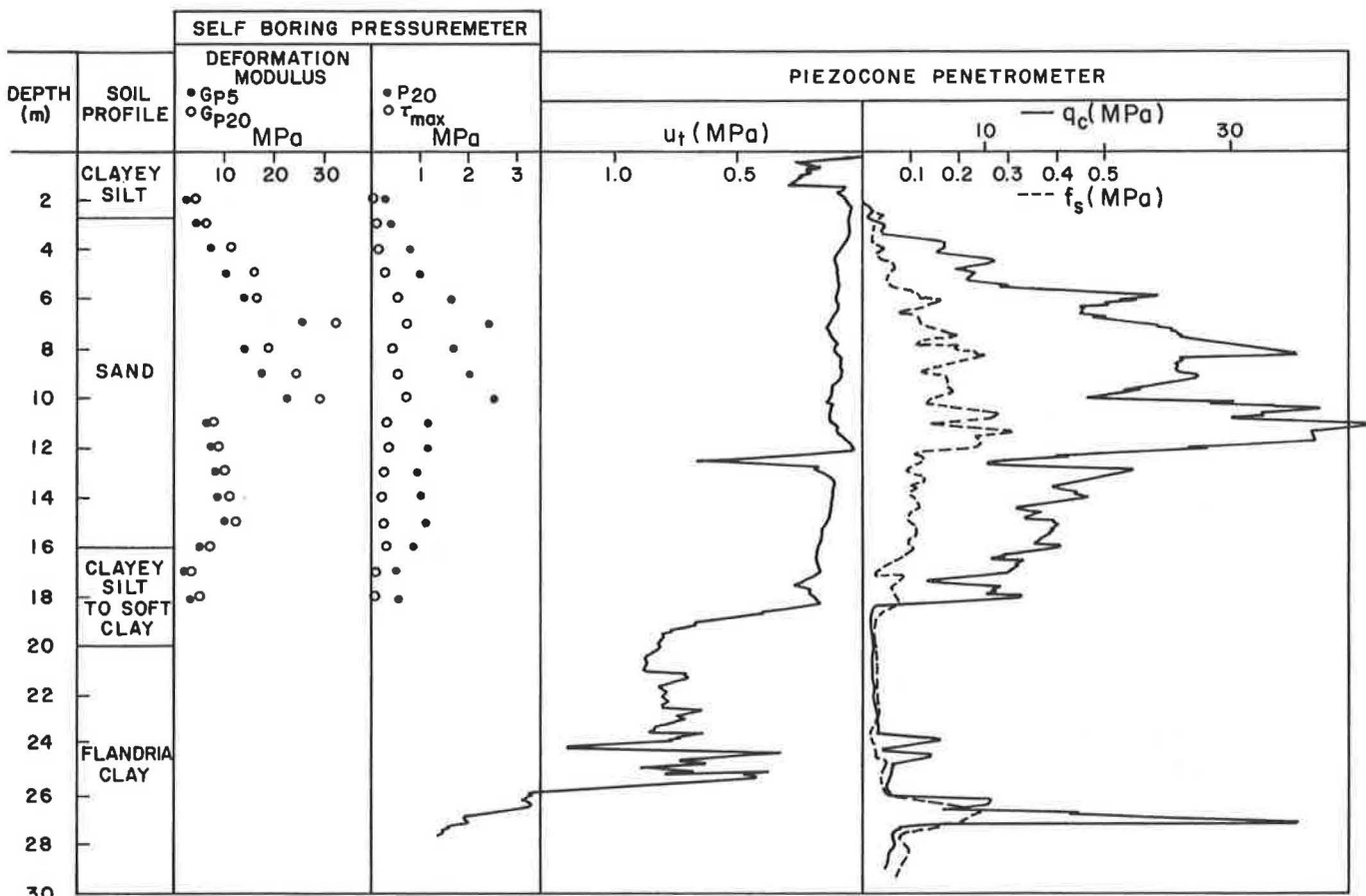
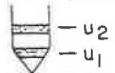
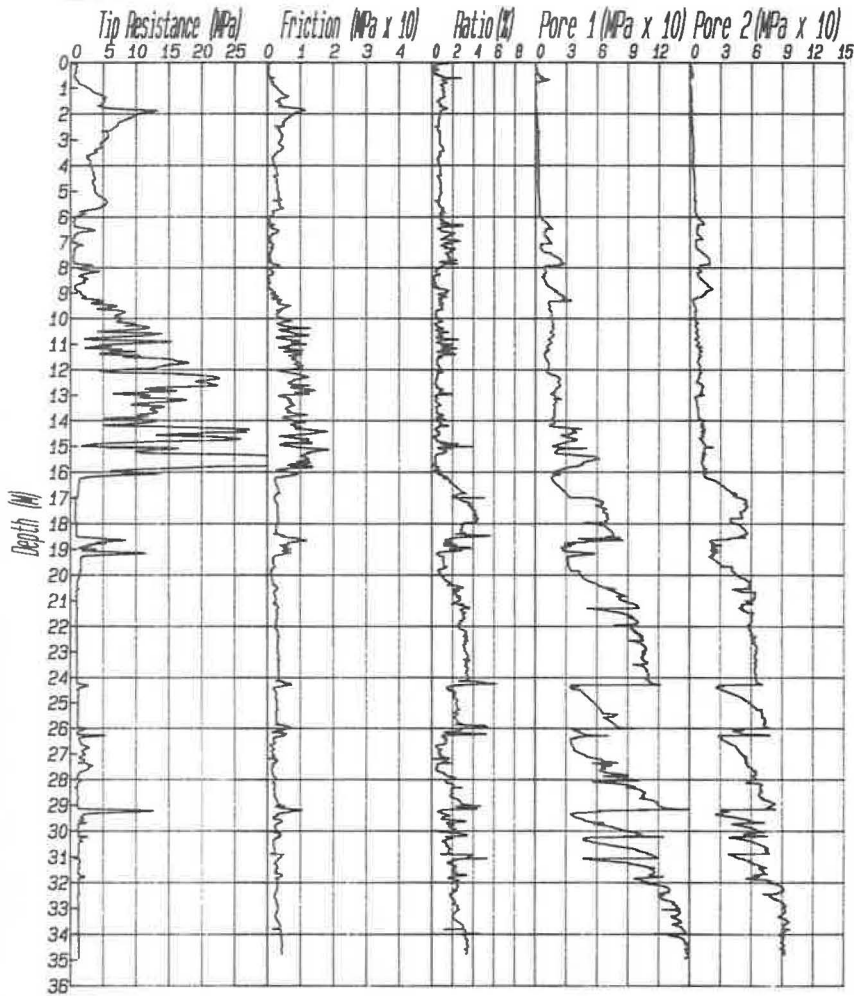



FIGURE 3 Soil profiles in the Dunkerque site.

(a)

LSU Cone Penetration Test Result		
Location : GRAND ISLE	Cone Type: F7.5CKEM	Remarks :
Site : BEACH	Cone No. : 01	2.5 meters pre-punched
Date : 06-04-86	Tip Angle: 60 degrees	
Time : 14:00	Area : 15 Sq. cm	
Test No. : 01	Water Table: .5 METER	



(b)

LSU Cone Penetration Test Result		
Location : GRAND ISLE	Cone Type: F7.5CKEM	Remarks :
Site : BEACH	Cone No. : 01	2.5 meters pre-punched
Date : 06-04-86	Tip Angle: 60 degrees	
Time : 14:00	Area : 15 Sq. cm	
Test No. : 01	Water Table: .5 METER	

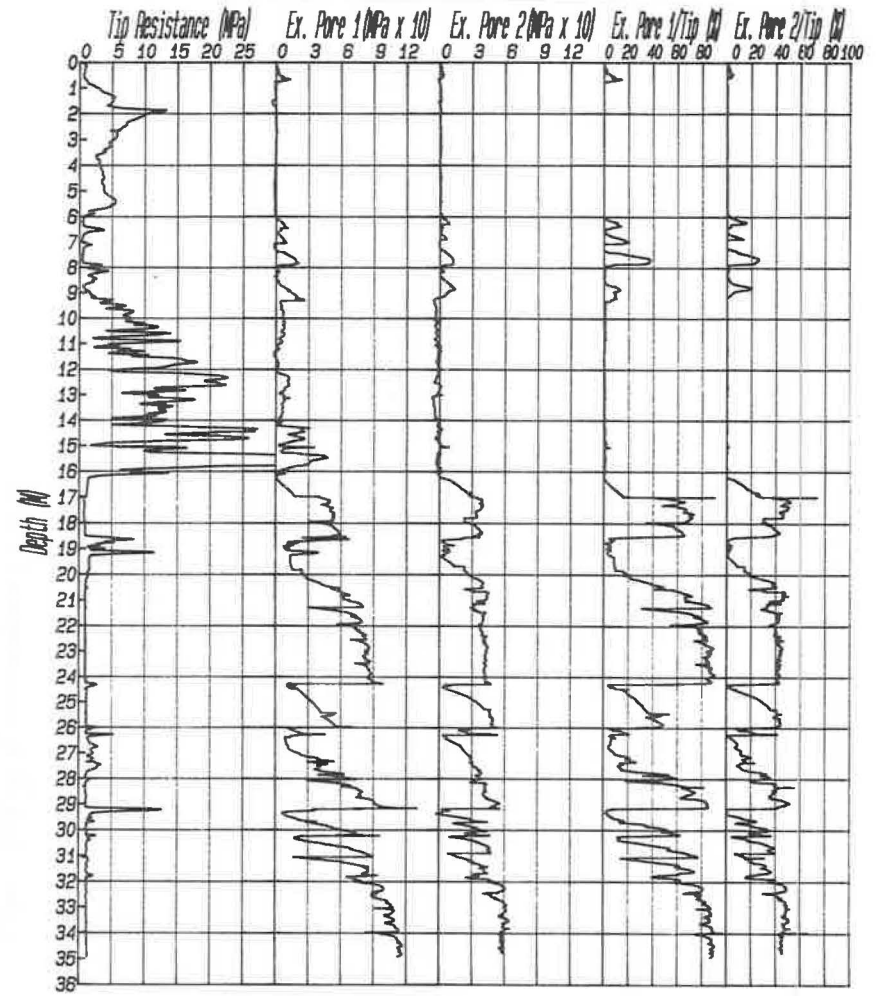


FIGURE 4 (a) Profiles of  $q_c$ ,  $f_s$ ,  $q_c/f_s$ ,  $u_1$ , and  $u_2$  at Grand Isle, Louisiana. (b) Profiles of  $q_c$ ,  $u_1$ ,  $u_2$ ,  $u_1/q_c$ ,  $u_2/q_c$  at Grand Isle, Louisiana.

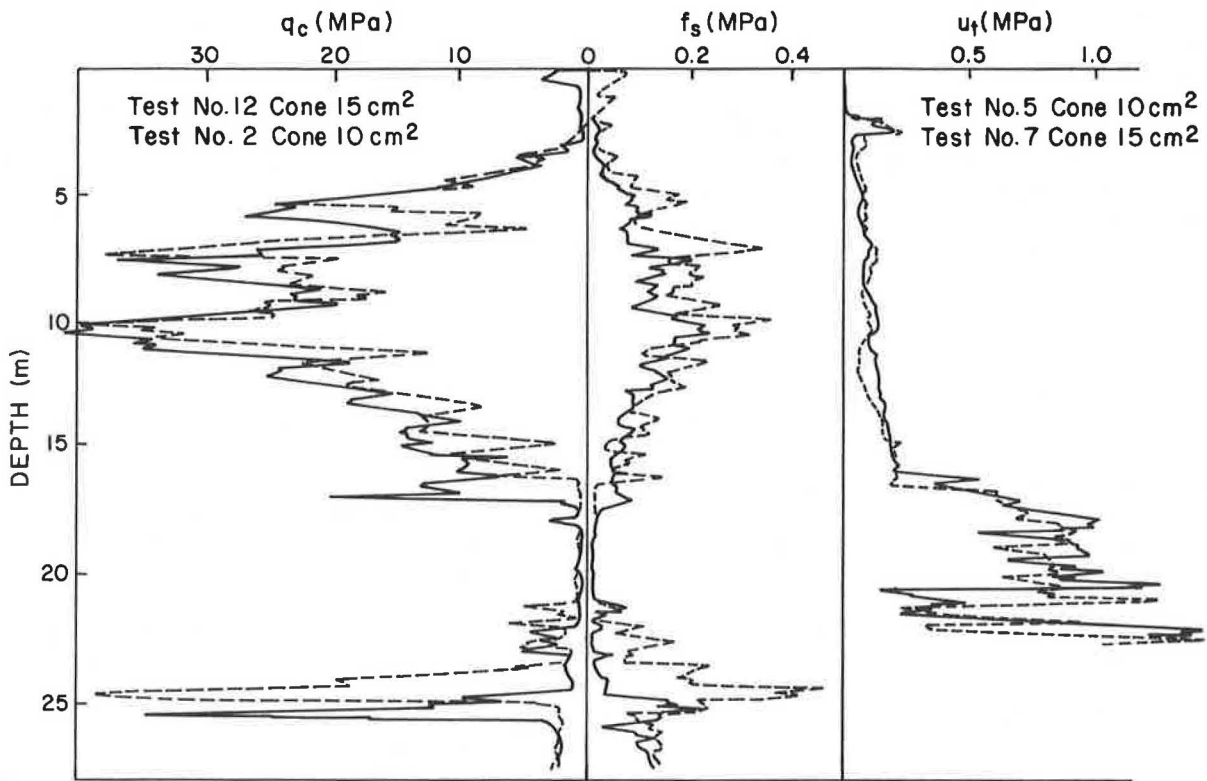


FIGURE 5 Effect of cone diameter on PCPT profiles in the Dunkerque site.

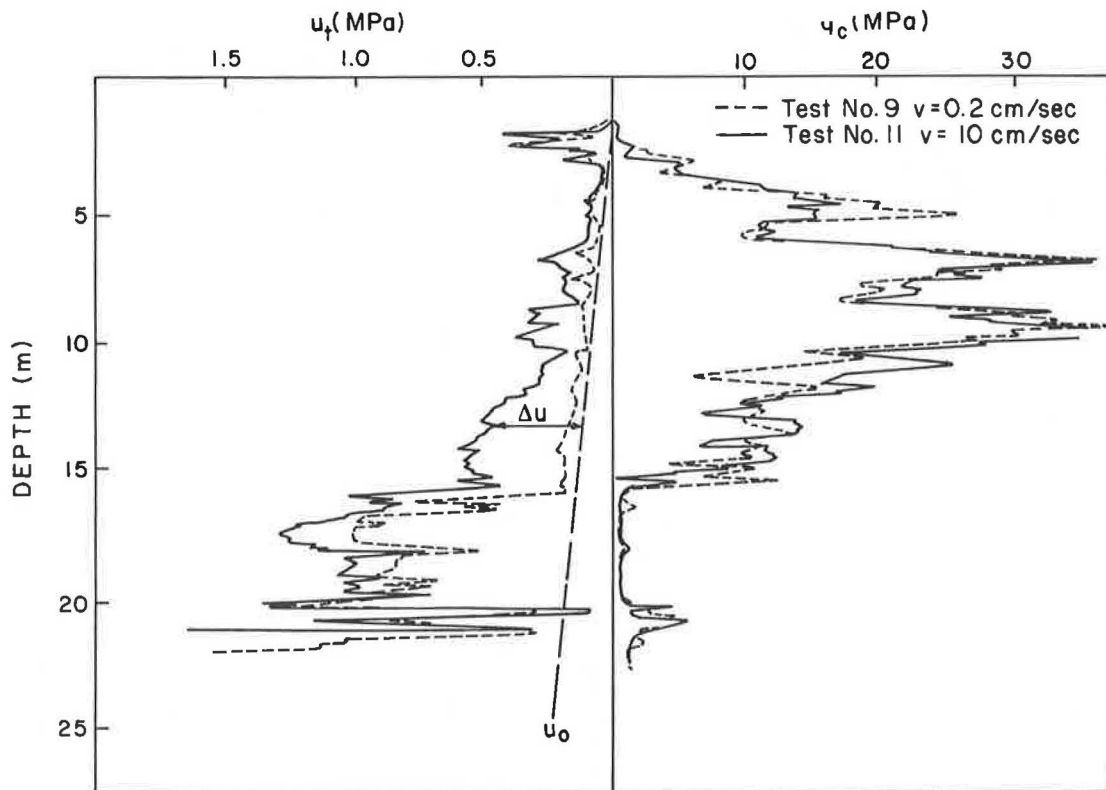


FIGURE 6 Effect of penetration rate on PCPT profiles in the Dunkerque site.

The measured excess pore water pressures ( $\Delta u$ ) are found to be highly sensitive to the existence of loose sand inclusions in the clay layer (at depths of 16 to 23 m at Dunkerque and 16.5 to 26 m at Grand Isle) (Figures 4 through 6). The excess pore water pressures decrease substantially due to dissipation in these highly permeable sand seams (at depths of 17, 18.6, 21, and 22 m at Dunkerque; 18.5, 19.2, and 24.2 m at Grand Isle), which cannot practically be detected using any other of the available in situ soil testing techniques.

### Effect of Location of Porous Stones

Figures 4 and 7 show typical DPCPT soil profiles obtained at the Grand Isle and Dunkerque sites, respectively, with the dual piezocone at the standard penetration rate of 2 cm/s. The location of the porous stone is found to have a significant effect on the recorded  $\Delta u$  profiles. The excess pore water pressures measured at the tip, both in the sand and the clay layers, are systematically positive and higher than those measured at the sleeve. In the upper sand layer, generally positive excess pore water pressures are measured at the tip, whereas those measured at the sleeve correspond to the hydrostatic  $u_0$  or somewhat below. In the normally consolidated clay layer (depth, 17 to 22 m at Dunkerque; 20 to 30+ m at Grand Isle), the excess pore water pressures measured at the tip are about double those measured behind the sleeve. It is of particular interest to note that the pore water pressure response in the upper dense sand layer is significantly different from that measured in the dense sand inclusions (depth, 25 to 26 m at Dunkerque; 18.5 to 19.5, and 29.5 m at Grand Isle)

located within the clay layer. This major difference is due to the boundary drainage conditions associated with a sand inclusion in a clayey deposit that substantially reduces the rate of dissipation. The excess pore water pressures measured at the tip in the sand inclusion are found to be several times (5 to 10 times) higher than those measured in the upper sand layer (depth, 7 to 12 m at Dunkerque; 1 to 5.5 m at Grand Isle), whereas the  $q_c$  and  $f_s$  values are about the same. Specifically, the very low to negative excessive pore water pressures measured at the sleeve in the dense sand inclusions illustrate that the effect of the location of the porous stone is much more significant in sand inclusions than in the relatively thick sand deposits. The dual piezocone thus appears to provide a significant and uniquely enhanced capacity to identify sand inclusions situated in clay deposits of low hydraulic conductivity.

### PIEZOCONE TESTING IN STRATIFIED SOIL SYSTEMS OF CLAY DEPOSITS WITH THIN SAND INCLUSIONS

Figure 8 illustrates the use of the dual piezocone in identifying loose and dense sand inclusions in a silty clay deposit. In the loose sand inclusion (depth, 22 to 23 m), the excess pore water pressures measured both at the tip and the sleeve are positive. In the dense sand inclusion (depth, 25 to 26 m), the high increase in the normal stress on the tip, associated with high  $q_c$  values, results in high positive excess pore water pressures (greater than 2 MPa, about 10 times  $u_0$ ) at the tip, whereas the excess pore water pressures measured at the sleeve are negative ( $-0.26$  MPa), indicating that the sand tends to dilate

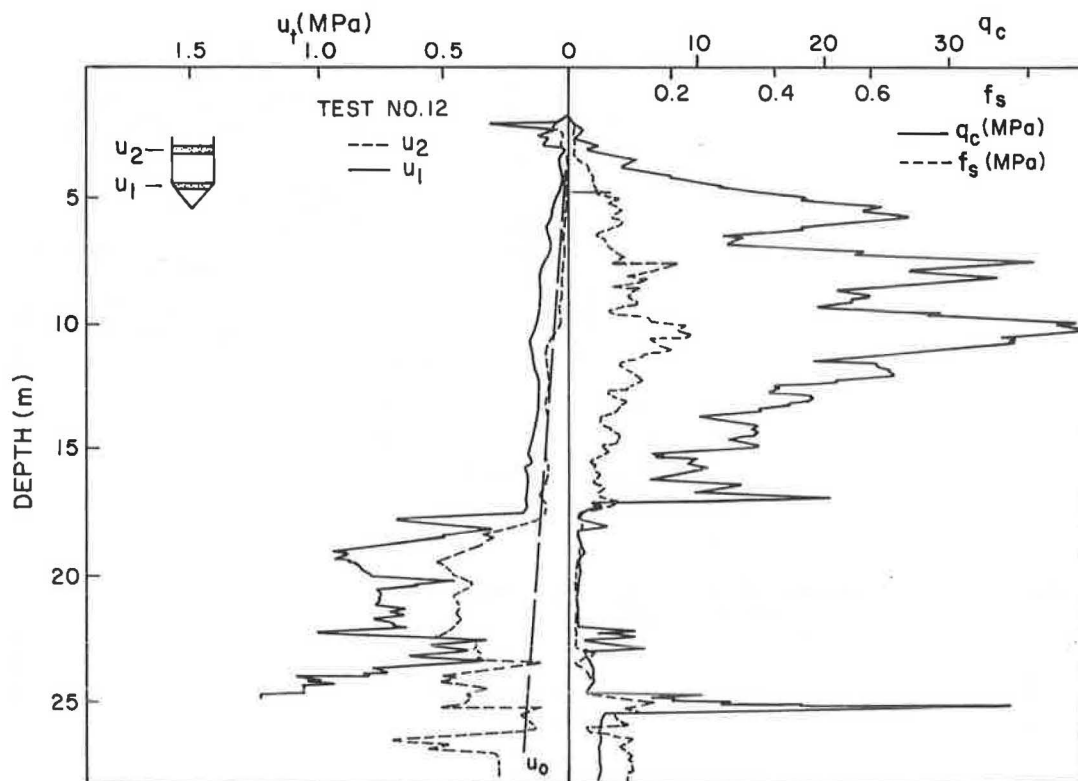


FIGURE 7 Dual piezocone penetration test profiles in the Dunkerque site.



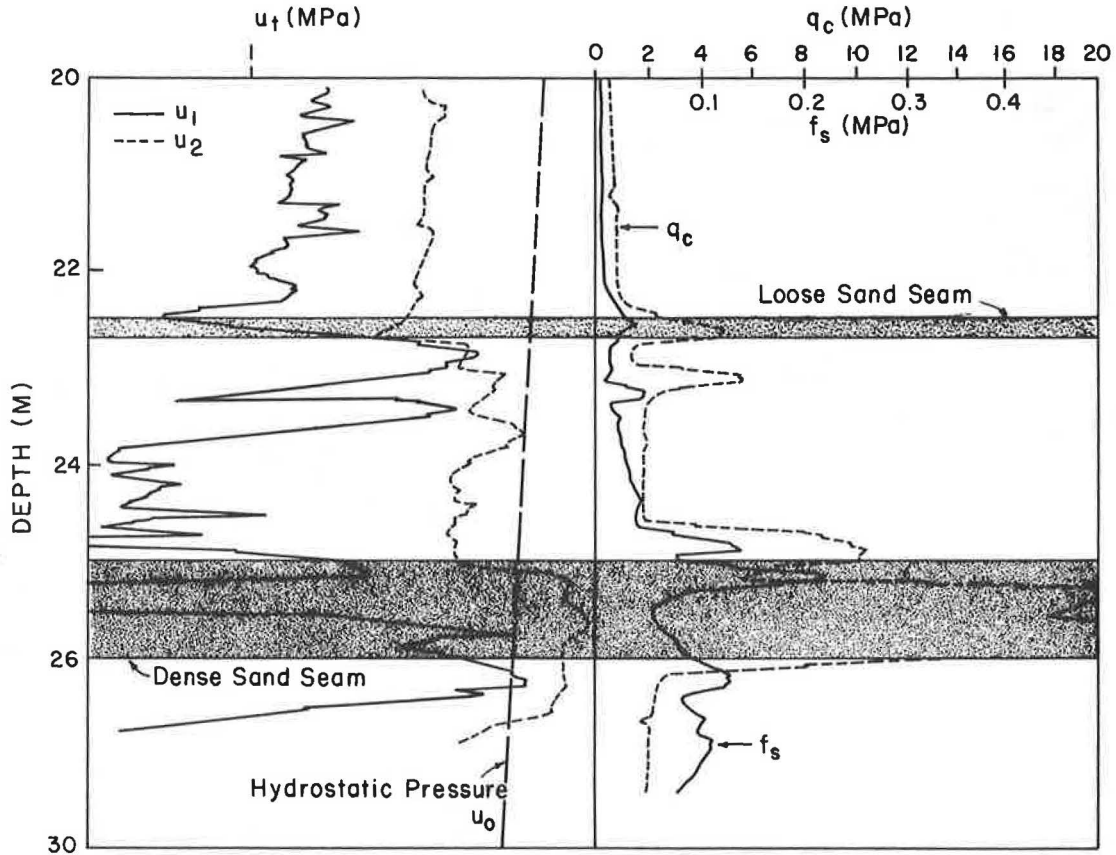


FIGURE 8 Dual piezocone penetration test profiles in clayey silt with sand inclusion (Dunkerque site).

during its shearing. Dissipation tests that provide useful means to evaluate in situ the hydraulic conductivity of the soil can significantly extend the data base for soil stratification. Figure 9 shows the dissipation curves measured in the silty clay layer at both the sleeve and the tip.

It is of interest to report at this point the results of a series of piezocone tests in a similar site of a 40-m-deep silty clay layer with inclusions of loose sand seams, namely the Nice harbor site in France. In this site, a conventional 10-cm<sup>2</sup> piezocone with a porous stone at the middle of the tip has been used (38) to identify potentially liquefiable sand layers that could have caused the quasi-instantaneous sliding collapse of the 10 Mm<sup>3</sup>-harbor dike. Figure 10 shows typical penetration profiles ( $q_c, u_t$ ) obtained in this site. These penetration profiles illustrate that subhorizontal loose sand seams less than 10 cm in thickness can be identified using the piezocone. As the penetration reaches a sand seam, there is an increase of the point resistance ( $q_c$ ), associated with an increase of positive excess pore water pressure exceeding that measured in the surrounding silty clay layer. Dissipation tests conducted both in the silty clay layer and the sand seams indicated significantly different hydraulic conductivities of the two soil layers (Figure 11) and thereby improved the data base for the soil stratification. However, it should be indicated that the excess pore water pressures measured at the tip in these loose sand inclusions are mainly governed by the soil compression around the penetrating cone and, to a lesser extent, by the mechanical compression of the piezometric element in the cone tip, and

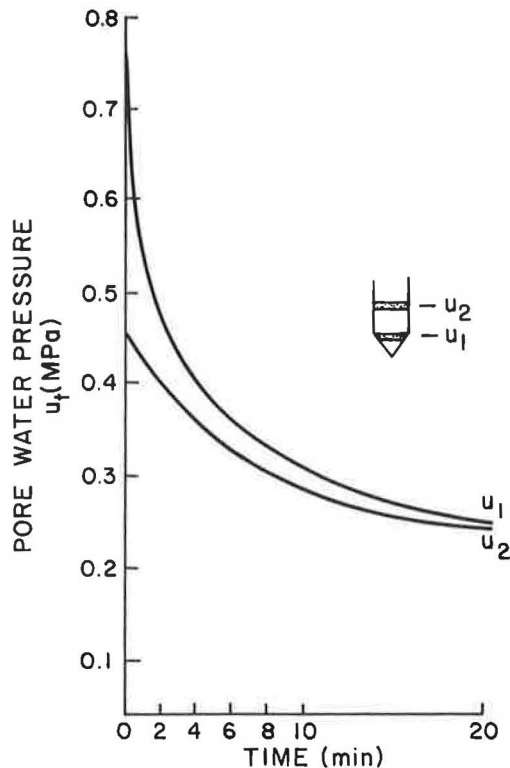


FIGURE 9 Dissipation tests in the Dunkerque site.

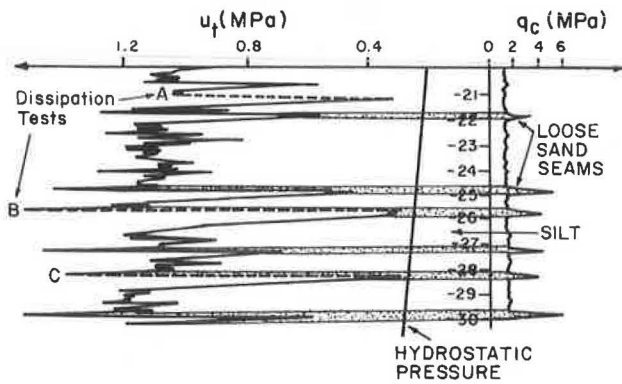


FIGURE 10 PCPT profiles in stratified silty soil with sand inclusions (Nice site).

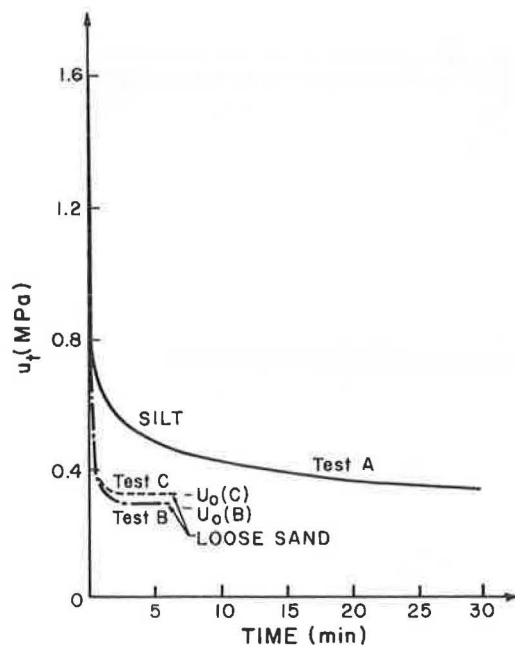


FIGURE 11 Dissipation tests for soil stratification in the Nice site.

therefore do not reflect their tendency to liquefy under rapid undrained shearing.

Interpretation of piezocone data in a stratified soil system of a clayey soil of low hydraulic conductivity containing loose or dense sand seams is a difficult task. The available classification charts for piezocone data (18,20) have been established for thick soil deposits. The drainage conditions at the boundaries of sand seams significantly reduce the dissipation rate and generally imply horizontal flow. Therefore, the pore water pressure response in such sand seams is significantly different from that measured in thick layers of similar sands at the same relative density (Figures 4 and 7). Figure 12 illustrates an attempt to use the classification charts proposed by Jones and Rust (18) for soil stratification in the Dunkerque site. The loose sand inclusion at the depth of 23 m (Figure 8) is characterized by the following piezocone data:  $\Delta u_{sleeve} = 400$  KPa,  $q_c = 4$  MPa (or  $q_c - \sigma_{v0} = 3.5$  MPa;  $\sigma_{v0}$  is the

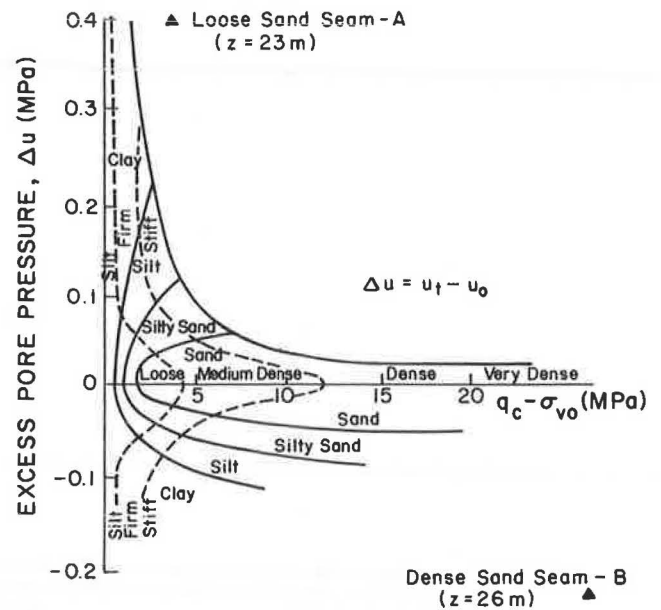


FIGURE 12 Classification of sand seams in Dunkerque site using Jones and Rust's (18) classification chart.

total overburden stress). For these piezocone data, the proposed chart would indicate that the sand seam under consideration cannot be classified because the measured excess pore water pressure is unexpectedly high. The dense sand inclusion at the depth of 25 to 26 m is characterized by piezocone data of  $\Delta u_{sleeve} = -200$  KPa,  $q_c = 35$  MPa. For these piezocone data, the classification chart would again indicate that the measured negative excess pore water pressures are unexpectedly high. An attempt is also made to use the classification charts proposed by Robertson and Campanella (20), depicted in Figure 13, for soil stratification in this site. These charts involve all the piezocone data:  $q_c$ ,  $\Delta u_{sleeve}$  and  $f_s$ , and use the normalized pore pressure parameter  $B_q = (u_t - u_0)/(q_t - \sigma_{v0})$  and the friction ratio  $F_R = f_s/q_c$ .

For the sand inclusions specified above, these classification charts indicated that:

- The loose sand layer (depth, 23 m) is identified as a silty sand using the  $q_c$ ,  $F_R$  data, but the high excess pore water pressure data would indicate a rather fine-grained soil (sandy to clayey silt) (Point A); and
- The dense sand layer (depth, 25 to 26 m) can be classified as gravelly sand to sand (Point B).

These charts, and specifically the use of the normalized pore water pressure parameter  $B_q$ , seem to be better adapted for the classification of sand inclusions in clayey soils. However, it is anticipated that a significant improvement of the data base for soil stratification can be gained by incorporating the difference in the pore water pressures measured at the tip and the sleeve in the classification charts.

## CONCLUSIONS

This paper presents a newly developed piezocone probe providing simultaneous measurement of pore pressures generated

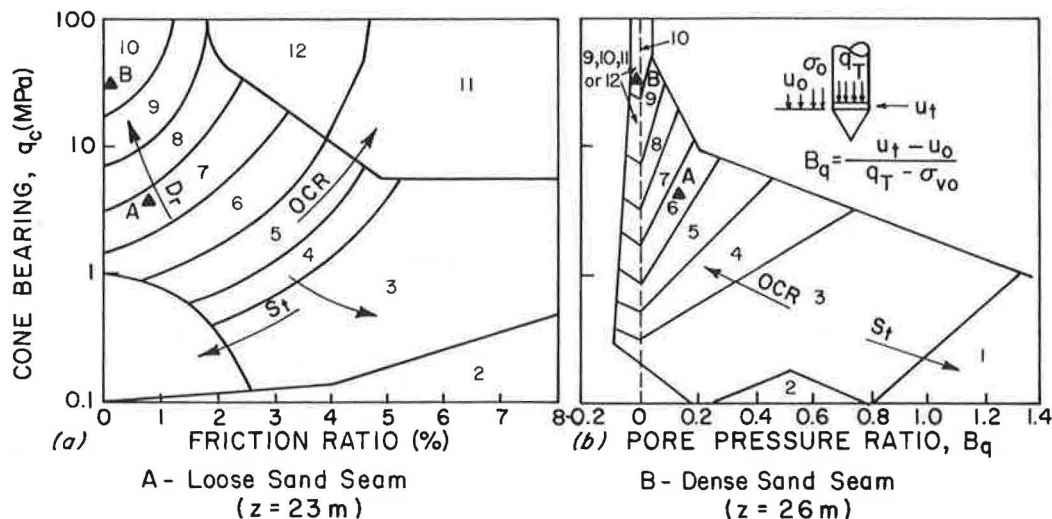


FIGURE 13 Classification of sand seams in the Dunkerque site using Robertson and Campanella's (20,21) classification chart.

both at the middle of the cone tip and along the penetrometer shaft behind the friction sleeve, together with monitoring of the tip resistance and sleeve friction. Design considerations and a novel de-airing technique are outlined.

The preliminary penetration tests conducted with the dual piezocone penetrometer illustrate that simultaneous measurement of excess pore water pressures at the middle of the cone tip and behind the friction sleeve provides valuable data for soil stratification. The pore water pressure response at both piezometric element locations is highly dependent on the strain path of the surrounding soil. Consequently, substantial differences are observed in the pore water pressures recorded during a sounding. In particular, the excess pore water pressure response at the middle of the tip is primarily governed by the increase of the normal stress and the cone tip, whereas the excess pore water pressure measured along the shaft (4 to 5 diameters behind the tip) is primarily dependent upon the tendency of the soil to contract or dilate during shearing. Therefore, the dual piezocone is of particular interest for the identification of potentially liquefiable loose sand seams often encountered in freshly deposited normally consolidated soils. However, in our present state of knowledge, the available classification charts do not provide appropriate means of identification of such inclusions. An attempt should be made to develop a reliable data base using the dual piezocone for the development of relevant classification charts.

REFERENCES

1. M. M. Baligh, V. Vivarant, and C. C. Ladd. *Exploration and Evaluation of Engineering Properties for Foundations Design of Offshore Structures*. Research Report R78-40, No. 607. Department of Civil Engineering, Massachusetts Institute of Technology, Cambridge, Mass., 1978.
2. M. M. Baligh and J. N. Levadoux. *Pore Pressure Dissipation after Cone Penetration*. Sea Grant Report No. 80-13. Massachusetts Institute of Technology, Cambridge, Mass., 1980, p. 368.
3. M. Roy, M. Tremblay, F. Tavenas, and P. LaRochelle. Induced Pore Pressures in Static Penetration Tests in Sensitive Clay. *Proc.*,

- 33rd Canadian Geotechnical Conference, Calgary, Alberta, Canada, 1980, pp. 11.3.1-11.3.13.
4. Y. B. Acar. *Piezocone Penetration Testing in Soft Cohesive Soils*. Fugro postdoctoral report, Geotechnical Engineering Report GE-81/01. Department of Civil Engineering, Louisiana State University, Baton Route, La., 1981, 31 pp.
5. M. T. Tumay, Y. B. Acar, and R. L. Boggess. *Subsurface Investigations with Piezocone Penetrometer*. ASCE Special Publication on Cone Penetration Testing. ASCE, New York, 1981, pp. 325-342.
6. M. T. Tumay, R. Yilmaz, Y. B. Acar, and E. DeSeze. Soil Exploration in Soft Clays with the Electric Cone Penetrometer. *Proc., 2nd European Symposium on Penetration Testing, ESOPT II*, Vol. 1, Amsterdam, The Netherlands, 1982, pp. 915-921.
7. I. Hajibakar and M. T. Tumay. *In situ Determination of Compressibility of Louisiana Soils Using Piezocone Penetration Tests (PCPT)*. Geotechnical Engineering Report FHWA/LA/LSU-GE-82/06. Department of Civil Engineering, Louisiana State University, Baton Route, La., 1982, 253 pp.
8. A. S. Chan, M. T. Tumay, and Y. B. Acar. *Analysis of Dissipation of Pore Pressures after Cone Penetration*. Geotechnical Engineering Report FHWA/LA/LSU-GE-82/05. Department of Civil Engineering, Louisiana State University, Baton Rouge, La., 1982, 131 pp.
9. R. G. Campanella, P. K. Robertson, and D. Gillespie. Cone Penetration Testing in Deltaic Soils. *Canadian Geotechnical Journal*, Vol. 20, No. 1, 1983, pp. 23-35.
10. R. G. Campanella, P. K. Robertson, D. G. Gillespie, and J. Greig. Recent Development in In Situ Testing of Soils. *Proc., 11th International Conference on Soil Mechanics and Foundation Engineering*, San Francisco, Calif., 1985.
11. M. Jamiolkowski, C. C. Ladd, J. T. Germaine, and R. Lancelotta. New Developments in Field and Laboratory Testing of Soils. State-of-the-Art Paper, *Proc., 11th International Conference of the Society for Soil Mechanics and Foundation Engineering (ICSMFE)*, San Francisco, Calif., 1985.
12. M. T. Tumay, Y. B. Acar, M. H. Cekirge, and N. Ramesh. Flow Fields around Cones in Steady Penetration. *Journal of Geotechnical Engineering*, Vol. 111, No. GT2, 1985, pp. 193-204.
13. N. Rad and M. T. Tumay. A Study of Pore Pressure Response of Piezocone Penetration Test (PCPT). *Geotechnical Testing Journal*, Vol. 8, No. 3, 1985, pp. 125-131.
14. T. Lunne, H. P. Christoffersen, and T. I. Tjelta. Engineering Use of Piezocone Data in North Sea Clays. *Proc., 11th International Conference on Soil Mechanics and Foundation Engineering*, San Francisco, Calif., 1985.
15. M. T. Tumay and Y. B. Acar. Piezocone Penetration Testing in

- Soft Cohesive Soil. In *Strength Testing of Marine Sediments: Laboratory and In Situ Measurements* (R. C. Chaney and K. R. Demars, eds.), ASTM STP 883, ASTM, Philadelphia, Pa., 1985, pp. 72–83.
16. Y. B. Acar and M. T. Tumay. Strain Field around Cones in Steady Penetration. *Journal of Geotechnical Engineering*, Vol. 112, No. GT2, 1986, pp. 207–213.
  17. P. D. Kioussis, G. Z. Voyiadjis, and M. T. Tumay. A Large Strain Theory and Its Application in the Analysis of Cone Penetration Mechanism. *International Journal for Numerical and Analytical Methods in Geomechanics*, Vol. 12, No. 1, 1988, pp. 45–60.
  18. G. A. Jones and E. A. Rust. Piezometer Penetration Testing CPTU. *Proc., 2nd European Symposium on Penetration Testing, ESOPT II*, Amsterdam, The Netherlands, Vol. 2, 1982, pp. 607–613.
  19. K. Senneset, N. Janbu, and G. Svanø. Strength and Deformation Parameters from Cone Penetrating Tests. *Proc., 2nd European Symposium on Penetration Testing, ESOPT II*, Amsterdam, The Netherlands, 1982, pp. 863–870.
  20. P. K. Robertson and R. G. Campanella. Liquefaction Potential of Sands Using the CPT. *Journal of Geotechnical Engineering*, Vol. 111, No. 3, 1985, pp. 384–403.
  21. P. K. Robertson and R. G. Campanella. Interpretation of Cone Penetration Tests—Part II (Clay). *Canadian Geotechnical Journal*, Vol. 20, No. 4, 1983.
  22. M. T. Tumay and I. Juran. *Fundamental Aspects of the Penetration Mechanism in Soft Soil*. Research Proposal Submitted to National Science Foundation for Project CEE-8113679. Department of Civil Engineering, Louisiana State University, Baton Rouge, La., 1981.
  23. M. T. Tumay. *Fundamental Aspects of the Penetration Mechanism in Soft Soil, Progress Report No. 1*. Department of Civil Engineering, Louisiana State University, Baton Rouge, La., 1983.
  24. M. T. Tumay. *Field Calibration of Electric Cone Penetrometer in Soft Soil—Executive Summary*. Report FHWA/LA/LSU-GE-85/02. Louisiana Transportation Research Center, Baton Rouge, La., 1985, 37 pp.
  25. N. Rad and M. T. Tumay. *Modification and Calibration of the Piezocone Penetrometer*. Fugro Post-Doctoral Report, Geotechnical Engineering Report GE-82/06. Department of Civil Engineering, Louisiana State University, Baton Rouge, La., 1983, 214 pp.
  26. A. Al-Awkati. *On Problems of Soil Bearing Capacity at Depth*. Ph.D. dissertation. Duke University, Durham, N.C., 1975, 204 pp.
  27. L. Parez, M. Bachelier, and B. Sechet. Pore Pressure Generated during Penetration of the Cone. *Proc., 6th European Conference on Soil Mechanics and Foundation Engineering*, Vienna, Vol. 3, 1976, pp. 533–538.
  28. P. K. Robertson and R. G. Campanella. Interpretation of Cone Penetration Tests—Part I (Sand). *Canadian Geotechnical Journal*, Vol. 20, No. 4, 1983.
  29. T. Lunne, T. Eidmoen, J. Powell, and R. Quartermann. *Piezocone Testing in Overconsolidated Clays*. Report No. 52155-42. Norwegian Geotechnical Institute, Oslo, 1986.
  30. D. Bruzzi and M. Battaglio. *Pore Pressure Measurements during Cone Penetration Test*. ISMES Research Report, Experimental Institute for Models and Structures, Bergamo, Italy, 1988, 125 pp.
  31. H. Zuidberg. Piezocone Penetration Testing—Probe Development. Specialty Session No. 14, *1st International Symposium on Penetration Testing, ISOPT-I*, Orlando, Fla., 1988, 21 pp.
  32. M. T. Tumay and R. Yilmaz. *In Situ Determination of Undrained Shear Strength of Louisiana Soils by Quasi-Static Cone Penetration Test*. Geotechnical Engineering Report FHWA/LA/LSU-GE-82/04. Department of Civil Engineering, Louisiana State University, Baton Rouge, La., 1981, 282 pp.
  33. A. S. Chan and M. T. Tumay. Piezocone Penetration Test—A New Deairing Technique. Technical Note, *Geotechnical Testing Journal*, in review, 1990.
  34. D. J. Bak. New Design Ideas—Degassing Liquids Requires No Heat. *Design News*, August 17, 1981.
  35. P. D. Kioussis, G. Z. Voyiadjis, and M. T. Tumay. *Large Strain Theory as Applied to Penetration Mechanism in Soils*. Geotechnical Engineering Report No. GE-85/01. Department of Civil Engineering, Louisiana State University, Baton Rouge, La., 1985, 97 pp.
  36. I. Juran and M. A. BenSaid. *Mesure in-situ des pressions interstitielles—Application à la reconnaissance des sols*. Research Report. École Nationale des Ponts et Chaussées, Paris, 1985.
  37. M. A. BenSaid. *Mesure in-situ des pressions interstitielles—Application à la reconnaissance des sols*. Ph.D. dissertation. École Nationale des Ponts et Chaussées, Paris, 1985.
  38. I. Juran. *In Situ Testing To Determine the Cause of Failure at the Nice Port*. Report submitted to TERRASOL, Paris, 1983.

---

*Publication of this paper sponsored by Committee on Soil and Rock Properties.*

# Load-Deflection Response of Piles in Sand: Performance Prediction Using the DMT

ROY H. BORDEN AND ROBERT S. LAWTER, JR.

The accurate prediction of the lateral load deflection response of piles is highly dependent on the proper modeling of the lateral soil stiffness. Recent papers have presented models that incorporate data obtained from the Marchetti dilatometer (DMT) to develop  $p$ - $y$  curves. As the DMT data are normally obtained at 8-in. depth intervals, these models provide a nearly continuous profile of lateral soil response. This paper presents a comparison of performance predictions made using three of these models with the measured response of two 24-in.-square, 25-ft-long, prestressed concrete piles in sand. The test piles were jettied the first 12 ft and driven the remaining 13 ft into the coastal plain deposits of eastern North Carolina. The measured load-deflection response of the two piles was very similar, and although none of the models that were investigated explicitly permits the consideration of installation effects, the measured response was found to be intermediate between that predicted by a model developed for driven piles and that predicted by a model applied to drilled piers.

A common technique used in the analysis of laterally loaded piles is to idealize the lateral stiffness of the soil adjacent to the foundation as a series of independent nonlinear springs. The Winkler model idealizes the soil-pile interaction mechanism by relating the pile displacement at a point to the soil pressure at that point through a spring constant, referred to as the coefficient of subgrade reaction ( $k$ ). Therefore, the accurate prediction of the lateral load-deflection response is highly dependent on the determination of the value of the coefficient of subgrade reaction, as well as its variation along the length of the pile.

Methods have been proposed for evaluating  $k$  from laboratory-determined soil modulus values and somewhat more directly from pressuremeter pressure-displacement data. Recent papers (1-4) have reported the validity of using data obtained from the Marchetti dilatometer test (DMT) in models to generate  $p$ - $y$  curves. The DMT is capable of providing a nearly continuous profile of the coefficient of subgrade reaction because test data are typically obtained at 8-in. increments. As an in situ test device that involves a lateral displacement of soil somewhat analogous to the lateral displacement of a pile, the DMT has been shown to be a reasonable tool for lateral pile analysis. This paper presents the results of performance predictions made using  $p$ - $y$  curves generated from three of these models.

## BACKGROUND

The flat dilatometer (DMT) developed by Silvano Marchetti (5,6) is essentially a penetration device capable of obtaining an estimate of lateral pressure and soil stiffness. The body of the dilatometer has an approximate width of 3.7 in. (95 mm) and a thickness of 0.6 in. (14 mm). When at rest, the external surface of the approximately 2.4-in.-diameter (60-mm-diameter) membrane is flush with the surrounding flat surface of the blade. The blade is usually pushed into the ground at conventional penetration test rates (1 in./sec). When the desired test depth is reached, the membrane is inflated by means of pressurized gas through a small control unit at the ground surface. Readings are taken of the pressure required to initiate movement of the membrane (related to the lateral stress existing in the ground) and the pressure required to move its center an additional approximate 0.04 in. (1 mm) into the soil (related to the soil stiffness). Both of these pressure readings are corrected for the effect of membrane stiffness. The first of these corrected pressures is called the " $p_0$ " pressure.

Gabr and Borden (2) proposed a subgrade reaction model, illustrated in Figure 1, that utilizes the difference between the " $p_0$ " pressure and the existing lateral pressure before penetration, approximating the nonlinear pressure-displacement relationship by a secant during the one-half-blade-thickness lateral displacement of the soil. This model will be referred to as Method A throughout the remainder of this paper. Schmertmann (3) has suggested a similar model, which expresses the coefficient of subgrade reaction in the following form:

$$k = \frac{(K_D - K_0) \cdot \sigma'_v}{0.5 \cdot t_b} \quad (1)$$

where  $\sigma'_v$  is the in situ vertical pressure at the test depth,  $t_b$  is the thickness of the dilatometer blade,  $K_0$  is the at-rest earth pressure coefficient, and  $K_D$  is the horizontal stress index, determined by the following equation:

$$K_D = \frac{(p_0 - u_0)}{\sigma'_v} \quad (2)$$

where  $u_0$  is the hydrostatic pore water pressure.

Both models require an estimate of the in situ lateral stress. The prediction of lateral stress in this study was based on the model proposed by Gabr and Borden (2) based on the evaluation of calibration chamber tests on normally consolidated

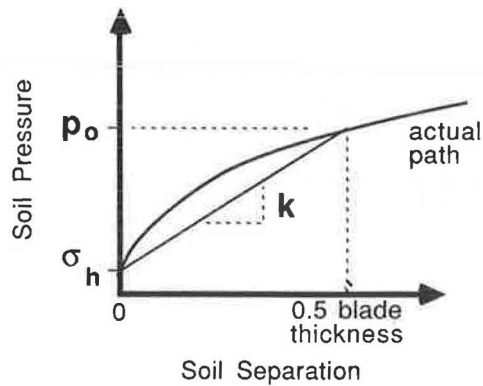


FIGURE 1 DMT subgrade reaction model.

sands. Reasonably good agreement between the predicted and measured response of three drilled piers was obtained (2) when this model was used in conjunction with the hyperbolic model for  $p$ - $y$  curves originally proposed by Parker and Reese (7) and modified by Murchison and O'Neill (8). The continuous hyperbolic tangent function is expressed as

$$p = \eta \cdot A \cdot p_u \cdot \tanh \left[ \left( \frac{k_h}{A \cdot \eta \cdot p_u} \right) \cdot y \right] \quad (3)$$

where  $p_u$  is the unmodified ultimate soil resistance, and  $\eta$  and  $A$  are empirical adjustment factors. For prismatic piles under static loading, the factor  $\eta$  is equal to 1, and  $A$  is a function of the depth from the ground surface to the point in question ( $z$ ) and of the pile diameter ( $D$ ), given by the formula  $3 - 0.8z/D > 0.9$ . The value of  $k_h$  in Equation 3 is obtained by multiplying  $k$  from Equation 1 by the pile width.

As the observed values of  $K_D$  in the sand at the field test site were much larger than  $K_0$  (generally on the order of a factor of 10), any reasonable estimate of  $K_0$  is sufficiently accurate for the determination of the in situ lateral stress used in Equation 1.

Schmertmann (3) also suggested that  $k$  determined from Equation 1 should be modified to account for size effects. In order to make this adjustment, Schmertmann estimated that for a reference width of 1 ft the  $k$  value is taken as equal to one-half of the value determined from the DMT data (i.e., Equation 1). Terzaghi's equation for size correction is then applied for widths greater than 1 ft. Thus, the corrected equation for  $k$  becomes:

$$k_{hsB} = 0.5 \left( \frac{B + 1}{2B} \right)^2 \frac{(K_D - K_0) \sigma'_v}{0.5 \cdot t_b} \quad (4)$$

and the value of  $k_h$  in Equation 3 is again obtained by multiplying  $k_{hsB}$  from Equation 4 by the pile width. This model, including the correction for size effects, will be referred to as Method B.

Robertson et al. (4) have suggested using DMT data in the cubic parabola model for  $p$ - $y$  curves proposed by Matlock (9) to predict the lateral response of driven piles. This expression has the form:

$$\frac{p}{p_u} = 0.5 \left( \frac{y}{y_c} \right)^{1/3} \quad (5)$$

where  $p_u$  is the lateral ultimate soil resistance and  $y_c$  is the critical deflection. The critical deflection is determined by the following equation:

$$y_c = \frac{4.17 \cdot \sin \phi \cdot \sigma'_{v0} \cdot D}{F_S \cdot E_D \cdot (1 - \sin \phi)} \quad (6)$$

where  $F_S$  is an empirical stiffness factor, with a value of 2 suggested, and  $E_D$  is the dilatometer modulus. This model will be referred to as Method C.

In each of the three models described, the ultimate soil resistance as a function of depth ( $p_u$ ) was determined according to the three-dimensional wedge model developed by Reese et al. (10).

## FIELD TEST SITE

The test site was located at the North Carolina Department of Transportation (NCDOT) marine maintenance facility in Manns Harbor, North Carolina. The current phase of construction at the facility is the bulkhead shown in Figure 2. Prior construction, begun in the late 1970s, had included a warehouse, material handling area, elevated water tank, and dry dock. The load test was conducted as a proof test of the lateral capacity of anchor piles designed to support the bulkhead. The 24-in.-square, 25-ft-long, prestressed concrete test piles were installed approximately 75 ft from the proposed bulkhead. The piles were manufactured using concrete with a compressive strength of 7,000 psi and were prestressed to an average stress of 1,320 psi. The uncracked pile stiffness and cracking moment were calculated to be  $0.11 \times 10^{11}$  lb-in.<sup>2</sup> and 365 k-ft, respectively. The piles were jetted 12 ft before being driven the remaining 13 ft with a Conmaco 100E5 hammer with an average pile blow count of 20 blows/ft. An enlarged view of the load test arrangement and the CPT and DMT locations is shown in Figure 3.

The site is located in the coastal plain of eastern North Carolina. NCDOT records indicated the typical soil profile

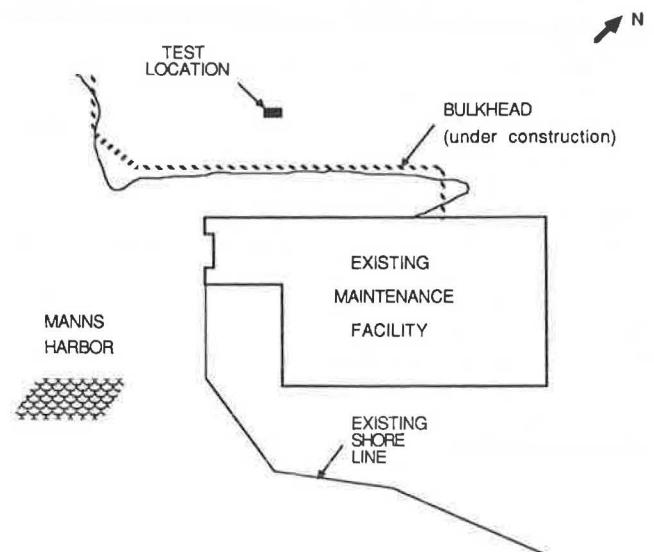
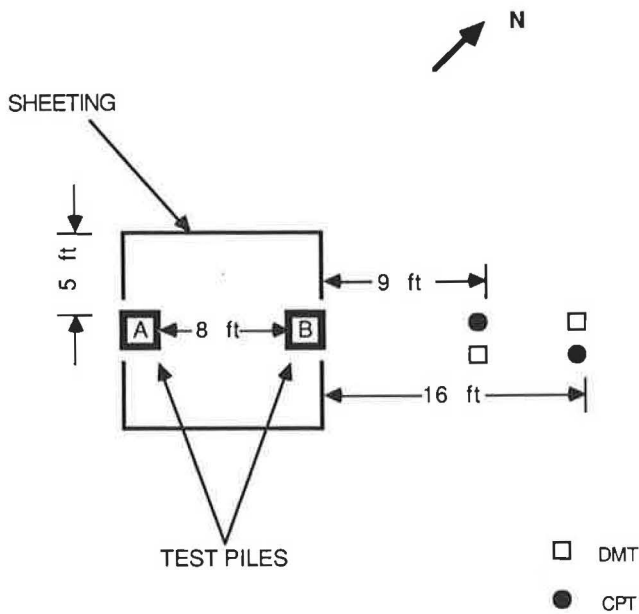


FIGURE 2 Site plan of NCDOT marine maintenance facility.



**FIGURE 3** Load test arrangement and penetration test locations.

around the facility to generally consist of a 1- to 4-ft-thick layer of hydraulically placed fill, which is composed of loose, uniform fine sand containing some organic material, SP according to the Unified Soil Classification System (USCS). The fill is underlain by a 2- to 7-ft-thick layer of soft organic silty clay with traces of sand. The clay soils were classified as CL. The clay deposit was underlain by medium-dense fine sand, also classified as SP.

After installation of the test piles, the DMT and CPT were performed. The averaged data from the two dilatometer tests, shown in Figure 4, indicated the sand fill layer at the test site location to be about 7.5 ft thick. The angle of internal friction ranged from 33 to 38 degrees, with the average value being approximately 37 degrees, as shown in Figure 5. The clay layer encountered between the depths of 7.5 and 12.5 ft on the basis of DMT data, had a predicted undrained shear strength ranging between 1.6 and 2.9 psi. The friction angles obtained

from the DMT for the underlying medium-dense sand ranged from 36 degrees at a depth of 13 ft to 41 degrees at 26 ft. These values were determined using the procedure proposed by Schmertmann (11), based on the Durgunoglu and Mitchell bearing capacity theory.

The CPT cone resistance and friction ratio are shown in Figure 6 in conjunction with the interpreted friction angles obtained using the method suggested by Schmertmann (12). The cone resistance ( $q_c$ ) for the fill layer ranged between 66 kg/cm<sup>2</sup> near the ground surface to 12 kg/cm<sup>2</sup> near the bottom of the fill layer. The corresponding friction angles for the fill layer ranged from 37 degrees in the upper 5 ft to 33 degrees in the lower 3 ft. Average cone resistances of 3 and 60 kg/cm<sup>2</sup> were measured for the clay and medium-dense sand layers, respectively. The value of the friction angle ranged from 33 to 38 degrees for the underlying medium-dense sand layer, with an average of approximately 35 degrees.

**LOAD TEST RESULTS AND PERFORMANCE PREDICTIONS**

The lateral load test was conducted by North Carolina Department of Transportation personnel in accordance with ASTM Standard D3966. The load was applied at a point 3 ft below the top of the pile, as shown in Figure 7. This depth corresponded to the location at which the tiebacks were to be connected to the anchor piles. Sheet piling was installed to allow the excavation of approximately 4 ft of soil below the pile tops. The measured load-deflection response of the two piles is shown in Figure 8.

The computer program LTBASE (13) was used to generate the  $p$ - $y$  curves at 8-in. intervals along the length of the pile and perform the load-deflection prediction. Program options were selected that incorporated the hyperbolic model previously described to generate the  $p$ - $y$  curves for the sand layers, and the unified method recommended by Sullivan (14) to generate the  $p$ - $y$  curves for the clay layer. Because the stress-strain response of the clay had not been determined from triaxial compression tests, the strain corresponding to the 50 percent stress level was estimated to be 0.02, and on the basis of the in situ determined undrained shear strength,  $k$  was

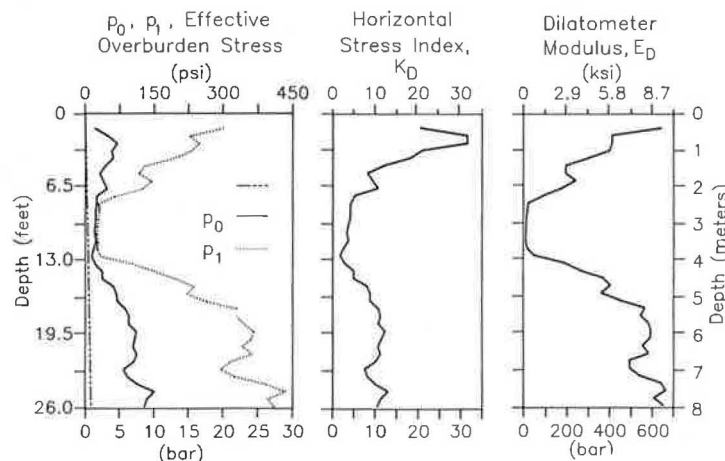


**FIGURE 4** Average DMT profiles.

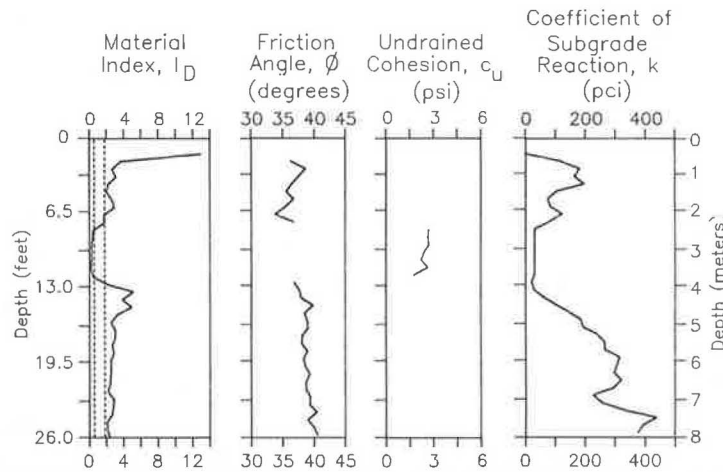


FIGURE 5 Average soil parameters and properties interpreted from DMT.

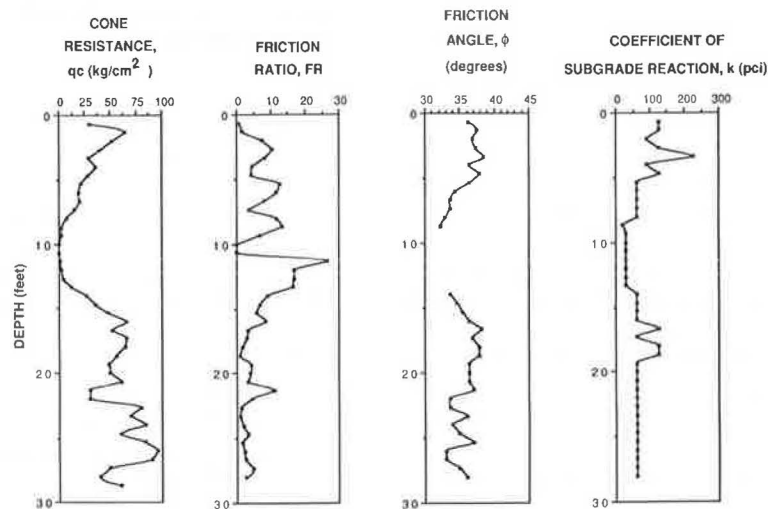


FIGURE 6 Average soil parameters and properties interpreted from CPT.

taken as 30 pci, as suggested by Reese (15). The values of the coefficient of subgrade reaction for the sand layers, as determined using Method A, and the estimated  $k$  values for the clay layer are presented in Figure 5.

In order to perform the load-deflection analysis for the situation encountered in this load test where the lateral load was applied 3 ft below the ground surface, the following analytical procedure was used:

1. The load-deflection response of the 22-ft portion below the point of load application was determined. To obtain  $p$ - $y$  curves appropriate for the actual 25-ft pile, the effect of the upper 3 ft of soil was modeled using a proportionately higher unit weight in the first 8-in. soil layer below the point of load application. Because of the installation of sheet piling and the excavation of soil from within the test pit (Figures 3 and 7), it was considered appropriate to model the stress reduction due to excavation by reducing the full height of sand above the top of the model pile by 50 percent.

2. Because the analysis described did not include the lateral resistance provided by the upper 3 ft of fill, it was necessary

to modify the predicted pile displacements. This modification was made by first performing an analysis using the entire 25-ft pile to determine the lateral resistance provided by the upper 3 ft of fill as a function of deflection. For example, the ultimate lateral resistance, ( $p_u$ ) of each pile increment above the point of loading is shown in Figure 9. This curve was then integrated to determine the equivalent shear and moment at the point of loading. Next, an analysis was made applying this shear and moment to the top of the model 22-ft pile to determine the resulting deflection. An iterative procedure was employed until the assumed deflection of the pile at the point of load application, from which the soil resistance in the upper 3 ft was determined, was approximately equal to the subsequently calculated displacement. The significance of this correction is shown in Figure 8 in conjunction with the uncorrected prediction. A similar correction procedure was applied to each of the subsequent predictions.

As shown in Figure 10, the predicted deflected shape of the pile below the point of loading suggests that the pile is behaving as a relatively rigid member. At a pile top deflection of 3 in., a maximum moment of 175 k-ft was predicted to



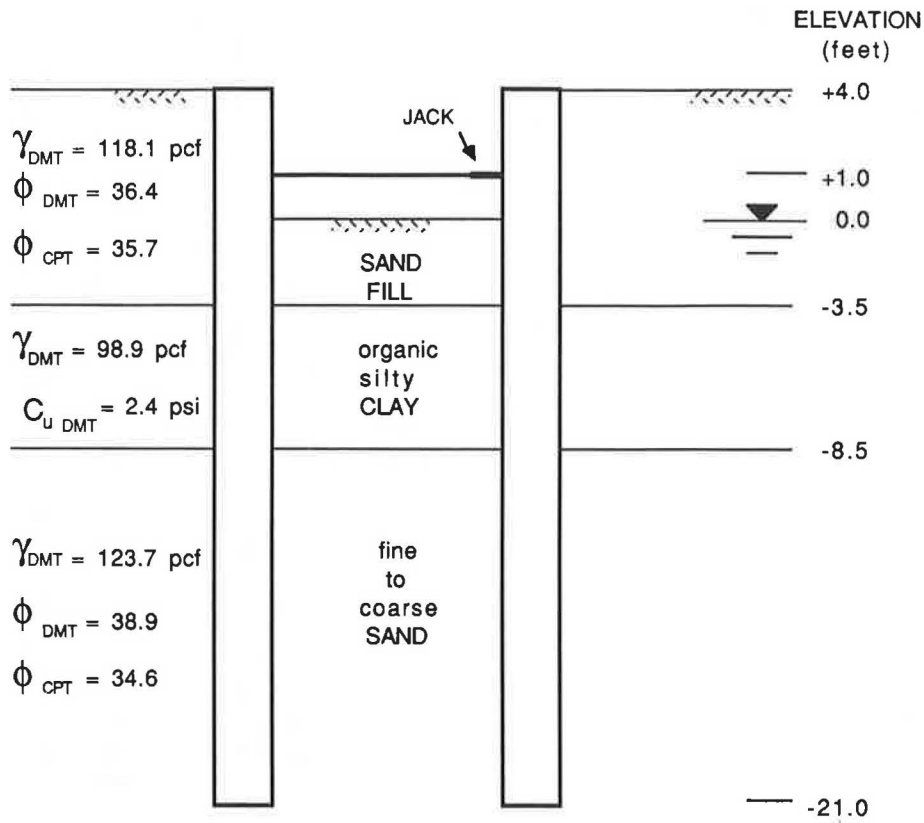


FIGURE 7 Load test configuration and soil profile.

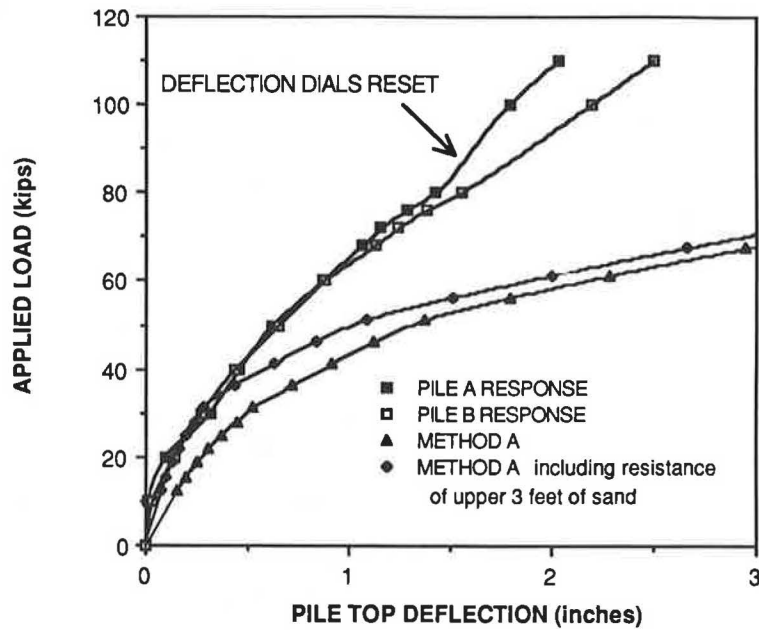


FIGURE 8 Comparison of measured pile response with predicted pile response using Method A.

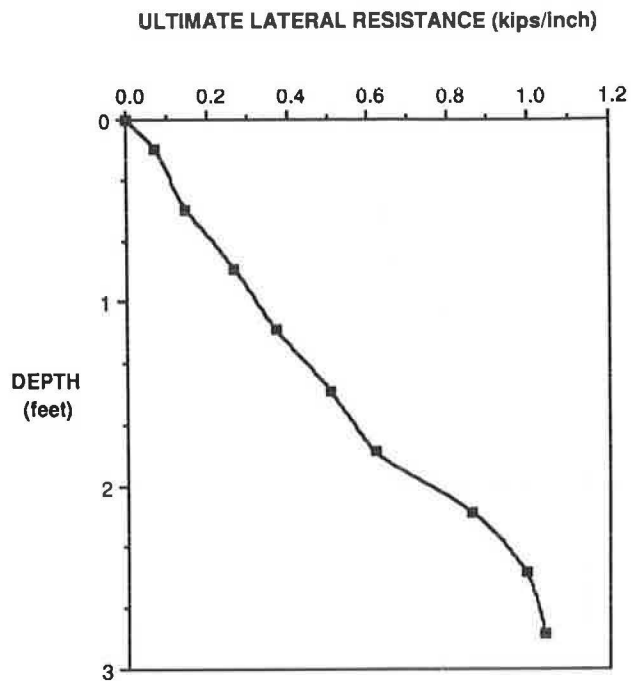


FIGURE 9 Ultimate lateral resistance in upper 3 ft.

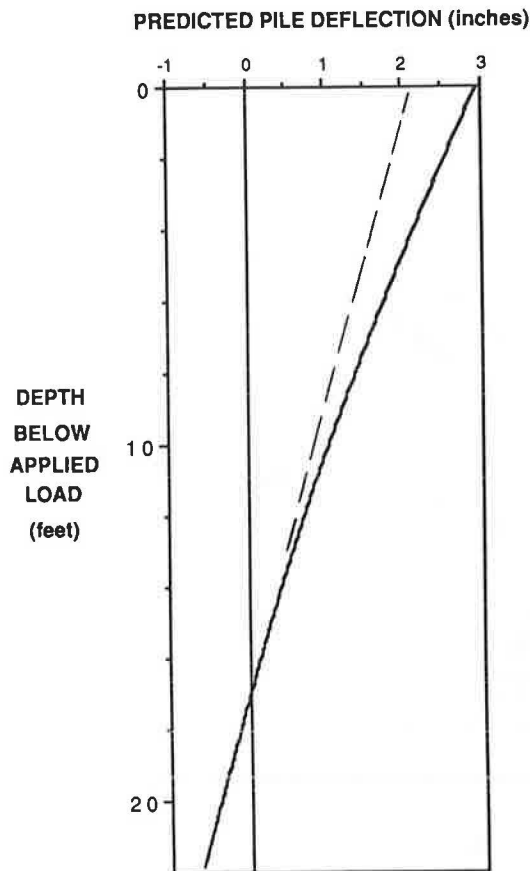


FIGURE 10 Pile deflection predicted using Method A.

occur in the pile. This is less than one-half of the calculated cracking moment of the pile.

Similarly, an analysis was made using Method B in conjunction with the hyperbolic  $p$ - $y$  curve formulation, as shown in Figure 11. As previously reported by Schmertmann (3), the  $k$  values from this model tend to underestimate  $k$ . J. H. Schmertmann (personal communication, 1988) also suggested that these  $k$  values might logically be used in bi-linear  $p$ - $y$  curves as they represent secant values. Figure 12 shows the improved predicted response obtained by using these  $k$  values in bi-linear  $p$ - $y$  curves.

Figure 13 shows the predicted load-deflection response based on the cubic parabola model of Method C, in conjunction with the measured response. With respect to the measured response, the predicted pile response is significantly stiffer. Because this method was developed for driven piles, this difference may be due to a reduction in lateral stress adjacent to the piles caused by jetting the piles the first 12 ft during installation and the subsequent excavation of the soil within the test pit.

For each of the predictions presented, the shape of the  $p$ - $y$  curves as a function of depth is the controlling factor, as the ultimate lateral resistance at large deflections is the same. In order to more clearly demonstrate the difference in these  $p$ - $y$  curves, the following comparison is presented. The  $p$ - $y$  curves generated by each of the above models for depths of 3 and 18 ft are shown in Figure 14. As evidenced in the preceding performance predictions, the softest  $p$ - $y$  curves are generated using Method B in hyperbolic  $p$ - $y$  curves. Modeling the  $p$ - $y$  curves as bi-linear significantly reduces the deflection for a given load, particularly once the load is greater than one-half of the ultimate. The stiffer  $p$ - $y$  curves generated using Method A in hyperbolic  $p$ - $y$  curves results in a slightly improved performance prediction when viewed over the first few inches of deflection. Method C produces a  $p$ - $y$  curve that is much stiffer than any of the other models. Because of the stiffness of the  $p$ - $y$  curves generated by this model, the deflection at any given load was underpredicted. From this information it appears that the stiffness of the  $p$ - $y$  curves should be between that generated by Method A and that generated by Method C.

For comparison purposes, a performance prediction was made using the CPT data. Predictions made using the CPT data will be referred to as generated by Method D. The relative density ( $D_r$ ) of the sand at 8-in. increments was estimated from Schmertmann's (12) correlation of  $D_r$  with  $\sigma'_v$  and  $q_c$ . The effective unit weight of the sand was estimated using typical values of the maximum and minimum unit weights of uniform fine sands (16). Values of  $k$  as a function of depth were chosen according to relative density as suggested by Reese and Allen (15) and are shown in Figure 6. Figure 15 presents a comparison of the prediction made using Method D with the prediction made using Method A. A review of Figures 5 and 6 indicates that the DMT soundings produced  $k$  and  $\phi$  values higher than those obtained from the CPT. However, the subgrade modulus profile for the CPT shown in Figure 16 is calculated by multiplying the Reese-determined value of  $k$  by the depth, while the DMT-developed  $k$  values are multiplied by the pile width. Although at shallow depths the DMT subgrade modulus values are somewhat greater, at increasing depths and in the sand underlying the clay layer

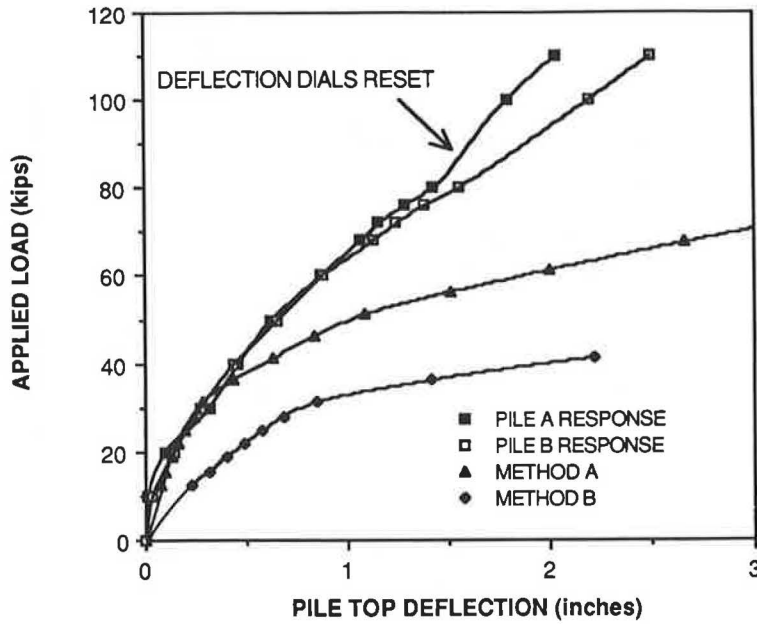


FIGURE 11 Pile response predicted using Method B.

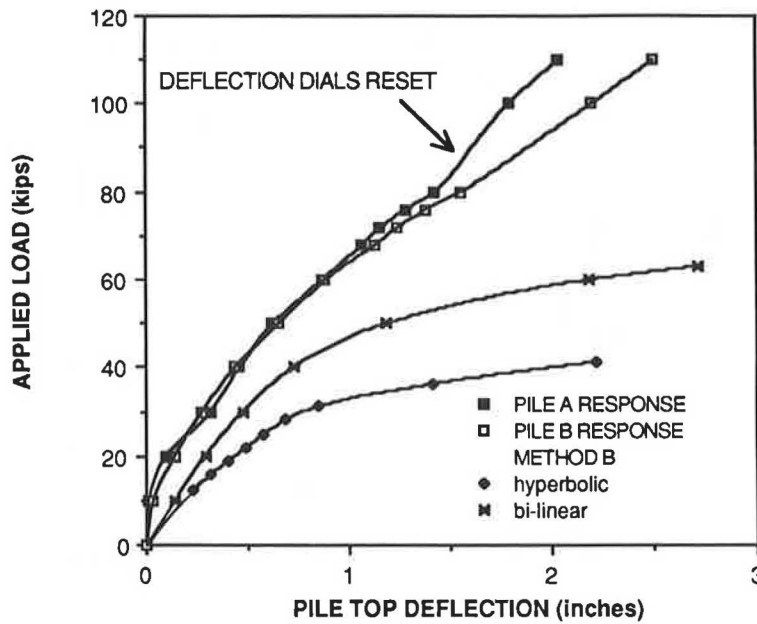


FIGURE 12 Pile response predicted using Method B in hyperbolic and bi-linear *p-y* curves.

the values interpreted from the CPT become almost twice as large as those from the DMT. The *p-y* curves at depths of 3 and 18 ft resulting from the CPT data are plotted in Figure 17 in conjunction with those previously shown in Figure 14. Because of the relatively rigid response of the pile, the effect of the stiffer *p-y* curves at depth from the CPT data very prominently influences the resultant load-deflection response.

In order to illustrate the insignificant influence of small variations in the angle of internal friction on the predicted load-deflection response in the first few inches of deflection, an analysis was performed utilizing the somewhat lower CPT

$\phi$  values in conjunction with *k* values from Method A. A comparison of this prediction, the prediction using Method D, and the prediction using Method A is shown in Figure 15. As there is virtually no difference in the predicted response as a result of the different friction angle profile produced by the CPT and DMT, this figure illustrates the significance of the early portion of the *p-y* curve in predicting the lateral response of these piles up to a displacement of 10 percent of the pile width. The value of an instrumented test pile is obvious when one tries to evaluate the likely deflected shape and actual soil response as a function of depth.

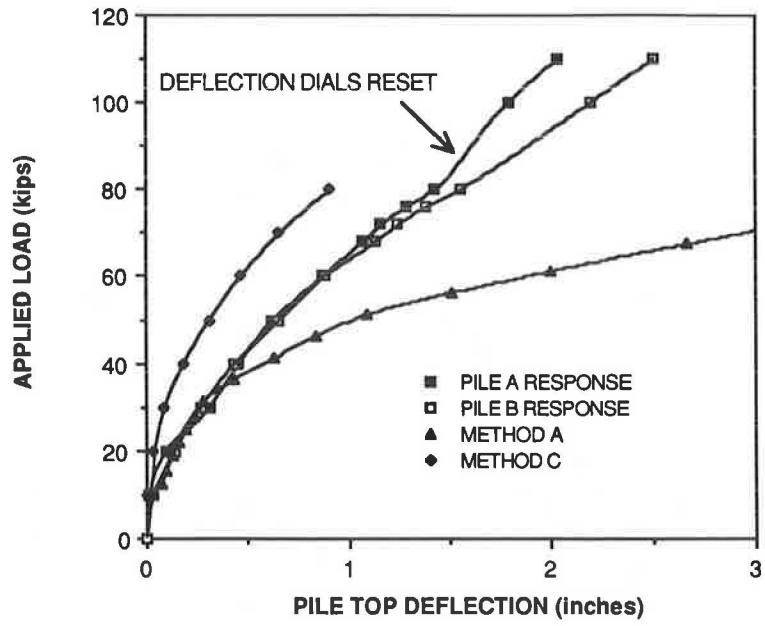


FIGURE 13 Pile response predicted using Method C.

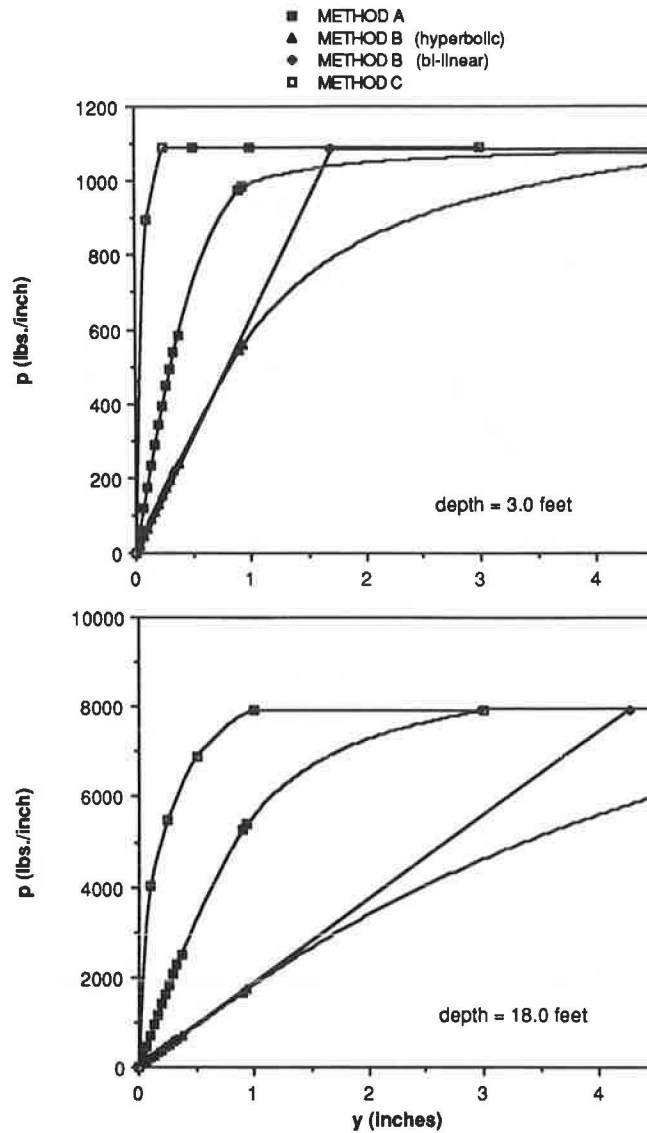


FIGURE 14 DMT-based  $p$ - $y$  curves at depths of 3 and 18 ft.

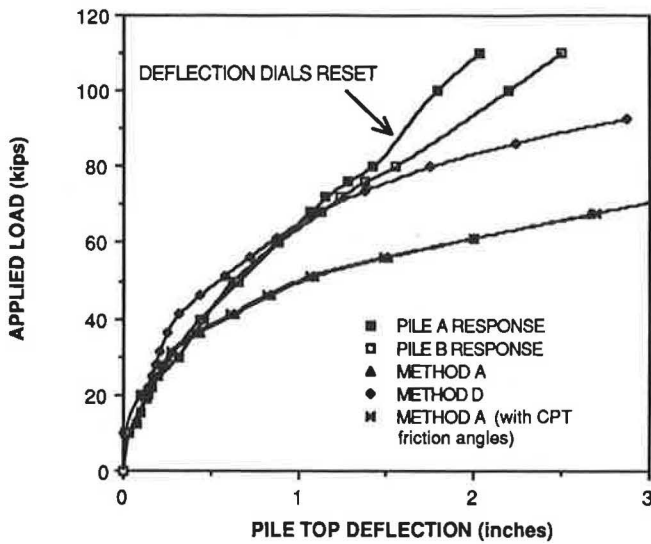


FIGURE 15 Pile response predicted using Method D.

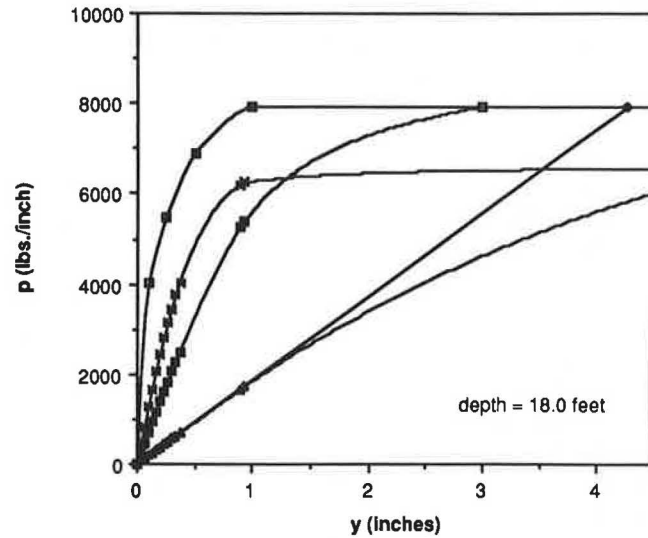
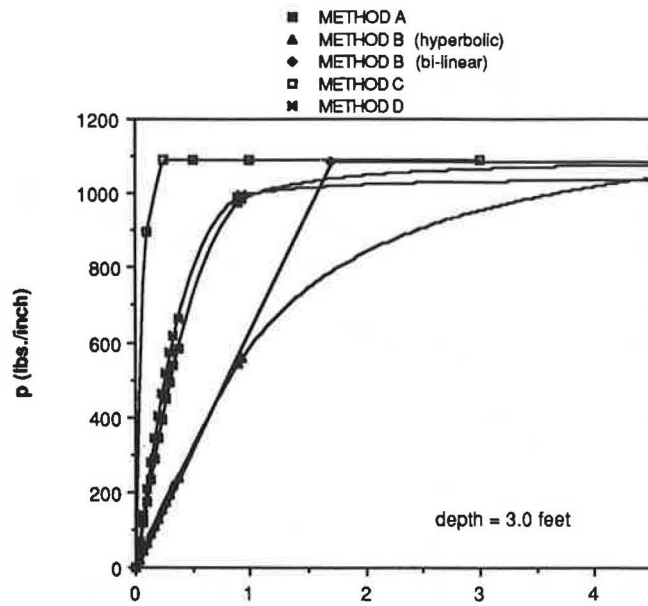


FIGURE 17 CPT-based  $p$ - $y$  curves at depths of 3 and 18 ft.

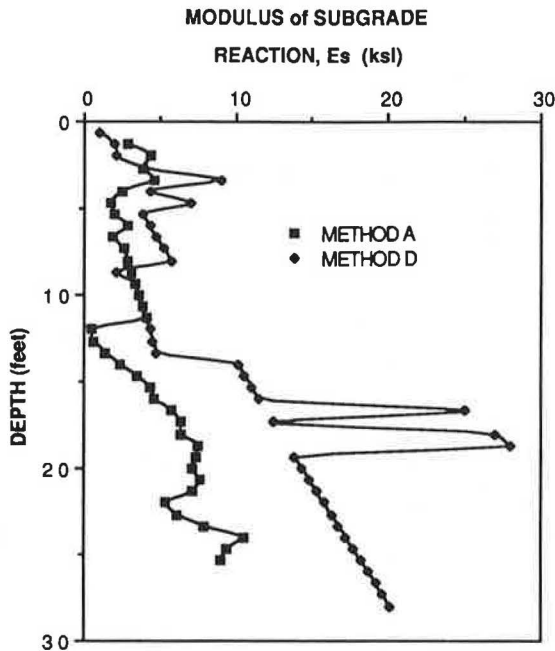


FIGURE 16 Modulus of subgrade reaction as determined by Methods A and D.

Finally, Figure 18 presents a comparison of the measured and predicted load-deflection responses over the first 1 in. of deflection. During the first 0.5 in. of deflection, the measured response was most closely approximated by the hyperbolic  $p$ - $y$  curves using the DMT secant model without consideration for size effects. The actual response was bounded by the stiffer response predicted using Method C and the softer response produced using Method B in conjunction with bi-linear  $p$ - $y$  curves. It is not the intention of this comparison to suggest that in all cases the best agreement should be expected to be obtained by the models showing the best performance in this study. However, in cohesionless profiles, the stiffness of the

predicted load-deflection responses of the three DMT-based models, with respect to each other, is expected to remain the same.

**SUMMARY AND CONCLUSIONS**

The results of performance predictions made using three proposed models for developing  $p$ - $y$  curves from DMT data are presented in conjunction with the measured response from lateral load tests on two 24-in.-square prestressed concrete piles that were installed by jetting the first 12 ft followed by driving to a depth of 25 ft. Over the first 1-in. deflection, a method for developing  $p$ - $y$  curves using a simple secant approximation based on the pressure increase needed to dis-

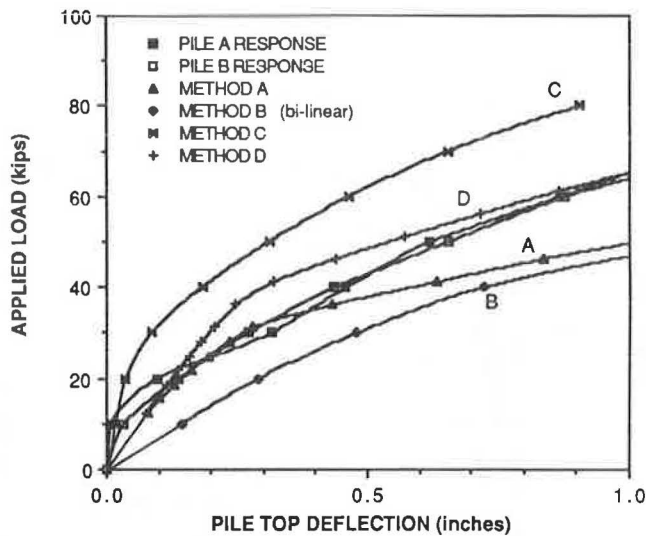


FIGURE 18 Predicted pile response over 1-in. deflection.

place the soil a distance equal to one-half of the DMT blade thickness produced a predicted response closest to that measured. The use of size effect corrections produced a significantly softer response than that measured, whereas the model of Robertson et al. produced a significantly stiffer response. It should be noted that this method was developed for driven piles and that the stiffer predicted response may in part be due to a lateral stress reduction due to the jetting. Although none of the models investigated allowed for the explicit consideration of the installation procedure, it is quite reasonable that the observed response was bracketed by procedures that previously had been applied to driven piles and drilled piers, respectively.

Although DMT soundings produced friction angles, based on the Durgunoglu and Mitchell bearing capacity theory, that were somewhat higher than those obtained from the CPT, this difference was shown to be of relatively minor importance in the first several inches of pile displacement in comparison to that of the inferred  $k$  values used to generate the  $p$ - $y$  curves.

#### ACKNOWLEDGMENTS

This project was sponsored by the North Carolina Department of Transportation. The authors would like to express appreciation to John Ledbetter, Don Moore, and the other NCDOT personnel who supported the dilatometer testing and conducted the cone penetration and lateral load testing. The authors also wish to thank Raja Elawar of the NCDOT for providing background information needed to prepare this paper, and Mohammed A. Gabr and Peter K. Robertson for their review comments. The financial support of the second author on a State of North Carolina Research Assistantship and the

Ralph E. Fadum Graduate Fellowship is gratefully acknowledged.

#### REFERENCES

1. E. S. Motan, and M. A. Gabr. Flat Dilatometer and Lateral Soil Modulus. In *Transportation Research Record No. 1022*, TRB, National Research Council, Washington, D.C., 1985, pp. 128–135.
2. M. A. Gabr, and R. H. Borden. Analysis of Load Deflection Response of Laterally Loaded Piers Using DMT. *Proc., 1st International Symposium on Penetration Testing, ISOPT 1*, Orlando, Fla., 1988, pp. 513–520.
3. J. H. Schmertmann. *Guidelines for Using the CPT, CPTU and Marchetti DMT for Geotechnical Design*, Vol. 3. Research Report FHWA-PA-024+84-24. FHWA, U.S. Department of Transportation, Washington, D.C., March 1988, pp. 4.59–4.60.
4. P. K. Robertson, M. P. Davies, and R. G. Campanella. Design of Laterally Loaded Driven Piles Using the Flat Plate Dilatometer. *Geotechnical Testing Journal*, Vol. 12, No. 1, 1989, pp. 30–38.
5. S. Marchetti. A New In Situ Test for the Measurement of Horizontal Soil Deformability. *Proc., Conference on Measurement of In Situ Soil Properties*, Raleigh, N.C., Vol. 2, ASCE, New York, 1975–1976, pp. 255–259.
6. S. Marchetti. In Situ Tests by Flat Dilatometer. *Journal of the Geotechnical Engineering Division, ASCE*, Vol. 106, No. GT3, 1980, pp. 299–321.
7. F. Parker, Jr., and L. C. Reese. *Experimental and Analytical Studies of Behavior of Single Piles in Sand under Lateral and Axial Loading*. Research Report 117-2. Center for Highway Research, University of Texas at Austin, 1970.
8. J. M. Murchison, and M. W. O'Neill. Evaluation of P-Y Relationships in Cohesionless Soils. *Proc., Analysis and Design of Pile Foundations*, San Francisco, Calif., ASCE, New York, 1984.
9. H. Matlock. Correlations for Design of Laterally Loaded Piles in Soft Clay. *Proc., 2nd Offshore Technology Conference*, Vol. 1, Houston, Tex., 1970, pp. 577–594.
10. L. C. Reese, W. R. Cox, and F. D. Koop. Analysis of Laterally Loaded Piles in Sand. *Proc., 6th Annual Offshore Technology Conference*, Houston, Tex., Vol. 2, 1974.
11. J. H. Schmertmann. A Method for Determining the Friction Angle in Sands from the Marchetti Dilatometer Test. *Proc., 2nd European Symposium on Penetration Testing, ESOPT II*, Amsterdam, The Netherlands, 1982, pp. 853–861.
12. J. H. Schmertmann. *Guidelines for Cone Penetration Test Performance and Design*. Manual FHWA-TS-78-209. U.S. Department of Transportation, Washington D.C., 1978, pp. 38–41.
13. R. H. Borden, and M. A. Gabr. *LTBASE: A Computer Program for the Analysis of Laterally Loaded Piers Including Base and Slope Effects*. In *Transportation Research Record 1169*. TRB, National Research Council, Washington, D.C., 1988, pp. 83–93.
14. W. R. Sullivan. *Development and Evaluation of a Unified Method for the Analysis of Laterally Loaded Piles in Clay*. Unpublished thesis. University of Texas at Austin, 1977.
15. L. C. Reese, and J. D. Allen. *Drilled Shaft Manual*, Vol. 2, *Structural Analysis and Design For Lateral Loading*. FHWA, Office of Research and Development, U.S. Department of Transportation, Washington, D.C., 1984.
16. R. D. Holtz, and W. D. Kovacs. *An Introduction to Geotechnical Engineering*. Prentice-Hall, Englewood Cliffs, N.J., 1981, pp. 104–105.

Publication of this paper sponsored by Committee on Foundations of Bridges and Other Structures.